UNIVERSITY OF SOUTHAMPTON

DEPARTMENT OF AERONAUTICS AND ASTRONAUTICS

COAXIAL CONTRAROTATING TWIN ROTOR AERODYNAMICS

by

MICHAEL JOHN ANDREW

Under the Supervision of Professor I.C. Cheeseman

Dissertion Submitted for the

Degree of Doctor of Philosophy

TABLE OF CONTENTS

UNIVERSITY OF SOUTHAMPTON

ABSTRACT

FACULTY OF ENGINEERING

AERONAUTICS & ASTRONAUTICS

Doctor of Philosophy

COAXIAL CONTRAROTATING TWIN ROTOR AERODYNAMICS

by Michael John Andrew

The modelling of a Coaxial Contrarotating Twin Rotor (CCTR) system has been developed from single rotor modelling techniques. Particular attention has been paid to the characteristics of the tip vortex, namely, vortex strength, structure and decay. Equations are presented which describe both the vortex core and the complete structure of a rolled-up tip vortex. These equations are utilised with conventional strip theory to enhance the predictive accuracy, and replace the arbitrary application of a tip loss factor. Using this combined approach, named Vortex-Strip theory, the full interference effects between the two rotors of a hovering CCTR have been successfully modelled.

By a similar approach, a Vortex-Glauert theory has been developed to model the wake of a CCTR in forward flight. Comparisons between theory and experimental results from model and full scale rotors are shown over a variety of hovering and forward flight conditions.

Both wake models have been written in Fortran IV computer language with a flexible input procedure. This feature allows a user to investigate a wide range of rotor parameters including different rotor radii, number of blades, CCTR rotor spacing, with variations in blade twist, taper and effective hinge offset.

The computer program, named ROTOR, was used in a preliminary optimisation study of a hovering CCTR. The results show that a conventional CCTR is a more efficient layout in hover than an equivalent single rotor; a finding which has been endorsed by experimental results.

Although the presented models have been developed for a CCTR, it should not be overlooked that they are equally applicable to single rotor configurations.

LIST OF FIGURES

NOTATAION

A	Tip vortex coefficient
A_r	Blade aspect ratio = R/C
a	Lift curve slope
a_o	Blade coning angle
a_1	First harmonic longnitudinal flapping coefficient
$a_1 a_2$	Landgrebe wake coefficients
B	Tip vortex coefficient
b	Number of blades
b_1	First harmonic lateral flapping coefficient
C	Tip vortex coefficient
C_L	Rotor lift coefficient
C_T	Rotor thrust coefficient
c	Blade chord
c_l	Local blade lift coefficient
c_{do}	Local blade profile drag coefficient
D	Drag, tip vortex coefficient
D_i	Induced drag
D_p	Profile drag
d	Vertical spacing between CCTR rotors
E	Tip vortex coefficient
E_v	Tip vortex rotational energy
F	Rotor figure of merit
H	Rotor H-force
I	Second moment of inertia
K	Vortex strength = $2\pi v_v r$
K_1	Tip vortex modelling constant
K_2	Tip vortex modelling constant
K_c	Tip vortex core strength
K_l	Maximum tip vortex strength in the logarithmic region

K_2 Total tip vortex strength

M Mach number

P Rotor power

Q Rotor torque

R Rotor radius

R_e Reynolds number based on blade chord

r Radial distance

r_c Tip vortex core radius

r_l Tip vortex logarithmic outer radius

r_o Tip vortex defect outer radius

T Rotor thrust

t Blade thickness

u Induced velocity, axial velocity

U_p Perpendicular velocity to blade section

U_T Tangential velocity to blade section

V Forward flight velocity

V_s Tip vortex induced velocity at vortex core edge ($r=r_c$)

V_T Rotor tip velocity

V_c Rotor climb velocity

v General velocity, radial velocity

v_i Induced velocity

v_v Tip vortex induced velocity

w Tangential velocity

x,y,z Cartesian coordinates

α Blade angle of attack

α_r Local blade angle of attack

β Blade flapping angle

Γ Blade bound circulation

Γ_{max} Maximum blade bound circulation

γ Lock number

θ Blade pitch

λ Rotor inflow ratio

μ Rotor advance ratio

π Pi = 3.145927

ρ Air density

σ Blade solidity

ϕ Inflow angle

ψ Degrees of azimuth

Ω Rotor angular velocity

ω Angular velocity

Suffixes

1,2,3 Blade number

u,l Upper and lower rotor respectively

x,y,z Componants associated with the (x,y,z) Cartesian coordinates

ACKNOWLEDGEMENTS

The author wishes to express his gratitude to Professor I.C. Chesseman for his guidance and supervision throughout this study; to Mr N.I. Powell and technical staff at Southampton University for their assistance during the experimental portion of the study;to Westland Helicopters Limited for supplying the experimental helicopter model rotor rig;to the Science Research Council for their financial support; and to Mrs W. Bull for typing the thesis.

1. INTRODUCTION

1.0 Introduction

Although a vast amount is now known about single rotor aerodynamics (1,2) and associated modelling techniques (3,4), current knowledge of the flow through a coaxial contrarotating twin rotor (CCTR) is extremely limited. Even Russian publications fail to disclose concise details of CCTR flow characteristics (5,6). The following historical note on CCTR development indicates that this particular layout is a serious contender to the conventional single rotor configuration. However, the dearth of knowledge in the literature needs to be rectified if the full potential of the CCTR helicopter is to be exploited in the future. The objective of this thesis is to partially fulfill this need.

1.1 Historical Notes

In 1784 two Frenchmen, Launoy and Bienvenu (7) were credited with the first working model of a helicopter. The device they constructed was a model CCTR, powered by twisted chord and bent whalebone. A similar layout was also proposed by Cayley in 1796. Although various designs followed it was not until the beginning of this century that Berliner (1909) built a CCTR system which lifted a pilot untethered. Similar attempts are attributed to Pescara (1919), d'Asanio (1930) and Breguet (1930).

With the main emphasis being placed on single rotor development in post-war years, relatively little attention has been paid to the CCTR layout. Apart from the Sikorsky Advancing Blade Concept (ABC) (8), work on this configuration effectively ceased in the mid 1950's. Nevertheless, the ABC verification program identified some of the salient features of a CCTR, and indicated great caution is necessary when applying single rotor type assumptions, even in the most simplified analysis.

The ABC exploits the fundamental properties of a CCTR system. That is, the resultant unbalanced aerodynamic moments and torques on

one rotor are reacted by the other rotor turning in the opposite direction, allowing trim to be maintained without the aid of a tail rotor. In addition, the ABC alleviates retreating blade stall by selectively loading only the advancing blades in each rotor. Although this necessitates very stiff blades with rigid root fittings, the forward flight speed capability of the helicopter has increased markedly over the conventional single rotor. In recent trials, the ABC craft was reported to have reached a forward flight speed of 240 knots (9). Further potential gains include good overall handling qualities, high hovering efficiency and compactness with low noise characteristics (10).

However, during preliminary flight trials, the ABC XH-59A demonstrator craft in a low advance ratio flight regime, experienced a high nose up pitching moment, rendering the craft uncontrollable. A heavy tail first landing resulted. Post-analysis of this incident revealed that the computation of the control range pilot input required to maintain trim, using simple momentum type theory, grossly underpredicted the resultant blade forces and moments. The 'K' factor in Glauerts well known forward flight equation was subsequently updated to allow for the interaction between the two rotors (11). With increasing forward flight speed, the influence between the two rotors diminishes. Even so, at the higher end of the speed range very large profile drag losses are incurred by the rotor hub and blade rigid root fittings. This to date, has been identified as the major disadvantage of the ABC.

Alternatively, the CCTR layout may also be exploited with semi-rigid or fully articulated rotors. CCTR's of this category have also been demonstrated as a viable option in both model (12) and full-scale helicopters (13). Under the guidance of Nikoi Kamov, the Russion 'Ka' series of CCTR helicopters was born. The first craft to fly successfully was the Ka-8 in 1947. Continuing success of this configuration is reflected by the Ka-25 anti-submarine helicopter, the Ka-25k flying crane and the Ka-26 general purpose helicopter. The Ka-25k is claimed to combine a high payload to all-up-weight ratio, with good manoeuvrability and minimum dimensions (13).

A further application of the CCTR has been utilised by Westland Helicopters Limited. With this layout the feasibility of using a small remotely piloted helicopter (RPH) for real time surveillance and reconnaissance was investigated. From the prototype RPH design, named Mote, through more advanced projects using CCTR crafts Wisp, Wide-eye and Supervisor, the overall handling qualities have been successfully demonstrated.

Although disjointed, the development of the CCTR has brought forth a variety of claims which if to be taken seriously and exploited in future development requires a greater indepth knowledge of this particular layout. The following section presents the research investigations which were carried out at Southampton University to increase the understanding of the aerodynamic properties of a CCTR.

1.2 Research Development

At the inception of the research study, the prototype RPH, developed by Westland Helicopters Ltd, was presented to the University for research investigations. Chapter 2 discusses the overall characteristics of the craft and the modifications made over the duration of the investigation.

The expansive experimental research already in existance on single rotor aerodynamics has over recent years, with advances in computer hardware, been supplemented with more refined theoretical treatments. Such theoretical approaches, although not necessarily producing a higher degeree of predictive accuracy, have often identified areas where current experimental data is lacking. For example, results from advanced wake modelling codes developed by Johnson (14), suggest much more effort is needed to ascertain the strength, decay and overall characteristics of the tip vortex, even when evaluating integrated effects on a helicopter rotor. Chapter 3 surveys the available literature reporting tip vortex data and presents equations defining the strength and circulation distribution of a tip vortex.

Chapters 4 and 5 describe the developed CCTR wake theories for hover and forward flight respectively. Included in these chapters are comparisons with results from model and full-scale rotors. The adaption of the CCTR theory to an overall computer program ROTOR, is presented in Chapter 6. The program refinements include a well defined input procedure with the option to run interactively, combined with a generally written set of modular codes which may be used as a continuing research tool. Chapter 7 discusses one application of program ROTOR to a preliminary optimisation study of a hovering CCTR.

Finally, a review of the research study and discussion of the results including conclusions and recommendations for future work is contained in Chapter 8.

2. EXPERIMENTAL RIG AND PROCEDURE

2.0 CCTR Rig

The CCTR rig used throughout this investigation was presented to the University of Southampton by Westland Helicopters Limited. Initially developed as a prototype design to explore the control characteristics and problems encountered with CCTR RPH's, the complete craft (named Mote) was extensively modified for adaption to experimental research.

All experimentally redundant structures were removed from the craft leaving only the main frame, drive shafts and rotor heads. The two 10cc glow plug motor power supplies were initially replaced by one large 1.5 horse power direct curent motor. This was later upgraded by two small electrical dc motors (max power of each = 0.4 horse power) which have been especially developed for model applications. Light in weight, very compact and low in cost the major disadvantage of a model motor is the high current drawn through its windings (e.g. amps =10, volts =12), and resulting low electrical efficiency. Nevertheless, these motors were easily integrated to the main frame and considered highly desirable, especially for forward flight testing.

The rig (Fig 1) was mounted on four strain gauged flexures which were calibrated to measure the overall lift. The power absorbed by the CCTR system was determined from recording the input power to each motor and correcting for known motor and mechanical losses. The latter was evaluated by running the rig at sample RPM's without blades, and generating representative opposing torques on the drive shafts using a frictional torquemeter. The torquemeter was constructed from a cord taken over a drive shaft and connected to a spring balance and freely hanging mass. As the rig is run-up, the cord produces an opposing frictional torque which can be determined from the change in tension registered by the spring balance. It was observed that changes in efficiency took place during prolonged running of the rig and was assumed to result from the increase in

temperature in the motor windings. To account for this when establishing thrust/power characteristics, on the spot efficiencies of the rig were determined using the torque meter for each separate thrust condition. Nominally however, the overall system efficiency was less than 30%.

The salient rig characteristics are:-

Configuration	Twin rotor, contra-rotating and coaxially mounted
No blades/rotor	Two
Rotor spacing	19.6cm
Rotor radius	76cm
Max RPM	600

A variety of blades were used during the course of the investigation and unless otherwise stated, the default blade characteristics assumed in program ROTOR are:-

Blade Fixing	Teetering
Lift curve slope (rads)	5.73
Profile drag coefficient	(after Bailey (15))

2.1 Experimental Procedure

CCTR hover was investigated with the rig thrusting downward (blades inverted) to minimise re-circulation affects. Wake detail was collected using:-

1) Smoke visualisation/photographic techniques to locate the tip vortices of each rotor.

2) A single non-directional hot wire anemometer developed at Southampton University (16) to determine the induced velocity flow field and the magnitude of the trailing tip vortex strengths. Hard copies of the tip vortex speed/time signatures were obtained from a graph pen recorder.

With the RPM (synchronous rotor RPM was achieved by an interconnecting toothed timing belt linking the two drive shafts) of each rotor being monitored by magnetic pickups connected to a tachometer, the power absorbed by each rotor was recorded. Differential collective was then applied to trim out any power (yaw) imbalance in the rotors. For this particular CCTR, differential pitch settings well under 1.0 degree were found adequate to maintain trim. Overall rotor thrust and power were then measured. This procedure was repeated for a variety of pitch settings.

Forward flight performance of the rig was similarly investigated in Southampton University's 7x5 feet wind tunnel. Initially, the tunnel wind speed was set as required, without the rotors turning, to zero the strain gauge outputs from the four supporting flexures. Thereafter, the rig was run-up to a predefined RPM with simultaneous application of the rotor controls to remove any differential forces on the flexures. The corresponding control settings, overall rotor thrust and power were then recorded. Further smoke visualisation tests were also carried out in the 10x8 feet working section to investigate tip vortex wake affects in low advance ratio flight conditions. In all, advance ratios, between 0 to 0.25 were investigated for a variety of rotor loading conditions.

Chapter 3 introduces the tip votex experimental data, while Chapter 4 presents the Mote hover performance results. Chapter 5 includes both the forward flight performance characteristics, and discusses some of the smoke visualisation photographs gathered during the experimental programme.

3. TIP VORTEX MODELLING

3.0 Introduction

Over the last decade, the complexity of rotor wake computer analysis has increased greatly. Nevertheless, underlying the theoretical models are basic assumptions not fully endorsed by experimental investigation. For example, the common practice of setting the strength of an assumed Rankine tip vortex ('solid body' rotational core with an irrotational outer region) equal to the peak circulation on the blade is immediately open to criticism. Following a similar viewpoint, Johnson (14) in a recent paper concludes that 'to correlate and develop non-uniform distorted wake models further requires experimental data that emcompass the details of rotor aerodynamics such as the measurement of the tip vortex circulation, core size and peak velocities even when the paramters of most interest are the integrated effects such as the first harmonic flapping motion'.

Considering the substantial influence of the tip vortex on blade air loads, especially in hover and at low advance ratios, a survey of the available vortex data was undertaken to check the validity of the currently used assumptions. The resultant salient findings covering the vortex core, vortex structure and decay are presented in sections 3.1 - 3.5.1, and collectivly discussed in section 3.6.

3.1 Vortex Core Maximum Induced Velocity and Radius Defined

For a Rankine vortex, the maximum tangential vortex induced velocity V_s is located at the 'solid body' rotational core edge. Within the 'solid body' region or vortex core, the general vortex induced velocity v_v, is directly proportional to the radial distance r, from the vortex centre, reaching a maximum value V_s at radial distance r_c, defining the core radius. (i.e. $v_v = V_s$, $r=r_c$). In utilising a vortex core model an estimation of the core radius and strength is required. Ideally, explicit equations determining V_s

and r_c are necessary to minimise computational time.

McCormick et al (17) have fitted empirical equations to a collocate of vortex data yielding,

$$V_s/V_T = 0.625C_L \qquad (3.1)$$

$$w/c = 0.02+0.035C_L \qquad (3.2)$$

$$R_e = 3.5*10^5$$

V_T is the rotor tip speed and w is defined as the distance from the vortex centre where the vorticity has reached half its centreline value (a logarithmic distribution of vorticity is assumed by McCormick). Considering the limited cases investigated (A_r <6, V_T= 31 m/s) to determine equations 3.1 - 3.2, the agreement shown in Figure 2 is very reasonable. However, the equations do lack universality which is best highlighted by comparisons with Carradonna et al (18) vortex data. Similarly, although good agreement was found by Andrew (19) by fitting expressions to a variety of vortex data taken at typical lift coefficients and tip Mach numbers of less than .55 (Figure 3), the equations become less valid for Mach numbers approaching unity. The equations reported in reference (19) are:-

$$r_c/c = \frac{(1-M)}{\sqrt{M}}\frac{t_\theta}{c} \qquad (3.3)$$

$$V_s/V_T = (1+(6.6/A_r))(tC_L/c)^{1/2} \qquad (3.4)$$

To obtain a better global fit, an extended collacate of vortex data was examined. Spivey (20) has concluded that for low Mach numbers, the tip vortex location and direction is not affected by

centrifugal forces or pressure gradients. Further, Chigier et al (21) argue that the vortex structure generated from a fixed wing and a rotating blade should be similar. Consequently, the presented vortex data has been accumulated from rotating blade and fixed wing investigations.

3.2 Problems of Data Correlation

Great care must be taken at all times when making comparisons with and using other sets of experimental data. The limitations of the experimental technique, the test conditions and the way the data have been derived and presented must be fully appreciated. The two sets of data obtained by Chigier and Corsiglia (21,22) serve as a typical example of where caution is necessary in interpreting the results. In reference (21) the triple hot wire anemometer was fixed at a single position for a 'sufficient length of time' to record a time mean averaged value. For a blade pitch setting of 12 degrees, the maximum vortex induced velocity recorded was $0.37V_T$. In contrast, the reported maximum induced velocity in reference (22), where almost identical test conditions were investigated was $0.68V_T$. In this case, the measuring probe was rapidly scanned many times through a vortex yielding a quantity of vortex peak velocities which were later averaged.

The discrepancies between probe fixed and probe moving data arise, in part, from the behaviour of the vortex itself. In both references (21) and (22), a measurable vortex meander was noted (a Crow type of instability). For the probe fixed case (21), this produced a fluctuating velocity field. Consequently the probe was, for substantial periods, recording velocity signatures with magnitudes less than the maximum values within the vortex. When averaged, the resultant 'peak' velocities produced were much less than the maximum velocity within the vortex. For the moving probe case (22) however, effectively instantaneous velocity values are recorded, yielding a much better estimate of the peak velocities within the vortex.

3.3 Salient Features of the Tip Vortex Core

Even with the problems of data correlation, a number of salient features are highlighted in the literature, giving adequate guidance for tip vortex modelling:-

1) The strength of the vortex core K_c, (given by $K_c = 2\pi V_s r_c$) increases with increase in pitch θ. (22,25,26,27,28). Generally, this results from an increase in both V_s, and r_c. However, exceptions are reported where r_c remains roughly constant (27), and may result from the experimental techniques used, or a possible redistribution of the vorticity throughout the vortex (see Section 3.4.)

2) V_s increases linerly with pitch (22,25,26,27). However, beyond maximum pitch, blade stall greatly modifies the vortex producing a diminished V_s and an uncharacteristically thickened vortex core (28).

3) Flow measurements of a rectangular tip section (29,30) evince that the vortex core initially forms at the side of the tip and moves over to the top surface at or beyond the region of maximum thickness (largest pressure gradient).

4) If a rolled up tip vortex is said to comprise of a 'solid body' rotational core surrounded by a further distribution of vorticity, then the rolling up process may take many wing tip chords. However, it must be emphasised that large velocities are induced back onto the wing immediately the core departs from the trailing edge.

Andrew's equation (3.5) can be simplified to reflect the extended set of vortex data by linearising V_s with respect to pitch θ, and redefining aspect ratio $A_r = R/c$, yielding

$$V_s/V_T = (1+(6.6/A_r))K_1\theta \qquad (3.5)$$

(θ in degrees)

McCormick et al (17) have indicated that the core radius r_c, could be as small as 2% of the blade chord, but theoretical analyses incorporate very wide ranging suppositions. Typically the core diameter is set to 10% of the blade chord (25) or 1% of the blade radius (31). More recently, it has been found that to guarantee predictive accuracy a theoretical core radius of 5% blade radius was used. (14,32). Consulting Figure 4, it is immediately obvious that for regular aspect ratio blades r_c is generally over-estimated and insensitive to changes in operating conditions.

An intersting observation (see Figure 4) is that the vortex core radius departing from the blade trailing edge is of the order of the turbulent boundary lower thickness i.e

$$r_c/c = R_e^{-1/5} K_2 V_s/V_T \qquad (3.6)$$

Where from the limited experimental data available, the best fit empirical constants are given by:

$K_1 = 2.64 \times 10^{-2}$, in equation (3.5)

$K_2 = 1.2$, in equation (3.6)

Combining equations 3.5 and 3.6 yields the vortex core strength K_c of,

$$K_c = 2\pi V_t c(((1+(6.6/A_r))K_1\theta)^2 K_2 R_e^{-1/5} \qquad (3.7)$$

Interestingly, equation (3.7) indicates that the vortex core strength is proportional to pitch squared; whereas the blade bound circulation Γ is proportional to θ giving the ratio:

$$K_c/\Gamma \propto \theta \qquad (3.8)$$

It must be emphasised that this expression does not violate the conservation of circulation. It simply states that the normalised vortex core strength grows with blade pitch; while the remaining blade circulation may be viewed as being shed as discrete vortex filaments.

This result is, perhaps, indirectly endorsed by the experimental difficulty encountered in generating a tip vortex at low pitch settings. Indeed, below pitch angles of 7 degrees, Tangler et al (26) had great difficulty in recording a trailing tip vortex.

Carradonna et al (18) similarly found that for a low pitch setting K_c / Γ was less than that for a higher pitch setting.

The effects of compressibility on the vortex core have not been included in equations (3.5) and (3.6) since to the author's knowledge, no substantial body of vortex data exists on this subject. However, Carradonna et al (18) have indicated that the vortex structure does change with Mach number reflecting transonic flow conditions. This is accompanied by a reduction in the maximum core edge induced velocity V_s. Nevertheless, the limited results indicate that the far field of the vortex remains unchanged with only the inner sections of the vortex changing appreciably. Such changes, if required, may be modelled by the developed equations in

the following section.

3.4 Tip Vortex Roll-Up

Landgrebe (23) has concluded that the induced downwash on the blade from the inboard vortex sheet is an order of magnitude less than the induced velocity distribution from the tip vortex wake. This results partly because the vorticity is not as concentrated and partly because it tends to be convected downward faster than the tip vortex. However, some of the vortex sheet may be captured by the tip vortex, modifying the induced velocity distribution outside of the vortex core.

From fixed wing experimental evidence, Nielsen and Schwind (33) modelled a completely rolled-up vortex based on an analogy with the structure of a turbulent boundary layer. This has been further utilised in reference (22). More recently, this analogy has also been applied to rotor tip vortices (34). Modifying the equation of reference (22) by non-dimensionalising with respect to the blade chord c, yields

Core region,

$$K/\Gamma_{max} = A(r/c)^2 \qquad (3.9)$$

$$0 \leqslant K \leqslant K_c$$

Logarithimic region,

$$K/\Gamma_{max} = B\ln(r/c) + C \qquad (3.10)$$

$$K_c \leqslant K \leqslant K_1$$

Defect region,

$$\ln(1-(K/\Gamma_{max})) = D(r/c) + E \qquad (3.11)$$

$$K_1 \leqslant K \leqslant K_o$$

References (22) and (34) identify 'best fit' coeficients for a particular set of vortex data. A more general approach to estimate the coefficients A-E for any individual vortex is suggested in the following procedure:-

For a "solid body" rotational core, the vortex strength may be given by:

$$K_c = 2\pi V_s r_c \qquad (3.12)$$

Comparing equations 3.9, 3.12 yields,

$$A = 2\pi V_s c^2/(r_c \Gamma_{max}) \qquad (3.13)$$

V_s and r_c are computed from equations (3.5) and (3.6).

For the logarithmic region, consider dK/dlnr:

$$dK/d\ln r = r dK/dr = 2\pi vr + 2\pi r^2 dv/dr$$

Whence,

$$(dK/d\ln r)_{r=r_c} = K_c, \quad (3.14) \text{ since } (dv/dr)_{r=r_c} = 0$$

Hence, comparing equations (3.10) and (3.14) yields,

$$B = K_c / \Gamma_{max} \qquad (3.15)$$

$$C = B(1-\ln(r_c/c)) \qquad (3.16)$$

To obtain the coefficients D and E, the radial distance to the perimeter of the logarithmic region r_1, and the outer radius of the vortex r_o, the following conditions are typically satisfied:-

1) Continuing the boundary layer analogy, the outer radius of the vortex r_o, is defined where the vortex circulation strength K_o, reaches 99 percent of the peak circulation on the blade Γ_{max}. However, research has indicated (28,35) that the final vortex strength may be much less than the expected value. Consequently a more general expression may be used:

$$K_o = n\Gamma_{max} \qquad (3.17)$$

$$0 \leqslant n \leqslant 0.99$$

Using equations 3.11 and 3.17 yields

$$\ln(1-n) = D(r_o/c) + E \qquad (3.18)$$

2) Continuity of circulation is satisfied at r_1, giving:

$$B\ln(r_1/c) + C = 1-\exp((Dr_1/c) + E) \qquad (3.19)$$

3) Similarly, in the outer regions of the vortex, sharp discontinuities in circulation are assumed not to exist, whence

$$(dK/dr)_{r=r_1} = B/r_1 = -(D/c)\exp((Dr_1/c) + E) \qquad (3.20)$$

To develop the remaining equation, a simple work/energy theorem has been postulated. That is, the total rotational energy per unit length of a fully rolled up tip vortex was equated to the induced drag on the blade from the points of peak circulation to the tip. The theorem which is presented in Appendix 1 produces the following equation:-

$$E_v = ((\rho\pi r_c^2 V_s^2)/4) + (VAR1)(VAR2 + VAR3) = \left[\text{induced drag}\right]_{r(\Gamma_{max})}^{r=1.0} \qquad (3.21)$$

where,

$$VAR1 = \rho\Gamma_{max}^2/4\pi$$

$$VAR2 = \int_{r_c}^{1} \left[B^2(0.33\ln^3 r - \ln^2 r \ln c + \ln r \ln^2 c) + BC(\ln^2 r - 2\ln r \ln c + C^2 \ln r\right]$$

$$VAR3 = \int_{r_1}^{r_o} \left[\ln r + \exp(2E)(\ln r + \sum_{1}^{m}(2Dr/c)^m/(m*m!) - 2\exp(E)(\ln r + \sum_{1}^{m}(Dr/c)^m/(m*m!))\right]$$

Equation (3.21) is solved with equations (3.9) - (3.20), yielding an initial value of the tip vortex rotational energy E_v. Further solutions are evaluated by iteration until the vortex rotational energy E_v, is equal to the induced drag on the blade between tip and $n\Gamma_{max}$ (the default value of n being 0.99); while simultaneously satisfying the conservation of circulation law, where the circulation contained in the vortex K_o equals $n\Gamma_{max}$. Both energy and circulation conservations laws are satisfied simultaneously by ajusting the vortex outer structure (equations (3.19) and (3.20)).

Thirty stations were located in the outer 10% of blade radius to compute the induced drag and peak blade bound circulation using two dimensional aerofoil theory as presented in Appendix 2.

3.5 Vortex Decay

A general observation of the tip vortex wake shed beneath a hovering rotor is that the tip vortex dissipative rate is much greater than ideal theory would suggest. Widnal (36) has shown that below a helical pitch of 32 degrees the filaments will become

unstable due to their strong interactions. Such interactional decay has been reported by Tangler et al (26) using schlieren flow visualisation techniques. They found that vortex instability was accentuated by the development of an asymetric wake which resulted from the finite tolerance limits of blade manufacture, pitch settings etc. Maximum interaction occurred at complete wake contraction where two adjacent vortices, generated by neighbouring rotor blades, began revolving about their common centroid of vorticity. While this is occurring the two vortices draw closer together becoming unstable and either destroy each other or combine to form a weak diffuse vortex.

By considering a two-dimensional representation (Figure 8), the respective velocities are:

$$v_1 = K_2/(2\pi a) \quad , \quad v_2 = K_1/(2\pi a)$$

Equating the strength of each vortex to an analogous mass, a centroid of vorticity c, lying on the line joining the vortices can be determined from,

$$K_1 a_1 + K_2 a_2 = 0$$

For the case where $K_1 = K_2$, the vortices would revolve about their centroid with angular speed w_c given by,

$$w_c = K_1/(\pi a^2) \qquad (3.22)$$

By increasing the number of blades (same blade loading) the axial separation between consecative vortices is reduced. For similar blade loadings, equation (3.22) indicates that the angular rate w_c, would similarly increase causing further instabilities and rapid diffusion.

This instability appears as sinusoidal fluctuations of the tip vortex which grow with time (26). Similarly, reducing the collective pitch decreases the axial vortex spacing enhancing rapid decay.

Another instability was also noted for independant vortices even in a four bladed rotor. The vortex core was seen to expand until only a diffuse vortex could be registered. An example of this decay is given in Figure 7.

3.5.1.Axial Velocity Effects on Vortex Decay

The description vortex decay is often interpreted as the time dependant decay of the vortex strength (circulation) as, for example, predicted by Lamb (65). Effectively the strength K, at time t, is given by $K = K_o \exp(-ct)$, where K_o, is the initial value of the vortex strength and c, either a predetermined constant or estimated from a 'best fit' experimental curve. Theoretically, the vortex strength decay is extremely slow and implies that a large number of rotor wake revolutions should be detectable beneath a lifting rotor. Experimental results however, indicate the the 'decay' of the helicopter tip vortex is much more rapid. This is often allowed for in wake modelling by simply increasing the value of the constant c, in the decay equation stated above.

It is suggested in the following argument that the assumption of rapid circulation decay can be a gross misrepresentation of the 'decay' mechanism. Take, for example, the well known incompressible flow expression describing the equilibrium state of the vortex, where the pressure gradient across the vortex matches the centrifugal force, namely:-

$$(1/\rho)dp/dr = w^2/r \qquad (3.23)$$

whence integrating between the core radius r_c and the vortex outer

radius r_o , where

$$K = K_c = \text{constant} \tag{3.24}$$

and ,

$$w^2 = K_c^2 / (4\pi^2 r^2) \tag{3.25}$$

yields ,

$$(p_o - p_c) / \rho = -\left[K_c / (8\pi^2 r^2)\right]_{r_c}^{r_o} \tag{3.26}$$

whence , assuming $r_c \ll r_o$,

$$(p_o - p_c) = \rho K_c^2 / (8\pi^2 r_c^2) \tag{3.27}$$

Applying the conservation of circulation low implies K_c remains constant. Therefore, any weakening of the pressure gradient across the vortex will be associated with a vortex core expansion.

Now Tangler et al (26) have reported rapid vortex core expansions resulted when two vortices come into close proximity. In this instance, as the two vortices approached each other, the static pressure p_o would reduce, weakening the stabilising vortex pressure gradient and, therefore, producing a vortex core expansion (equation

3.27).

However, Tangler et al (26) also report that at low pitch settings (< 7 degrees), the strength of the rotor tip vortex is reduced, and the vortex core axial velocity is seen to diminish quickly. This also results in a rapid vortex core expansion. Equally, Logan (40) has found that for weak vortices, axial velocities diminish with downstrem distance and remain unchanged for strong vortices. Again, as the vortex axial velocity falls, the static pressure within the vortex core will increase, weakening the vortex stabilising pressure gradient. The same vortex core expansion results.

Interestingly, the actual strength (circulation) decay may be extremely slow as theoretically predicted; yet as a result of the vortex core expansion, may occupy such a large volume that the corresponding velocity field is greatly diminished.

3.6 Discussion and Conclusion

The modelling equations 3.5 and 3.6 used to evaluate vortex core radius r_c, and corresponding vortex induced velocity V_s, are compared with experimental data in Figures 9 and 10. Figure 9 indicates an increase in V_s is found with increasing blade pitch. Other researchers have also reported this trend (22, 25, 26, 27). Figure 10 also shows a similar connection between core radius r_c, and blade pitch. However, other investigators have concluded that the core radius does not vary substantially throughout an incidence range of 8 to 12 degrees (22), at least for the fixed wing case. This may partially result from the limitations of an experimental technique or the variability in data obtained, as can be similarly seen on Figure 10. Nevertheless, such conclusions cannot be wholly ignored and place a level of uncertainty in the universality of equation 3.6. The core radius magnitude, however, is more accurately defined with values much less than commonly used in theoretical analyses (14, 25, 31, 32).

For completeness, Figure 11 has been included to indicate

possible affects of compressibility on the tip vortex. The salient changes are a reduction in peak induced velocity V_s, and a redistribution of vorticity throughout the vortex. Interestingly, the far field remains unaltered, allowing an incompressible solution to adequately model the effects of the vortex on a point away from the immediate vicinity of the core. Plotted with the data on Figure 11 is the function $r_c(\sqrt{1-M^2})$. Although, with the limited data available this solution can only be proposed as a possible approximation, it may partially explain that within the limits of experimental variability, Rorke (25) found no marked changes in V_s, from test ranging from free stream Mach numbers of 0.2 to 0.6.

The equations developed in Section 3.4 to describe the complete structure of a trailing tip vortex have been used to evaluate the circulation distribution through a known rotor tip vortex structure (39). In this case, the value of 'n' in equation (3.17) was reported to be 0.99. Figures 13 and 14 show the comparison between the resultant predicted circulation curves for a rotor with an aspect ratio of 13.7 and blade pitch settings of eight and twelve degrees respectively. Both the circulation distribution and outer vortex radius are well predicted. The associated velocity distributions are given in Figure 12, while Figure 15 highlights an equivalent Rankine vortex with the same core radius producing an identical velocity far field. As can be seen from Figure 15, this is accomplished at the expense of the near field velocity distribution.

Figure 16 indicates, however, that the final vortex strength may be much less than the peak circulation on the blade. The data, which was taken from reference (28), shows that for a given thrust, the strength may vary substantially and furthermore, is not constant over a thrust range. This may result from the affects of a high blade aspect ratio (20.5) and the corresponding relatively low circulation strength of the vortex core (Figure 17). For comparison, the generalised logarithimic constant B ($=K_c/\Gamma_{max}$) in equation 3.10, is given in reference (34) as 0.39. However, interpreting the results presented in reference (34), the following simple relationship may be postulated;

$$n\Gamma_{max} = 3.1K_c \qquad (3.28)$$

Applying this relationship to Cook's (28) full-scale rotor data, produces vortex circulation strengths much less than the blade's peak circulation. However, expression (3.28) yields a general underestimate of the vortex strength over most of the thrust range as shown in Figure 18.

Using the same procedures to evaluate a theoretical vortex structure for Cook's rotor, initial convergence between induced drag and vortex rotational energy could not be established. The corresponding vortex energy with 'n' set to 0.99 was always in excess of the induced drag value. Using just the 'solid body' and logarithimic regions to define the vortex structure, the vortex parameters were re-evaluated, converging firstly on the induced drag value computed as before and secondly, on a mean experimental value for the vortex strength.

The corresponding values of the outer rotor radius for the two cases were .472m and .165m respectively. The experimentally measured value of .162m, indicates that the latter method of convergence more accurately defined the vortex parameters. That is, from knowing the total strength of the vortex, a good approximation to the structure can be predicted with equations (3.9) and (3.10). Moreover, if the vortex strength is much less than the peak circulation on the blade, computation of the vortex structure may be achieved without using the defect vortex equation (3.11). The resultant velocity distribution is depicted in Figure 19. The theoretically predicted curve over-estimates the velocity distribution outside the vortex core and is seen to arise from estimating a core radius in excess of the measured vlaue. However, taking into consideration the spread of vortex strength data for a given thrust (Figure 16), this discrepancy is well within the experimental tolerances.

For low aspect ratio rotor blades most of the blade circulation

is found in the vortex core. Indeed, for a blade aspect ratio of 6 and a collective pitch of twelve degrees, Carrandonna et al (18) report that all the circulation was found within the vortex core. Such findings indicate that a generalised circulation curve and associated logarithimic constant B equal to 0.39, as expounded in reference (34) is highly questionable. Alternatively, equations 3.5 and 3.6 allow greater flexibility in evaluating the core circulation ratio B, and reflect the experimentally found tends of varying vortex structure with rotor blade aspect ratio.

Section 3.5 indicated that vortex decay is not necessarily a feature of strength or circulation decay, but may result from a rapid vortex core expansion. The vortex core expansion takes place when the presure gradient across the vortex is weakened. This may happen when,

1. a vortex-vortex interaction occurs

2. the vortex core axial velocity diminishes

The falling vortex axial velocity is more often seen to occur in weaken rather than stronger vortices.

More recently, the variation in vortex core radius over the first 90 degrees of azimuth (until the following blade passage) has been published (41) for a four bladed rotor with a blade aspect ratio of 15 and a chord of 0.05m. The data, shown in Figure 20, indicates the rapidity of the expanding vortex core which has more than doubled in less than a quarter of a rotor revolution.

With the equations developed for defining the vortex core and subsequent rolled up vortex structure, combined with an appreciation for the vortex core expansion process, the overall wake modelling techniques may now be described. Chapters 4 and 5 present the hover and forward flight models respectiely; both of which use extensively the vortex equations presented in this Chapter.

4. COAXIAL COUNTERROTATING TWIN ROTOR AERODYNAMICS IN HOVER

4.0 Introduction

Wake flows generated by hovering rotors have been studied in great detail (3, 18, 23, 31, 44). Except for the most simple momentum/blade element approaches to rotor performance prediction, the modelling of rotor wakes has relied heavily upon the availability of computer hardware. Offsetting this availability however, is the ever increasing need to reduce computational costs by decreasing the time required to achieve a successful run. Consequently, a suitable compromise between the degree of complexity incorporated in any wake model and the computational time required has to be reached.

Many researchers have identified a general weakness in modelling routines to date. Notably, Cheeseman (43), Miller (44) and Johnson (14) indicate that the forthcoming models require a better understanding of the structure, strength and decay of rotor tip vortices. In the following sections a number of wake models are presented for guidance in selecting a possible optimum method which could incorporate the tip vortex information presented in Chapter 3.

4.1 General Wake Approaches

The problem of evaluating the induced downwash distribution along a rotor blade has been paid much attention. The resulting theories and wake models include the simple Glauert type strip analysis (45), a Fourier series representation of blade airloads (46), local momentum approaches (4,47) and vortex theories ranging from prescribed wakes (23), to the more advanced free-wake analyses (44, 48). Blade representation by a lifting line has been superseeded by the more exacting lifting surface methods (49).

The combined momentum-blade element approach of strip theory recognises the major design parameters and yields an estimate of the induced velocity at any specified blade element. However, the theory

in general, requires the application of a tip loss factor to increase the rotor performance predictive accuracy. This restriction, combined with the inability of the theory to model temporal variations in the flow, limit its usage.

To overcome these limitations, vortex theory has been developed to provide a more physical representation of blade airloads. With advances in computer hardware more exacting theories have been presented. Such theories usually require extensive computer code with many iterative and numerical routines necessitating large run times. Unfortunately, this does not always guarantee good predictive accuracy. For example, reference (50) indicates that a free-wake model can produce severe wake distortion, leading to blade vortex interactions not apparent in actual hovering tests. Ultimately, 'relaxed' procedures are often necessary to fine tune the desired output. Nevertheless, vortex theory can be most readily applied to compute temporal variations in the flow and is important when estimating the influence of one blade or rotor on another.

4.1.1.CCTR Wake Approaches

The most fundamental approach to CCTR hover performancce prediction is that reported by Harrington (51). The CCTR is represented by a single rotor with the same radius and number of blades (equivalent blade solidity). The predicted performance for a test CCTR shows reasonable agreement over a large thrust range and is, therefore, a useful model for a first approximation. Another simple model was used in the Advancing Blade Concept CCTR verification programme (52). Applying momentum theory, the induced velocities of the lower rotor is assumed to increase by the average downwash from the upper rotor. This was later modified with the supposition that the upper rotor wake is fully developed and only the inner 50% of the lower rotor area is exposed to the fully developed wake; with the outer sections taking in clean air. Similarly, Stepniewski (2) incorporated strip theory into the evaluation of the affect of one rotor on another, yielding a better blade loading distribution. However, as with all the aforementioned approaches, this method assumes averaged or fully developed wake

flows and is inadequate, for example, in determining the full influence of varying the inter-rotor spacing.

A more concise method is that developed by Cheeseman (53), who combined a lifting line approximation to translational lift plus a stream tube model for propeller lift. The trailing helical tip vortex wake is approximated by a straight line horeshoe vortex system with strengths set equal to the peak circulation on the blade. Wake contraction is not considered.

Recently, renewed interest has been shown by the Japanese in CCTR configurations. In reference (32), momentum theory is developed by modelling the two rotors as actuator discs, to predict the optimum load sharing ratio for a given inter-rotor spacing. Implicit in the optimisation is the reliance of ideal flow conditions and the formation of an associated optimum wake geometry which as cited, does not adequately allow for the mutual influence of the two rotors. To overcome this limitation, a more rigorous treatement is also presented. Using a simplified free-wake analysis, the tip vortex wake is approximated by inviscid ring vortices. Each blade is represented by a lifting line. Of most interest are the results from a sensitivity analysis which was undertaken to guarantee predictive accuracy. The conclusions from the analysis indicated that the bounds for good accuracy were given by a rotor azimuth step ψ = 20 degrees, the number of vortex rings for each rotor N = 8, and the vortex core radius r_c = 0.05R (32). The large number of rings are required to prevent instabilities in the numerical convergence of the wake in close proximity to the rotors. It is suggested that such instabilities will be remedied by introducing viscosity into the flow equations. The incremental step of 20 degrees of azimuth is derived from a trade off between a realistic run time required for wake convergence, and the acceptable finite errors incurred during the integration procedures. Finally, the poor physical representation of vortex core radius may be an indicator of the useful applications of this model. For example, a rotor blade with an aspect ratio of 15 would have a vortex core radius of 75% blade chord. Referring to Figure 4, it can be seen that this approximation is an order of magnitude greater than actual results, and does not

allow for the substantial influence of changing rotor conditions.

Finally, the application of local momentum theory (54) to CCTR performance prediction has shown good overall agreement and endorses the findings of Andrew (19), when comparing two and four bladed single rotors with a four bladed CCTR. The theory equates the local instantaneous momentum of fluid with the blade elemental lift to yield the elemental induced downwash. To estimate the timewise variation of the induced downwash after a blade pass, simplified vortex theory is applied, using a combination of a vortex ring (nearest vortex to the rotational plane) and a vortex cylinder (remaining vortices). Although the vortex model could be improved upon, the low computational time required for a successful run highlights the major advantage of this approach.

4.2 CCTR Vortex-Strip Theory

The collection of aforementioned theories have emphasised specific modelling advantages. In general, momentum approaches require a low computational time, whereas vortex theory enhances the blade loading predictive accuracy. The present theory uses a simplified method, combining vortex and momentum theory in an attempt to exploit the advantages of each.

Strip theory (15) (Appendix 2) yields an initial estimate of the induced downwash at a blade element vis:-

$$v_{im} = \left(\frac{V_c}{2} + \frac{\sigma_r a \Omega R}{16}\right)\left(-1 + \left(1 + \frac{2(\theta r \Omega - V_c)}{\frac{4V_c}{\sigma_r a \Omega R} + \frac{V_c + \sigma_r a \Omega R}{16}}\right)^{1/2}\right) \qquad (4.1)$$

Traditionally, a tip loss factor is introduced to allow for the finite span of the blade and the associated formation of the tip

vortex. Such tip loss factors are often applied such that they confusingly truncate the blade radius so that in the tip region no lift is generated. More realistically, the 'tip loss' is caused by the lift impairment resulting from the tip vortex induced velocities over the complete blade. This loss is not simply a result of the interference between a blade and its own tip vortex, but the summation of the velocities induced by the helical tip vortex wake propagating from all blades in the rotor(s).

To incorporate a better estimation of the losses incurred by a finite rotor radius system while allowing for the lift contribution generated at the tip, strip theory has been combined with a vortex model. The latter represents the three-dimensional helical tip vortex wake by a series of straight line filaments, and using the Biot-Savart law to calculate the induced velocities at any specified point. The vortex filaments are either made to follow the empirical prescribed paths reported by Landgrebe (23), or alternatively, may be relaxed using the free-wake facility in program ROTOR (see Chapter 6). The vortex filament structure, degrees of azimuth step and number of wake revolutions, are all optional parameters input by the user of ROTOR. Furthermore, the time history of vortex core radius and associated velocity may be computed applying the assumptions and equations presented in Chapter 3.

Each helical vortex trail is attached to its respective blade at the tip, with the solid body rotational vortex core already formed as defined by equation 3.5 and 3.6. If the turbulent boundary layer vortex structure is required, a roll-up of 60 degrees is assumed before the logarithmic and defect rotational regions are fully formed. This assumption has been endorsed by other researchers findings (18).

For hover, by definition, the vertical climb velocity V_c, in equation (4.1), is exactly zero. However, the present theory suggests that each blade element perceives an additional induced velocity v_v, due to the tip vortex wake, which may be interpreted as a local climb velocity. That is, the induced velocity v_v, calculated at each elemental annular ring, replaces V_c, in equation (4.1), to

produce a modified elemental strip velocity The resulting additional loss of useful angle of attack at each blade element reflects the losses associated with a finite radius rotor system, replacing the arbitrary tip loss factor.

Figure 21 is a schematic representation of the presented model. The downwash from a given rotor is bounded by its respective tip vortex wake. The initial flow conditions at the entrance to the upper rotor disc are given by the induced velocities from the upper and lower rotor tip vortex wakes, v_{vu} and v_{vlu} respectively; plus the strip contribution v_{im} from equation (4.1) where $V_c(r) = V_{vu} + V_{vlu}$ More precisely, the inflow of any radial station point r, is given by:-

$$v_{iu}(r) = v_{vu}(r) + v_{vlu}(r) + v_{imu}(r) \qquad (4.2)$$

The inflow in the section of the lower rotor immersed in the downwash of the upper rotor may be approximated by:-

$$v_{il}(r') = v_{iu}(r)(R_u/R_c)^2 \qquad (4.3)$$

$$0 \leqslant r' \leqslant R_c$$

(conservation of momentum)

where

$$r' = r(R_c/R_u) \qquad (4.4)$$

Finally, the inflow in the outboard section of the lower rotor taking in clean air is given by:-

$$v_{il} = v_{vl} + v_{vul} + v_{iml} \qquad (4.5)$$

$$R_c < r \leq R_l$$

Equation (4.3) however, does not take into account the effect of the further pressure jump across the inner section of the lower rotor. This pressure jump, resulting from the lift generated on the lower rotor blades, is more noticeable with increasing radius. Figure 27, indicates that the downwash magnitude is underpredicted for both the upper and lower rotors in this region using equation 4.1 - 4.4. Stepniewski (2) hypothesised that the lower rotor immersed in the upper rotor wake share a common rate of flow; and assuming that the final induced velocity reaches twice the value of the upper rotor disc in the fully developed wake where the static pressure tends to the ambient value, produced on expression for the CCTR induced flow.

However, Stepniewski's model does not take into account the vertical separation between the rotors, the tip vortex wake effects from both the upper and lower rotors and the influence of upper rotor wake contraction at the lower rotor disc plane R_c. Using Stepniewski's premise that the lower rotor immersed in the upper rotor wake share a common rate of flow, and considering the elemental thrusts generated on the upper and lower rotors simultaneously from momentum and blade element theories, including the above effects, it may be postulated:-

momentum:

$$dT_u(r) + dT_l(r') = 4\pi\rho r(\bar{v}_v(r) + v_{im}(r))v_{im}(r)dr \qquad (4.6)$$

blade element:

$$dT_u(r) = b_u \tfrac{1}{2}\rho \Omega_u^2 r^2 a_u \left(\theta_u - \frac{(v_v(r)+v_{im}(r))}{\Omega_u r}\right) c_u dr \qquad (4.7)$$

$$dT_l(r') = b_l \tfrac{1}{2}\rho \Omega_l^2 r'^2 a_l \left(\theta_l - \frac{(v_v(r)+v_{im}(r))(R_u/R_c)^2}{\Omega_l r'}\right) c_l dr' \qquad (4.8)$$

That is, the tip vortex induced velocity $v_v(r)$, is computed at each radial station r, from the tip vortex wakes of both the upper and lower rotors. For the momentum expression (4.6), the total tip vortex induced velocity is averaged around a specified annular ring of radius r, yielding $\bar{v}_v(r)$. with the inclusion of the upper rotor wake contraction, a radial station on the upper rotor r is associated with a radial station r' on the lower rotor (Equation 4.8).

Now, $$r' = r(R_c/R_u) \qquad (4.9)$$

and, $$dr' = dr(R_c/R_u) \qquad (4.10)$$

Substituting equation (4.9) and (4.10) into (4.8) and equating equations (4.7) and (4.8) to equation (4.6) yields:-

$$b_u \tfrac{1}{2}\rho \Omega_u^2 r^2 a_u (\theta_u - \frac{(v_v + v_{im})}{\Omega_u r}) c_u dr + b_l \tfrac{1}{2}\rho \Omega_l^2 r^2 a_l (\theta_l (R_c/R_u)^3 - \frac{(v_v + v_i)}{\Omega_l r}) c_l dr$$

$$= 4\pi\rho r (\bar{v}_v + v_{im}) v_{im} dr \qquad (4.11)$$

Expanding and rearranging (4.11) yields:-

$$4\pi v_{im}^2 + (4\pi\bar{v}_v + b_u \tfrac{1}{2} \Omega_u a_u c_u + b_l \tfrac{1}{2} \Omega_l a_l c_l) v_{im}$$
$$- b_u \tfrac{1}{2} c_u \Omega_u^2 r a_u c_u (\theta_u - \frac{v_v}{\Omega_u r}) - b_l \tfrac{1}{2} c_l \Omega_l^2 r a_l c_l (\theta_l (R_c/R_u)^3 - \frac{v_v}{\Omega_l r}) = 0 \qquad (4.12)$$

Where, solving the quadratic in v_{im} produces the solution:-

$$v_{im} = (\frac{v}{2} v + \frac{b_u \Omega_u a_u c_u}{16\pi} + \frac{b_l \Omega_l a_l c_l}{16\pi})(-1 + E_l) \qquad (4.13)$$

where,

$$E_1 = \sqrt{1 + \frac{2\Omega_u r(\theta_u - v_v/(\Omega_u r)) + \frac{2b_1\Omega_1^2 a_1 c_1 r}{b_u\Omega_u a_u c_u}(\theta_1(R_u/R_c)^3 - v_v/(\Omega_1 r))}{\frac{4\pi v^2}{b_u a_u c_u \Omega_u} + v_v(1 + \frac{b_1 a_1 c_1 \Omega_1}{b_u a_u c_u \Omega_u}) + \frac{b_u a_u c_u \Omega_u}{16\pi}(E_2)}}$$

and,

$$E_2 = (1+(\frac{b_1 a_1 c_1 \Omega_1}{b_u a_u c_u \Omega_u})^2 + 2(\frac{b_1 a_1 c_1 \Omega_1}{b_u a_u c_u \Omega_u})) \qquad (4.14)$$

Note that when the vertical separation tends to zero for a convential CCTR (i.e. $b_1\ a_1\ c_1\ \Omega_1 = b_u a_u c_u\ \Omega_u$ and $R_c \rightarrow R_u$, $r' \rightarrow r$), the above equation collapses, to the text book solution for the equivalent single rotor (equation 4.1) where $b_s = b_u + b_1$.

Equations (4.13) and (4.14) were used to generate the inflow curves (labelled as theory No 2) on Figure 27. As can be clearly seen, the further pressure jump across the outboard section of the lower rotor immersed in the upper rotor wake is now more adequately represented, relfecting the experimental data.

Knowing the total downwash, the inflow angle at any blade element is evaluated vis,

$$\phi = \frac{v_v + v_{im}}{\Omega r} \qquad (4.15)$$

Overall rotor thrust and torque are computed by summing the individual differential thrusts and torques at each specified blade element using two-dimensional aerofoil characteristics (see Appendix

2).

4.3.1 Principal Features of Vortex-Strip Theory model

Hot wire recordings of the tip vortex signatures from the Mote rig indicated that the vortex was essentially Rankine in nature. Although some circulation could be seen outside of the vortex core it was not considered, in the first instance, significant. Consequently, initial evaluation of the Vortex-Strip model was undertaken using equations 3.5 and 3.6 to define the tip vortex strength.

Figure 22 depicts the downwash velocity component distribution for a single two bladed rotor. The modified strip induced velocity distribution v_{im} incorporates the effect of the apparent vertical climb velocity v_v The slight depression at 90% blade radius results from the upwash effect of the previous blade trailing tip vortex. The total theoretical velocity distribution compares well with experimental data. The largest discrepancies in velocities beyond 70% blade radius results, firstly, from the differences in the predefined vortex position and strength, and secondly, in the limitations of the hot wire recorded data which are discussed later in this section.

Figure 23 compares the present theory with conventional strip theory for a two bladed untwisted rotor set at a collective pitch, of 10.5 degrees. Over the complete blade radius, the vortex-strip theory predicts a higher induced downwash with a corresponding reduction in blade angle of attack at any specified blade element. These losses, reflecting those associated with a finite aspect ratio rotor blade, although a maximum at the tip are nevertheless, spread over the complete blade radius.

For the CCTR, the mutual interference effects are accounted for by evaluating the increments in inflow at one disc resulting from the velocity field generated by the other disc. To start the computation in program ROTOR (details given in Chapter 6), the inflow at the upper rotor disc is calculated using equations (4.13)

and (4.14) including the induced effects of its own tip vortex wake. The inflow at the inboard section of the lower rotor disc immersed in the upper rotor wake reflects the distribution at the upper rotor disc corrected for wake contraction. The net effect of the tip vortex velocity field on the upper rotor on the inner portion of the lower rotor over one complete revolution is given by evaluating the averaged vortex induced velocity over the upper disc. (The averaging process, calculation procedure and further potential savings in computational time are discussed in Chapter 6). Figure 24 compares the averaged vortex induced velocities around the upper disc with the velocities induced at the blade. The latter distribution defines the initial apparant vertical ascent velocity v_v, used in equation (4.13), to determine the strip downwash distribution along the upper rotor. The total downwash from the upper rotor on the lower rotor is given in Figure 25. The outboard velocities on the lower rotor are computed from the average upper tip vortex induced velocities at the lower disc plane. With the lower rotor downwash distribution established from the upper rotor, the lower rotor tip vortex wake effects on both the outboard sections of the lower rotor and the complete disc of the upper rotor are computed. The latter constitutes the interference effects of the lower rotor on the upper rotor (Figure 26), and by simultaneously updating the inflow conditions at the upper rotor disc, modifies the subsequent downwash along the inboard sections of the lower rotor.

The final downwash distributions for the respective rotors are compared with experimental data in Figure 27. The experimental data was recorded using a single non-directional hot wire probe placed beneath each rotor and aligned along the blade chord at each blade pass. The absolute velocity magnitudes recorded at a plane .12R below the upper disc, and the associated wake contraction, was used to scale back the velocities into the plane of the disc. A similar procedure was adopted for the outboard sections of the lower disc, while the inboard distribution was evaluated from measuring the actual values ·12R below the disc and correcting for any further wake contraction. The corresponding blade loading distributions are given in Figure 28. The lower rotor lift distribution is degraded on the inboard sections of the lower rotor with a slight negative

distribution to 36% blade radius. Thereafter, the loading remains below that of the upper rotor until approximately 80% blade radius whereupon the lift distribution exceeds that of the upper rotor loading. This results from the required increment in lower rotor pitch (~0.5 deg) to maintain yaw trim. Clearly, the combined vortex-strip theory yields a much more representative blade loading than strip theory alone.

The wake contraction used in the computation of the aforementioned figures was prescribed using updated Landgrebe wake coefficients. A study of the actual wake contraction indicated that a variation in tip vortex loaction occurred with time. Such variations for the single rotor are well known (18). Utilising the free-wake facility of program ROTOR, the initial prescribed wake was relaxed to allow for the influences of all the vortex helicies from both rotors. Figure 29 shows the final converged wake, indicating a severe upper rotor wake contraction with little change in the lower rotor vortex locations from the initial prescribed paths. It is evident from the figure that the free wake facility did not increase the overall predictive accuracy of the vortex paths. Furthermore, the computational time required to converge the wake, using the free-wake facility, was approximately two orders of magnitude greater than the prescribed computational time. Considering these facts the only modification retained in the program was an allowance for the increase in the axial translation of the upper rotor tip vortex wake as it traverses the lower rotor disc. This feature, depicted in Figure 30, although did not produce any significant differences for the Mote geometry, was incorporated to allow for the effects of reducing CCTR inter-rotor spacing (Chapter 7).

Introducing an allowance for the effects of vortex core expansion (reflecting the trend depicted in Figure 20) into the flow computations did not significantly change the overall rotor perfomance prediction. This results because even with the core expansion, the vortex blade interactions generally took place outside of the vortex core.

4.3 Application of Vortex-Strip Theory

Figure 31 shows the perfomance characteristics of the Mote CCTR run at a tip speed of 35m/s. For direct comparison with the perfomance curves generated in Chapter 7, CCTR optimisation, the data is presented as thrust per unit power versus thrust coefficient. Although the performance curves of both the CCTR and one of the rotors operating independantly are well predicted, the general trend is on over prediction of the thrust power ratio for a given thrust. A further comparison with a conventional four bladed CCTR with a tip speed of 119.4m/s (Fig 32) also highlights this trend when using equations 3.5 and 3.6 to define the tip vortex strengths. This, in part, may result from neglecting the circulation distribution outside of the vortex core in the vortex induced velocity calculations. This discrepancy however, diminishes with increasing thrust, and is a direct consequence of the vortex modelling equations where the normalised vortex core strength was found in Chapter 3, to be directly proportional to collective pitch setting.

A further comparison with predicted CCTR perfomance is given in Figure 33 for the Sikorsky's Advancing Blade Concept two, three bladed CCTR (52), operating at a tip speed of 198.3m/s, with both blade twist and taper. Both equations 3.5 - 3.6 and the fully rolled up tip vortex equations were used to predict the ABC performance; the latter equations converging on the peak blade bound circulation. The results shown in Figure 33 imply that a vortex strength greater than defined by equations 3.5 - 3.6, yet less than the peak bound circulation would best fit the test data. This conclusion reflects the full-scale vortex data reported by Cook (28) and, as will be seen latter, is endorsed by the forward flight findings in Chapter 5.

Recently Stepniewski (55) has shown that the hovering efficiencies of both the Russian CCTR's and Sikorsky's ABC CCTR are greater than a wide range of conventional single rotors. Utilising program ROTOR, the perfomance curves of the Mote CCTR was compared with an equivalent single rotor. The latter having the same number of blades, blade solidity, rotor radius, tip speed and aerofoil

section (same thrust potential) as the CCTR. Figure 34 presents the data which indicates that for a given thrust the CCTR absorbs approximately 5% less power than the equivalent single rotor. Included among Stepniewski's (55) full scale rotor data are the figures of merit of the Aerospatiale SA-365N, F_A, (R_A = 7.5m, b = 4) and the Kamov Ka -25, F_K, (R_K = 7.87m, b = 6) which are 0.572 and 0.674 respectively. Both helicopters have a gross weight of approximately 7360kg.

Now the figure of merit F, is given by:

$$F = \frac{\text{Ideal Power}}{\text{Actual Power}}$$

where, Ideal Power = $T(T/(2\pi R^2 \rho))^{\frac{1}{2}}$

Whence, for the same thrust generation, the actual power ratios between the Kamov Ka -25, P_K, and the Aerospatiale SA-365N, P_A, is given by:

$$P_K/P_A = (R_A F_A)/(R_K F_K)$$

yielding $P_K = .87P_A$

Although such a deduction does not take into account the differing number of blades, the previous figure of merit ratios indicate that a 13% saving in power is achieved in hover by operating a CCTR with the same all-up-weight as the conventional single rotor. Also presented in reference (55) is the shaft horse power in hover per unit gross weight for a variety of helicopters. The lowest power to weight ratio is given for a Kamov CCTR helicopter as 0.096. This compares very favourably with a variety of conventional Western World single rotor helicopters with power to weight ratios ranging from 0.11 to 0.133.

Such increases in CCTR efficiency is seen to result from;

1) the contraction of the upper wake of a CCTR allows clear air with a slight upwash to be taken by the outboard sections of the lower rotor. Consequently, the effective disc area has increased with a corresponding reduction in induced power. This is seen most clearly when comparing the downwash distributions for the Mote CCTR and an equivalent single rotor (Figure34). In the outboard sections ($r>0.8$) of the rotor disc the momentum velocity contribution for the equivalent single rotor is in excess of both the upper and lower rotors of the CCTR.

2) the vertical spacing of the two rotors in the CCTR layout reduces the severity of the total vortex induced velocity, especially on the upper rotor.

3) the recapture of the upper rotor wake rotational losses on the lower rotor. Such losses have been calculated for a typical single rotor by Bramwell (1) and Gessow et al (15) indicating the loss to be less than 0.5% of the total rotor power. Consequently this feature is considered a secondary effect.

4.4 Conclusion

The conventional Glauert type strip analysis has been modified to incorporate the influence of the trailing helical tip vortices from all blades at any specified blade element. Furthermore, Stepniewski's (2) simple model of a CCTR has been greatly extended to incorporate the effects of the tip vortices shed from both rotors, including the influence of wake contraction. The theory has been applied to both model and full-scale rotors with different tip speeds, rotor radii, number of blades and blade aspect ratios, including blade twist and taper. Over representative CCTR thrust loadings, the vortex equations (3.5) and (3.6), used in program ROTOR, to determine the vortex strengths, produced a reasonable predictive accuracy. The remaining discrepancies, in part, are seen to result from neglecting the additional 'captured' circulation outside of the vortex core. Unfortunately, precise evaluation of

this circulation, at present, is not possible since it varies between rotors. Nevertheless, actual tip vortex strength would seem, in general, to be less than the peak circulation on the blade, endorsing Cooks results (28). However, the vortex core equations establish an effective strength which reflects the variations in rotor parameters, including blade aspect ratio and rotor tip Reynolds number. Equally important is the much more representative blade loading distribution predicted by the combined Vortex-Strip theory, especially in the blade tip region, updating the arbitrary application of the tip loss factor when using strip theory alone.

The developed theory also indicates that a CCTR in hover produces more thrust per unit power than an equivalent single rotor. This conclusion has been endorsed by other CCTR operators (10), and in comparisons between full-scale CCTR and single rotor helicopters (55). Such comparisons suggest a potential 5% saving (neglecting the tail rotor power of the conventional single rotor) when operating a CCTR with the same all-up-weight as the conventional single rotor.

5. COAXIAL CONTRAROTATING TWIN ROTOR AERODYNAMICS IN FORWARD FLIGHT

5.0 Introduction

The wake concepts, modelling techniques and associated limitations expounded in the previous chapter are also largely applicable to the forward flight analysis of a CCTR. An exception is the blade element-momentum strip theory which is limited to hover and vertical translation of the helicopter. For a forward flight condition Glauert approximated a rotor by a circular wing with an elliptic loading; yielding the well known constant induced velocity distribution $\bar{v}_i$.

$$\bar{v}_i = T/(2\rho AV') \tag{5.1}$$

where, $$V' = \sqrt{V^2 + v_i^2} \tag{5.2}$$

In addition, to incorporate an allowance for the azimuthal variation of the induced downwash, Glauert postulated;

$$v_i = \bar{v}_i(1 + K\bar{r}\cos\psi) \tag{5.3}$$

where K is traditionally given by:-

$$K = -\tan(\mu/2\lambda) \tag{5.4}$$

or resulting from experience gained at the Royal Aircraft Establishment, the factor is often given by:

$$K = -\tan(\mu/\lambda) \qquad (5.5)$$

The usefulness of equations (5.1) to (5.5) is reflected by their continued application in rotor analyses, offering as they do a reasonable description of the induced flow through the rotor with the added benefits of simplicity and low computational time. Nevertheless, the Glauert model often underpredicts the downwash distribution for a variety of forward flight modes with the largest discrepancies occuring at low advance ratios (52). During the ABC CCTR verification program the required control range required to maintain trim was grossly underpredicted by a Glauert type analysis. At a forward flight speed of 25 kts (μ = 0.067), the ABC helicopter experienced a high nose up pitching moment which could not be countered by the pilot. The craft struck the ground with a 'heavy tail first landing' (56). Similarly Johnson (14) has identified substantial inaccuracies in momentum and classical wake modelling techniques. Applying such models to the analysis of an articulated rotor, it was found that the lateral b_1 flapping coefficient was constantly under estimated for advanced ratios of less than 0.15. By using a free wake facility, a more accurate representation of the close proxity of the tip vortex wake to the longitudinal plane of the rotor disc was achieved, resulting in a much better theoretical prediction of the b_1 flapping coefficient.

5.1 CCTR Forward Flight Model

As with the variety of hovering theories, the forward flight models have specific advantages for a certain range of flight conditions. Generally, it may be concluded that:-

1) The Glauert model has simplicity which is reflected in the low computational time. Nevertheless, blade loading prediction for low advance ratio flight is poor and partially results from the absence of modelling the finite number of blades in a rotor layout.

2) The classical wake approach where the vortex filament positions are assumed to be influenced only by the local free-stream conditions, neglecting vortex-vortex interactions, yields more accurate rotor performance predictions at higher advance ratios. Again, with low advance ratio flight, large discrepancies can occur resulting from the high degree of wake distortion, commonly found in experimental investigations (see Figures 47-50).

3) At low advance ratios, the vortex interactions substantially modify the tip vortex locations from the classical representation. Consequently the 'free-wake' model and associated lengthy computational time has been found essential for accurate temporal blade loading predictions.

Using similar principles as presented for the vortex-strip hover model, a forward flight hybrid model may be developed. The aim of such an approach is to allow for greater flexibility in application without diminishing the specific advantages of each modelling technique.

Referring to Figure 36, the slipstream of each of the two rotors is represented by a Glauert expression for the induced velocity, modified to account for the induced velocity effects of the tip vortex wake. That is, the effect of the tip vortex wake is

approximated by updating equation (5.2) to incorporate the vortex induced velocity through the centre of the disc, giving:-

$$V' = \sqrt{V^2 + (\bar{v}_i + \bar{v}_v)^2} \qquad (5.6)$$

Substituting the expression for the resultant velocity V' at the centre of the disc into equation (5.2), and rearranging, yields a quartic in the mean induced flow through the rotor v_i of,

$$\bar{v}_i^4 + 2\bar{v}_v \bar{v}_i^3 + \bar{v}_i^2(V^2 + \bar{v}_v^2) - (T^2/(4\rho^2 A^2)) = 0 \qquad (5.7)$$

For the classical wake option (wake limits defined by the free stream conditions only) in program ROTOR, a further allowance for the influence of the tip vortex wake on a specified blade element is established by evaluating the downwash at that element via:-

$$v_i = \bar{v}_i + v_v \qquad (5.8)$$

Furthermore, if any portion of the lower rotor is immersed in the upper rotor wake, equation (5.8) is retained with the added term of $(2\bar{v}_i)$ to evaluate the flow in this region of the lower rotor. This assumes that the wake from the upper rotor is fully developed on intersection with the lower rotor plane.

Alternatively, the free-wake option not only updates the positions of vortex filements, including vortex interactional

effects as the blades rotate around the disc, but assumes an induced velocity distribution given by equation (5.3), (5.5) and (5.7).

Equation (5.8) is correspondingly updated to give:

$$v_i = \bar{v}_i(1 + K\bar{r}\cos\psi) + v_v \qquad (5.9)$$

As previously assumed, the portion of the lower rotor immersed in the upper rotor wake is effected by the fully developed velocities. This however, is computed on a local, level where v_i lower = fn (v_i upper).

One limitation of the free-wake tip vortex model is the assumption that the vortex core departs the trailing edge of the blade at the tip ($\bar{r} = 1.0$). This assumption neglects the fact that the vortex core location is not only effected by the free-stream conditions but is substantially modified by the large pressure gradients existing at the tip. Indeed, Chigier et al (21) have reported that a vortex core moves inboard, and for the tests conducted, suggested the path taken by the forming vortex was a deflection inboard by the the order of 10 degrees to the tip. For comparative purposes, the free-wake model was used with and without assuming a 10 degrees deflection of the tip vortex from quarter chord to the blade's tailing edge. Figure 37 shows the predicted blade loading results in the lateral plane for an inflight H-34 rotor with an advance ratio of 0.03. Effectively the results show the influence of the vortex position on blade loading. With the blade pressure gradient term assuming a 10 degrees vortex core path deflection on the top surface of the blade, the resultant blade loading at the tip reaches a higher value. This reflects the experimentally determined blade loadings; but as will be established in the next section, it is also equally sensitive to the final rolled-up tip vortex strength.

Throughout the computational procedures, the assumption of rigid blade flapping has been imposed. The corresponding flapping coefficients have been approximated (where actual experimental data was not available) by the following expressions allowing for the effective hinge offset and varying inflow distribution across the rotor (1):-

$$a_o = \frac{\gamma}{8(1+\varepsilon)}(\theta_o(1+\mu^2) + 4\lambda/3) \tag{5.10}$$

$$a_1 = \frac{2\mu((4\theta_o/3)+\lambda)}{1-\mu^2/2} + \left(\frac{8}{\gamma}\ \frac{\varepsilon b_1}{1+\mu^2/2}\right) \tag{5.11}$$

$$b_1 = \frac{(4\mu a_o/3)+K\lambda_i}{1+\mu^2/2} - \left(\frac{8}{\gamma}\ \frac{\varepsilon a_1}{1+\mu^2/2}\right) \tag{5.12}$$

$$\text{where,}\quad \lambda_i = v_i/\Omega R \tag{5.13}$$

and $\varepsilon=1.5e$, for a uniform blade mass distribution neglecting the effect of root cutout. The effective hinge offset e, is normalised by the blade radius. Only the first harmonics are considered since higher harmonics are of the order of further elastic blade deflections which have been ignored. Furthermore, it has been noted (1) that the second flapping harmonics are generally an order of magnitude less than the first harmonics and, therefore, only have importance in vibration or control load computations.

The corresponding flapping angle β, at any azimuthal position is given by:

$$\beta = a_o - a_1 \cos\psi - b_1 \sin\psi \qquad (5.14)$$

The computational approach and the full equations used in the forward flight code are presented in Chapter 6 and Appendix 2 respectively.

5.2 Application of the Vortex-Glauert Model

One of the most testing flight regimes for any forward flight rotor wake model is the low advance ratio case (μ <0.15). In this transition zone between hover and well established forward flight, the trailing wake deformation has a substantial influence on the induced velocity and blade loading distributions.

To ascertain the potential of the present model, the Vortex-Glauert approach was used to predict the blade loading distribution of an H-34 rotor in flight with an advance ratio of 0.03. The predicted results are compared with both experimentally measured inflight data (57), and the results from a full vortex lattice free-wake code (58). Four blade positions of 0, 90, 180 and 270 degrees of azimuth were examined. The input to the present model included the measured pitch distribution, and the flapping coefficients up to the first harmonic.

As can be seen from Figures 38-41, the full-vortex lattice method generally over predicted the blade loading distribution on the inner portion of the blade; while for the 90, 180 and 270 degrees of azimuth cases did not forecast the substantial peak loading toward the blade tip.

The H-34 rotor, with aspect ratio rotor blades of 20.5, falls

into the category of the rotor blade investigated by Cook (28). As presented in Chapter 3, one of the major difficulties in using the vortex turbulent boundary layer analogy equations is that the final rolled-up tip vortex strength may be a fraction of the peak bound circulation. Indeed, Figures 16 to 18 depict Cook's full-scale vortex data where, in general, it was found that the vortex strength was found to be less than half the expected value.

Using this research work for guidance, two finalised vortex strength values were investigated. The first value used in the Vortex-Glauert approach represented the generalised Carradonna et al (34) vortex model which yielded a final vortex strength K_O, equal to 3.1 times the vortex core strength K_C. A second estimation of the final strength of the vortex was obtained by using an expression developed by Cook (59), to predict the local mean value of blade circulation given by:-

$$K_o = \frac{T}{\rho N R \Omega R((1/2)-(3/16)\mu^2)}(1-(3/2)\mu\sin\psi) \qquad (5.15)$$

For the H-34 rotor the mean vortex strength evaluated using Cook's expression was nearly twice the value set by Carradonna's approximation. The roll-up of each vortex was assumed complete after 60 degrees of azimuth (before next blade passage) whereapon the full value was set to the trailing vortex filament. The free-wake facility was used in program ROTOR to evaluate the tip vortex locations around the disc.

Figures 38-41 indicate that the predicted blade loading distribution more accurately reflects the experimentally measured results. Furthermore, with the fully rolled up vortex strength set equal to the local blade mean circulation value, the peak loadings at the blade tips were more accurately defined. However, the blade

loading is sensitive to both vortex position and strength; the former being directly coupled to the latter in the free-wake model. This coupling effect is most readily highlighted in Figure 40 for the blade loading distribution at a blade azimuth position of 180 degrees. With the final vortex strength set to the blade mean circulation, the free-wake model indicates a second vortex blade interaction at $\bar{r} = 0.75$. (blue curve).

Overall, the agreement between the Vortex-Glauert model and the experimentally measured data is quite reasonable, especially in the tip region where the mean blade circulation value was taken as the strength of the fully rolled-up tip vortex. This circulation value, based on a mean rotor thrust estimation, correlates well with Cook's (28) research data. Indeed, the finalised vortex strength values were found to be just less than half the peak circulation on the blade.

In contrast to the vortex-lattice model predictions, the inboard blade loading distribution was underpredicted using the present model. This feature is thought, in part, to be affected by the simplification of the Glauert momentum inflow distribution, assuming a substantial mean value at the centre of the disc. Indeed, the constant Glauert induced velocity distribution in the 90 - 270 degrees plane, shown on Figures 43 and 45, suggests an equal circulation weighting along the blade radius. This supposition may lead to measurable discrepancies, especially near the blade root. Figures 42 and 44 show a similar breakdown of the inflow distributions for the 0 and 180 degrees azimuth positions. Again, Figure 40, clearly identifies two vortex 'strikes' occuring at the front of the disc. Figure 46 details the tip vortex paths computed using the free-wake facility in the longitudinal plane of the H-34 rotor (i.e. the 0-180 degrees of azimuth plane where Z/R is the normalised axial displacement of the tip votices on Figure 46). The vortices generated at the front of the disc initially move upward and inboard before descending through the blade plane (vortex coordinates at the front of the disc were determined relative to blade axes located at 180 degrees of azimuth). This feature is reflected in the smoke visualization photograph (Figure 48) for the

lower rotor of a CCTR operating at a low advance ratio. In contrast, the tip vortices of the trailing edge of the disc are convected away at a much faster rate. Landgrebe et al (60) has shown similar trends for the tip vortex wake generated by a single rotor operating at low advance ratios.

However, the major limitation of this 'free-wake' option is highlighted by the subsequent locations of the tip vortices after they pass through the front portion of the disc. The combined effects of assuming a limited number of wake revolutions, neglecting the blade bound vorticity in the computation of the tip vortex locations, and the relative flow magnitudes at the front of the disc operating at a low advance ratio, create the conditions whereby the vortex-vortex interactions produce a macro wake roll-up. That is, the formation of a larger vortex composed of a number of tip vortices. The second vortex strike prediction is a result of this feature.

Although there is much less detailed blade loading data for CCTR's, the heavy tail first landing incident of the ABC helicopter provoked a revision of the methods used in forecasting the inflow through the two rotors. The revised inflow distributions based on experimental measurements for a forward flight velocity of 25 knots (μ = 0.067) are given in reference (56). Converging on the ABC helicopters gross weight of 90001b by varying the blade collective pitch, the inflow variation in the longitudinal plane was evaluated. Figure 51 compares the revised inflow values of reference (56) with the generated values from program ROTOR, using the free-wake facility. It is interesting to note the build-up of inflow over the rear section of the lower rotor.

Figures 52 and 53 show comparisons between theory and experimental forward flight Mote CCTR data for a constant thrust coefficient of 0.006 and advance ratio of 0.174 respectively. In both cases, the classical wake option was found adequate for estimating the overall performance of the Mote CCTR.

5.3 Discussion

Applying the Vortex-Glauert model to predict the blade loading distribution of an H-34 rotor in flight with an advanced ratio of 0.03, produced some very interesting results. As detailed in the previous section, a variety of tip vortex strengths were used when computing the total inflow through the rotor. Of these the tip vortex strengths set equal to the localised mean blade circulation gave the most accurate blade loading prediction, especially, near the tip region. Indeed, this mean value reflects the full scale rotor data (Figure 16) collected by Cook (28). Both rotors have a blade aspect ratio of 20.5.

Nevertheless, inboard blade loadings at this low advance ratio, in general, were under predicted, suggesting that the computed inflow was excessive. Perhaps, the most plausible reason for this is the "global" momentum representation of the Glauert model. The comparatively large inflow through the central regions of the disc, implicit in the Glauert model, may be more accurately modelled by a local momentum theory, as proposed by Azuma et al (47). Infact, the incorporation of the local momentum theory into a tip vortex - momentum approach would be a straightforward extension of the proposed model. Alternatively, explanations seem common to most other wake modelling methods. That is, a different blade loading prediction results when the initial computer input is either the rotor thrust or blade pitch. In the latter case, for high aspect ratio rotor blades, the final blade thrust is generally underpredicted. This feature, is often explained by the omission of the blade elastic deflections. Although such a discrepancy can be the order of a degree in pitch between experiment and theory to obtain equivalent blade loadings, Kawachi (61) has shown that the blade aspect ratio has a substantial effect on this trend. For a hovering rotor with a blade aspect ratio of 6.54, equivalent theoretical/experimental blade loadings were achieved when Kawachi's program converged on a blade pitch over one degree less than the actual value. Converging on the experimental pitch value gave an excessive blade loading distribution, especially at the blade tip. Interestingly, the vortex core model expounded in Chapter 3 would reflect the overall trend, indicating an increasing degredation of

rotor thrust per degree of blade pitch as the blade aspect ratio is decreased, independant of blade elastic deflections.

Resulting from a conversation with Kawachi, it was indicated that 'good' values of the lift curve slope were 5.73 and 6.28 for momentum and vortex approaches respectively. Infact, Kawachi in reference (61) uses a lift curve slope value of 6.05 as a good universal representative value. Obviously this approach is questionable and may well relfect the uncertainty of many of the currently used models.

The free-wake solution of the tip vortex locations suggested two blade vortex interactions at the front of the disc. The experimental blade loading (Figure 38) does not indicate a second vortex strike. This disparity is seen to result from neglecting the blade bound vorticity (especially the next blade pass) in the present model.

In contrast, the vortex lattice method, in general, overpredicted the inboard blade loading distribution and failed to reflect the substantial peak loading at the tip. The former limitation may be improved by comparing the downwash at a specified blade element with that required to conserve momentum for a given elemental thrust. It is proposed that if a mismatch occurs then the inflow value should be updated accordingly. Peak loading predictions at the blade tip may be enhanced by including a more accurate description of the substantial tip vortex core which is formed on the blade surface.

Using the results from the H-34 rotor as guidance for future rotor blade loading predictions, program ROTOR was initiated to generate the inflow values through the upper and lower rotor of the ABC CCTR. Setting the tip vortex strengths to the local mean blade circulation value, the inflow distributions for an advanced ratio of 0.067 were computed. Figure 51 shows that a reasonable inflow prediction in both magnitude and trend, especially in the aft region of the lower rotor. Further comparisons using the classical wake option with perfomance figures generated from the Mote experimental

programme show reasonable agreement throughout a range of advance ratios (Figure 52) and blade collective pitch settings (Figure 53).

The previous computations have used, in general, finalised tip vortex strengths much less than the peak blade bound circulation values. This, however, does not necessarily violate the conservation of circulation principle. Indeed, it is proposed that if a concentrated tip vortex core has a comparatively "short life" with an expanding core, then the much weaker inboard shed vorticity may be dissipated at an even greater rate. That is, the circulation is still conserved, yet, because of the expansion process it occupies such a large volume that the related velocity field rapidly diminishes.

5.4 Conclusion

The Vortex-Glauert model presented here has given reasonable agreement with experimental data from both single rotor and CCTR systems. Furthermore, it shows considerable promise for low advance ratio modelling. The general underprediction of blade loading distributions when converging on the experimental blade collective pitch reflects current findings from a wide variety of modelling approaches (61). This is often remedied by increasing the blade collective pitch during the computation (allowing for blade elastic deflections) or selecting a larger lift curve slope value.

Alternatively, it has been proposed that a more accurate representation of the rotor may be achieved by coupling the tip-vortex momentum approach with a local momentum theory. Updating the approach in this way does not limit the flexibility of the model in that either classical or free-wake routines could still be used.

Further investigations are required to ascertain the fully rolled up tip vortex strengths generated from a variety of different rotor blades. The present model sets this strength to a mean bound circulation value which reflected the full scale rotor data reported by Cook (28). Equally, as indicated in Chapter 3, the tip vortex, core strength is substantially effected by the blade aspect ratio

which other wake models do not adequately account for (61).

6. PROGRAM ROTOR

6.0 Introduction

The main objective in developing program ROTOR was to produce a computer package written for the general case, with high flexibility and the option to run interactively. Furthermore, structured in a module format, the code may be easily updated, allowing it to be used as a continuing research tool. After compilation, the program is initiated by a well defined input procedure (see Appendix 3). During this stage, a number of questions are first posed to the user, to determine whether a hover or forward flight computation is required. Further input includes blade radius, blade pitch (including twist distribution), blade chord (including taper distribution), rotor RPM, the number of rotor wake revolutions, the degrees of azimuth spacing between integration procedures and if an allowance for tip vortex roll-up required.

Both single rotors (read as upper rotor) and CCTR's may be analysed with up to a total of twenty blades. Other blade variables including twist, taper and hinge offset are easily handled by the code. It must be emphasised, however, that the flapping equations given in Chapter 5 could be improved upon to incorporate a more accurate description of blade twist and taper effects. Additional features include the option for differing rotor radii, number of blades and vertical spacing between the two rotors in the CCTR layout. A full input procedure for an arbitrary rotor plus a full program listing containing extended Fortran IV code is detailed in Appendix 3.

6.1 The Hover Facility

The flow chart in Figure 55 depicts the salient features of the Hover Code. After setting the input parameters, subroutine STRIP is called to compute an initial estimate of the rotor thrust coefficient. Initially, conventional strip theory is used with a tip loss factor to estimate the rotor thrust. Thereafter, LANDG is

initialised to define the Landgrebe empirical prescribed tip vortex paths. The helical vortex wake is stepped out to the number of requested wake revolutions, using the straight line vortex filament approximation. The accuracy of the approximation is dependant upon the degrees of azimuth spacing parameter defined in the input procedure. The vortex filament cartesian coordinates are computed for all blades in the rotor(s) by subroutine BLVOCO. With the vortex filament locations known and the vortex core parameters V_s, and r_c, established, subroutine CAL is called to evaluate the apparent vertical accent velocity distribution v_v. Recalling STRIP yields a modified momentum downwash contribution effected by the tip vortex wake. After summing the total downwash at each blade station, subroutine PERM is initialised to evaluate the overall thrust, torque, location and magnitude of the peak circulation. The fourteen blade stations are distributed such that the first nine are separated by 0.1R to 90 percent blade radius with the remaining five stations equally spaced over the last 10 percent of blade. Lift and torque are summed using mean two-dimensional aerofoil characteristics as presented in Appendix 2.

The aforementioned procedures are repeated until the rotor thrust-vortex location inter-relationship has converged. At this stage, if the single rotor performance calculation was requested, the program would output a variety of data depending upon the number of WRITE statements 'released' in the current program. Throughout the program a variety of WRITE statements are included such that maximum access to the computed data may be achieved. However, to suppress the output listing the majority of WRITE statements have a 'C' in column one of their line. With this arrangement, the computer ignores the WRITE statement, but before compilation, may be activated by simply removing the 'C' character during an edit of the program.

For a CCTR computation the program continues to evaluate the perfomance of the lower rotor in a similar manner to that explained for the upper rotor. Initially, the performance calculation is perfomed allowing for the upper rotor wake interaction and altering the pitch on the lower rotor until the torques on both rotors are

within .01 of each other. Thereafter a full computation is initiated which allows for the elongation of the upper rotor wake under the influence of the lower rotor (using subroutine ZUPDATE), and the lower rotor tip vortex wake effect on the upper rotor inflow distribution. At this stage, the extended Stepniewski equations are utilised in subroutine STRIP 2, to complete the calculation of the lower rotor influence on the upper rotor.

Re-calculation of the upper and lower rotor performances follows until, the upper and lower rotor thrust-vortex locations are fully converged. The final data output represents the complete interference effects between upper and lower rotor.

6.2 The Forward Flight Facility

The pertinent features of the forward flight code are represented by the flow chart in Figure 56. After initialising the input parameters and selecting the type of wake required the program commences by calling subroutine GLAUERT, to estimate an initial value for the mean induced flow through the rotors. Directly proceeding this calculation, the advance ratio, inflow ratio and blade flapping coefficients up to the first harmonic are determined. Knowing the wake step in degrees of azimuth (input parameter), the flapping angle and the flapping rate are evaluated at each future blade azimuth position.

The wake computations immediately follow. The rotors are started from the rest with each blade moving through two wake stations, trailing their corresponding tip vortex filaments (two per blade). For the CCTR configuration, the upper and lower rotors rotate anticlockwise and clockwise respectively. Although started from rest, the rotors assume the correct tip speed immediately with the locations of the initial two vortex filaments per blade being determined solely by the local freestream conditions. Thereafter, subroutine RANKINE is called to establish the vortex filament strengths which vary around the disc. If the free-wake option has been selected, subroutine IND is called to evaluate the induced velocities from all other vortex wake filaments on the end points of

any specified wake filament. Repeated calculations are performed until all the interactions have been computed. The subsequent update of filament end points is managed in subroutine POSTN.

The velocities in the x, y, z directions of the coordinate system, shown in Figure 57, of the filament end points are assumed constant over a time equivalent to one blade step. For the classical wake option, these velocities ar set to the local freestream conditions.

The aforementioned procedures are continued until the predefined number of wake revolutions are completed. Wake convergence may be checked in the interactive mode by comparing the filament locations between completed rotor revolutions. This check may be continued until the user is satisfied that sufficient repeatibility has occurred, usually after two further wake revolutions.

Thus far, the preceeding calculations have been with respect to the no-feathering axes with the origin located at the centre of the upper rotor disc. Figure 56 shows the direction of the axes system. Following computations, however, are simplified by a transfer of axes to a set rotating with and in a specified blade, denoted by a suffix 'b' in Figure 56. Thereafter, RANKINE, IND, GLAUERT and INCEPT are called to evaluate the tip vortex strengths, the vortex induced velocity distribution along a specified blade and the modified Glauert velocity through the rotors. Tangential and perpendicular velocities to a given blade are then summed, and using subroutine PERM, the elemental and overall blade thrust, torque and H-force contributions are determined. The procedures are repeated for each blade in the rotor layout. Complete rotor thrust, torque and H-force are then output with the blades 'frozen' at their specified locations. Subsequent runs may be initialised to trim out any rotor imbalance.

6.3 Conclusions

The development, running and debugging of program ROTOR formed

a substantial part of the research programme. Partly for this reason, the program was structured in a module format to allow future users the option of updating certain features when more information becomes available. Equally, other approaches could be integrated with various routines with ROTOR, avoiding unnecessary duplication of work.

The version of program ROTOR presented in Appendix 3 is configured for use in the interactive mode. However, when using the free-wake facility during a time sharing session, the run time can be prohibative. Consequently, it is recommended that when using the free wake facility, program ROTOR should be configured to run in batch, avoiding this difficulty.

7. PRELIMINARY OPTIMISATION STUDY OF A CCTR IN HOVER

7.0 Introduction

As a result of the spiralling costs of energy and the highly competitve commercial market, the need for more efficient rotor systems is becoming increasingly important. Although gains in rotor thrust of a few percent for a given power may at first seem trivial, the corresponding payload increment is amplified. For example, a gain in payload of 20% may result if a thrust increment of only 5% is attained for a given power. Such gains are becoming feasible with the aid of computers in advanced blade design; and the application of composites during manufacturing processes which allow greater flexibility in blade structure with varying planform, twist and aerofoil distributions.

The outcome of any optimisation study is heavily constrained by the 'specification', defining the requirements of the helicopter. Generally, a number of tradeoffs emerge between hover, fast forward flight, autorotating characteristics and avoidence of blade stall on the retreating blade and during maneuvers. Although complete helicopter studies have been undertaken, notably by Stepneiwski (55), considerable effort has been concentrated on main rotor design.

For a single rotor Bingham (62) found that the initiation of blade taper and taper ratio had a significant influence on the efficiency of rotor in both hover and forward flight. For the hover case, Bingham concludes that the favourable influences of taper result from, 1) the increased inboard loading of the rotor which reduces the induced torque and, 2) the reduction of chord in the outboard regions decreased the profile torque. Although similar gains could be achieved by twisting the blade (washout) in hover, it was established that blade taper had the more beneficial effect in forward flight. Again, the main reason proposed was the reduction in blade profile drag as proportionately more blade area is moved

inboard. However, it should be noted that the influence of taper and taper ratio decreases as blade solidity increases.

Another interesting optimisation programme was undertaken (63) to study the problems of blade wake interactions and designing a rotor which capitalised on the findings. The outcome was the Variable Geometry Rotor (VGR). The VGR system consisted of two rotors turning in the same direction (corotating rotors). By varying the vertical spacing, blade radii, collective pitch and phasing between the two rotors, the performance characteristics of a wide variety of combinations were obtained. Indeed, the full programme included analytical studies and experimental investigations on model and full-scale rotors.

The key parameter in effecting a desirable change in rotor efficiency was the vertical rotor spacing. For an vertical rotor spacing of two chord lengths, the hover performance was increased by 12%. At an advance ratio of 0.2, 5.06% less torque for a given thrust was required with a rotor vertical spacing of one chord length. Increasing the spacing had a negligible effect. Further testing at an advance ratio of 0.3 with a rotor axial spacing of one chord length indicated that 3.4% less torque at the same lift as the regular rotor was required. The reason attributed to this result was the lower induced flow through the upper rotor, especially in the inboard regions. Both differential collective pitch and radii reduced the forward flight performance for the one chord vertical rotor spacing.

With regard to the CCTR layout very little emphasis has been placed on optimising the rotors. An exception is the preliminary work reported by Nagashima and Makanishi (32) on the optimisation of a hovering CCTR and the associated wake geometry. They conclude that for a given vertical rotor spacing, differential collective pitch may be applied, obtaining the optimal thrust sharing ratio. This thrust sharing ratio was found to be almost equivalent to the contraction ratio of the upper rotor wake at the plane of the lower rotor. However, such an optimum thrust sharing ratio would, in general, be achieved at the expence of generating a torque imbalance

between the two rotors and therefore of little practical value.

Jones (64), however, in a preliminary study comparing the ABC CCTR with a conventional single rotor, for a given mission, indicated that the ABC CCTR could operate with a smaller rotor radius and possibly fuel load.

7.1 Single Rotor Hovering Performance

Useful insights into the effects of number of blades, blade aspect ratio and blade solidity on the hovering performance of a single rotor were gathered by running program ROTOR. The generated information is presented in Figures 57-61. The only constraints imposed on the data acquisition were:-

Rotor radius = .76m (Mote dimension)
Tip speed = 35m/s

The measure of rotor efficiency used throughout the program has been defined as the thrust generated per unit power.

Figure 57 indicates that for the same mean lift coefficient ($6C_T/\sigma$), the highest efficiences are obtained by keeping the number of blades to a minimum. This is not surprising since adding blades into a rotor system increases the disc loading which increases the induced power. Equally, increasing the blade aspect ratio while keeping the number of blades constant (Figure 58) reduces the rotor disc loading for a given mean lift coefficient.

At all stages in interpreting the efficiency of a rotor system, great caution is necessary. For example, it is unimportant to an operator that a two bladed rotor is more efficient per unit lift coefficient than a four bladed rotor (double solidity), if the former was unable to lift a specified all-up-weight.

A second set of curves shows efficiency with respect to constant blade solidity (Figure 59) and thrust coefficient (Figure 60). Figure 60 highlights the variation of the number of blades

combined with varying aspect ratio, to maintain a constant blade solidity of 0.08. The graph indicates that a more efficient rotor may be obtained for a given thrust if a large number of high aspect ratio blades are used as opposed to a small number of low aspect ratio blades.

Completing the overall view of the parametric trends, Figures 57 and 58 have been replotted against thrust coefficient (Figures 60-61). At low thrust coefficients, the most efficient rotor system has the minimum number of rotor blades (lowest solidity). This results directly from minimising the profile drag which forms a substantial part of the total power absorbed at low thrust settings. Increasing the thrust reduces the initial efficiency gain of a low solidity rotor. That is, the blades in a low solidity rotor have to operate at a greater collective pitch, increasing the induced power of the rotor. Although a similar trend is seen with varying blade aspect ratio (Figure 58), the potential gain is greater even for high thrust loadings. In essence, this reflects the beneficial effects that aspect ratio has on the resultant induced rotor power.

7.2 CCTR Hovering Performance

For direct comparison, Figure 62-65 are plotted with an abcissa based on a regular Mote rotor thrust coefficient C_{T_M} defined as;

$$C_{TM} = T/(\rho V_M^2 \pi R_m^2)$$

where,

V_M = 35m/s

R_M = 0.76m (maximum permissible radius)

This parameter allows absolute comparisons between a variety of design options to be made. Figure 62 shows the effect of interrotor spacing on the thrust per unit power generated by a CCTR. The greatest efficiency is achieved when the two rotors are infinately separated, inferring no mutual rotor interference. Effectively, the disc area has doubled. The lower efficiency limit is reached as the inter rotor spacing tends to zero (from practical reasoning, the

zero vertical rotor spacing curve on Figure 62 was computed assuming the same rotor rotational directions and therefore not technically a CCTR). Over a midrange spacing, allowing for adequate blade tip clearance, no gain is predicted from increasing the separation from 10% to 20% blade radius. This result reflects the findings of the VGR programme (63) where little further gain in performance was achieved after a rotor separation of two chord lengths.

Figures 63 and 64 show the effect of reducing the upper rotor radius, with the same RPM and tip speed between the upper and lower rotors, respectively. A definate benefit can be seen by reducing the upper rotor radius by a small amount (approximately on 8% reduction with respect to the lower rotor). However, a further reduction in the upper rotor radius produces a degrading effect with a thrust coefficient exceeding 0.005. This trend results from a tradeoff between reducing the upper rotor radius and, therefore, increasing the upper rotor induced power, with the enhanced performance of a larger portion o the lower rotor taking in clean air.

To verify the encouraging findings on rotor blade aspect ratio, a second set of blades, with an aspect ratio of 19.0, were constructed and fitted to the Mote rig. Figure 65 shows the hovering performance of this CCTR (b=4, R=0.76) compared with the standard Mote blades with an aspect ratio of 14.1. (The performance data was averaged from five separate tests). At a thrust coefficient of 0.007, a increase in hovering efficiency of 4.0% can be seen. Replotting the data presented in Reference (51), for two CCTRs with equal blade radii of 3.8 metres, but differing blade aspect ratios of 8.33 and 11.65, shows the same trend.

7.3 Conclusion and Recommendations

This limited study of a hovering CCTR has shown three areas where potential gains in hovering efficiency may be obtained. Firstly, the vertical rotor spacing has a beneficial effect on the CCTR performance. Interestingly, this gain is quickly attained by small vertical rotor spacing (< 10% rotor radius). Consequently, the rotor spacing necessary to avoid the possibility of a mutual blade

strike will invariably be sufficient to exploit this feature. Secondly, there is a tradeoff between reducing the upper rotor radius and, therefore, increasing the induced power, with the benefits resulting from a larger portion of the lower rotor taking in clean air. For the example given, an 8% reduction in upper rotor radius produced the most promising results. Thirdly, blade aspect ratio has a significant effect on the hovering efficiency of a CCTR (also applies to a single rotor). The trend of increased hovering efficiency with higher aspect ratio rotor blades has been endorsed by experimental data. This, in part, is considered to result from a reduction in the induced power, analogous to the reduction in induced drag found in fixed wing operations with increasing aspect ratio.

It is recommended that this preliminary study be continued, using program ROTOR. Besides investigating blade twist and taper distributions, root cut-out etc, unconventional CCTR layouts should be explored. That is, differing rotor radii, number of blades and RPMs should be investigated, not only with the view of increased performance, but perhaps with the aim of minimising the overall helicopter vibration levels. This, of course, will have to be investigated over the complete flight envelope of the CCTR, as undoubtedly trade offs will emerge.

8. CONCLUSIONS

8.0 Conclusions

At the inception of the research work, the appropriate literature was surveryed to obtain a suitable wake theory which would adequately model the flow through a Coaxial Contratrotating Twin Rotor (CCTR). Initially, the large variety of single rotor wake models were investigated. This investigation, although producing the various advantages of momentum and vortex approaches, indicated that a more indepth understanding of wake generated flows was essential. One fundamental area where a lack of information was reported (14, 43, 44) was the characteristics of the helicopter tip vortex, namely vortex strength, and structure. Bearing this fact in mind, the available CCTR models were examined to determine their suitability. In general, the CCTR models investigated as presented in Chater 4, were greatly simplified and did not satisfactorily allow for the effect of one rotor on another. Equally, all the CCTR models contained the same single rotor wake assumptions.

It was therefore considered necessary in developing a suitable CCTR wake model that:-

1) The experienced gained from single rotor modelling techniques, and the limitations thereof, would be used as guidance in the development of a CCTR model.

2) Fundamental weaknesses, namely the understanding of tip vortex characteristics would be improved apon.

Consequently, in developing a CCTR model, considerable effort was expanded on single rotor concepts and tip vortex experimental and theoretical considerations. The results of this work, in part, generated a frame-work in which a CCTR model was developed. However, the findings are also applicable to single rotor wake modelling which for completeness have been reported herein.

The tip vortex literature survey presented in Chapter 3, highlighted possible areas where traditional modelling techniques are limited. The results of the survey indicated that although a large amount of experimental data was available, very little cross-correlation had been done. To overcome this limitation, the vortex data was condensed and used to establish a better understanding of the tip vortex. Initially, only the vortex 'solid body' rotational core was studied in detail. As a result, two equations were developed defining the vortex core radius and associated tangential velocity (Equations 3.5 and 3.6). It was found that, for example, a high aspect ratio rotor blade generated a comparatively weaker tip vortex core than a lower aspect ratio rotor blade. Equally, the vortex core radius, as it departs from the trailing edge of the blade, was found to be the order of the turbulent boundary layer thickness. This result was in conflict with many typical suppositions used in a variety of wake models. For example, although the actual vortex core radius could be as small as 2% blade chord, typical analyses often use anything between 0.5% (31) to 2.5% (14,32) blade radius to define the vortex core radius.

Further research on the complete structure of a rolled-up tip vortex highlighted more ambiguities in the literature. Although to a good approximation, the complete vortex structure may be considered analogous to the structure of the turbulent boundary layer (33), the coefficients in the describing equations (see Equations 3.9 - 3.11) cannot be considered universal, as it is sometimes suggested (34). To ascertain a good description of the structure of a tip vortex from a variety of rotor blades, a theoretical model was developed. The theoretical procedures and solution are described in Section 3.4 and Appendix 1 respectively, and compared with experimental data in Figure 13 and 14 where excellent agreement was found. Unlike the turbulent boundary layer solution however, where the outer limit of the layer is defined where the velocity approaches 99% of the free stream value, the outer radius of a vortex may not always be defined where the vortex strength approaches 99% of the maximum bound circulation on the blade. This feature was reported by Cook (28), who found that the tip vortex strengths shed from a rotor blade with an aspect ratio of 20.5 was, in general, less than half the expected

value. Indeed, for the vortex data reported by Cook (i.e. from a high aspect ratio rotor blade), Equations 3.9 and 3.10 were found adequate to described the resultant vortex structure (i.e. ignoring the defect region) once the finalised vortex strength was known (see Figure 19).

Lastly, Section 3.5 of Chapter 3 has identified that the large strength (circulation) decay sometimes assumed in wake modelling, may be a gross misrepresentation of what actually happens. Rotor tip vortex 'decay' is, infact, often associated with a vortex core expansion. It was shown in section 3.5 that this can take place when either a vortex-vortex interaction occurs or when the vortex axial velocity diminishes. Consequently, the associated velocity field of a expanding vortex core is, for points contained in the core, diminishing. The core strength, however, may not have changed by a significant amount. An example of this type of decay is given in Figure 7.

The difficulty in developing a suitable CCTR hover model is determining the correct tradeoff between avoiding unnecessary complicated computation without loosing a full description of the interference effects between the two rotors. Furthermore, increasing the complication of a theoretical model does not necessarily guarantee better predictive accuracy (50).

Chapter 4 presents a survey of a wide variety of wake modelling techniques. In essence, momentum approaches offer simplicity in application with a low computational time, while vortex theories can be most readily applied to compute temporal variations in the flow, and become important when estimating the influence of one blade or rotor on another. To exploit the advantages of each, a method was developed which combined the vortex, momentum and blade element theories into one approach.

The well known strip theory (15), which uses blade element and momentum theories to yield an initial estimate of the induced downwash at the blade element is still widely used. Its major limtiations, however, are the arbitrary application of a tip loss

factor to enhance the rotor performance prediction, and the poor physical representation of the rotor blade airloads. The tip loss, infact, results from a finite radius rotor system, which allows air to flow around the lower surface of the blade to the upper blade surface, creating a tip vortex. It is argued in section 4.2 of Chapter 4, that the 'tip loss' may be more accurately described by the lift impairment resulting from the total tip vortex wake(s) induced velocities over the complete blade. Now for hover, by definition, the vertical climb velocity in the strip equation (4.1), is exactly zero. However, the developed theory suggests that each blade element perceives an additional induced velocity due to the tip vortex wake, which may be interpreted as a local climb velocity. That is, the total tip vortex induced velocity calculated at each elemental annular ring, replaces the global vertical climb velocity in the strip equation (Equation 4.1), modifying the resultant strip induced velocity. The resultant additional loss of angle of attack at each blade element reflects the losses associated with a finite radius rotor system, replacing the arbitary application of the tip loss factor. Based on this method, Stepniewski's (2) simple model of a CCTR was greatly extended to include the effects of the tip vortex wake and wake contraction.

The resultant CCTR hover model named Vortex-Strip theory, was applied to both model and full-scale rotors (see Chapter 4), with different tip speeds, rotor radii, number of blades and blade aspect ratios, including blade twist and taper, Overall, the full interference effects between the two rotors was found to be well predicted and produced a much more representative blade loading prediction, especially in the tip region (see Figure 27 and 28). Equally, single rotor blade loading and performance prediction, using Vortex-Strip theory, was also very encouraging.

This approach, combined with the aforementioned vortex equations, implies the tip loss, for example, is strongly related to the blade aspect ratio. Interestingly, even the most current analyses (61) encounter substantial difficulties in predicting the perfomance and blade loading distributions of different aspect ratio single rotor systems. Kawachi (61), found that by entering the

actual blade pitch into a variety of rotor wake computer programs, produced a gross over prediction of the blade loading for a rotor with a blade aspect ratio of 6.54. The presented Vortex-Strip theory however, using equations (3.5) and (3.6), suggest that for such a low aspect ratio rotor blade, the tip vortex core strength would be high, tending to produce substantial rotor losses.

The Vortex-Strip theory was also used to compare the Mote CCTR with an equivalent single rotor. The latter being defined by collapsing the two rotor systems into one plane and spacing the blades equally around the disc. It was found that for a given thrust, the CCTR is approxiamtely 5% more efficient than the equivalent single rotor and is considered to result from :-

1) The contraction of the upper wake of a CCTR allows clean air with a slight upwash to be taken by the outboard sections of the lower rotor. Consequently, the effective rotor disc area has increased with a corresponding reduction in the induced power.

2) The vertical CCTR rotor spacing effectively reduces the severity of the total vortex induced velocity, especially on the upper rotor.

Using similar principles to those developed for the hover theory, a forward flight hybrid model was developed, and is presented in Chapter 5. Combining Glauert's approximate forward flight equations with an allowance for the tip vortex wake (named the Vortex-Glauert approach), the resultant model was applied to both single rotor and CCTR systems. The model incorporated a facility to allow the tip vortices to either modify the wake limits (free-wake), or remain prescribed. The former was considered essential from the experienced gained with single rotor modelling techniques (14), to adequately described the flow pattern during low advanced ratio conditions. Since only very limited published data is available on CCTR aerodynamic characteristics in forward flight, the model was initially developed and tested on comprehensive full scale single H34 rotor data (57). The condition investigated was a low

advance ratio case of 0.03, with blade loading predictions at 0, 90, 180 and 270 degrees of azimuth. The most reasonable agreement ensued when the finalised tip vortex strengths, used in the fully rolled-up tip vortex equations were set to a local mean blade circulation, as suggested by the full-scale ABC hover findings, and results reported by Cook. Moreover, using this condition to predict the inflow distribution through the ABC rotor system, for an advance ratio of 0.067, produced very promising results. Figure 51 shows the high values of inflow which are generated over the rear portion of lower rotor of an ABC CCTR when operating at this low advance ratio.

Using the classical wake option in program ROTOR, the theoretical performance predictions were compared with experimental results for varying advance ratios with a constant thrust coefficient of 0.006, and varying rotor collective pitch with a constant advance ratio of 0.174 (Figure 52 and 53). The agreement in these ranges was found to be good through out.

During the verification and testing of the presented helicopter rotor wake models an extensive computational code was developed. Indeed, the construction, running and 'de-bugging' of the final program ROTOR formed a substantial portion of the research programme. The program refinements include a well defined input procedure with the option to run interactively, combined with a set of codes written for the general case. This feature allows an operator to investigate a wide range of rotor parameters including different rotor radii, number of blades, CCTR rotor spacing, with variations in blade twist, taper and hinge offset. Equally, the program has been constructed around a modular format, making future improvements and modification less time consuming. It is envisaged that the developed code will continue to be used as a research and development tool. The wide application of the program is reflected in the variation in runtimes, from a few seconds for a single rotor hovering condition, to many hundred of seconds for a fully converged solution of a free-wake CCTR computation.

The favourable finding of improved hovering performance of a CCTR when compared with a single rotor, prompted a preliminary

optimisation study of a hovering CCTR. The results of this study, presented in Chapter 7, indicate three factors which enhance the CCTR hovering perfomance, namely:-

1) Vertical CCTR rotor spacing. The practical optimal gain in hovering efficiency is quickly attained for a small vertical rotor spacing (<10% blade radius). Thereafter no further gain results.

2) A reduction in the upper rotor radius. There is a trade off between the increase in induced power of the upper rotor with a reduction in the upper rotor radius, and the enhanced perfomance of the lower rotor as proportionately more disc is exposed to clean air. For the example shown in Chapter 7, the most promising results were obtained for an 8% reduction in upper rotor radius.

3) Increasing the blade aspect ratio. Both theoretical and experimental findings indicate that an increase in hovering efficiency may be obtained with high aspect ratio rotor blades. For a thrust coefficient of 0.007, the standard Mote, with a blade aspect ratio of 14.1 was compared with the perfomance of a CCTR, with the same rotor radius of 0.76 metres, but with higher aspect ratio rotor blades of 19.0. At this thrust coefficient an increase in hovering efficiency of 4% was recorded by the higher aspect ratio CCTR.

Although condition 3) is equally applicable to the single rotor, and condition 1) is generally built into a CCTR to avoid any possibility of a blade tip strike btween rotors, condition 2) represents a further modification to a CCTR, increasing its hovering efficiency over the equivalent single rotor. For example taking a thrust coefficient of 0.006, and combining conditions 1) and 2) above in a CCTR design, a potential gain in the CCTR hovering perfomance over a equivalent single rotor of 9% is predicted; and this is neglecting the further power absorbed by the tail rotor in the single rotor configuration.

8.1 Recommendations for Further Work

The developed forward flight and hovering theories, combined with the tip vortex modelling equations presented in Chapter 3, have shown considerable promise for both single rotor and CCTR configurations. The vortex analysis and modelling equations are based on a wide collection of experimental data. Not only do these equations help describe some of the difficulties encountered by other modelling techniques, but may be readily adapted, if necessary, for other applications in 'stand alone' vortex models. Further work is required however, to enhance the understanding of the finalised tip vortex strength and the conditions which effect it.

The increased hovering performance which may be achieved for a given rotor plan area demonstrates a significant advantage of the CCTR over the single rotor. As indicated in Chapter 7, further gains in efficiency are possible, and suggestions are made to investigate unconventional CCTR rotor layouts with different rotor radii, blades number, rotor RPM etc between rotors. This programme of work may be undertaken using program ROTOR without any further modification being necessary.

Equally, the full flight enveloped of a CCTR may be further explored with program ROTOR. For example, although the increased hub drag of the CCTR layout is often cited as a major drawback to its forward flight performance, this alone should not prevent active research in this area. Afterall, the Russians have successfully developed both milatary and civil CCTR variants which have continued to be a popular option. This fact, coupled with the encouraging findings reported herein, present an alternative rotor layout which has yet to be fully exploited by the Western World.

REFERENCES

1. A.R.S. Branwell. Helicopter Dynamics. Edward Arnold, London 1976.

2. W.Z. Stepniewski. Basic Aerodynamics and Performance of the Helicopter. AGARD-LS-63, 1973.

3. M.C. Cheney and A.J. Landgrebe. Rotor Wakes-Key to Performance Prediction. AGARD.

4. R. Stricker and W. Gradl. Rotor Prediction with Different Downwash Models. Forth European Rotorcraft and Powered Lift Aircraft Forum, Paper No 6, 1978.

5. M.L. Mil et al. Helicopter Calculation and Design. Volume I, Aerodynamics NASA TT-823, 1976.

6. V.E. Boskin, L.S. Vil´dgrube, Ye. S. Vozhdayev and G.I. Maykapar. Theory of the Lifting Airscrew.

7. D.W. Wragg. Flight Before Flying, Osprey Publishing Ltd, 1974.

8. R.K. Burgess. Development of the ABC Rotor, 27th Annual National V/Stol Forum of the American Helicopter Society, 1971.

9. J.J. Ventribo (Editor). Sikorsky News, Nov 1981.

10. D.S. Jenney. ABC Aircraft Development Status, Paper No 8, Sixth European Rotorcraft and Powered Lift Aircraft Forum, 1980.

11. V.P. Bailey. The Advancing Blade Concept (ABC) Rotor Program. SAE Specialist Meeting, Las Angeles, 1977.

12. J.A. Faulkner and I.A. Simons. The Remotely Piloted Helicopter Vertica Vol 1, 1977.

13. J.W.R. Taylor and K. Munson. Jane's All the Worlds Aircraft 1979-80.

14. W. Johnson. Comparison of Calculated and Measured Helicopter Rotor Lateral Flapping Angles. Jnl. of the American Helicopter Society. April 1978.

15. A. Gessow and G.C. Myers. Aerodynamics of the Helicopter. Frederick Ungar Publishing Co. New York, 1978.

16. P.O.A.L. Davies and M.R. Davis. ISVR Report No 155, University of Southampton. October 1966.

17. B.W. McCormick, J.L. Tangler and Harold E. Sherrieb. Structure of Trailing Vortices. Jnl of Aircraft Vol 5, No 3, 1968.

18. F.X. Carradonna and C. Tung. Experimental and Analytical Studies of a Model Helicopter Rotor in Hover. Vertica, Vol 5, No 2, 1981.

19. M.J. Andrew. Co-axial Rotor Aerodynamics in Hover Vertica, Vol 15, No 2, 1981.

20. R.F. Spivey. Blade Tip Aerodynamics - Profile and Platform Effects. 24th Annual National V/Stal Forum of the American Helicopter Society, 1968.

21. N.A. Chigier and V.R. Carsiglia. Tip Vortices - Velocity Distributions 27th Annual National V/Stol Forum of the American Helicopter Society, 1971.

22. V.R. Carsiglia, R.G. Schwind and N.A. Chigier. Rapid Scanning, Three-Dimensional Hot-Wire Anemometer Surveys of Wing-Tip Vortices. Jnl of Aircraft, Vol 10, No 12, 1973.

23. A.J. Landgrebe. The Wake Geometry of a Hovering Helicopter Rotor and its Influence on Rotor Performance 28th Annual National V/Stal Forum of the American Helicopter Society, 1972.

24. P.G. Wilby. The Aerodynamic Characteristics of some New RAE - Blade Sections and their Potential Influence on Rotor Perfomance. Vertica. Vol 14, No 2-4.

25. J.B. Rorke, R.C. Moffitt and J.F. Ward. Wind Tunnel Simulation of full Scale Vortices. 28th Annual National V/Stal Forum of the Americn Helicopter Society, 1972.

26. J.L. Tangler, R.M. Wohlfeld and S.J. Miley. An Experimental Investigation of Vortex Stability, Tip Shapes, Compressibility, and Noise for Hovering Model Rotors. NASA CR-2305, 1973.

27. N.A. Chigier and V.R. Corsiglia. Wind Tunnel Studies of Wind Wake Turbulence. Jnl of Aircraft, Vol 19, No 12, 1972.

28. C.V. Cook. The Structure of a Rotor Balde Tip Vortex AGARD CP-111, 1972.

29. J.D. Hoffman and H.R. Velkoff. Vortex Flow over Helicopter Rotor Tips. Jnl of Aircraft, Vol 18, No 9, 1971.

30. M.S. Francis and D.A. Kennedy. Formation of a Trailing Tip Vortex. Jnl of Aircraft. Vol 16, No3, 1979.

31. A.J. Landgrebe. An analytical Method for Predicting Rotor Wake Geometry. Jnl of the American Helicopter Society. Oct 1969.

32. T. Nagashima dn K. Nakanishi. Optimum Performance and Wake Geometry of Co-Axial Rotor in Hover. Seventh European Rotorcraft and Powered Lift Aircraft Forum. Paper No 41, 1981.

33. J.N. Nielsen and R.G. Schwind. Decay of a Cortex Pair Behind An Aircraft. Aircraft Wake Turbulence and its Detection. Plenum Press, 1971.

34. C. Tung, S.L. Pucci, F.X. Carradonna and H.A. Morse. The

Structure of Trailing Vortices Generated by Model Rotor Blades. Seventh European Rotorcraft and Powered Lift Aircraft Forum. Paper No 4, 1981.

35. D.S. Dasanjh, E.D. Gaspaek, and S. Eskinazi. Decay of a Viscous Trailing Vortex. The Aeronautical Quarterly, May 1962.

36. S.E. Widnall, D. Bliss and A. Zalay. Theoretical and Experimental Study of the Stability of a Vortex Pair. Aircraft Wake Turbulence and its Detection Plenum Press, 1971.

37. G.K. Batchelor. Axial Flow in Trailing Line Vortices. Jnl of Fluid Mechanics. Vol 20, Part 4, 1964.

38. Lord Rayleigh. On the Dynamics of Revolving Fluids Proceedings of the Royal Society. Ser. A, 93(1916).

39. S. Leibovia. Structure of Vortex Breakdown. Annual Review of Fluid Mechanics (In Libaray under Q).

40. A.H. Logan. Vortex Velocity Distributions at Large Downstream Distances. Jnl of Aircraft 1619, No 12, 1972.

41. C. Maresca, M. Nsi Mba and D. Favier. Prediction et Verification Experimentale du Champ des Vitesses d'un Rotor en Vol Stationnaire. Ref 9. AGARD-CPP-334, 1982.

42. P.B. MacCready, Jr. An Assessment of Dominant Mechanisms in Vortex-Wake Decay. Aircraft Wake Turbulence and its Detection. Plenum Press 1971.

43. I.C. Cheeseman. Development in Rotory Wing Aircraft Aerodyanics. Seventh European Rotorcraft and Powered Lift Aircraft Forum. Paper No 1, 1981.

44. R.H. Miller. A Simplified Approach to the Free Wake Analysis of a Hovering Rotor. Seventh European Rotorcraft and powered Lift Aircraft Forum. Paper No 1, 1981.

45. H. Glauert. On the Vertical Ascent of a Helicopter. ARC R&M No 1132, 1927.

46. K.W. Mangler and H.B. Squire. The Induced Velocity Field of a Rotor ARC R&M No 2642, 1953.

47. A. Azuma and K. Kawachi. Local Momentum Theory and its Application to the Rotory Wing. Jnl of Aircraft Vol 16, No 1, 1979.

48. D.R. Clark. The Free Wake Analysis. 25th Annual National V/Stol Forum of the American Helicopter Society, 1969.

49. J.D. Kacurek and J.L. Tangler. A Prescribed Wake Lifting Surface Performance Analysis. 32nd Annual National V/Stol Forum of the American Helicopter Society, 1976.

50. S.G. Sadler. A Method for Predicting Helicopter Wake Geometry, Wake Induced Flow and Wake Effects on Blade Airloads. 27th Annual National V.Stol Forum of the American Helicopter Society, 1971.

51. R.D. Harrington. Full Scale Tunnel Investigation of the Static Thrust Performance of a Coaxial Rotor. NACA Tn 2318, 1951.

52. A.J. Rudell. Advancing Blade Concept (ABC) Development 32nd Annual National V/Stol Forum of the American Helicopter Society, 1976.

53. I.C. Cheeseman. A Method of Calculating the Effect of One Helicopter Rotor on Another. ARC Tech Rep. C.P. No 406, 1958.

54. S. Saito and A. Azuma. A Numerical Appraoch to Co-Axial Rotor Aerodynamics. Seventh European Rotor craft and Powered Lift Aircraft Forum. Paper No 42. 1981.

55. W.Z. Stepniewski and L.H. Sloan. Some Thought on the

Optimisation of Transport Helicopters. Vertica, Vol 6, No 1. 1982.

56. V.P. Bailey. The Advancing Blade Concept (ABC) Rotor Program SAE Specialist Meeting, Los Angeles, 1977.

57. J. Scheiman. A Tabulation of Helicopter Rotor Blade Differential Pressures, Stresses and Motions in Forward Flight. NSAS TMS-952, March 1964.

58. V.G. Sekaran. A Free Wake Model for Predicting Rotor Wake and Blade Loads. University of Southampton, AASU Memo 82/1, Jan 1982.

59. C.V. Cook. Induced Flow Through a Helicopter Rotor in Forward Flight. Westland Helicopter Ltd, Research Paper 374, Jan 1980.

60. A.J. Landgrebe, R.B. Taylor, T.A. Egolf and J.C. Bennett. Helicopter Airflow and Wake Characteristics for Low Speed and Hovering Flight from Racket Interference Investigations. 37th Annual Forum of the American Helicopter Society, May 1981.

61. K. Kawachi. Extension of Local Momentum Theory to Hover in Rotor with Distorted Wake. Journal of Aircraft, Vol 19. No 7.

62. G.J. Bingham. The Aerodynamic Influences of Rotor Blade Airloads, Twist Taper and Solidity on Hover and Forward Flight Perfomance. 37th Annual Forum of the American Helicopter Society, May 1981.

63. W.R. Mantoy and J.B. Rorke. The Evolution of the Variable Geometry Rotor. Presented at Symposium on Rotor Technology of American Helicopter Society, Mideast Region, August 1976.

64. J.P. Jones. A Comparison of ABC and Conventional Rotors. Westland Helicopters Ltd, Research Paper No 385.

65. H. Lamb. Hydrodynamics. Cambridge, 1932.

66. I.A. Simons, R.E. Pacifico and J.P. Jones. The Movement, Structure and Breakdown of Trailing Vortices from a Rotor Blade. CAL/USAA Avlabs Symposium,June 1966.

67. R.L. Panton,W.L. Oberampf,N. Soskic. Flight Measurements of a Wing Tip Vortex. Journal of Aircraft, Volume 17,No 4, April,1980.

68. A.D. Zalay. Hot Wire and Vorticity Meter Wake Vortex Surveys. AIAA Journal,Volume 14,No 5,1976.

69. J.M. Pouradier and E. Horowitz. Aerodynamic Study of a Hovering Rotor. Presented at the Sixth European Rotorcraft and Powered Lift Forum. 1980.

70. J.D. Iversen, V.R. Corsiglia,D.R. Backus and R.A. Brickman Hot-Wire,Laser-Anemometer,and Force Measurements of Interacting Trailing Vortices. Journal of Aircraft,Volume 16, No 7, 1979.

APPENDIX 1

A1.0 Solution of the Vortex Turbulent Boundary Layer Analogy Energy Equation

The following solution, relevant to section 3.4 in the main text, is derived from a postulated work/energy theorem. That is, the work done by the blade in creating a trailing tip vortex is considered equal to the rotational kinetic energy within the vortex. Now, the elemental rotational kinetic energy $d\varepsilon$, of an air particle of mass dm, angular velocity w and at a radial distance r from the axis of rotation is given by:

$$d\varepsilon = \frac{1}{2}(wr)^2\, dm \qquad (A1.1)$$

where,

$$w = K/2\pi r^2 \qquad (A1.2)$$

$$dm = \rho 2\pi r dr \qquad (A1.3)$$

whence the energy per unit length $d\varepsilon$, becomes;

$$d\varepsilon = (\rho/4\pi) \int (K^2/r)dr \qquad (A1.4)$$

For the vortex core region,

$$K/\Gamma_{max} = A(r/c)^2 \qquad (A1.5) \qquad 0 \leq r \leq r_c$$

Substituting (A1.5) into (A1.4) yields a vortex core energy E_c of:

$$E_c = (\rho\, \Gamma_{max}^2\, A^2/(4\pi c^4)) \int_0^{r_c} r^3\, dr \qquad (A1.6)$$

$$E_c = (\rho\, \Gamma_{max}^2\, A^2\, r_c^4)/(16\pi c^4)$$

For the vortex logarithmic region,

$$K/\Gamma_{max} = B\ln(r/c) + C \qquad \text{(A1.7)} \qquad r_c \leq r \leq r_b$$

Substituting A1.7 into A1.4 yields a vortex logarithmic energy E_l of:

$$E_l = (\rho\,\Gamma_{max}^2/4\pi) \int_{r_c}^{r_l} \frac{1}{r} (B\ln(r/c) + C)^2\, dr$$

$$E_l = (\rho\Gamma_{max}^2/4\pi) \Bigg| B^2 \left|\frac{1}{3}\ln^3 r - \ln^2 r\ln c + \ln r\ln^2 c\right) + BC(\ln^2 r - 2\ln r\ln c + C^2\ln r \Bigg|_{r_c}^{r_l} \qquad \text{(A1.8)}$$

For the vortex defect region

$$K/\Gamma_{max} = 1 - \exp((Dr/c) + E) \qquad \text{(A1.9)} \qquad r_l \leq r \leq r_o$$

Substituting (A1.9) into (A1.4) yields a vortex defect energy E_d of:

$$E_d = (\rho\Gamma_{max}^2/4\pi) \int_{r_l}^{r_o} \frac{1}{r} (1 - \exp((Dr/c) + E))^2\, dr \qquad \text{(A1.10)}$$

Now

$$\int_{r_l}^{r_o} \frac{1}{r} (1 - \exp((Dr/c) + E))^2 dr = \int_{r_l}^{r_o} \frac{1}{r} (1 - 2\exp((Dr/c) + E) + \exp2((Dr/c) + E))dr \qquad \text{(A1.11)}$$

where,

$$\int_{r_l}^{r_o} \frac{1}{r}\, dr = \Big|\ln r\Big|_{r_l}^{r_o} \qquad \text{(A1.12)}$$

and

$$-\int_{r_1}^{r_o} (2\exp(Dr/c + E)/r)dr = -\,2\exp(E) \int_{r_1}^{r_o} (\exp(Dr/c)/r)dr \qquad (A1.13)$$

similarly,

$$\int_{r_1}^{r_o} (\exp 2(D\,r/c + E)/r)dr = \exp(2E) \int_{r_1}^{r_o} (\exp 2(Dr/c)/r)dr \qquad (A1.14)$$

Integrals (A1.13) and (A1.14) are solved using the expansion

$$\int (e^{ax}/x)dx = \left(\ln x + \frac{ax}{1x1!} + \frac{(ax)^2}{2x2!} + \frac{(ax)^3}{3x3!} \cdots \frac{(ax)^m}{mxm!} \right) \qquad (A1.15)$$

Whence, using (A1.12-A1.15) and substituting into (A1.10) yields:

$$E_d = (\rho \Gamma_{max}^2/4\pi) \Bigg| \ln r + \exp(2E)\left(\ln r + \sum_{1}^{m} (2Dr/c)^m/(mxm!)\right)$$

$$- 2\exp(E)\left(\ln r + \sum_{1}^{m} (Dr/c)^m/(mxm!)\right)\Bigg|_{r_1}^{r_o} \qquad (A1.16)$$

The total rotational vortex energy per unit length E_v, is given by

$$E_v = E_c + E_1 + E_d$$

where E_c E_1 and E_d are computed from equations (A1.6) (A1.8) and (A1.16) respectively.

APPENDIX 2

A2.0 Salient Hover Equations

The axes system used throughout are given in Figure 56. However, exceptions to this axes set are the downwash velocity V_c, and vortex induced 'apparent vertical ascent' velocity V_v, where a positive magnitude indicates flow passing down through the rotor. Blade numbering commences with blade 1 located in the upper rotor at zero degrees of azimuth, blade 2, 3 etcfollowing in an anticlockwise manner until the number of upper rotor blades have been reached. Therefore, the next blade number $(b_u + 1)$ refers to a specified lower rotor blade with remaining blades being indentified in a clockwise manner.

Using the well known strip equation (15) on initial estimate of the induced flow through the upper rotor is given by,

$$V_{im} = \left(\frac{V_c}{2} + \frac{\sigma_r awR}{16} \right) \left(-1 + \left(1 + \frac{2(\theta rw - V_c)}{\frac{4V_c}{\sigma_r waR} + V_c + \frac{\sigma_r awR}{16}} \right)^{\frac{1}{2}} \right)$$

(A2.1)

where initially $V_c = 0$.

Blade elemental thrust is computed at 14 separate station points of elemental span dr, where

$$dr = .1R \qquad r \leq 0.9R \qquad \text{(9 inboard station points)} \qquad \text{(A2.2)}$$

$$dr = .02R \qquad 0.9R < r \leq R \qquad \text{(5 tip station points)} \qquad \text{(A2.3)}$$

and elemental thrust dT,

$$dT = \frac{1}{2} \rho V^2 c_l c \cos\phi \, dr \qquad (A2.4)$$

$$V = V_T$$

$$c_l = a (\theta - \phi) \frac{1}{\sqrt{1 - M^2}} \qquad (A2.5)$$

$$\phi = \frac{v_i + v_v}{wr} \qquad (A2.6)$$

(again v_v initially being 0)

Total thrust T, is then evaluated,

$$T = b \times \sum_{m=1}^{14} dT_m \qquad (A2.7)$$

and corrected using a tip loss factor of,

$$B = 1 - \sqrt{2.0 C_T/b} \qquad (A2.8)$$

to yield an initial estimate of the thrust coefficient.

$$C_T = T/\rho V_T^2 \, 2\pi R^2 \qquad (A2.9)$$

Thereafter, Landgrebe (31) prescribed wake coefficients a_1, a_2 and a_3 are used to determine the tip vortex paths,

$$a_1 = -0.25 (C_T/\sigma) \qquad (A2.10)$$

$$a_2 = -1.41 \sqrt{C_T/2} \qquad (A2.11)$$

$$a_3 = 0.145 + (27 * C_T) \qquad (A2.12)$$

yielding vertical z_v and radial r_v coordinates of the tip vortex limits via,

$$z_v = a_1 wt \qquad wt < 2\pi/b \qquad (A2.13)$$

$$z_v = a_1 2\pi/b + a_2(wt - 2\pi/b) \qquad wt \geq 2\pi/b \qquad (A2.14)$$

$$r_v = 0.78 + 0.22 \exp(-a_3 wt) \qquad (A2.15)$$

The upper rotor is then stepped around the disc by predefined azimuth steps $\Delta\psi$, producing straight line vortex filaments lying on the paths described by equations A3.13 - A3.15.

On reaching the required number of rotor revolutions, the apparent vertical ascent velocity V_v, from the upper rotor wake is computed using equation A2.38. Thereafter, the aforementioned procedures are repeated with $V_c = v_v$ and continue with an initial estimate of the upper rotor performance via

$$\text{Elemented induced drag} \quad dD_i = dL \sin\phi \tag{A2.16}$$

$$\text{Elemented profile drag} \quad dD_p = \frac{1}{2} \rho V^2 C_{do} c\, dr$$

$$\text{where} \quad C_{do} = 0.0087 - 0.0216\, \alpha_r + 0.400\, \alpha_r^2 \tag{A2.17}$$

Total blade thrust T is given by

$$T = b \left(\sum_{m=1}^{m=14} dL \cos\phi_m + \sum_{m=1}^{14} dD_p \sin\phi \right) \tag{A2.18}$$

and rotor torque Q by

$$Q = b \left(\sum_{m=1}^{14} dD_p \cos\phi\, r_m + \sum dL \sin\phi\, r_m \right) \tag{A2.19}$$

The procedures are repeated as described in Chapter 4, 4.3 with the inclusion of interference effects , evaluating thrust and torque on the lower and upper rotors until convergence has been achieved. The final inflow, computations use the extended Stepniewski equation 4.13, given in Chapter 4.

A2.1 Salient Forward Flight Equations

As with the previous section, the following equations are presented for the general case and only were necessary are the computational differences between the upper and lower rotors highlighted. Resulting from the opposite rotations of the two rotors in the CCTR, sign changes can occur. These changes are shown by (±) where the top and bottom signs refer to upper and lower rotors respectively. A single sign indicates no change occurs when transferring from one rotor to the other.

Glauerts approximation for the mean induced downwash $\bar{v}_i$ yields

$$\bar{v}_i = T/(2\rho AV') \tag{A2.20}$$

where $V' = \sqrt{V^2 + (\overline{v_i + v_v})^2}$ (A2.21)

whence substituting (A2.21) into (A2.20) yields

$$\overline{v_i}^4 + 2\bar{v}_v\overline{v_i}^3 + v_i^2\left(V^2 + v_v^2\right) - \left(T^2/(4\rho^2A^2)\right) = 0 \tag{A2.22}$$

The quartic equation in $\overline{v_i}$ is solved by using a NAG computer library routine named COZAEF.

Initial condition are set by

$$T = (\theta/3 + \mu^2\theta/2 + \lambda/2)\tfrac{1}{2}\rho\, abc\, \Omega^2R^3 \tag{A2.23}$$

$$v_v = 0.0$$

and defining

advance ratio $\mu = V\cos\alpha/\Omega R$ (A2.24)

inflow ratio $\lambda = (V\sin\alpha + v_v - v_i)/\Omega R$ (A2.25)

Subsequent $\overline{v_i}$ computations are performed throughout the program when the tip vortex wake effects are known.

Using the initial estimates of $\overline{v_i}$, λ and μ the source program computes the flapping characteristics of the blades around the disc. Using the coordinate system shown in Figure 56, where the top and bottom rotors have positive and negative rotations respectively. Simple flapping theory (1) yields,

$$\beta = a_o - a_1 \cos\psi \mp b_1 \sin\psi \qquad \text{(A2.26)}$$

$$d\beta/dt = \Omega(\mp a_1 \sin\psi - b_1 \cos\psi) \qquad \text{(A2.27)}$$

where the flapping coefficients are given by equations (5.10) - (5.12), presented in Chapter 5.

The rotors are stepped around the disc with the trailing tip vortex filaments coordinates being generated with respect to the no-feathering axes, the origin of which is located at the centre of the upper rotor. Two options are possible for computing the vortex filament positions.

1) Classical Wake

The velocity and subsequent position of the jth vortex filament station from the kth blade is given by the local flow conditions without considering the interactions between filaments, namely.

$$x_{v_{j=1}} = - \sin\psi_k \cos\beta_k \qquad \text{(A2.28)}$$

$$y_{v_{j=1}} = + \cos\psi_k \cos\beta_k \qquad \text{(A2.29)}$$

$$z_{v_{j=1}} = \sin\beta_k \qquad \text{(A2.30)}$$

for $k > b_u$, $z_{v_{j=1}} = \sin\beta_k - (d/R)$

where $v_x = 0.0$ (A2.31)

$$v_y = V \cos\alpha \qquad \text{(A2.32)}$$

$$V_z = V \sin\alpha - v_i \qquad \text{(A2.33)}$$

Subsequent j filament positions are computed for k blades via.

$$\sum_{k=1}^{k=b_u+b_b} \sum_{i=2}^{m} x_v = \sum_{k=1}^{k=b_u+b_l} \left(\sum_{j=2}^{j=m} x_{v_{j-1}} + \sum_{j=z}^{j=m} V_{x_{j-1}} \Delta t/R \right) \qquad \text{(A2.34)}$$

where $\Delta t = \frac{\Delta\psi}{\Omega}$ (A2.35)

(similar summations for y_v and z_v)

2) Free-wake

Using this facility, the interaction between the vortex filaments is computed using the Biot-Savart Law. The salient equations used in subroutine IND, with suffixes a b and p representing the vortex filaments end points (a,b) and a general point (p) respectively:-

$$v_{vx} = \pm \frac{K_o C}{4\pi} \left(\left(\left(y_p - y_a \right) \left(z_p - z_b \right) \right) - \left(\left(z_p - z_a \right) \left(y_p - y_b \right) \right) \right) \qquad \text{(A2.36)}$$

$$v_{vy} = \pm \frac{K_o C}{4\pi} \left(\left(\left(z_p - z_a \right) \left(x_p - x_b \right) \right) - \left(\left(x_p - x_a \right) \left(z_p - z_b \right) \right) \right) \qquad \text{(A2.37)}$$

$$v_{vz} = \pm \frac{K_o C}{4\pi} \left(\left(\left(x_p - x_a \right) \left(y_p - y_b \right) \right) - \left(\left(y_p - y_a \right) \left(x_p - x_b \right) \right) \right) \qquad \text{(A2.38)}$$

where, $C = (AP + BP)/((AP \times BP)R((AP \times BP + I + J + K)$ (A2.39)

and, $I = (x_p - x_a)(x_p - x_b)$ (A2.40)

$J = (p_p - y_a)(y_p - y_b)$ (A2.41)

$K = (z_p - z_a)(z_p - z_b)$ (A2.42)

For the Rankine vortex, the strength K is given by:-

$$K = \oint_0^{2\pi} q \cos\alpha \, ds \tag{A2.43}$$

where for the vortex core $q = V_s$, $ds = r_c d\alpha$

yielding $K_c = 2\pi V_s r_c$ (A2.44)

From Chapter 3, V_s and r_c are given by:-

$$V_s = V_T' (1.0 + 6.6/A_r) \, 2.64 \times 10^{-2}\theta \qquad (\theta \text{ in degrees}) \tag{A2.45}$$

$$r_c = 1.2R_e^{-0.2} V_s c/V_T' \tag{A2.46}$$

where V_T' is the local tip speed given by;

$$V_T' = \Omega R + V\sin\psi \tag{A2.47}$$

Note that for the forward flight case the strength of the vortex filaments vary around the disc. For computational purposes the average strength between the two filament end points is set equal to the strength of the filament. The velocity induced on the j^{th} station on the k^{th} vortex helix is given by:-

$$V_{vx_j} = \sum_{l=1}^{l=b_u+b_l} \sum_{m=l}^{m=n-1} V_{vx_{ml}} \tag{A2.48}$$

where n = number of stations per helix.

When $k = 1$, $V_{vx_{m=j}}$, $V_{vx_{m=j-1}}$, $V_{vx_{m=j+1}} = 0$

Similarly for V_{vy} and V_{vz}.

Further

$$v_i = \overline{\overline{v_i}} \, (1 + \bar{r} \cos\psi) \tag{A2.49}$$

where $$\overline{\overline{v_i}} = \overline{\overline{v_i}} \, (V_{vz \; \bar{r}=0}) \tag{A2.50}$$

The wake is continually stepped around the disc until the desired number of stations have been reached for the classical wake, or until wake convergence is satisfied for the free-wake. The user of the program ROTOR may determine wake convergence by either comparing filament locations for consecative revolutions of the disc, or by comparing the tip vortex induced velocity distribution for various blade locations. To compute the tip vortex induced values along the blade, a transfer of axes from the no feathering plane to axes inserting in and rotating with a given blade, is performed.

The transformation is given by

$$x_b = x_{nf} \cos\psi + y_{nf} \sin\psi \tag{A2.51}$$

$$y_b = (y_{nf} \cos\psi - x_{nf} \sin\psi) \cos\beta + z_{nf} \sin\beta \tag{A2.52}$$

$$z_b = z_{nf} \cos\beta - (y_{nf} \cos\psi - x_{nf} \sin\psi) \sin\beta \tag{A2.53}$$

$$(\text{if} \quad k > b_u \qquad z_{nf} = z_{nf} + d/R)$$

Using coordinate system (x_b , y_b , z_b),

$$v_v = V_{vz} \tag{A2.54}$$

The total velocities at any blade element radial station r is given by:-

Upper rotor

Perpendicular blade velocity U_p,

$$U_{pu} = (V \sin\alpha - v_{iu})\cos\beta - r\frac{d\beta}{dt} - V\cos\alpha\cos\psi\sin\beta + V_{vz} \qquad (A2.55)$$

Tangential blade velocity U_t

$$U_{tu} = \Omega r + V\cos\alpha\sin\psi \qquad (A2.56)$$

For the lower rotor immersed in the upper rotor wake

$$U_{pl} = (V\sin\alpha - 2v_{iu})\cos\beta - r\frac{d\beta}{dt} - V\cos\alpha\cos\psi\sin\beta + V_{vz} \qquad (A2.57)$$

$$U_{tl} = \Omega r + V\cos\alpha\sin\psi \qquad (A2.58)$$

For the sections of the lower rotor taking in clear air,

$$U_{pl} = (V\sin\alpha - v_{il})\cos\beta - r\frac{d\beta}{dt} - V\cos\alpha\cos\psi\sin\beta + V_{vz} \qquad (A2.59)$$

At each blade station, the blade lift, drag and H-force is computed via:-

$$\text{Elemental lift} \quad dl = \frac{1}{2}\rho U^2 c_l c\,\Delta r \qquad (A2.60)$$

$$\text{where} \quad c_l = a(\theta + (U_p/U_r)) \qquad (A2.61)$$

$$\text{Elemental induced drag} \quad dD_i = dL\sin\phi \qquad (A2.62)$$

$$\text{Elemental profile drag} \quad dD_p = \frac{1}{2}\rho c U^2 c_{do}\Delta r \qquad (A2.63)$$

$$\text{where} \quad c_{do} = 0.0087 - 0.0216\,\alpha_r + 0.400\,\alpha_r^2 \qquad (A2.64)$$

$$\text{Elemental drag} \quad dD = dD_p + dD_i \qquad (A2.65)$$

Elemental H-force dH,

$$dH = (dD_p \cos\phi - dL \sin\phi)\sin\psi - (dL \cos\phi + dD \sin\phi) \sin\beta \cos\psi \qquad (A2.66)$$

Total blade thrust T_b is given by

$$T_b = \left(\sum_{m=1}^{m=14} dL \cos\phi_m + \sum_{m=1}^{m=14} dD_p \sin\phi \right) \cos\beta \qquad (A2.67)$$

and blade torque Q_b by

$$Q_b = r \cos\beta \left(\sum_{m=1}^{m=14} dD_p \cos\phi - \sum_{m=1}^{m=14} dL \sin\phi \right) \qquad (A2.68)$$

Total rotor thrust T, torque Q, power P and H-force H is given by:-

$$T = \sum_{b=1}^{b_u+b_l} T_b \qquad (A2.69)$$

$$Q = \sum_{b=1}^{b_u+b_l} Q_b \qquad (A2.70)$$

$$P = Q \times \Omega \qquad (A2.71)$$

$$H = \sum_{b=1}^{b_u+b_l} H_b \qquad (A2.72)$$

APPENDIX 3

3.0 Input procedure

```
*****************************************
*                                       *
*                                       *
*            PROGRAM ROTOR              *
*                                       *
*                                       *
*****************************************
```

THE PROGRAM CALCULATES THE HOVER AND FORWARD FLIGHT PERFORMANCE OF EITHER A SINGLE OR TWIN COAXIAL ROTOR LAYOUT. BEFORE RUNNING THE PROGRAM A NUMBER OF QUESTIONS ARE FIRST POSED. TO ANSWER EITHER INPUT A Y FOR YES OR AN N FOR NO,FOLLOWED BY THE REQUESTED DATA.

***** INPUT ALL LENGTHS IN METRES *****

DO YOU REQUIRE THE PERFORMANCE OF A SINGLE ROTOR?

/-N

THE TWO ROTORS IN A TWIN CONFIGURATION ARE LABELLED UPPER AND LOWER ROTOR RESPECTIVELY.

***** ALL PROCEEDING INPUTS ARE FOR THE UPPER ROTOR UNLESS OTHERWISE STATED. *****

INPUT NUMBER OF BLADES

/-2.0

INPUT ROTOR RADIUS

/-0.76

ARE THE BLADES TAPERED?

/-Y

EACH BLADE IS DIVIDED UP INTO 9 INBOARD ELEMENTS AND 5 TIP ELEMENTS.EACH INBOARD ELEMENT SPANS 0.1R,STARTING AT THE ROOT.EACH TIP ELEMENT SPANS 0.02R,STARTING AT 0.9R.INPUT THE MIDPOINT CHORD OF EACH ELEMENT STARTING AT THE ROOT END.(14 CHORDS IN ALL)

I.E. THE CHORD AT 0.05R,0.15R.....0.85R,0.91R,0.93R 0.99R

/-0.12 0.11 0.10 0.09 0.08 0.07 0.06 0.05 0.04 0.038 0.036

/-0.034 0.032 0.03

Input procedure continued

```
ARE THE BLADES TWISTED?
/-Y
INPUT EACH MIDPOINT BLADE ELEMENT PITCH,STARTING
AT THE ROOT END.(14 PITCHES IN ALL)
/-12.0 11.0 10.0 9.0 8.0 7.0 6.0 5.0 4.0 3.8 3.6 3.4
/-3.2 3.0
INPUT ROTOR RPM
/-440.0
INPUT MASS OF BLADE IN KG
/-1.5
DO YOU REQUIRE A FORWARD FLIGHT COMPUTATION?
/-Y
INPUT FORWARD FLIGHT VEL IN M/S
/-5.0
INPUT ROTOR SHAFT ANGLE OF ATTACK,ALPHA,IN DEGS
/--3.0
DO YOU WANT TO INCLUDE VORTEX ROLL-UP?
/-Y
HOW MANY WAKE REVOLUTIONS DO YOU REQUIRE?
INPUT AN INTEGER:
/-2
INPUT FILAMENT INCREMENT (INTEGER) IN DEGS OF AZIMUTH
/-20
***** ALL PROCEEDING INPUTS ARE FOR THE LOWER ROTOR *****
INPUT NUMBER OF ROTOR BLADES
/-2.0
INPUT ROTOR RADIUS
/-0.76
ARE THE BLADES TAPERED
/-N
INPUT BLADE CHORD
/-0.054
ARE THE BLADES TWISTED?
/-N
```

Input procedure continued

INPUT BLADE PITCH IN DEGREES

/-7.5

INPUT ROTOR RPM

/-440.0

INPUT MASS OF BLADE IN KG

/-1.35

INPUT VERTICAL SEPARATION BETWEEN ROTORS

/-0.196

3.1 Program ROTOR listing

```
LINE NUMBER    FORTRAN TEXT

    1                REAL MASSU,MASSL,MUU,MUL,LANDAU,LANDAL,LOCKU,LOCKL,MU
    2                REAL KC,KL,KO,MACHNO,MACHNOU,MACHNOL,KU,KLOW
    3                REAL LANDIU,LANDIL
    4                INTEGER YES,TOTALSTP,DELTAZIM
    5                DIMENSION HF(40),HFORCE(40),HFORCEU(40),HFORCEL(40)
    6                DIMENSION XPT(40),YPT(40),ZIN(100,20),YIN(100,20),ZI(100)
    7                DIMENSION YI(100),ZIF(100),YIF(100),VMOM(40),VFLAP(40)
    8                DIMENSION THRUSTU(40),TORQUEU(40),THRUSTL(40),TORQUEL(40)
    9                DIMENSION XFVT(100,20),YFVT(100,20),ZFVT(100,20),ZFV1(100,20)
   10                DIMENSION THETAR(40),CHORDR(40),BSR(40)
   11                DIMENSION VELFV(100,20),VELFVT(100,20),THI(40),UTI(40),THRUST(40)
   12               C,UP(100,20),UT(100,20),TORQUE(40),TH(40),TOR(40),RADB(40)
   13                DIMENSION XFVNEW(100,20),YFVNEW(100,20),ZFVNEW(100,20)
   14                DIMENSION XVEL(100,20,20),YVEL(100,20,20),ZVEL(100,20,20)
   15                DIMENSION CIRV(100,20)
   16                DIMENSION TIME(20),RAD(20),EPSI(100,20),BETA(100,20)
   17                DIMENSION DBETA(100,20),XFV(100,20),YFV(100,20),ZFV(100,20)
   18                DIMENSION XVELT(100,20),YVELT(100,20),ZVELT(100,20)
   19                DIMENSION THETAL(40),CHL(40),VINU(40),VECMUL(40),XLDU(40)
   20                DIMENSION YLDU(40),ZLDU(40),VECUL(40),VIL(40),THLO(40)
   21                DIMENSION BSL(40),XVL(100,20),YVL(100,20),ZVL(100,20),VVUL(100,20)
   22                DIMENSION CIRL(100,20),VECL(40),VVL(100,20),VITL(40),THL(40)
   23                DIMENSION XVU(100,20),YVU(100,20),ZVU(100,20),VVU(100,20)
   24                DIMENSION CIRU(100,20),CU(40),BSU(40),XP(40),YP(40)
   25                DIMENSION ZP(40),VECU(40),VIU(40),THETAU(40),VIT(40),THU(40)
   26                DIMENSION TORL(40),THEO(40),TORU(40),NO(1),TOT(40)
   27                DIMENSION RC1(2000),RCD1(2000)
   28                DIMENSION RCU(2000),RCDU(2000),RCL(2000),RCDL(2000)
   29                DIMENSION VORTEXA(100,20),VORTEXB(100,20),VORTEXC(100,20)
   30               C,VORTEXD(100,20),VORTEXE(100,20),VORTEXKC(100,20)
   31               C,VORTEXKL(100,20),VORTEXKO(100,20),VORTEXRC(100,20)
   32               C,VORTEXRL(100,20),VORTEXRO(100,20)
   33               C,XVL1(100,20),YVL1(100,20),ZVL1(100,20),VVLU(100,20),VVI(40)
   34               C,VECUI(40),VIUI(40),VITI(40),THUI(40),TORUI(40)
   35                COMMON/BL2/ A1,A2,A3
   36                COMMON/BL5/ W,ALPHA,V
   37                COMMON/BL9/ VA,VB,VC,VD,VE
   38                COMMON/BL21/ TOTALSTP,NFILASTP
   39                COMMON/BL22/ BET,A7M,SIGN
   40                COMMON/BL25/ VSOU,RCU
   41                CALL ICL9HEMASK(64,I)
   42                DATA A/5.7J/,NTYPV/0/
   43                DATA NO/1HN/,M7/1HN/
   44                DATA YES/1HY/
   45                DATA VIS,ROE,PI/1.455E-5,1.225,3.1415927/
   46                DATA M/12/
   47                DATA EU/0.5/,EL/0.5/
   48                WRITE(6,5)
   49             5  FORMAT('          **********************************')
   50                WRITE(6,6)
   51             6  FORMAT('          *                                *')
   52                WRITE(6,7)
   53             7  FORMAT('          *          PROGRAM ROTOR         *')
   54                WRITE(6,6)
   55                WRITE(6,5)
   56                WRITE(6,10)
```

```
LINE NUMBER     FORTRAN TEXT

   57              1    FORMAT(/,'THE PROGRAM CALCULATES THE HOVER AND FORWARD FLIGHT')
   58                   WRITE(6,11)
   59              11   FORMAT('PERFORMANCE OF EITHER A SINGLE OR TWIN COAXIAL ROTOR')
   60                   WRITE(6,15)
   61              15   FORMAT('LAYOUT.BEFORE RUNNING THE PROGRAM ROTOR A NUMBER OF')
   62                   WRITE(6,18)
   63              18   FORMAT('QUESTIONS ARE FIRST POSED.TO ANSWER EITHER INPUT A  Y')
   64                   WRITE(6,20)
   65              20   FORMAT('FOR YES OR AN  N  FOR NO,FOLLOWED BY THE REQUESTED DATA.
   66                  C')
   67                   WRITE(6,21)
   68              21   FORMAT(/'***INPUT ALL LENGTHS IN METRES***'/)
   69              29   WRITE(6,30)
   70              30   FORMAT(//'DO YOU REQUIRE THE PERFORMANCE OF A SINGLE ROTOR?.')
   71                   READ(5,35)M1
   72              35   FORMAT(1A4)
   73                   IF(M1.EQ.YES) GOTO 65
   74                   WRITE(6,50)
   75              50   FORMAT('THE TWO ROTORS IN A TWIN CONFIGURATION ARE LABELLED')
   76                   WRITE(6,52)
   77              52   FORMAT('UPPER ROTOR AND LOWER ROTOR.')
   78                   WRITE(6,55)
   79              55   FORMAT('THE UPPER ROTOR CENTRE IS ALWAYS SITUATED AT THE')
   80                   WRITE(6,58)
   81              58   FORMAT('REFERENCE AXES ORIGIN')
   82                   WRITE(6,60)
   83              60   FORMAT(/'*** ALL PROCEEDING INPUTS ARE FOR THE UPPER ROTOR')
   84                   WRITE(6,63)
   85              63   FORMAT('UNLESS OTHERWISE STATED ***'/)
   86              65   WRITE(6,70)
   87              70   FORMAT('INPUT NUMBER OF ROTOR BLADES')
   88                   READ(5,*)BU
   89                   IF(M1.EQ.YES) NOBLADES=IFIX(BU+0.2)
   90                   NBU=IFIX(BU+0.2)
   91                   WRITE(6,75)
   92              75   FORMAT('INPUT ROTOR RADIUS')
   93                   READ(5,*)RU
   94                   WRITE(6,80)
   95              80   FORMAT('ARE THE BLADES TAPERED?.')
   96                   READ(5,35)M2
   97                   IF(M2.EQ.YES) GOTO 100
   98                   WRITE(6,90)
   99              90   FORMAT('INPUT BLADE CHORD')
  100                   READ(5,*)C
  101                   DO 95 I=1,14
  102                   CU(I)=C
  103              95   CONTINUE
  104                   CAVU=CU(8)
  105                   GOTO 128
  106             100   WRITE(6,105)
  107             105   FORMAT('EACH BLADE IS DIVIDED UP INTO 9 INBOARD ELEMENTS AND 5')
  108                   WRITE(6,106)
  109             106   FORMAT('TIP ELEMENTS')
  110                   WRITE(6,110)
  111             110   FORMAT('EACH INBOARD ELEMENT SPANS 0.1R,STARTING AT THE ROOT')
  112                   WRITE(6,112)
```

```
LINE NUMBER    FORTRAN TEXT

 113           112 FORMAT('END.EACH TIP ELEMENT SPANS ).02R,STARTING AT 0.9R.')
 114               WRITE(6,115)
 115           115 FORMAT('INPUT THE MIDPOINT CHORD OF EACH SEGMENT,STARTING AT')
 116               WRITE(6,118)
 117           118 FORMAT('ROOT END.(14 CHORDS IN ALL).')
 118               WRITE(6,125)
 119           125 FORMAT('I.E. THE CHORD AT 0.05R,0.15R,....0.75R,0.85R,0.91R,')
 120               WRITE(6,126)
 121           126 FORMAT('0.93R,....0.99R')
 122               READ(5,*)(CU(I),I=1,14)
 123               CAVU=CU(8)
 124           128 WRITE(6,130)
 125           130 FORMAT('ARE THE BLADES TWISTED?.')
 126               READ(5,35)M3
 127               IF(M3.EQ.YES) GOTO 148
 128               WRITE(6,140)
 129           140 FORMAT('INPUT BLADE PITCH IN DEGREES')
 130               READ(5,*) THETA
 131               DO 145 I=1,14
 132               THETAU(I)=THETA*PI/180.0
 133           145 CONTINUE
 134               THETAVU=THETAU(8)
 135               GOTO157
 136           148 IF(M2.EQ.YES) GOTO 150
 137               WRITE(6,105)
 138               WRITE(6,106)
 139               WRITE(6,110)
 140               WRITE(6,112)
 141           149 FORMAT('THE ROOT END.(14 PITCHES IN ALL).')
 142           150 WRITE(6,155)
 143               WRITE(6,149)
 144           155 FORMAT('INPUT EACH MIDPOINT BLADE ELEMENT PITCH,STARTING AT')
 145               READ(5,*)(THETAU(I),I=1,14)
 146               DO 170 K=1,14
 147               THETAU(K)=THETAU(K)*PI/180.0
 148           170 CONTINUE
 149               THETAVU=THETAU(8)
 150           157 THETASW=THETASW*PI/180.0
 151               WRITE(6,158)
 152           158 FORMAT('INPUT ROTOR RPM')
 153               READ(5,*) OMEGAU
 154               WU=OMEGAU*PI/30.0
 155               DO 200 K=1,14
 156               BSU(K)=(BU*CU(K))/(PI*RU)
 157               VECU(K)=0.0
 158           200 CONTINUE
 159               BS=BSU(8)
 160               DO 210 K=1,9
 161               XP(K)=0.0
 162               YP(K)=(0.05*K)+((K-1)*0.05)
 163               ZP(K)=0.0
 164           210 CONTINUE
 165               DO 215 K=10,14
 166               XP(K)=0.0
 167               YP(K)=YP(9)+0.05+((K-9)*0.01)+((K-10)*0.01)
 168               ZP(K)=0.0
```

```
LINE NUMBER    FORTRAN TEXT

  169            215 CONTINUE
  170                VTU=WU*RU
  171                MACHNOU=VTU/340.0
  172                REU=VTU*CU(8)/VIS
  173                ARU=RU/CU(8)
  174           C    CALCULATION OF VORTEX MAX SWIRL VEL AND CORE RADIUS.
  175                VSOU=(1.0+(6.6/ARU))*(2.64E-2)*THETAU(12)*VTU*180.0/PI
  176                RCOU=CU(12)*1.2*(REU**(-0.2))*VSOU/VTU
  177                WRITE(6,5022)
  178             5022 FORMAT('INPUT MASS OF BLADE IN KG')
  179                READ(5,*) MASSU
  180                WRITE(6,216)
  181              216 FORMAT('DO YOU REQUIRE A FORWARD FLIGHT COMPUTATION?')
  182                READ(5,35) M6
  183                NAA=2
  184                IF(M6.EQ.YES) NAA=1
  185                IF(NAA.EQ.2) GOTO 5364
  186                WRITE(6,5021)
  187             5021 FORMAT('INPUT FORWARD FLIGHT VEL. IN M/S')
  188                READ(5,*) V
  189                WRITE(6,5472)
  190             5472 FORMAT('INPUT ROTOR SHAFT ANGLE OF ATTACK,ALPHA,IN DEGS')
  191                READ(5,*) ALPHA
  192             5364 WRITE(6,219)
  193              219 FORMAT('DO YOU WANT TO INCLUDE VORTEX ROLL-UP?')
  194                READ(5,35) M51
  195                WRITE(6,217)
  196              217 FORMAT('HOW MANY WAKE REVOLUTIONS DO YOU REQUIRE?')
  197                WRITE(6,218)
  198              218 FORMAT('INPUT AN INTEGER:')
  199                READ(5,*) NREV
  200                WRITE(6,701)
  201              701 FORMAT('INPUT FILAMENT INCREMENT(INTEGER) IN DEGS OF AZIMUTH')
  202                READ(5,*) DELTAZIM
  203                ALPHA=ALPHA*PI/180.0
  204                NFILASTP=(360/DELTAZIM)+1
  205                TOTALSTP=(NREV*(NFILASTP-1))+1
  206                IF(M6.EQ.YES) GOTO 409
  207                CALL STRIP(VECU,YP,TOT,CTU,VIU,RU,THETAU,CU,BSU,BU,A,WU)
  208                CALL LANDG(XVU,YVU,ZVU,CTU,BU,BS,RU)
  209                IF(NBU.EQ.1) GOTO 221
  210                DO 220 K=2,NBU
  211                CALL BLVOCO(XVU,YVU,ZVU,BU,K)
  212              220 CONTINUE
  213              221 WRITE(6,222)VSOU,RCOU
  214              222 FORMAT('VSU=',1F8.4,'M/S, RCU=',1F8.4,'M')
  215                NCOUNT=1
  216              223 DO 230 K=1,NBU
  217                CALL CAL(XVU,YVU,ZVU,XP,YP,ZP,1,VVU,0,RU,BU,K,KC,KL,KO,RCU
  218               C,VRL,RO,VA,VB,VC,VD,VE,NCOUNT,GAMAXU,RCOU,VSOU,CAVU,NTYPV
  219               C,SIGN,1,CIRV)
  220              230 CONTINUE
  221                DO 240 K=1,14
  222                VECU(K)=VVU(K,1)
  223              240 CONTINUE
  224                IF(NBU.EQ.1) GOTO 251
```

```
LINE NUMBER    FORTRAN TEXT

 225                DO 250 K=2,NBU
 226                DO 251 J=1,14
 227                VECU(J)=VECU(J)+VVU(J,K)
 228             250 CONTINUE
 229             251 WRITE(6,*)(VECU(L),L=1,14)
 230                 CALL STRIP(VECU,YP,TOT,CTU,VIU,RU,THETAU,CU,BSU,BU,A,WU)
 231                 DO 260 K=1,14
 232                 VIT(K)=VECU(K)+VIU(K)
 233             260 CONTINUE
 234                 WRITE(6,5561)
 235            5561 FORMAT('TOTAL DOWNWASH DISTRIBUTION(VIT) ON UPPER ROTOR IS:')
 236                 WRITE(6,*)(VIT(L),L=1,14)
 237                 CALL PERM(VIT,YP,THU,TORU,THEO,RU,THETAU,CU,BSU,BU,ENU,GAMAXU
 238                C,A,WU,THI,1,UTI,HF)
 239                 KC=2.0*PI*VSOU*RCUU
 240                 ENU=ENU*(KC/GAMAXU)**2
 241                 WRITE(6,7033) ENU
 242            7033 FORMAT('ENU=',1F10.4)
 243                 WRITE(6,*)(THU(14),TORU(14))
 244                 CTU=(BU*THU(14))/(ROE*(WU*RU)**2*PI*RU**2)
 245                 CQU=(RU*TORU(14))/(ROE*(WU*RU)**2*PI*RU**3)
 246                 WRITE(6,600) CTU
 247             600 FORMAT(' ','THRUST COEFF,CTU,FOR UPPER ROTOR IS:',1F8.6)
 248                 WRITE(6,2) CQU
 249               2 FORMAT(' ','TORQUE COEFF. FOR UPPER ROTOR IS:',1F10.8)
 250                 IF(NCOUNT.EQ.2) GOTO 409
 251                 CALL TIPVOR(ENU,GAMAXU,VTU,ARU,CAVU,THETAVU,THETASW,REU,KC
 252                C,KL,KO,VRL,RO,NTYPV,MACHNOU)
 253                 IF(KC.GT.GAMAXU) GOTO 8041
 254                 GOTO 8042
 255            8041 VSOU=VSOU*GAMAXU/KC
 256                 KC=GAMAXU
 257            8042 CALL DECAY(RCOU,VSOU,WU,RU,RCU,RCOU,BU,ENU)
 258                 DO 261 J=1,TOTALSTP
 259                 NVAR1=(DELTAZIM*(J-1))+1
 260                 NVAR2=(DELTAZIM*J)+1
 261                 RCU(J)=(RCU(NVAR1)+RCU(NVAR2))/2.0
 262             261 CONTINUE
 263                 N21=1
 264                 NCOUNT=2
 265                 GOTO 223
 266           C     START OF LOWER ROTOR COMPUTATION.
 267           C
 268             409 IF((M1.EQ.YES).AND.(M6.EQ.YES)) GOTO 1510
 269                 IF(M1.EQ.YES) GOTO 580
 270             408 WRITE(6,410)
 271             410 FORMAT(/'*** ALL PROCEEDING INPUTS ARE FOR THE LOWER ROTOR ***'/)
 272                 WRITE(6,70)
 273                 READ(5,*) BL
 274                 NBL=IFIX(BL+0.2)
 275                 WRITE(6,75)
 276                 READ(5,*) RL
 277                 WRITE(6,80)
 278                 READ(5,35) M2
 279                 IF(M2.EQ.YES) GOTO 420
 280                 WRITE(6,90)
```

```
LINE NUMBER    FORTRAN TEXT

 281                READ(5,*)C
 282                DO 415 I=1,14
 283                CHL(I)=C
 284            415 CONTINUE
 285                CAVL=CHL(8)
 286                GOTO 425
 287            420 WRITE(6,105)
 288                WRITE(6,106)
 289                WRITE(6,110)
 290                WRITE(6,112)
 291                WRITE(6,115)
 292                WRITE(6,116)
 293                WRITE(6,125)
 294                WRITE(6,126)
 295                READ(5,*)(CHL(I),I=1,14)
 296                CAVL=CHL(8)
 297            425 WRITE(6,130)
 298                READ(5,35) M3
 299                IF(M3.EQ.YES) GOTO 435
 300                WRITE(6,140)
 301                READ(5,*) THETA
 302                DO 430 I=1,14
 303                THETAL(I)=THETA*PI/180.0
 304            430 CONTINUE
 305                THETAVL=THETAL(8)
 306                GOTO 441
 307            435 IF(M2.EQ.YES) GOTO 440
 308                WRITE(6,105)
 309                WRITE(6,106)
 310                WRITE(6,110)
 311                WRITE(6,112)
 312            440 WRITE(6,155)
 313                WRITE(6,149)
 314                READ(5,*)(THETAL(I),I=1,14)
 315                DO 443 KK=1,14
 316                THETAL(KK)=THETAL(KK)*PI/180.0
 317            443 CONTINUE
 318                THETAVL=THETAL(8)
 319            441 WRITE(6,158)
 320                READ(5,*) OMEGAL
 321                WRITE(6,5022)
 322                READ(5,*) MASSL
 323                WL=OMEGAL*PI/30.0
 324                VTL=WL*RL
 325                MACHNOL=VTL/340.0
 326                REL=VTL*CHL(8)/VIS
 327                WRITE(6,460)
 328            460 FORMAT('INPUT VERTICAL SEPARATION BETWEEN ROTORS')
 329                READ(5,*) VSEP
 330                VSEP=ABS(VSEP)
 331                DO 445 K=1,14
 332                BSL(K)=(BL*CHL(K))/(PI*RL)
 333            445 CONTINUE
 334                BS=(BL*CHL(8))/(PI*RL)
 335                ARL=RL/CHL(8)
 336                VSOL=(1.0+(6.6/ARL))*(2.62E-2)*THETAL(8)*VTL*180.0/PI
```

```
LINE NUMBER    FORTRAN TEXT

 337                RCOL=CHL(6)*1.2*(REL**(-0.2))*VSOL/VTL
 338                IF(P6.EQ.YES) GOTO 1510
 339                THETAV=(((-VSEP/RU)-(A1*2.0*PI/BU))/A2)
 340                R2=0.78+(0.22*EXP(-A3*THETAV))
 341                R3=R2*RU/RL
 342                WRITE(6,300)R3
 343           300  FORMAT('VORTEX INTERSECTS LOWER ROTOR AT',1F8.4,'(NON-D WRT RL)')
 344                THETAV=THETAV*180.0/PI
 345                WRITE(6,305)THETAV
 346           305  FORMAT('AND AT AN AGE OF',1F8.4,' DEGS.')
 347           C
 348           C       THE COMPUTATION OF THE MOMENTUM INDUCED DOWNWASH VELOCITY COMPUT
 349           C       ON THE LOWER ROTOR FROM THE UPPER ROTOR ALLOWING FOR THE
 350           C       POSSIBILITY OF DIFFERENTIAL RADII AND WAKE CONTRACTION NOW
 351           C       FOLLOWS:
 352           C
 353           C       IF(ABS(RL-RU).LT.0.02) GOTO 340
 354           309  K=1
 355           310  IF(K.GT.14) GOTO 347
 356                KK=1
 357           C
 358           C       YP(KK) IS THE NON-D DISTANCE ON THE UPPER ROTOR.
 359           C       (YP(K)*RL/RU) IS THE DISTANCE OF THE STATION PT 'K' ON THE LOWER
 360           C       ROTOR,NON-D WRT THE UPPER ROTOR.
 361           C
 362                IF(YP(KK).GT.R2) GOTO 325
 363           312  IF(YP(KK).GT.(1.0/R2)*(YP(K)*RL/RU)) GOTO 315
 364                KK=KK+1
 365                IF(KK.GT.14) GOTO 326
 366                GOTO 312
 367           315  IF(KK.EQ.1) GOTO 320
 368                WRITE(6,*) K,KK
 369                GRAD=(VIT(KK)-VIT(KK-1))/(YP(KK)-YP(KK-1))
 370                CONS=VIT(KK)-(GRAD*YP(KK))
 371                VINU(K)=(GRAD*(1.0/R2)*YP(K)*RL/RU)+CONS
 372                VECMUL(K)=VINU(K)*(1.0/R2)**2
 373                K=K+1
 374                GOTO 310
 375           320  GRAD=VIT(KK)/YP(KK)
 376                VINU(K)=GRAD*(1.0/R2)*YP(K)*RL/RU
 377                VECMUL(K)=VINU(K)*(1.0/R2)**2
 378                K=K+1
 379                GOTO 310
 380           325  IF(K.LT.14) GOTO 326
 381                VECMUL(K)=0.0
 382                GOTO 347
 383           326  DO 327 L=K,14
 384                VECMUL(L)=0.0
 385           327  CONTINUE
 386                GOTO 347
 387           C 340  DO 345 K=1,14
 388           C       IF(YP(K).GT.R2) GOTO 335
 389           C       VECMUL(K)=VIU(K)*(1.0/R2)**2
 390           C       GOTO 345
 391           335  VECMUL(K)=0.0
 392           345  CONTINUE
```

```
LINE NUMBER    FORTRAN TEXT

 393           C
 394           C      END OF MOMENTUM COMPUTATION.
 395           C
 396             347 WRITE(6,360)
 397             360 FORMAT('VECMUL DISTRIBUTION IS:',/)
 398                 WRITE(6,365)(VECMUL(L),L=1,14)
 399             365 FORMAT(7(1F8.4,1X),/)
 400                 KAZM=1
 401                 AZML=(KAZM-1)*PI/3.0
 402                 AZMLD=AZML*180.0/PI
 403                 WRITE(6,370)AZMLD
 404             370 FORMAT('LOWER ROTOR AT AZIMUTH POSTN OF',1F8.4,' DEGS',/)
 405                 DO 375 K=1,14
 406                 ZLDU(K)=-VSEP/RU
 407                 YLDU(K)=YP(K)*COS(AZML)*RL/RU
 408                 XLDU(K)=YP(K)*SIN(AZML)*RL/RU
 409             375 CONTINUE
 410                 DO 380 JK=1,NBU
 411                 CALL CAL(XVU,YVU,ZVU,XLDU,YLDU,ZLDU,2,VVUL,KAZM,RU,BU,JK,KC,KL
 412                C,K0,RCU,VRL,RC,VA,VB,VC,VD,VE,NCOUNT,GAMAXU,RCOU,VSOU,CAVU
 413                C,NTYPV,SIGN,1,CIRV)
 414             380 CONTINUE
 415                 DO 385 K=1,14
 416                 VECUL(K)=VVUL(K,1)
 417             385 CONTINUE
 418                 DO 390 K=2,BU
 419                 DO 390 J=1,14
 420                 VECUL(J)=VECUL(J)+VVUL(J,K)
 421             390 CONTINUE
 422                 K=1
 423             536 IF(YP(K).GT.R3) GOTO 537
 424                 K=K+1
 425                 IF(K.GT.14) GOTO 538
 426                 GOTO 536
 427             537 M21=K
 428                 GOTO 592
 429             538 M21=14
 430             592 DO 391 K=1,14
 431                 IF(K.LT.M21) GOTO 393
 432                 VECUL(K)=VECUL(K)
 433                 GOTO 391
 434             393 VECUL(K)=VECMUL(K)
 435             391 CONTINUE
 436                 WRITE(6,395)
 437             395 FORMAT('VECUL DISTRIBUTION IS:',/)
 438                 WRITE(6,400)(VECUL(L),L=1,14)
 439             400 FORMAT(7(1F8.4,1X),/)
 440             401 CALL STRIP(VECUL,YP,TOTL,CTL,VIL,RL,THETAL,CHL,BSL,BL,A,WL)
 441                 CALL LANDG(XVL,YVL,ZVL,CTL,BL,BS,RL)
 442                 IF(NBL.EQ.1) GOTO 511
 443                 DO 510 K=2,NBL
 444                 CALL BLVOCO(XVL,YVL,ZVL,BL,K)
 445             510 CONTINUE
 446             511 VSOL=(1.0+(6.6/ARL))*(2.64E-2)*THETAL(12)*VTL*180.0/PI
 447                 RCOL=CHL(8)*1.2*(REL**(-0.2))*VSOL/VTL
 448                 WRITE(6,515)VSOL,RCOL
```

```
LINE NUMBER    FORTRAN TEXT

  515 FORMAT('VSL=',1F8.4,'M/S, RCL=',1F8.4,'M')
      NCOUNT=1
  516 DO 520 K=1,NBL
      CALL CAL(XVL,YVL,ZVL,XP,YP,ZP,1,VVL,0,RL,BL,K,KC,KL,KO,RCL,VRL
     C,RO,VA,VB,VC,VD,VE,NCOUNT,GAMAXL,RCOL,VSOL,CAVL,NTYPV,SIGN,1
     C,CIRV)
  520 CONTINUE
      DO 525 K=1,14
      VECL(K)=VVL(K,1)
  525 CONTINUE
      IF(NBL.EQ.1) GOTO 531
      DO 530 K=2,NBU
      DO 530 J=1,14
      VECL(J)=VECL(J)+VVL(J,K)
  530 CONTINUE
  531 DO 535 K=1,14
      IF(K.LT.M21) GOTO 532
      VECL(K)=VECL(K)+VECUL(K)
      GOTO 535
  532 VECL(K)=VECMUL(K)
  535 CONTINUE
      CALL STRIP(VECL,YP,TOTL,CTL,VIL,RL,THETAL,CHL,BSL,BL,A,WL)
      DO 540 K=1,14
      IF(K.LT.M21) GOTO 541
      VITL(K)=VECL(K)+VIL(K)
      GOTO 540
  541 VITL(K)=VECMUL(K)
  540 CONTINUE
      WRITE(6,545)
  545 FORMAT('VITL DISTRIBUTION IS:',/)
      WRITE(6,550)(VITL(L),L=1,14)
  550 FORMAT(7(1F8.4,1X),/)
      CALL PERM(VITL,YP,THL,TORL,THLO,RL,THETAL,CHL,BSL,BL,ENL,GAMAXL
     C,A,WL,THI,1,UTI,HF)
      KC=2.0*PI*VSOL*RCOL
      ENL=ENL*(KC/GAMAXL)**2
      IF(NCOUNT.EQ.2) GOTO 552
      CALL TIPVOR(ENL,GAMAXL,VTL,ARL,CAVL,THETAVL,THETASW,REL,KC,KL
     C,KO,VRL,RO,NTYPV,MACHNOL)
      IF(KC.GT.GAMAXL) GOTO 8043
      GOTO 8044
 8043 VSOL=VSOL*GAMAXL/KC
      KC=GAMAXL
 8044 CALL DECAY(RCOL,VSOL,WL,RL,RCL,RCOL,BL,ENL)
      DO 551 J=1,TOTALSTP
      NVAR1=(DELTAZIM*(J-1))+1
      NVAR2=(DELTAZIM*J)+1
      RCL(J)=(RCL(NVAR1)+RCL(NVAR2))/2.0
  551 CONTINUE
      NCOUNT=2
      GOTO 516
  552 DEGSU=THETAU(8)*180.0/PI
      DEGSL=THETAL(8)*180.0/PI
      WRITE(6,555)THU(14),DEGSU,THL(14),DEGSL
  555 FORMAT('THU=',1F8.4,'N. THETAU=',1F8.4,'DEGS. THL=',1F8.4,'N
     CTHETAL=',1F8.4,'DEGS.')
```

```
LINE NUMBER    FORTRAN TEXT

 505                WRITE(6,560)TORU(14),TORL(14)
 506             560 FORMAT('TORU=',1F8.4,'NM TORL=',1F8.4,'NM.')
 507                 THC=(BU*THU(14))+(BL*THL(14))
 508                 TORC=(BU*TORU(14))+(BL*TORL(14))
 509                 CTL=(BL*THL(14))/(ROE*(WL*RL)**2*PI*(RL**2))
 510                 CQL=(BL*TORL(14))/(ROE*(WL*RL)**2*PI*(RL**3))
 511                 EFFU=CTU/CQU
 512                 CLU=6.0*CTU/BSU(8)
 513                 EFFL=CTL/CQL
 514                 CLL=6.0*CTL/BSL(8)
 515                 CTC=CTU+CTL
 516                 CQC=CQU+CQL
 517                 CLC=6.0*CTC/(BSU(8)+BSL(8))
 518                 EFFC=CTC/CQC
 519                 WRITE(6,561)
 520             561 FORMAT('CTU',8X'CQU',8X,'CTL',8X,'CQL',8X,'CTC',8X,'CQC',/)
 521                 WRITE(6,562)CTU,CQU,CTL,CQL,CTC,CQC
 522             562 FORMAT(6(1F8.6,3X),/)
 523                 WRITE(6,563)
 524             563 FORMAT('CTU/CQU',3X,'CLU',5X,'CTL/CQL',1X,'CLL')
 525                 WRITE(6,564) EFFU,CLU,EFFL,CLL
 526             564 FORMAT(4(1F8.4))
 527                 WRITE(6,565)
 528             565 FORMAT(/'*** OVERALL COAXIAL ROTOR PERFORMANCE FIGURES ***'/)
 529                 WRITE(6,566)
 530             566 FORMAT('CTC',8X,'CQC',8X,'CLL',8X,'CTC/CQC'/)
 531                 WRITE(6,567) CTC,CQC,CLC,EFFC
 532             567 FORMAT(6(1F10.6),/)
 533                 WRITE(6,568) THC
 534             568 FORMAT('OVERALL COAXIAL ROTOR THRUST=',1F10.4,'N')
 535                 WRITE(6,569) TORC
 536             569 FORMAT('OVERALL COAXIAL ROTOR TORQUE=',1F10.4,'NM')
 537                 DELTOR=TORU(14)-TORL(14)
 538                 IF(ABS(DELTOR/TORU(14)).LT.0.05) GOTO 580
 539                 DTOR=ABS(DELTOR)/TORL(14)
 540                 FACTOR=DTOR**(3.0/2.0)
 541                 IF(DELTOR.LT.0.0) FACTOR=-FACTOR
 542           C     CON4=0.5*ROE*(VTL**2)*(RL**4)*A*CHL(8)
 543                 DO 570 K=1,14
 544                 THETAL(K)=THETAL(K)*(1.0+FACTOR)
 545             570 CONTINUE
 546                 GOTO 401
 547             580 IF(M1.EQ.YES) GOTO 582
 548                 IF(N21.GT.1) GOTO 582
 549                 N21=N21+1
 550           C      COMPUTATION OF INTERFERENCE OF LOWER ROTOR ON UPPER
 551                 DO 601 K=1,NBL
 552                 DO 601 J=1,TOTALSTP
 553                 XVL1(J,K)=XVL(J,K)*RL/RU
 554                 YVL1(J,K)=YVL(J,K)*RL/RU
 555                 ZVL1(J,K)=(ZVL(J,K)*RL/RU)-(VSEP/RU)
 556             601 CONTINUE
 557           C     ROTOR FOR WHICH INDUCED VELS ARE GOING TO BE CALCULATED IN
 558           C     'CAL'=R,B
 559           C     ROTOR FROM WHICH THE VORTEX WAKE IS GENERATED=C
 560                 DO 602 K=1,NBL
```

```
LINE NUMBER    FORTRAN TEXT

 561                CALL CAL(XVL1,YVL1,ZVL1,XP,YP,ZP,1,VVLU,0,RU,BU,K,KC,KL,KU
 562               C,RCL,VRL,RU,VA,VB,VC,VD,VE,2,GAMAXL,RCOL,VSOL,CAVL,NTYPV
 563               C,SIGN,1,CIRV)
 564              602 CONTINUE
 565                DO 603 K=1,14
 566                VVI(K)=VVLU(K,1)
 567              603 CONTINUE
 568                IF(NBL.EQ.1) GOTO 609
 569                DO 604 K=2,NBL
 570                DO 604 J=1,14
 571                VVI(K)=VVI(K)+VVLU(J,K)
 572              604 CONTINUE
 573              609 DO 605 K=1,14
 574                VECUI(K)=VECU(K)+VVI(K)
 575              605 CONTINUE
 576                CALL STRIP(VECUI,YP,TOT,CTUI,VIUI,RU,THETAU,CU,BSU,BU,A,WU)
 577                DO 606 K=1,14
 578                VITI(K)=VECUI(K)+VIUI(K)
 579              606 CONTINUE
 580                CALL PERM(VITI,YP,THUI,TORUI,THEO,RU,THETAU,CU,BSU,BU,ENUI
 581               C,GAMAXI,A,WU,THI,1,UTI,HF)
 582                WRITE(6,607) THU(14),THUI(14)
 583              607 FORMAT('OLD THRUST(U.ROTOR)=',1F12.6,' NEW THRUST=',1F12.6)
 584                WRITE(6,608) TORU(14),TORUI(14)
 585              608 FORMAT('OLD TORQUE=',1F12.6,' NEW TORQUE=',1F12.6)
 586                WRITE(6,583)
 587              583 FORMAT(//,'**** RE-CAL OF LOWER ROTOR PERMFORMANCE ****',//)
 588                DO 584 K=1,14
 589                VIT(K)=VITI(K)
 590              584 CONTINUE
 591                THU(14)=THUI(14)
 592                TORU(14)=TORUI(14)
 593                GOTO 309
 594              582 WRITE(6,581)
 595              581 FORMAT('DO YOU REQUIRE FURTHER PERFORMANCE COMPUTATIONS?')
 596                READ(5,35) M4
 597                IF(M4.EQ.YES) GOTO 29
 598                GOTO 2056
 599          C      ******************************************************
 600          C
 601          C              START OF FORWARD FLIGHT COMPUTATION
 602          C
 603          C      ******************************************************
 604           1510 AU=A
 605                AL=A
 606                MAND=0
 607          C     COMPUTATION OF GLAUERT MEAN INDUCED DOWNWASH,ROTOR ADVANCE AND
 608          C     INFLOW RATIOS AND FLAPPING COEFFICIENTS.
 609          C     ************************************************************
 610                VVV=0.0
 611                CALL GLAUERT(AU,BU,CAVU,WU,RU,THETAVU,ALPHA,V,VIGU,VVV,TGU)
 612                IF(M1.EQ.YES) GOTO 1511
 613                VVV=0.0
 614                CALL GLAUERT(AL,BL,CAVL,WL,RL,THETAVL,ALPHA,V,VIGL,VVV,TGL)
 615           1511 LANDAU=((V*SIN(ALPHA))-VIGU)/VTU
 616                MUU=(V*COS(ALPHA))/VTU
```

```
LINE NUMBER    FORTRAN TEXT

 617                IF(M1.EQ.YES) GOTO 1514
 618                LANDAL=((V*SIN(ALPHA))-(VIGL))/VTL
 619                MUL=(V*COS(ALPHA))/VTL
 620           C    BLADE FLAPPING COEFFS A0,A1,B1
 621            1514 PAR1=(THETAU(8)/4.0)*(1.0+(MUU*MUU))+(LANDAU/3.0)
 622                LOCKU=3.0*CU(8)*ROE*AU*RU*PU/MASSU
 623                EPSILONU=1.5*EU
 624                A0U=(LOCKU/(2.0*(1.0+EPSILONU)))*PAR1
 625                PAR2=MUU*((8.0*THETAU(8)/3.0)+(2.0*LANDAU))
 626                PAR3=1.0-(0.5*MUU*MUU)
 627                LANDIU=VIGU/VTU
 628                VAR66=-LANDAU
 629                KU=ATAN(MUU/VAR66)
 630                PAR4=(4.0*MUU*A0U/3.0)+(KU*LANDIU)
 631                PAR5=1.0+(0.5*MUU*MUU)
 632                PAR5B=8.0*EPSILONU/(PAR3*LOCKU)
 633                PAR5C=PAR4/PAR5
 634                PAR5D=8.0*EPSILONU/(PAR5*LOCKU)
 635                WRITE(6,*) KU,LANDIU,PAR4,PAR5,PAR5D
 636                PAR5A=PAR2/PAR3
 637                A1U=(PAR5A+(PAR5B*PAR5C))/(1.0+(PAR5B*PAR5D))
 638                B1U=(PAR5C-(PAR5D*PAR5A))/(1.0+(PAR5B*PAR5D))
 639                WRITE(6,5000) A0U,A1U,B1U
 640            5000 FORMAT('A0U=',1F8.4,' A1U=',1F8.4,' B1U=',1F8.4)
 641           C    WRITE(6,5001)
 642            5001 FORMAT('INPUT A0,A1,B1')
 643           C    READ(5,*) A0U,A1U,B1U
 644                IF(M1.EQ.YES) GOTO 1512
 645                PAR6=(THETAL(8)/4.0)*(1.0+(MUL*MUL))+(LANDAL/3.0)
 646                LOCKL=3.0*CHL(8)*ROE*RL*RL*AL/MASSL
 647                EPSILONL=1.5*EL
 648                A0L=(LOCKL/(2.0*(1.0+EPSILONL)))*PAR6
 649                PAR7=MUL*((8.0*THETAL(8)/3.0)+(2.0*LANDAL))
 650                PAR8=1.0-(0.5*MUL*MUL)
 651                LANDIL=VIGL/VTL
 652                VAR67=-LANDAL
 653                KLOW=ATAN(MUU/VAR67)
 654                PAR9=(4.0*MUL*A0L/3.0)+(KLOW*LANDIL)
 655                PAR10=1.0+(0.5*MUL*MUL)
 656                PAR10A=PAR7/PAR8
 657                PAR10B=8.0*EPSILONL/(PAR8*LOCKL)
 658                PAR10C=PAR9/PAR10
 659                PAR10D=8.0*EPSILONL/(PAR10*LOCKL)
 660                A1L=(PAR10A+(PAR10B*PAR10C))/(1.0+(PAR10B*PAR10D))
 661                B1L=(PAR10C-(PAR10D*PAR10A))/(1.0+(PAR10B*PAR10D))
 662                WRITE(6,5926) A0L,A1L,B1L
 663            5926 FORMAT('A0L=',1F8.4,' A1L=',1F8.4,' B1L=',1F8.4)
 664                NOBLADES=NBU+NBL
 665           C    ***************************************************************
 666           C    TOTAL NUMBER OF VORTEX FILAMENT STATION PTS PER HELIX,TOTALSTP
 667            1512 TOTALSTP=(NREV*(NFILASTP-1))+1
 668           C    TIME BETWEEN SUCCESSIVE BLADE AZIMUTH STEPS
 669                DO 1520 K=1,NOBLADES
 670           C    WRITE(6,1537)K
 671            1537 FORMAT('K=',I2)
 672                IF(FLOAT(K).GT.(BU+0.2)) GOTO 1521
```

```
LINE NUMBER    FORTRAN TEXT

  673                TIME(K)=2.0*PI/(FLOAT(NFILASTP-1)*WU)
  674                RAD(K)=RU
  675                GOTO 1520
  676           1521 TIME(K)=2.0*PI/(FLOAT(NFILASTP-1)*WL)
  677                RAD(K)=RL
  678           1520 CONTINUE
  679           C
  680           C       THE REFERENCE AXES USED ARE: *
  681           C                                    *
  682           C                                    * V,+VE ALONG +VE Y
  683           C                                    *
  684           C                                    *
  685           C                        X***********V
  686           C                                  * * *
  687           C                                *   *     *K'TH BLADE
  688           C                              *     *       *
  689           C                            *       *     *
  690           C                          *         *       *
  691           C                        Z           Y  EPSI(J,K)
  692           C                  +VE UPWARD    +VE FROM CENTRE
  693           C                                TO AFT OF DISC
  694           C
  695           C       FLAPPING PARAMETERS EVALUATED FOR ALL BLADES AROUND THE DISC
  696           C       ***********************************************************
  697                   DO 2000 K=1,NOBLADES
  698                   DO 2000 J=1,TOTALSTP
  699                   FOR1=FLOAT(J-1)
  700                   FOR2=FLOAT(NFILASTP-1)
  701                   IF(FLOAT(K).GT.(BU+0.2)) GOTO 2001
  702                   EPSI(J,K)=(FOR1*2.0*PI/FOR2)+(FLOAT(K-1)*2.0*PI/BU)
  703                   A0=A0U
  704                   A1=A1U
  705                   B1=B1U
  706                   W=WU
  707                   GOTO 2002
  708           2001    EPSI(J,K)=-(FOR1*2.0*PI/FOR2)+((-BU+FLOAT(K-1))*PI*2.0/BL)
  709                   A0=A0L
  710                   A1=A1L
  711                   B1=-B1L
  712                   W=WL
  713           2002    BETA(J,K)=A0-(A1*COS(EPSI(J,K)))-(B1*SIN(EPSI(J,K)))
  714                   IF(K.GT.NBU) A1=-A1L
  715                   IF(K.GT.NBU) B1=B1L
  716                   DBETA(J,K)=W*((A1*SIN(EPSI(J,K)))-(B1*COS(EPSI(J,K))))
  717           2000    CONTINUE
  718           C       WRITE(6,5639)
  719           5639    FORMAT('BETA DISTRIBUTION IS:')
  720           C       DO 5005 MGI=1,4
  721           C       WRITE(6,*)(BETA(MG,MGI),MG=1,TOTALSTP)
  722           C5005   CONTINUE
  723           C       WRITE(6,5009)
  724           5009    FORMAT('DBETA DIS. FOR BLADE ONE IS:',/)
  725           C       WRITE(6,*)(DBETA(MG,1),MG=1,TOTALSTP)
  726           C       ***********************************************************
  727           C       INITIALLY SET UP THREE HELICAL STATION PTS PER BLADE
  728           C       (TWO FILAMENTS PER BLADE)
```

```
LINE NUMBER    FORTRAN TEXT

 729          C       THE ROTOR WAKE TIP VORTEX COORDINATES ARE GIVEN BY
 730          C       THE ARRAYS XFV,YFV,ZFV.FOR XFV(J,K),J REFERS TO THE
 731          C       STATION POINT ON THE K'TH HELIX.I.E.THE HELICAL VORTEX
 732          C       FILAMENT GENERATED BY THE K'TH BLADE.
 733          C      ****************************************************************
 734                 HORV=V*COS(ALPHA)
 735                 VERV=V*SIN(ALPHA)
 736                 DO 2010 K=1,NOBLADES
 737                 XFV(1,K)=-SIN(EPSI(1,K))*COS(BETA(1,K))
 738                 YFV(1,K)=COS(EPSI(1,K))*COS(BETA(1,K))
 739                 IF(K.GT.NBU) GOTO 2011
 740                 ZFV(1,K)=SIN(BETA(1,K))
 741                 GOTO 2012
 742           2011  ZFV(1,K)=SIN(BETA(1,K))-(VSEP/RU)
 743           2012  XFV(2,K)=XFV(1,K)
 744                 XFV(1,K)=-SIN(EPSI(2,K))*COS(BETA(2,K))
 745                 YFV(2,K)=YFV(1,K)+(HORV*TIME(K)/RAD(K))
 746                 YFV(1,K)=COS(EPSI(2,K))*COS(BETA(2,K))
 747                 IF(M6.EQ.YES) VERV=V*SIN(ALPHA)
 748                 IF(M6.EQ.YES) GOTO 2210
 749                 RVORT=SQRT(XFV(1,K)**2+YFV(1,K)**2)
 750                 R=RU
 751                 V10=VIGU
 752                 IF(K.GT.NBU) R=RL
 753                 IF(K.GT.NBU) V10=VIGL
 754                 IF(RVORT.GT.1.0) VERV=(V*SIN(ALPHA))-(2.0*V10)
 755                 IF(RVORT.GT.1.0) GOTO 2210
 756                 IF(M7.EQ.YES)VERV=(V*SIN(ALPHA))-V10
 757                 IF(M7.EQ.YES) GOTO 2210
 758                 EPSV=ATAN2(-XFV(1,K),YFV(1,K))
 759                 IF(K.GT.NBU) EPSV=ATAN2(XFV(1,K),YFV(1,K))
 760                 VERV=(V*SIN(ALPHA))-(V10*(1.0+(RVORT*COS(EPSV))))
 761           2210  ZFV(2,K)=ZFV(1,K)+(VERV*TIME(K)/RAD(K))
 762                 IF(FLOAT(K).GT.(BU+0.2)) GOTO 2014
 763                 ZFV(1,K)=SIN(BETA(2,K))
 764                 GOTO 2015
 765           2014  ZFV(1,K)=SIN(BETA(2,K))-(VSEP/RU)
 766           2015  XFV(3,K)=XFV(2,K)
 767                 XFV(2,K)=XFV(1,K)
 768                 XFV(1,K)=-SIN(EPSI(3,K))*COS(BETA(3,K))
 769                 YFV(3,K)=YFV(2,K)+(HORV*TIME(K)/RAD(K))
 770                 YFV(2,K)=YFV(1,K)+(HORV*TIME(K)/RAD(K))
 771                 YFV(1,K)=COS(EPSI(3,K))*COS(BETA(3,K))
 772                 IF(M6.EQ.YES) VERV=V*SIN(ALPHA)
 773                 IF(M6.EQ.YES) GOTO 2211
 774                 RVORT=SQRT(XFV(2,K)**2+YFV(2,K)**2)
 775                 R=RU
 776                 V10=VIGU
 777                 IF(K.GT.NBU) R=RL
 778                 IF(K.GT.NBU) V10=VIGL
 779                 IF(RVORT.GT.1.0) VERV=(V*SIN(ALPHA))-(2.0*V10)
 780                 IF(RVORT.GT.1.0) GOTO 2211
 781                 IF(M7.EQ.YES) VERV=(V*SIN(ALPHA))-V10
 782                 IF(M7.EQ.YES) GOTO 2211
 783                 EPSV=ATAN2(-XFV(2,K),YFV(2,K))
 784                 IF(K.GT.NBU) EPSV=ATAN2(XFV(2,K),YFV(2,K))
```

```
LINE NUMBER    FORTRAN TEXT

 785                VERV=(V*SIN(ALPHA))-(V10*(1.0+(RVORT*COS(EPSV))))
 786           2211 ZFV(3,K)=ZFV(2,K)+(VERV*TIME(K)/RAD(K))
 787                IF(M6.EQ.YES) VERV=V*SIN(ALPHA)
 788                IF(M6.EQ.YES) GOTO 2212
 789                RVORT=SQRT(XFV(1,K)**2+YFV(1,K)**2)
 790                R=RU
 791                V10=VIGU
 792                IF(K.GT.NBU) R=RL
 793                IF(K.GT.NBU) V10=VIGL
 794                IF(RVORT.GT.1.0) VERV=(V*SIN(ALPHA))-(2.0*V10)
 795                IF(RVORT.GT.1.0) GOTO 2212
 796                IF(M7.EQ.YES) VERV=(V*SIN(ALPHA))-V10
 797                IF(M7.EQ.YES) GOTO 2212
 798                EPSV=ATAN2(-XFV(1,K),YFV(1,K))
 799                IF(K.GT.NBU) EPSV=ATAN2(XFV(1,K),YFV(1,K))
 800                VERV=(V*SIN(ALPHA))-(V10*(1.0+(RVORT*COS(EPSV))))
 801           2212 ZFV(2,K)=ZFV(1,K)+(VERV*TIME(K)/RAD(K))
 802                IF(FLOAT(K).GT.(BU+0.2)) GOTO 2016
 803                ZFV(1,K)=SIN(BETA(3,K))
 804                GOTO 2015
 805           2016 ZFV(1,K)=SIN(BETA(3,K))-(VSEP/RU)
 806           2015 CONTINUE
 807                NOSTPS=3
 808           5791 IF(M50.EQ.YES) GOTO 3016
 809              C      COMPUTATION OF THE INTERACTION BETWEEN FILAMENTS COMMENCES
 810              C      ************************************************************
 811                NOM1=2
 812                IF(M1.EQ.YES) NOM1=1
 813                DO 2043 JKL=1,NOM1
 814                IF(JKL.EQ.2) GOTO 2041
 815                W=WU
 816                R=RU
 817                AR=ARU
 818                C=CU(8)
 819                THETA=THETAU(8)
 820                VI=VIGU
 821                B=BU
 822                EN=ENU
 823                GAMAX=GAMAXU
 824                MACHNO=MACHNOU
 825                GOTO 2042
 826           2041 W=WL
 827                R=RL
 828                AR=ARL
 829                C=CHL(8)
 830                THETA=THETAL(8)
 831                VI=VIGL
 832                B=RL
 833                EN=ENL
 834                GAMAX=GAMAXL
 835                MACHNO=MACHNOL
 836           2042 CALL VORPRAM(W,R,AR,C,THETA,0.0,VI,EN,GAMAX,1,0,7,DELTAZIM
 837              C,TOTALSTP,V,B,NTYPV,MACHNO)
 838                CALL VORTEXAV(VORTEXKC,VORTEXKL,VORTEXKO,VORTEXRC,VORTEXRL
 839              C,VORTEXRO,NOSTPS,NOBLADES,VORTEXA,VORTEXB,VORTEXC,VORTEXD
 840              C,VORTEXE,DELTAZIM,B,R,C,GAMAX)
```

```
LINE NUMBER    FORTRAN TEXT

  841          2043 CONTINUE
  842         C     WRITE(6,3300)
  843          3300 FORMAT('AVERAGE VORTEX FILAMENT VALUES:',/)
  844               DO 3310 K=1,NOBLADES
  845         C     WRITE(6,3320)K
  846          3320 FORMAT('FOLLOWING DATA RFOR HELIX',I2,/)
  847         C     WRITE(6,3330)
  848          3330 FORMAT(7X,'RC',7X,'A',7X,'B',7X,'C',7X,'D',7X,'E')
  849         C     WRITE(6,3340)(VORTEXRC(J,K),VORTEXA(J,K),VORTEXB
  850         C    C,VORTEXC(J,K),VORTEXD(J,K),VORTEXE(J,K),J=1,TOTALSTP-1)
  851          3340 FORMAT(6(1PE8.4))
  852          3310 CONTINUE
  853               GOTO 3015
  854          3016 DO 3017 K=1,NOBLADES
  855               SIGN=1.0
  856               IF(K.GT.NBU) GOTO 3018
  857               W=WU
  858               T=TGU
  859               B=BU
  860               MU=MUU
  861               R=RU
  862               AR=ARU
  863               C=CU(8)
  864               THETA=THETAU(8)
  865               GOTO 3019
  866          3018 W=WL
  867               SIGN=-1.0
  868               T=TGL
  869               B=BL
  870               MU=MUL
  871               R=RL
  872               AR=ARL
  873               C=CHL(8)
  874               THETA=THETAL(8)
  875          3019 NTYPV=1
  876               CALL RANKINE(V,W,R,AR,C,THETA,EPSI,CIRV,K,NOSTPS,SIGN,M51,T,MU,B)
  877          3017 CONTINUE
  878          3015 IF(M7.EQ.YES) GOTO 2031
  879               IF(M8.EQ.YES) GOTO 2031
  880          2017 DO 2020 K=1,NOBLADES
  881               DO 2020 L=1,NOBLADES
  882               SIGN=1.0
  883               MMM=2
  884               IF(K.GT.NBU) GOTO 3350
  885               GAMAX=GAMAXU
  886               R=RU
  887               GOTO 3353
  888          3350 GAMAX=GAMAXL
  889               SIGN=-1.0
  890               R=RL
  891          3353 IF(K.EQ.L) MMM=1
  892               CALL IND(XFV,YFV,ZFV,K,L,XVEL,YVEL,ZVEL,MMM,NOSTPS,R
  893              C,VORTEXKC,VORTEXKO,VORTEXRC,VORTEXRL,VORTEXRO,VORTEXA
  894              C,VORTEXB,VORTEXC,VORTEXD,VORTEXE,NTYPV,GAMAX,CIRV,SIGN)
  895          2020 CONTINUE
  896         C     ******************************************************************
```

```
LINE NUMBER    FORTRAN TEXT

  897          C      SUMMATION OF THE VORTEX INDUCED VELOCITIES AT EACH HELICAL
  898          C      STATION POINT NOW COMMENCES.E.G.THE TOTAL INDUCED VELOCITY
  899          C      IN THE X DIRECTION AT STATION POINTS 1 AND 2 ON HELIX 1
  900          C      IS GIVEN BY XVELT(1,1),XVELT(2,1) RESPECTIVELY.
  901          C      ***************************************************************
  902           2031  DO 2030 J=1,NOSTPS
  903                 DO 2030 K=1,NOBLADES
  904                 XVELT(J,K)=0.0
  905                 YVELT(J,K)=0.0
  906                 ZVELT(J,K)=0.0
  907           2030  CONTINUE
  908                 IF(M7.EQ.YES) GOTO 2441
  909                 IF(M8.EQ.YES) GOTO 2441
  910                 DO 2040 K=1,NOBLADES
  911                 DO 2040 J=1,NOSTPS
  912                 DO 2040 L=1,NOBLADES
  913                 XVELT(J,K)=XVEL(J,K,L)+XVELT(J,K)
  914                 YVELT(J,K)=YVEL(J,K,L)+YVELT(J,K)
  915                 ZVELT(J,K)=ZVEL(J,K,L)+ZVELT(J,K)
  916           2040  CONTINUE
  917          C      GOTO 2441
  918                 DO 6041 K=1,NOBLADES
  919                 DO 6041 J=1,1
  920                 SIGN=1.0
  921                 C=CU(14)
  922                 W=WU
  923                 R=RU
  924                 IF(K.GT.NBU) GOTO 6042
  925                 GOTO 6043
  926           6042  SIGN=-1.0
  927                 W=WL
  928                 R=RL
  929                 C=CHL(14)
  930           6043  VLOCAL=(W*R)+(V*SIGN*SIN(EPSI(J,K)))
  931                 VVOR=0.176*VLOCAL
  932                 XVELT(J,K)=XVELT(J,K)+(VVOR*(SIN(EPSI(NOSTPS,K))*COS(BETA(NOSTP
  933                C))))
  934                 YVELT(J,K)=YVELT(J,K)-(VVOR*COS(EPSI(NOSTPS,K))*COS(BETA(NOSTPS
  935                C))
  936                 ZVELT(J,K)=ZVELT(J,K)-(VVOR*SIN(BETA(NOSTPS,K)))
  937           6041  CONTINUE
  938          C      ***************************************************************
  939          C      EVALUATION OF NEW VORTEX FILAMENT LOCATIONS COMMENCES
  940          C      ***************************************************************
  941           2441  DO 2050 K=1,NOBLADES
  942                 VIG=VIGU
  943                 IF(K.GT.NBU) VIG=VIGL
  944                 CALL POSTN(XFV,YFV,ZFV,XVELT,YVELT,ZVELT,K,XFVNEW,YFVNEW,ZFVNEW
  945                CNOSTPS,RAD,TIME,VIG,NBU,M7,M8,M6)
  946           2050  CONTINUE
  947                 NOSTPS=NOSTPS+1
  948                 IF(NOSTPS.GT.TOTALSTP) NOSTPS=TOTALSTP
  949           2051  DO 2060 K=1,NOBLADES
  950                 DO 2060 J=2,NOSTPS
  951                 XFV(J,K)=XFVNEW((J-1),K)
  952                 YFV(J,K)=YFVNEW((J-1),K)
```

```
LINE NUMBER    FORTRAN TEXT

 953                ZFV(J,K)=ZFVNEW((J-1),K)
 954             2060 CONTINUE
 955           C      ******************************************************************
 956           C      SETTING UP THE NEW J=1 VORTEX FILAMENT STATION PT FOR ALL BLADES
 957           C      ******************************************************************
 958                DO 2070 K=1,NOBLADES
 959                XFV(1,K)=-SIN(EPSI(NOSTPS,K))*COS(BETA(NOSTPS,K))
 960                YFV(1,K)=COS(EPSI(NOSTPS,K))*COS(BETA(NOSTPS,K))
 961                IF(K.GT.NBU) GOTO 2061
 962                ZFV(1,K)=SIN(BETA(NOSTPS,K))
 963                GOTO 2070
 964             2061 ZFV(1,K)=SIN(BETA(NOSTPS,K))-(VSEP/RU)
 965             2070 CONTINUE
 966           C      ******************************************************************
 967                IF(NOSTPS.EQ.TOTALSTP) GOTO 2080
 968                GOTO 5791
 969             2080 WRITE(6,2085)
 970             2085 FORMAT('WAKE REVOLUTIONS COMPLETE,PERM CAL COMMENCES',/)
 971                DO 2088 JM=1,NOBLADES
 972                DO 2088 J=1,14
 973                VELFVT(J,JM)=0.0
 974             2088 CONTINUE
 975                IF(M1.EQ.YES) GOTO 9091
 976           C      CLASSICAL WAKE INTERCEPT,YINCEPT2
 977             7888 YINCEPT2=(-1.0*RU/RL)-(MUU*VSEP/(LANDAU*RL))
 978                WRITE(6,3007) YINCEPT2
 979             3007 FORMAT('CLASSICAL WAKE INTERCEPT IS:',1F12.6)
 980                IF(M7.EQ.YES) YINCEPT=YINCEPT2
 981                IF(M7.EQ.YES) GOTO 3008
 982                CALL INCEPT(WU,V,ALPHA,VIGU,KU,VSEP,RU,RL,YINCEPT)
 983             3008 WRITE(6,4022) YINCEPT
 984             4022 FORMAT('INCEPT FROM HELIX INTERSECTION IS:',1F12.6)
 985           C      CALCULATION OF VORTEX INDUCED VELOCITIES ON THE BLADES
 986           C      BEGINS.TRANSFER OF AXES FROM STATIONARY AXES IN THE NO
 987           C      FEATHERING PLANE TO AXES ROTATING WITH THE K'TH BLADE
 988           C      IS ALSO PERFORMED.
 989           C      ******************************************************************
 990             9091 K=1
 991             2089 DO 2222 J=1,14
 992                REPEAT=((0.05*J)+((J-1)*0.05))
 993                IF(J.GT.9)REPEAT=(0.9+((J-9)*0.01)+((J-10)*0.01))
 994                XP(J)=0.0
 995                YP(J)=REPEAT
 996                ZP(J)=0.0
 997             2222 CONTINUE
 998                DO 8500 LM=1,NOBLADES
 999                DO 8500 J=1,NOSTPS
1000                ANG=EPSI(NOSTPS,K)
1001                BET=BETA(NOSTPS,K)
1002                ZFV1(J,LM)=ZFV(J,LM)
1003                IF(K.GT.NBU)ZFV1(J,LM)=ZFV(J,LM)+(VSEP/RU)
1004                XFVT(J,LM)=(XFV(J,LM)*COS(ANG))+(YFV(J,LM)*SIN(ANG))
1005                AN1=(YFV(J,LM)*COS(ANG))-(XFV(J,LM)*SIN(ANG))
1006                YFVT(J,LM)=(AN1*COS(BET))+(ZFV1(J,LM)*SIN(BET))
1007                ZFVT(J,LM)=(ZFV1(J,LM)*COS(BET))-(AN1*SIN(BET))
1008             8500 CONTINUE
```

```
LINE NUMBER    FORTRAN TEXT

1009                ANG21=2.0*PI
1010                ANG=(AMOD(EPSI(NOSTPS,K),ANG21))*180.0/PI
1011          C     WRITE(6,2223)
1012           2223 FORMAT(7X,'XP',7X'YP',7X,'ZP')
1013          C     WRITE(6,2224)(XP(J),YP(J),ZP(J),J=1,14)
1014           2224 FORMAT(3(2X,1F8.2))
1015          C     WRITE(6,2081)K,ANG
1016           2081 FORMAT('INDUCED VEL ON BLADE',I2,' AT AZTH POS',1F10.4,'DEGS')
1017                DO 3000 L=1,NOBLADES
1018                IF(L.GT.NBU) GOTO 3001
1019                R=RU
1020                T=TGU
1021                B=BU
1022                MU=MUU
1023                B=BU
1024                RCO=RCOU
1025                VSO=VSOU
1026                C=CU(8)
1027                SIGN=1.0
1028                GOTO 3003
1029           3001 R=RL
1030                T=TGL
1031                B=BL
1032                MU=MUL
1033                B=BL
1034                RCO=RCOL
1035                VSO=VSOL
1036                C=CHL(8)
1037                IF(L.GT.NBU) SIGN=-1.0
1038           3003 CALL RANKINE(V,W,R,AR,C,THETA,EPSI,CIRV,L,NOSTPS,SIGN,M51,T,MU,
1039          C     IF((L.EQ.1).AND.(K.EQ.1)) WRITE(6,5555)(CIRV(J,L),J=1,NOSTPS-1)
1040           5555 FORMAT('CIR=',1F10.4)
1041                CALL CAL(XFVT,YFVT,ZFVT,XP,YP,ZP,1,VELFV,0,R,B,L,KC,KL,KO,RC,RL
1042               C,VA,VB,VC,VD,VE,1,GAMAX,RCO,VSO,C,1,SIGN,2,CIRV)
1043          C     WRITE(6,3004)L,K
1044           3004 FORMAT(/,'FROM HELIX',I2,'WITH COORDS WRT',I2,' BLADE AXES IS:'
1045          C     WRITE(6,3333)
1046           3333 FORMAT(7X,'XV',7X,'YV',7X,'ZV')
1047          C     WRITE(6,2224)(XFVT(J,L),YFVT(J,L),ZFVT(J,L),J=1,NOSTPS)
1048          C     WRITE(6,400)(VELFV(J,L),J=1,14)
1049                DO 3009 J=1,14
1050                VELFVT(J,K)=VELFVT(J,K)+VELFV(J,L)
1051           3009 CONTINUE
1052           3000 CONTINUE
1053                K=K+1
1054                IF(K.LE.NOBLADES) GOTO 2089
1055          C     ************************************************************
1056                NOM21=0
1057                K=1
1058           3006 IF(K.GT.NBU) GOTO 7016
1059                R=RU
1060                W=WU
1061                SIGN=1.0
1062                GOTO 7017
1063           7016 R=RL
1064                W=WL
```

```
LINE NUMBER    FORTRAN TEXT

1065                SIGN=-1.0
1066             7017 VVV=VELFVT(1,1)
1067                NOM21=NOM21+1
1068                IF(NOM21.GT.1) GOTO 7018
1069                CALL GLAUERT(AU,BU,CAVU,WU,RU,THETAVU,ALPHA,V,VIGU,VVV,TGU)
1070                IF(M1.EQ.YES) GOTO 7018
1071                IJ=NBU+1
1072                VVV=VELFVT(1,IJ)
1073                CALL GLAUERT(AL,BL,CAVL,WL,RL,THETAVL,ALPHA,V,VIGL,VVV,TGL)
1074             7018 DO 3005 J=1,14
1075                RADB(J)=((0.05*J)+((J-1)*0.05))*COS(BETA(NOSTPS,K))
1076                IF(J.GT.9)RADB(J)=(0.9+((J-9)*0.01)+((J-10)*0.01))
1077               C*COS(BETA(NOSTPS,K))
1078                IF(K.LE.NBU) GOTO 3011
1079             C     COMPUTATION OF UPPER ROTOR WAKE VELOCITIES ON LOWER ROTOR
1080                XPT(J)=-RADB(J)*SIN(EPSI(NOSTPS,K))
1081                YPT(J)=(RADB(J)*COS(EPSI(NOSTPS,K)))-((1.0*RU/RL)+YINCEPT)
1082                RG=SQRT(XPT(J)**2+YPT(J)**2)
1083                GG=RU/RL
1084                IF(RG.GT.GG) GOTO 3011
1085                IF(RG.LE.GG) VELFVT(J,K)=VELFVT(1,1)
1086             3011 UP1=(V*SIN(ALPHA)*COS(BETA(NOSTPS,K)))-VELFVT(J,K)
1087                UP2=-(R*RADB(J)*DBETA(NOSTPS,K))-(V*COS(ALPHA)*COS(EPSI(NOSTPS,K))
1088               C*SIN(BETA(NOSTPS,K)))
1089                IF(M7.EQ.YES) GOTO 7014
1090             C     IF(M6.EQ.YES) GOTO 7014
1091                IF(K.LE.NBU) UP3=-VIGU*(1.0+(RADB(J)*KU*COS(EPSI(NOSTPS,K))))
1092                IF(K.GT.NBU) UP3=-VIGL*(1.0+(RADB(J)*KLOW*COS(EPSI(NOSTPS,K))))
1093                IF(YINCEPT.GT.1.0) GOTO 7012
1094                IF(ABS(YPT(J)).LT.1E-4) GOTO 3012
1095                IF(ABS(XPT(J)).LT.1E-4) GOTO 8734
1096                ANGRG=ATAN2(XPT(J),YPT(J))
1097                GOTO 3014
1098             3012 IF(YPT(J).LT.0.0) ANGRG=3.0*PI/2.0
1099                IF(XPT(J).GT.0.0) ANGRG=PI/2.0
1100                GOTO 3014
1101             8734 IF(YPT(J).LT.0.0) ANGRG=PI
1102                IF(YPT(J).GT.0.0) ANGRG=0.0
1103             3014 IF((RG.LE.GG).AND.(K.GT.NBU)) UP3=(-2.0*VIGU*(GG+(RG*COS
1104                C(ANGRG)*KU)))+UP3
1105                GOTO 7012
1106             7014 IF(K.LE.NBU) UP3=-VIGU
1107                IF(K.GT.NBU) UP3=-VIGL
1108                IF(YINCEPT.GT.1.0) GOTO 7012
1109                IF((RG.LE.GG).AND.(K.GT.NBU)) UP3=-2.0*VIGU
1110             7012 VMOM(J)=-UP3
1111                VFLAP(J)=-UP2
1112                UP(J,K)=-(UP1+UP2+UP3)
1113                UT(J,K)=(W*RADB(J)*R)+(V*SIGN*COS(ALPHA)*SIN(EPSI(NOSTPS,K)))
1114                THI(J)=UP(J,K)/UT(J,K)
1115                UTI(J)=UT(J,K)
1116             3005 CONTINUE
1117             C     WRITE(6,8888)
1118              8888 FORMAT(6X,'THI',7X,'UT',/)
1119             C     WRITE(6,8889)(THI(J),UTI(J),J=1,14)
1120              8889 FORMAT(2(1F10.4,6X))
```

```
LINE NUMBER    FORTRAN TEXT

1121                IF(K.GT.NBU) GOTO 9001
1122                SIGN=1.0
1123                BET=BETA(NOSTPS,K)
1124                AZM=EPSI(NOSTPS,K)
1125                R=RU
1126                B=BU
1127                W=WU
1128                DO 9002 J=1,14
1129                THETAR(J)=THETAU(J)
1130                CHORDR(J)=CU(J)
1131                BSR(J)=BSU(J)
1132             9002 CONTINUE
1133                GOTO 9004
1134             9001 R=RL
1135                B=BL
1136                W=WL
1137                SIGN=-1.0
1138                BET=BETA(NOSTPS,K)
1139                AZM=EPSI(NOSTPS,K)
1140                DO 9003 J=1,14
1141                THETAR(J)=THETAL(J)
1142                CHORDR(J)=CHL(J)
1143                BSR(J)=BSL(J)
1144             9003 CONTINUE
1145             9004 IJKL=2
1146           C     COMPUTATION OF BLADE PERFORMANCE
1147           C     ********************************************************************
1148                 CALL PERM(VIT,RADB,TH,TOR,THEO,R,THETAR,CHORDR,BSR,B,ENERGY
1149                C,GAMAX,A,W,THI,IJKL,UTI,HF)
1150           C     WRITE(6,8091)
1151             8091 FORMAT('I AM HERE TOO')
1152                 HFORCE(K)=HF(14)
1153                 THRUST(K)=TH(14)
1154                 TOPQUE(K)=TOR(14)
1155           C     ********************************************************************
1156           C     OUTPUT DATA
1157           C     ********************************************************************
1158                 ANG12=2.0*PI
1159                 ANGBLADE=(AMOD(EPSI(NOSTPS,K),ANG12))*180.0/PI
1160                 WRITE(6,7778) ANGBLADE
1161              7778 FORMAT('BLADE AT AZIMUTH POSTN ',1F12.6,' DEGS')
1162                 WRITE(6,7001) BETA(NOSTPS,K),DBETA(NOSTPS,K)
1163              7001 FORMAT('BETA=',1F12.6,' DBETA=',1F12.6)
1164           C     WRITE(6,7002)
1165              7002 FORMAT('TOTAL VORTEX INDUCED VELOCITY IS:')
1166           C     WRITE(6,400)(VELFVT(J,K),J=1,14)
1167           C     WRITE(6,7003)
1168              7003 FORMAT('MOMENTUM VELOCITY DISTRIBUTION IS:')
1169           C     WRITE(6,400)(VMOM(J),J=1,14)
1170           C     WRITE(6,7005)
1171              7005 FORMAT('FLAP VELOCITY DISTRIBUTION IS:')
1172           C     WRITE(6,400)(VFLAP(J),J=1,14)
1173           C     WRITE(6,7004)
1174              7004 FORMAT('TOTAL VELOCITY DISTRIBUTION IS:')
1175           C     WRITE(6,400)(UP(J,K),J=1,14)
1176                 WRITE(6,7777) THRUST(K),TORQUE(K),K
```

```
LINE NUMBER    FORTRAN TEXT

1177          7777 FORMAT('THRUST=',1F9.3,' TORQUE=',1F9.3,' (BLADE',I2,')')
1178               K=K+1
1179               IF(K.LE.NOBLADES) GOTO 3006
1180               NOSTPS=TOTALSTP
1181               MAND=MAND+1
1182               HFORCEU(MAND)=0.0
1183               THRUSTU(MAND)=0.0
1184               TORQUEU(MAND)=0.0
1185               HFORCEL(MAND)=0.0
1186               THRUSTL(MAND)=0.0
1187               TORQUEL(MAND)=0.0
1188               DO 2094 K=1,NOBLADES
1189               IF(K.GT.NBU) GOTO 2095
1190               HFORCEU(MAND)=HFORCEU(MAND)+HFORCE(K)
1191               THRUSTU(MAND)=THRUSTU(MAND)+THRUST(K)
1192               TORQUEU(MAND)=TORQUEU(MAND)+TORQUE(K)
1193               GOTO 2094
1194          2095 THRUSTL(MAND)=THRUSTL(MAND)+THRUST(K)
1195               HFORCEL(MAND)=HFORCEL(MAND)+HFORCE(K)
1196               TORQUEL(MAND)=TORQUEL(MAND)+TORQUE(K)
1197          2094 CONTINUE
1198               ALPHACU=-(HFORCEU(MAND)/THRUSTU(MAND))*180.0/PI
1199               IF(M1.EQ.YES) GOTO 5003
1200               ALPHACL=-(HFORCEL(MAND)/THRUSTL(MAND))*180.0/PI
1201          5003 WRITE(6,2098) THRUSTU(MAND),TORQUEU(MAND)
1202          2098 FORMAT('UPPER ROTOR,THRUST=',1F12.6,'N',' TORQUE=',1F12.6,'N/M
1203              C,')
1204               WRITE(6,8021) HFORCEU(MAND),ALPHACU
1205          8021 FORMAT('CORRESPONDING H FORCE=',1F12.6,'N',' ALPHA=',1F8.4,'DEGS
1206               IF(M1.EQ.YES) GOTO 1010
1207               WRITE(6,2099) THRUSTL(MAND),TORQUEL(MAND)
1208          2099 FORMAT('LOWER ROTOR,THRUST=',1F12.6,'N',' TORQUE=',1F12.6,'N/M
1209              C,')
1210               WRITE(6,8021) HFORCEL(MAND),ALPHACL
1211          C    ************************************************************
1212          C    ****NOTE THE FOLLOWING DOES NOT TAKE INTO ACCOUNT OF VARIABLE
1213          C        BLADES STEPPED FULLY AROUND IN EACH ROTOR******
1214          C
1215           1010 VARA=360.0/(BU*DELTAZIM)
1216          C    WRITE(6,1011)VARA,MAND
1217           1011 FORMAT('VARA=',1F12.6,' MAND=',I2)
1218               IF(FLOAT(MAND).GE.VARA) GOTO 2092
1219               FOR1=FLOAT(TOTALSTP+MAND-1)
1220               DO 2090 K=1,NOBLADES
1221               IF(K.GT.NBU) GOTO 2091
1222               EPSI(NOSTPS,K)=(FOR1*2.0*PI/FOR2)+(FLOAT(K-1)*2.0*PI/BU)
1223               FLAP=-(A1U*COS(EPSI(NOSTPS,K)))-(B1U*SIN(EPSI(NOSTPS,K)))
1224               BETA(NOSTPS,K)=A0U+FLAP
1225               DBETA(NOSTPS,K)=WU*((A1U*SIN(EPSI(NOSTPS,K)))-(B1U*COS
1226              C(EPSI(NOSTPS,K))))
1227               GOTO 2090
1228          2091 ANL=(-BU+FLOAT(K-1))*2.0*PI/BL
1229               EPSI(NOSTPS,K)=-(FOR1*2.0*PI/FOR2)+ANL
1230               FLAP=-(A1L*COS(EPSI(NOSTPS,K)))+(B1L*SIN(EPSI(NOSTPS,K)))
1231               BETA(NOSTPS,K)=A0L+FLAP
1232               DBETA(NOSTPS,K)=WL*((-A1L*SIN(EPSI(NOSTPS,K)))-(B1L*COS
```

```
LINE NUMBER    FORTRAN TEXT

1233                C(EPSI(NOSTPS,K))))
1234           2090 CONTINUE
1235                GOTO 5791
1236           2092 WRITE(6,2093)
1237           2093 FORMAT('BLADES SUCCESSFULLY STEPPED AROUND DISC')
1238                THAV=0.0
1239                TORAV=0.0
1240                HFAV=0.0
1241                DO 2096 K=1,MAND
1242                IF(M1.EQ.YES) THRUSTL(K)=0.0
1243                IF(M1.EQ.YES) TORQUEL(K)=0.0
1244                IF(M1.EQ.YES) HFORCEL(K)=0.0
1245                HFAV=HFORCEU(K)+HFORCEL(K)+HFAV
1246                THAV=THRUSTU(K)+THRUSTL(K)+THAV
1247                TORAV=TORQUEU(K)+TORQUEL(K)+TORAV
1248           2096 CONTINUE
1249                THAV=THAV/FLOAT(MAND)
1250                TORAV=TORAV/FLOAT(MAND)
1251                HFAV=HFAV/FLOAT(MAND)
1252                WRITE(6,2097)THAV,TORAV
1253           2097 FORMAT('TOT THRUST=',1F12.6,'N',' TOT TORQUE=',1F12.6,'N/M')
1254                ALPHAF=(-HFAV/THAV)*180.0/PI
1255                WRITE(6,8021) HFAV,ALPHAF
1256                GOTO 582
1257           2056 STOP
1258                END
```

```
LINE NUMBER    FORTRAN TEXT

1259                SUBROUTINE RANKINE(V,W,R,AR,C,THETA,EPSI,CIR,K,NOSTPS,SIGN,M51
1260               C,T,MU,B)
1261                REAL MU
1262                INTEGER YES
1263                DIMENSION EPSI(100,20),VT(100,20),VSO(100,20),RCO(100,20)
1264                DIMENSION RE(100,20),CIR(100,20),CIROLL(100,20)
1265                DATA YES/1HY/
1266                DATA VIS/1.455E-5/,PI/3.1415927/,ROE/1.225/
1267                VAR1=T/(ROE*B*R*W*R*(0.5-(3.0*(MU**2)/16.0)))
1268                DO 10 J=1,NOSTPS
1269                L=NOSTPS-(J-1)
1270                VT(J,K)=(W*R)+(SIGN*V*SIN(EPSI(L,K)))
1271                VSO(J,K)=(1.0+(6.6/AR))*(2.64E-2)*THETA*VT(J,K)*180.0/PI
1272                RE(J,K)=VT(J,K)*C/VIS
1273                RCO(J,K)=C*1.2*(RE(J,K)**(-0.2))*VSO(J,K)/VT(J,K)
1274                CIR(J,K)=2.0*PI*VSO(J,K)*RCO(J,K)
1275                CIROLL(J,K)=VAR1*(1.0-(1.5*MU*SIGN*SIN(EPSI(L,K))))
1276           10   CONTINUE
1277                DO 20 L=1,NOSTPS-1
1278                CIR(L,K)=(CIR(L,K)+CIR(L+1,K))/2.0
1279                IF((L.GT.3).AND.(M51.EQ.YES)) CIR(L,K)=(CIROLL(L,K)+CIROLL(L+1,K)
1280               C/2.
1281           20   CONTINUE
1282                RETURN
1283                END
```

```
LINE NUMBER    FORTRAN TEXT

1284                SUBROUTINE CAL( XV,YV,ZV,XP,YP,ZP,NO,VINDV,J,R,B,JJ,KC,KL,KO
1285               C,RC,RL,PO,VA,VB,C,D,E,NCOUNT,GAMAx,RCO,VSO,CC,NTYPV,SIGN,NTYPC
1286               C,CIR)
1287                REAL KC,KL,KO
1288                DIMENSION RC(2000)
1289                DIMENSION XP(40),YP(40),ZP(40)
1290                DIMENSION XV(100,20),YV(100,20),ZV(100,20),VINDV(100,20)
1291                DIMENSION CIR(100,20),VIV(100),VIVT(100)
1292                DIMENSION THETA(100)
1293                COMMON/BL1/WY(40)
1294                COMMON/BL21/ N,NFILASTP
1295                DATA ROE,PI/1.225,3.1415927/
1296                M=1
1297          C     WRITE(6,2010)NCOUNT,N,NTYPV
1298           2010 FORMAT('NCOUNT=',I2,' N=',I2,' NTYPV=',I2)
1299          C     WRITE(6,90)
1300            90  FORMAT('H',10x,'VORTEX X COORD',10X,'VORTEX Y COORD',10X,'VORTEX Z
1301               C COORD')
1302          C     WRITE(6,91)(XV(L),YV(L),ZV(L),L=1,7)
1303            91  FORMAT(' ',10X,1F14.4,10X,1F14.4,10X,1F14.4)
1304            22  DO 40 K=1,N-1
1305                THETA(K)=(K-1)*2*PI/(NFILASTP-1)
1306                CD1=(XP(M)-XV((K+1),JJ))*(YP(M)-YV(K,JJ))
1307                CD2=(YP(M)-YV((K+1),JJ))*(XP(M)-XV(K,JJ))
1308                CD=(CD1-CD2)
1309                C1=(XP(M)-XV((K+1),JJ))**2
1310                C2=(YP(M)-YV((K+1),JJ))**2
1311                C3=(ZP(M)-ZV((K+1),JJ))**2
1312                AP=SQRT(C1+C2+C3)
1313                C4=(XP(M)-XV(K,JJ))**2
1314                C5=(YP(M)-YV(K,JJ))**2
1315                C6=(ZP(M)-ZV(K,JJ))**2
1316                BP=SQRT(C4+C5+C6)
1317                A4=XV((K+1),JJ)*XV(K,JJ)
1318                A5=(YP(M)-YV((K+1),JJ))*(YP(M)-YV(K,JJ))
1319                A6=ZV((K+1),JJ)*ZV(K,JJ)
1320                A7=(AP+BP)/(AP*BP)
1321                A8=R*((AP*BP)+A4+A5+A6)
1322                F=A7/A8
1323                IF(NTYPC.EQ.1) CIR(K,JJ)=2.0*PI*VSO*RCO
1324          C     IF(K.EQ.1) GOTO 540
1325          C      CORE
1326          C     CHECK IF BLADE TIP STATION POINTS ARE LOCATED INSIDE VORTEX
1327                VN1=(XV(K+1,JJ)-XV(K,JJ))**2
1328                VN2=(YV(K+1,JJ)-YV(K,JJ))**2
1329                VN3=(ZV(K+1,JJ)-ZV(K,JJ))**2
1330                AB=SQRT(VN1+VN2+VN3)
1331                IF((BP.LT.1E-3).OR.(AB.LT.1E-3)) GOTO 2020
1332                GOTO 2021
1333           2020 WRITE(6,2030)
1334           2030 FORMAT('BP OR AP LESS THAN 1E-3')
1335                GOTO 540
1336           2021 IF(NCOUNT.EQ.1) GOTO 778
1337                ANGLEB=ACOS(((BP**2)+(AB**2)-(AP**2))/(2.0*BP*AB))
1338                H=ABS(BP*SIN(ANGLEB))*R
1339                IF(NTYPV.EQ.1) GOTO 531
```

```
LINE NUMBER    FORTRAN TEXT

1340                IF(NTYPV.EQ.2) GOTO 532
1341                IF(H.GT.R0) GOTO 500
1342                IF((H.GT.RL).AND.(H.LE.R0)) GOTO 510
1343                IF((H.GT.RC(K)).AND.(H.LE.RL)) GOTO 520
1344                IF(H.LE.RC(K)) GOTO 530
1345             500 CIR(K,JJ)=K0
1346                 GOTO 778
1347             510 CIR(K,JJ)=(1.0-EXP((D*H/CC)+E))*0.99*GAMAX
1348                 GOTO 778
1349             520 CIR(K,JJ)=((VE*ALOG(H/CC))+C)*0.99*GAMAX
1350                 GOTO 778
1351             530 CIR(K,JJ)=KC*(H/RC(K))**2
1352                 GOTO 778
1353             531 IF(H.GT.RC(K)) GOTO 778
1354                 CIR(K,JJ)=KC*(H/RC(K))**2
1355                 GOTO 778
1356             532 IF(H.GT.R0) GOTO 533
1357                 IF((H.LE.R0).AND.(H.GT.RC(K))) GOTO 534
1358                 CIR(K,JJ)=KC*(H/RC(K))**2
1359                 GOTO 778
1360             533 CIR(K,JJ)=K0
1361                 GOTO 778
1362             534 FF=KC/(((RC0+0.0018)/CC)**(.778))
1363                 CIR(K,JJ)=FF*(((H+0.0018)/CC)**(.778))
1364                 GOTO 778
1365             540 IF((YV(K,JJ).LT.1.01).AND.(YV(K,JJ).GT.0.99))GOTO 777
1366                 GOTO 778
1367             777 IF(NO.EQ.1) GOTO 779
1368                 GOTO 778
1369             779 SM=(1-YP(M))*R
1370                 IF(SM.LT.RC0) GOTO 801
1371                 GOTO 778
1372             801 VIV(K)=VS0*SM/RC0
1373                 GOTO 40
1374             778 VIV(K)=SIGN*((CIR(K,JJ)*F)/(4*PI))*CD
1375           C     WRITE(6,2000)K,JJ,CIR(K,JJ)
1376            2000 FORMAT('CIR(',I2,I2,')=',1F12.6)
1377           C     CHECK COMPLETE
1378              40 CONTINUE
1379           C     WRITE(6,51)
1380              51 FORMAT('H',' ')
1381                 VIVT(1)=VIV(1)
1382                 DO 45 I=2,N-1
1383                 VIVT(I)=VIV(I)+VIVT(I-1)
1384              45 CONTINUE
1385                 VINDV(M,JJ)=VIVT(N-1)
1386                 M=M+1
1387                 IF(M.LE.14)GOTO 22
1388           C     WRITE(6,80)
1389              80 FORMAT('H','TOTAL VORTEX INDUCED VELOCITY AT EACH STATION
1390                CPOINT IS')
1391           C     WRITE(6,*)(VINDV(L),L=1,14)
1392                 RETURN
1393                 END
```

```
LINE NUMBER    FORTRAN TEXT

1394                SUBROUTINE BLVOCO(XV,YV,ZV,BB,I)
1395                DIMENSION XV(100,20),YV(100,20),ZV(100,20),THETA(100)
1396                COMMON/BL21/ N,NFILASTP
1397                PI=3.1415927
1398          C     VORTEX COORDS FROM OTHER BLADES
1399                DO 31 K=1,N
1400                THETA(K)=(K-1)*2*PI/(NFILASTP-1)
1401                AB=SQRT(YV(K,1)**2+XV(K,1)**2)
1402                YV(K,I)=AB*COS(((2*PI)/BB)+THETA(K))
1403                XV(K,I)=AB*SIN(((2*PI)/BB)+THETA(K))
1404                ZV(K,I)=ZV(K,1)
1405             31 CONTINUE
1406                RETURN
1407                END

LINE NUMBER    FORTRAN TEXT

1408                SUBROUTINE LANDG(XV,YV,ZV,CT,B,BS,R)
1409                DIMENSION XV(100,20),YV(100,20),ZV(100,20)
1410                DIMENSION THETA(100),RV(100)
1411                COMMON/BL2/A1,A2,A3
1412                COMMON/BL21/ N,NFILASTP
1413                DATA ROE,PI/1.225,3.1415927/
1414          C     LANDGREBE WAKE COEFFS.
1415                A1=-0.25*(CT/BS)
1416                A2=-1.41*SQRT(CT/2)
1417                A3=0.145+(27*CT)
1418          C     VORTEX FILAMENT ANGLE
1419                DO 30 K=1,N
1420                THETA(K)=(K-1)*2*PI/(NFILASTP-1)
1421                IF(THETA(K)-PI)3,4,4
1422             3  ZV(K,1)=A1*THETA(K)
1423                GOTO 5
1424             4  ZV(K,1)=(A1*2*PI/B)+A2*(THETA(K)-2*PI/B)
1425             5  RV(K)=0.78+0.22*EXP(-A3*THETA(K))
1426                XV(K,1)=RV(K)*SIN(THETA(K))
1427                YV(K,1)=RV(K)*COS(THETA(K))
1428             30 CONTINUE
1429                RETURN
1430                END
```

```
LINE NUMBER    FORTRAN TEXT

1431                SUBROUTINE STRIP(VO,Y,TOT,CT,VI,R,BETA,C,BS,B,A,W)
1432                REAL MACHNO
1433                DIMENSION EBETA(40),VAR7(40),BETA(40),C(40)
1434                DIMENSION Y(40),BS(40)
1435                DIMENSION VO(40),T(40),VI(40),TT(40)
1436                DIMENSION AN(40)
1437                DIMENSION AA(40)
1438                DATA ROE,PI/1.225,3.1415927/
1439                VAR8=BETA(8)*180/PI
1440                DO 5 I=1,14
1441                EBETA(I)=TAN(VO(I)/(W*Y(I)*R))
1442              5   CONTINUE
1443            C     WRITE(6,300)VAR8
1444              300 FORMAT('H','GEOMETRIC ANGLE OF INCIDENCE (75%R) IS:',1F8.4,'DEGS
1445            C     WRITE(6,400)R
1446              400 FORMAT(' ','BLADE RADIUS IS:',1F8.4,'M')
1447            C     WRITE(6,401)(C(L),L=1,14)
1448              401 FORMAT(' ','BLADE CHORD AT .75R IS:',1F8.4,'M')
1449            C     WRITE(6,402)(BS(L),L=1,14)
1450              402 FORMAT(' ','ROTOR SOLIDITY IS:',1F8.4)
1451            C     WRITE(6,301)
1452              301 FORMAT(' ','ELEMENTAL INFLOW ANGLES FROM APPARENT VERTICAL FLIGH
1453                 C INCIDENT VELOCITIES ARE:')
1454            C     WRITE(6,302)(EBETA(L),L=1,14)
1455              302 FORMAT(' ',2F8.4)
1456                DO 10 I=1,14
1457                VAR1=(VO(I)/2)+(BS(I)*A*W*R/16)
1458                VAR2=2*((BETA(I)*Y(I)*W*R)-VO(I))
1459                VAR3=(4*VO(I)*VO(I))/(BS(I)*A*W*R)
1460                VAR4=BS(I)*A*W*R/16.
1461                VAR7(I)=1.0+((VAR2)/(VAR3+VO(I)+VAR4))
1462                VI(I)=VAR1*(-1.0+SQRT(ABS(VAR7(I))))
1463                AN(I)=(VI(I)+VO(I))/(W*Y(I)*R)
1464                MACHNO=(W*R*Y(I))/340.0
1465                PRANDTL=1.0/SQRT(1.0-(MACHNO**2))
1466                VVV=COS(AN(I))*PRANDTL
1467                AA(I)=(BETA(I)-AN(I))*180.0/PI
1468                IF(AA(I).LT.0.0) GOTO 36
1469                IF(I.LE.9) GOTO 20
1470                GOTO 21
1471              20  T(I)=0.5*ROE*(W*R*Y(I))**2*A*C(I)*0.10*R*(BETA(I)-AN(I))*VVV
1472                GOTO 10
1473              21  T(I)=0.5*ROE*(W*R*Y(I))**2*A*C(I)*0.02*R*(BETA(I)-AN(I))*VVV
1474                GOTO 10
1475              36  T(I)=0.0
1476              10  CONTINUE
1477            C     WRITE(6,303)
1478              303 FORMAT(' ','INDUCED VELOCITY(STRIP) SQRT QUANTITY:')
1479            C     WRITE(6,304)(VAR7(L),L=1,14)
1480              304 FORMAT(' ',2F8.4)
1481            C     WRITE(6,305)
1482              305 FORMAT(' ','EFFECTIVE ELEMENTAL ANGLE OF INCIDENCE IS:')
1483            C     WRITE(6,306)(AA(L),L=1,14)
1484              306 FORMAT(' ',2F8.4)
1485                VAR9=1.0
1486                TT(1)=T(1)
```

```
LINE NUMBER    FORTRAN TEXT

1487                DO 80 I=2,14
1488                TT(I)=T(I)+TT(I-1)
1489              80  CONTINUE
1490                CT=(B*TT(14))/(ROE*(W*R)**2*PI*R**2)
1491           C    WRITE(6,100)
1492              100 FORMAT(' ','THRUST WITHOUT TIP LOSS IS:')
1493           C    WRITE(6,*) TT(14)
1494           C    WRITE(6,91)CT
1495              91  FORMAT(' ','THRUST COEFF. WITHOUT TIP LOSS IS:',1F8.4)
1496           C    TIP LOSS FACTOR
1497                IF(CT.LT.0.0) GOTO 592
1498                VAR5=1-(SQRT(2.0*CT)/B)
1499           C    WRITE(6,800)VAR5
1500              800 FORMAT(' ','TIP LOSS FACTOR IS:',1F8.4)
1501                GOTO 806
1502              592 VAR5=1.0
1503              806 DO 30 I=1,14
1504                IF(Y(I).GT.VAR5) GOTO 31
1505                GOTO 30
1506              31  T(I)=0.0
1507              30  CONTINUE
1508           C    DO 33 K=1,14
1509           C    IF(VI(K).LT.0.0) GOTO 34
1510           C    GOTO 33
1511           C    VI(K)=0.0                    LINE=34
1512           C    T(K)=0.0
1513           C    CONTINUE            LABEL=33
1514           C    WRITE(6,89)
1515              89  FORMAT(' ','STRIP INDUCED VELS. ARE:')
1516           C    WRITE(6,*)(VI(L),L=1,14)
1517           C    WRITE(6,90)
1518              90  FORMAT(' ','STRIP ELEMENTAL LIFTS ARE:')
1519           C    WRITE(6,*)(T(L),L=1,14)
1520                DO 32 I=2,14
1521                TT(I)=T(I)+TT(I-1)
1522              32  CONTINUE
1523                TOT=TT(14)
1524                CT=(B*TT(14))/(ROE*(W*R)**2*PI*R**2)
1525           C    WRITE(6,200) TOT
1526              200 FORMAT(' ','THRUST VALUE WITH TIP LOSS IS:',1F12.6,'N')
1527                RETURN
1528                END
```

```
LINE NUMBER    FORTRAN TEXT

1529                SUBROUTINE PERM(VIT,Y,TH,TOR,DT,R,THETA,C,BS,B,ENERGY,GAMAX
1530               C,A,W,THI,NUM,UT,DHSUM)
1531                REAL MACHNO
1532                DIMENSION DL(40),DPD(40),DH(40),DHSUM(40)
1533                DIMENSION GAMA(14),TORITIP(14),DL2D(40)
1534                DIMENSION TORIS(40),BS(40),CL(40),TORPS(40)
1535                DIMENSION  Y(40),THI(40),VIT(40),DT(40),CDO(40),TORI(40),
1536               C TORP(40),TH(40),TOR(40),C(40),THETA(40),UT(40)
1537                COMMON/BL22/ BETA,AZIMUTH,SIGN
1538                DATA ROE,PI/1.225,3.1415927/
1539                DO 50 I=1,14
1540                IF(NUM.EQ.2) GOTO 95
1541                THI(I)=VIT(I)/(W*Y(I)*R)
1542             95 IF(ABS(THETA(I)-THI(I)).GT.0.21) GOTO 81
1543                IF((THETA(I)-THI(I)).LT.0.0) WRITE(6,84) I
1544                VELR=W*R*Y(I)
1545                IF(NUM.EQ.2) VELR=UT(I)
1546                IF(VELR.LT.0.0) GOTO 81
1547                MACHNO=VELR/340.0
1548                VV=COS(THI(I))
1549                VVV=1.0/(1.0-(MACHNO**2))
1550                IF(I.LE.9) GOTO 36
1551                GOTO 37
1552             36 DL(I)=0.5*ROE*(VELR**2)*A*C(I)*0.10*R*(THETA(I)-THI(I))*VVV
1553                DL2D(I)=DL(I)/(0.1*R)
1554                GAMA(I)=DL(I)/(ROE*VELR*0.1*R)
1555                GOTO 38
1556             37 DL(I)=0.5*ROE*(VELR**2)*A*C(I)*0.02*R*(THETA(I)-THI(I))*VVV
1557                IF((I.EQ.14).AND.(DL(I).LT.0.0)) DL(I)=0.0
1558                DL2D(I)=DL(I)/(0.02*R)
1559                GAMA(I)=DL(I)/(ROE*VELR*0.02*R)
1560          C     PROFILE DRAG COEFF.
1561             38 PAR1=ABS(THETA(I)-THI(I))
1562                CDO(I)=0.0087-(0.0216*PAR1)+(0.4*PAR1**2)
1563          C     INDUCED TORQUE
1564                TORI(I)=DL(I)*Y(I)*THI(I)*R
1565                IF(I.LE.9) GOTO 39
1566                GOTO 40
1567          C     PROFILE TORQUE
1568             39 TORP(I)=0.5*ROE*(VELR**2)*Y(I)*R*C(I)*0.10*CDO(I)*R*VV
1569                GOTO 50
1570             40 TORP(I)=0.5*ROE*(VELR**2)*Y(I)*R*C(I)*0.02*CDO(I)*R*VV
1571                GOTO 50
1572             81 DL(I)=0.0
1573                TORI(I)=0.0
1574                TORP(I)=0.0
1575          C     WRITE(6,82)I
1576             82 FORMAT('BLADE AT STATION PT.',I2,' IS STALLED')
1577             84 FORMAT('BLADE ELEMENT AT STATION PT.',I2,' IS AT A -VE A-O-A')
1578             50 CONTINUE
1579                DO 51 I=1,14
1580                DPD(I)=TORP(I)/(Y(I)*R*COS(THI(I)))
1581                DT(I)=(DL(I)*COS(THI(I)))-(DPD(I)*SIN(THI(I)))
1582                IF(NUM.EQ.2) DT(I)=DT(I)*COS(BETA)
1583                IF(NUM.EQ.2) GOTO 52
1584                GOTO 51
```

```
LINE NUMBER    FORTRAN TEXT

1585              52  VAR1=(DPD(I)*COS(THI(I)))+(DL(I)*SIN(THI(I)))
1586                  VAR2=(DL(I)*COS(THI(I)))-(DPD(I)*SIN(THI(I)))
1587                  DH(I)=(VAR1*SIGN*SIN(AZIMUTH))-(VAR2*SIN(BETA)*COS(AZIMUTH))
1588              51  CONTINUE
1589            C     WRITE(6,60)
1590              60  FORMAT(' ','ELEMENTAL LIFTS ARE:')
1591            C     WRITE(6,*)(DL(L),L=1,14)
1592            C     WRITE(6,53)
1593              53  FORMAT('ELEMENTAL THRUST DISTRIBUTION IS:')
1594            C     WRITE(6,*)(DT(L),L=1,14)
1595            C     WRITE(6,61)
1596              61  FORMAT('2-DIMENSIONAL LIFT DISTRIBUTION IS:')
1597            C     WRITE(6,*)(DL2D(L),L=1,14)
1598            C     WRITE(6,70)
1599              70  FORMAT(' ','INDUCED TORQUE DISTRIBUTION IS:')
1600            C     WRITE(6,*)(TORI(L),L=1,14)
1601            C     WRITE(6,71)
1602              71  FORMAT(' ','PROFILE DRAG COEFF. DISTRIBUTION IS:')
1603            C     WRITE(6,*)(CDO(L),L=1,14)
1604            C     WRITE(6,72)
1605              72  FORMAT(' ','PROFILE TORQUE DISTRIBUTION IS:')
1606            C     WRITE(6,*)(TORP(L),L=1,14)
1607                  TORIS(1)=TORI(1)
1608                  TORPS(1)=TORP(1)
1609                  DO 30 M=2,14
1610                  TORIS(M)=TORI(M)+TORIS(M-1)
1611                  TORPS(M)=TORP(M)+TORPS(M-1)
1612              30  CONTINUE
1613                  WRITE(6,31)
1614              31  FORMAT(' ','INDUCED TORQUE VALUE IS:')
1615                  WRITE(6,*) TORIS(14)
1616                  WRITE(6,35)TORPS(14)
1617               35 FORMAT('PROFILE TORQUE VALUE IS:',1F10.5)
1618                  TH(1)=DT(1)
1619                  TOR(1)=TORI(1)+TORP(1)
1620                  IF(NUM.EQ.2) DHSUM(1)=DH(1)
1621                  DO 20 K=2,14
1622                  IF(NUM.EQ.2) DHSUM(K)=DH(K)+DHSUM(K-1)
1623                  TH(K)=DT(K)+TH(K-1)
1624                  TOR(K)=TORI(K)+TORP(K)+TOR(K-1)
1625              20  CONTINUE
1626                  GAMAX=0.0
1627                  DO 500 L=1,14
1628                  GAMAX=AMAX1(GAMAX,GAMA(L))
1629              500 CONTINUE
1630                  DO 110 L=1,14
1631                  IF(ABS(GAMA(L)-GAMAX).LT.1E-3) NUM=L
1632              110 CONTINUE
1633                  WRITE(6,120) Y(NUM)
1634              120 FORMAT('THE MAXIMUM CIRCULATION IS LOCATED AT',1F4.2,' RADIUS')
1635                  WRITE(6,121) GAMAX
1636              121 FORMAT(/,'MAXIMUM BOUND CIRCULATION IS:',1F8.4)
1637                  WRITE(6,*)(GAMA(L),L=NUM,14)
1638                  TORITIP(NUM-1)=0.0
1639                  DO 130 L=NUM,14
1640                  TORITIP(L)=TORITIP(L-1)+(DT(L)*THI(L))
```

```
LINE NUMBER    FORTRAN TEXT

1641               130 CONTINUE
1642                   ENERGY=TORITIP(14)
1643                   RETURN
1644                   END
```

```
LINE NUMBER    FORTRAN TEXT

1645                SUBROUTINE POSTN(XFV,YFV,ZFV,XVELT,YVELT,ZVELT,KO,XFVNEW,YFVNEW
1646               C,ZFVNEW,M,RAD,TIME,VIG,NBU,M7,M8,M6)
1647                REAL YES
1648                DIMENSION VELG(100,20)
1649                DIMENSION XVELT(100,20),YVELT(100,20),ZVELT(100,20)
1650                DIMENSION XFV(100,20),YFV(100,20),ZFV(100,20),XFVNEW(100,20)
1651                DIMENSION YFVNEW(100,20),ZFVNEW(100,20),DELTAXFV(100,20)
1652                DIMENSION DELTAYFV(100,20),DELTAZFV(100,20),TIME(20),RAD(20)
1653                COMMON/BLS/ OMEGA,ALPHA,V
1654                DATA YES/1HY/
1655                DO 10 K=1,M
1656          C      M7=YES,CLASSICAL WAKE REQUIRED.
1657                IF(M7.EQ.YES) GOTO 22
1658                DELTAXFV(K,KO)=XVELT(K,KO)*TIME(KO)/RAD(KO)
1659                DELTAYFV(K,KO)=(YVELT(K,KO)+(V*COS(ALPHA)))*TIME(KO)/RAD(KO)
1660                IF(M6.EQ.YES) VERV=V*SIN(ALPHA)
1661                IF(M6.EQ.YES) GOTO 21
1662                RVORT=SQRT(XFV(K,KO)**2+YFV(K,KO)**2)
1663                IF(YFV(K,KO).GT.1.0) VERV=(V*SIN(ALPHA))-(2.0*VIG)
1664                VELG(K,KO)=2.0*VIG
1665                IF((RVORT.GT.1.0).AND.(YFV(K,KO).GT.1.0)) GOTO 21
1666                EPSV=ATAN2(-XFV(K,KO),YFV(K,KO))
1667                IF(KO.GT.NBU) EPSV=ATAN2(XFV(K,KO),YFV(K,KO))
1668                IF(RVORT.GT.1.0) RVORT=1.0
1669                VERV=(V*SIN(ALPHA))-(VIG*(1.0+(RVORT*COS(EPSV))))
1670                VELG(K,KO)=VIG*(1.0+(RVORT*COS(EPSV)))
1671             21 DELTAZFV(K,KO)=(ZVELT(K,KO)+(VERV))*TIME(KO)/RAD(KO)
1672                GOTO 23
1673             22 DELTAXFV(K,KO)=0.0
1674                DELTAYFV(K,KO)=(V*COS(ALPHA))*TIME(KO)/RAD(KO)
1675                DELTAZFV(K,KO)=((V*SIN(ALPHA))-VIG)*TIME(KO)/RAD(KO)
1676             23 XFVNEW(K,KO)=XFV(K,KO)+DELTAXFV(K,KO)
1677                YFVNEW(K,KO)=YFV(K,KO)+DELTAYFV(K,KO)
1678                ZFVNEW(K,KO)=ZFV(K,KO)+DELTAZFV(K,KO)
1679             10 CONTINUE
1680          C     WRITE(6,20)M,KO
1681             20 FORMAT('ROTOR AT POSTN',1X,I2,' FOR HELIX NO',I2,/)
1682          C     WRITE(6,7)
1683             7  FORMAT('GLAUERT DISTRIBUTION IS:',/)
1684          C     WRITE(6,8)(VELG(L,KO),L=1,M)
1685             8  FORMAT(1F12.6)
1686          C     WRITE(6,60)
1687             60 FORMAT(7X,'DELTAXFV',7X,'DELTAYFV',7X,'DELTAZFV')
1688          C     WRITE(6,61)(DELTAXFV(L,KO),DELTAYFV(L,KO),DELTAZFV(L,KO),L=1,M)
1689             61 FORMAT((6X,1F8.4,2(7X,1F8.4)))
1690          C     WRITE(6,62)
1691             62 FORMAT(/,7X,'XVELT',7X,'YVELT',7X,'ZVELT')
1692          C     WRITE(6,63)(XVELT(L,KO),YVELT(L,KO),ZVELT(L,KO),L=1,M)
1693             63 FORMAT(3(4X,1F8.4))
1694          C     WRITE(6,30)
1695             30 FORMAT(/,7X,'XP',7X,'XP1',7X,'YP',7X,'YP1',7X,'ZP',7X,'ZP1')
1696          C     WRITE(6,40)(XFV(L,KO),XFVNEW(L,KO),YFV(L,KO),YFVNEW(L,KO)
1697          C    C,ZFV(L,KO),ZFVNEW(L,KO),L=1,M)
1698             40 FORMAT((4X,1F8.2,5(1X,1F8.2)))
1699                RETURN
1700                END
```

```
LINE NUMBER    FORTRAN TEXT

1701                SUBROUTINE GLAUERT(A,B,C,W,R,THETA,ALPHA,FORVEL,VI,VVV,T)
1702                DIMENSION COF(5),ZP(5),RP(5)
1703                REAL MU,LANDA
1704                DATA PI/3.1415927/,ROE/1.225/
1705                VI=0.0
1706                NUM=0
1707              5 P1=0.1E0
1708                TOL=X02AAF(P1)
1709              C WRITE(6,2000)NUM
1710           2000 FORMAT('NUM=',I2)
1711                NUM=NUM+1
1712                LANDA=((FORVEL*SIN(ALPHA))-(VI+VVV))/(W*R)
1713                MU=(FORVEL*COS(ALPHA))/(W*R)
1714                VAR1=((THETA/3.)+(((MU**2)*THETA)/2.)+(LANDA/2.))
1715                VAR2=0.5*ROE*A*B*C*(W**2)*(R**3)
1716                T=VAR1*VAR2
1717              C WRITE(6,8)
1718              8 FORMAT('GLAUERT THRUST IS:')
1719              C WRITE(6,*)T
1720                IF(NUM.GT.10)GOTO 10
1721                VIAPPROX=T/(2.0*ROE*PI*(R**3)*FORVEL)
1722                COF(1)=1.0
1723                COF(2)=2.0*VVV
1724                COF(3)=FORVEL**2+VVV**2
1725                COF(4)=0.0
1726                COF(5)=-(T**2)/(4.0*((ROE*PI)**2)*(R**4))
1727                NC=5
1728                IFAIL=0
1729                CALL C02AEF(COF,NC,RP,ZP,TOL,IFAIL)
1730                DO 60 K=1,4
1731                IF(ZP(K).LT.0.1E-2) GOTO 70
1732                GOTO 60
1733             70 IF(RP(K).GT.0.1E-2) GOTO 80
1734                GOTO 60
1735             80 VI=RP(K)
1736                IF(T.LT.0.0) VI=-VI
1737              C WRITE(6,90)VI
1738             90 FORMAT('VI=',1F12.6)
1739             60 CONTINUE
1740              C WRITE(6,30)(RP(L),ZP(L),L=1,4)
1741             30 FORMAT('RP=',1F8.4,'IP=',1F8.4,//)
1742              C VIHOVER=SQRT(T/(2.0*ROE*PI*R**2))
1743              C WRITE(6,40) VIAPPROX,VIHOVER
1744             40 FORMAT('VIAPPROX=',1F3.4,'VIHOVER=',1F8.4)
1745                GOTO 5
1746             10 RETURN
1747                END
```

```
LINE NUMBER    FORTRAN TEXT

1748                SUBROUTINE IND(XFV,YFV,ZFV,KO,LO,XVEL,YVEL,ZVEL,MMM,
1749               CNOSTPS,R,VORTEXKC,VORTEXKO,VORTEXRC,VORTEXRL,VORTEXRO,VORTEXA
1750               C,VORTEXB,VORTEXC,VORTEXD,VORTEXE,NTYPV,GAMAX,CIRAV,SIGN)
1751                DIMENSION VX(200),VY(200),VZ(200)
1752                DIMENSION VIX(200),VIY(200),VIZ(200)
1753                DIMENSION XV(200),YV(200),ZV(200),XV1(200),YV1(200),ZV1(200)
1754                DIMENSION VIXT(200),VIYT(200),VIZT(200)
1755                DIMENSION XFV(100,20),YFV(100,20),ZFV(100,20),CIRAV(100,20)
1756                DIMENSION XVEL(100,20,20),YVEL(100,20,20),ZVEL(100,20,20)
1757                DIMENSION VORTEXKC(100,20),VORTEXKO(100,20),VORTEXRC(100,20)
1758               C,VORTEXRL(100,20),VORTEXRO(100,20),VORTEXA(100,20)
1759               C,VORTEXB(100,20),VORTEXC(100,20),VORTEXD(100,20)
1760               C,VORTEXE(100,20)
1761                REAL I,J,K
1762                COMMON/BL25/ VSO,RCC
1763                CALL ICL9HEMASK(64,IRES)
1764          C                   VIZ                          Z(+VE UPWARD)
1765          C                    *                           *
1766          C                    *                          *
1767          C      **********P(XP,YP,ZP)                    *
1768          C      VIX       *  *  *                       *
1769          C              *   *   *                      *
1770          C            *     *    *  X************       *
1771          C          *     VIY     *              *      *
1772          C        A     *         *              *      *
1773          C     (XA,YA,ZA)  *      *              *      *
1774          C                        *  *           *      *
1775          C                           *           *      *
1776          C                             R         Y
1777          C                       (XR,YR,ZR)
1778          C
1779                DO 100 LL=1,NOSTPS
1780                XP=XFV(LL,KO)
1781                YP=YFV(LL,KO)
1782                ZP=ZFV(LL,KO)
1783                DO 110 L=1,(NOSTPS-1)
1784          C     WRITE(6,*)L
1785                IF(MMM.EQ.2) GOTO 310
1786                IF(L.EQ.LL) GOTO 300
1787                IF((L+1).EQ.LL) GOTO 300
1788                IF(NTYPV.EQ.1) GOTO 310
1789                GOTO 310
1790             300 VIX(L)=0.0
1791                VIY(L)=0.0
1792                VIZ(L)=0.0
1793                GOTO 110
1794             310 CIR=CIRAV(L,LO)
1795                XA=XFV(L,LO)
1796                YA=YFV(L,LO)
1797                ZA=ZFV(L,LO)
1798                XB=XFV(L+1,LO)
1799                YB=YFV(L+1,LO)
1800                ZB=ZFV(L+1,LO)
1801                PI=3.1415927
1802                VAR1=(XP-XA)**2
1803                VAR2=(YP-YA)**2
```

```
LINE NUMBER    FORTRAN TEXT

1804                VAR3=(ZP-ZA)**2
1805                AP=SQRT(VAR1+VAR2+VAR3)
1806                VAR4=(XP-XB)**2
1807                VAR5=(YP-YB)**2
1808                VAR6=(ZP-ZB)**2
1809                BP=SQRT(VAR4+VAR5+VAR6)
1810                IF((BP.LT.1E-3).OR.(AP.LT.1E-3)) GOTO 997
1811                I=(XP-XA)*(XP-XB)
1812                J=(YP-YA)*(YP-YB)
1813                K=(ZP-ZA)*(ZP-ZB)
1814                VAR7=(AP*BP)/(AP*BP)
1815                VAR8=(AP*BP)+I+J+K
1816                CON1=VAR7/(R*VAR8)
1817                AB=SQRT((XA-XB)**2+(YA-YB)**2+(ZA-ZB)**2)
1818                IF(AB.LT.1E-3) GOTO 997
1819                ANGLEB=ACOS(((BP**2)+(AB**2)-(AP**2))/(2.0*BP*AB))
1820                H=ABS(BP*SIN(ANGLEB))
1821                IF((H.LT.RCO).AND.(NTYPV.EQ.1)) CIR=CIR*(H/RCO)**2
1822                IF(NTYPV.EQ.1) GOTO 629
1823                IF(H.GT.(VORTEXRO(L,LO)/R)) GOTO 500
1824                VORT1=VORTEXRL(L,LO)/R
1825                VORT2=VORTEXRC(L,LO)/R
1826                VORT3=VORTEXRC(L,LO)/R
1827                IF((H.GT.VORT1).AND.(H.LT.VORT2)) GOTO 510
1828                IF((H.GT.VORT3).AND.(H.LE.VORT1)) GOTO 520
1829                IF(H.LE.(VORTEXRC(L,LO)/R)) GOTO 530
1830           500  CIR=VORTEXKO(L,LO)
1831                GOTO 629
1832           510  CIR=(1.0-EXP((VORTEXD(L,LO)*H*R/C)+VORTEXE(L,LO)))*0.99*GAMAX
1833                GOTO 629
1834           520  CIR=((VORTEXB(L,LO)*ALOG(H*R/C))+VORTEXC(L,LO))*0.99*GAMAX
1835                GOTO 629
1836           530  CIR=((H*R/VORTEXRC(L,LO))**2)*VORTEXKC(L,LO)
1837           629  CON2=SIGN*CIR*CON1/(4.0*PI)
1838                VARX=((YP-YA)*(ZP-ZB))-((ZP-ZA)*(YP-YB))
1839                VIX(L)=CON2*VARX
1840                IF(ABS(VIX(L)).GT.VSO) WRITE(6,710)
1841           710  FORMAT('VIX.GT.VSO')
1842                IF(ABS(VIX(L)).GT.VSO) VIX(L)=VSO
1843                VARY=((ZP-ZA)*(XP-XB))-((XP-XA)*(ZP-ZB))
1844                VIY(L)=CON2*VARY
1845                IF(ABS(VIY(L)).GT.VSO) WRITE(6,711)
1846           711  FORMAT('VIY.GT.VSO')
1847                IF(ABS(VIY(L)).GT.VSO) VIY(L)=VSO
1848                VAR7=((XP-XA)*(YP-YB))-((YP-YA)*(XP-XB))
1849                VIZ(L)=CON2*VARZ
1850                IF(ABS(VIZ(L)).GT.VSO) WRITE(6,712)
1851           712  FORMAT('VIZ.GT.VSO')
1852                IF(ABS(VIZ(L)).GT.VSO) VIZ(L)=VSO
1853                GOTO 110
1854           997  WRITE(6,379)
1855           379  FORMAT('I AM HERE')
1856                VIX(L)=0.0
1857                VIY(L)=0.0
1858                VIZ(L)=0.0
1859          C     WRITE(6,10)
```

```
LINE NUMBER    FORTRAN TEXT

1860              10   FORMAT(7X,'XA',7X,'YA',7X,'ZA',7X,'XB',7X,'YB',7X,'ZB')
1861            C      WRITE(6,20)XA,YA,ZA,XB,YB,ZB
1862              20   FORMAT(4X,1F8.2,5(1X,1F8.2),//)
1863            C      WRITE(6,30)
1864              30   FORMAT(7X,'XP',7X,'YP',7X,'ZP')
1865            C      WRITE(6,40)XP,YP,ZP
1866              40   FORMAT(3(2X,1F8.2))
1867              110  CONTINUE
1868            C      WRITE(6,740)
1869              740  FORMAT('VIX DISTRIBUTION IS:')
1870            C      WRITE(6,*)(VIX(JJJ),JJJ=1,(NOSTPS-1))
1871            C      WRITE(6,741)
1872              741  FORMAT('VIY DISTRIBUTION IS:')
1873            C      WRITE(6,*)(VIY(JJJ),JJJ=1,(NOSTPS-1))
1874            C      WRITE(6,750)
1875              750  FORMAT('VIZ DISTRIBUTION IS:')
1876            C      WRITE(6,*)(VIZ(JJJ),JJJ=1,(NOSTPS-1))
1877                   VIXT(1)=VIX(1)
1878                   VIYT(1)=VIY(1)
1879                   VIZT(1)=VIZ(1)
1880                   DO 250 N=2,(NOSTPS-1)
1881                   VIXT(N)=VIXT(N-1)+VIX(N)
1882                   VIYT(N)=VIYT(N-1)+VIY(N)
1883                   VIZT(N)=VIZT(N-1)+VIZ(N)
1884              250  CONTINUE
1885            C      LL=STATION POINT.
1886            C      KO=HELIX NUMBER STATION POINT LL IS LOCATED.
1887            C      LO=HELIX NUMBER THE INDUCED VELOCITIES ARE FROM.
1888                   XVEL(LL,KO,LO)=VIXT(NOSTPS-1)
1889                   YVEL(LL,KO,LO)=VIYT(NOSTPS-1)
1890                   ZVEL(LL,KO,LO)=VIZT(NOSTPS-1)
1891              100  CONTINUE
1892                   RETURN
1893                   END
```

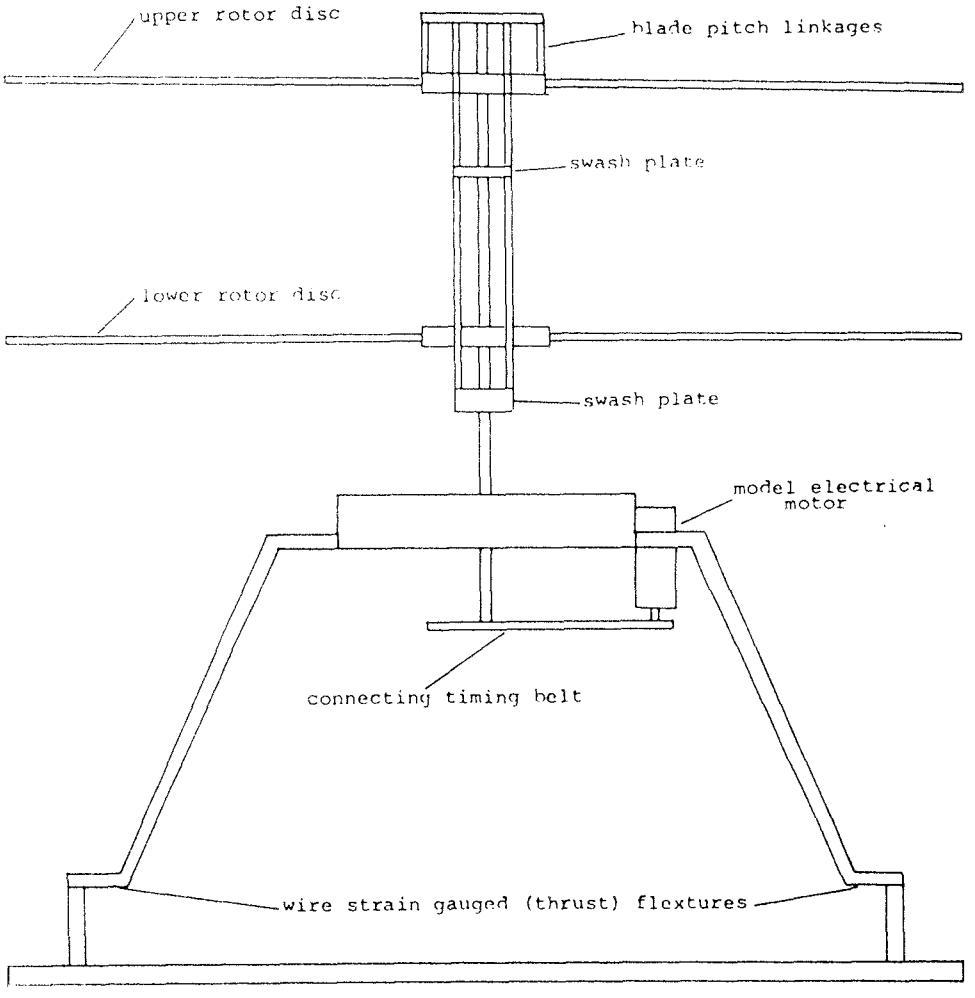

FIG.1 SCHEMATIC DIAGRAM OF THE MOTE CCTR RIG.

Source	C_L (mean)	Expt r/c	McCormick et al(17) w/c=0.02+ $0.035C_L$	Expt V_s/V_T	McCormick et al(17) $V_s/V_T=0.625C_L$	Comments
Cook (28)	0.69	0.016	0.044	0.31	0.43	
Andrew (19)	0.65	0.074	0.043	0.3	0.41	Vortex decay in expt apparent
Simons (66)	0.5	.05-.075	0.0375	0.23	0.28	Aged vortex
Carradonna et al (18)	0.446	0.056-0.075	0.0356	0.68	0.28	Rotor blade aspect ratio=6.0
Panton (67)	0.87	0.046	0.05	0.72	0.54	
Zalay (68)	0.57	.03-.05	0.04	0.6	0.36	
Rorke (25)	0.4*	0.03	0.034	0.58	0.25	*Estimate
Chigier et al (21)	0.72	0.079	0.045	0.37	0.45	
Chigier et al (22)	0.84	0.053	0.049	0.68	0.53	Aged vortex
Pouradier (69)	0.45			0.22	0.26	

FIG.2 TABLE OF McCORMICK'S ET AL VORTEX DATA.

Source	Comments	A_r	M	Vortex Position	Experimental V_s/V_T	Approximating V_s/V_T $(\frac{t}{c}\overline{C}_L)^{\frac{1}{2}}$	Approximating V_s/V_T $(1+\frac{6.6}{A_r})(\frac{t}{c}\overline{C}_L)^{\frac{1}{2}}$	Experimental r/c	Approximating r/c $(\frac{1-M}{\sqrt{M}})\alpha_g\frac{t}{c}$
Cook (28)	Rotor blade hot wire probe	41	0.53	75° azimuth	0.3	0.29	0.34	0.016	0.013
Simons et al (66)	Rotor blade hot wire probe	54	0.125	300° azimuth	0.23	0.25	0.28	0.05 to 0.075	0.042
Present Author	Rotor blade hot wire probe	28	0.102	120° azimuth	0.3 ± 0.03	0.25	0.31	0.074	0.068
Rorke et al (25)	Fixed wing wind tunnel test hot wire probe	4.2	0.2	2c downstream	0.48	0.22	0.57	0.02 to 0.03	0.018
Zalay (68)	Fixed wing wind tunnel test hot wire probe vorticity meter	5.6	0.133	6.5c downstream	0.6	0.26	0.57	0.03 to 0.05	0.036
Panton et al (67)	Fixed wing free flight hot wire probe	9.2	0.123	39.6c downstream	0.72 +.12 -.25	0.36	0.62	0.046	0.045
Iversen et al (70)	Fixed wing wind tunnel test hot wire probe elliptic tip *based on 92% chord	11.4*	0.135	3.25c downstream	0.42	0.35	0.55	0.050	0.049
Chiger et al (21)	Fixed wing wind tunnel test hot wire probe	5.33	.089	trailing edge	0.37	0.33	0.74	.079	.095

FIG.3 TABLE OF ANDREW'S ET AL VORTEX DATA.

Source	$0.37R_e^{-\frac{1}{5}}$	Expt r_c/c	Andrew $r_c/c=R_e^{-0.2}K_2V_s/v_T$	Expt V_s/V_T	Andrew $V_s/V_T=(1+(6.6/A_r)*K_1\theta$
Andrew	0.035	0.074	0.049	0.3	0.43
Carradonna et al (18)	0.02	0.056-0.075	0.044	0.68	0.67
Cook (28)	0.017	0.016	0.021	0.31	0.38
Simons (66)	0.03	.05-.075	.032	0.23	0.33
Chigier et al (21)	0.024	0.079	0.056	0.37	0.73
Chigier et al (22)	0.024	0.053	0.056	0.68	0.73
Panton (67)	0.017	0.046	0.045	0.72	0.79
Rorke (25)	0.027	0.0475	0.05	0.58	0.6
Zalay (68)	0.02	.03-.05	0.039	0.6	0.57

FIG.4 TABLE OF VORTEX DATA COMPARISONS.

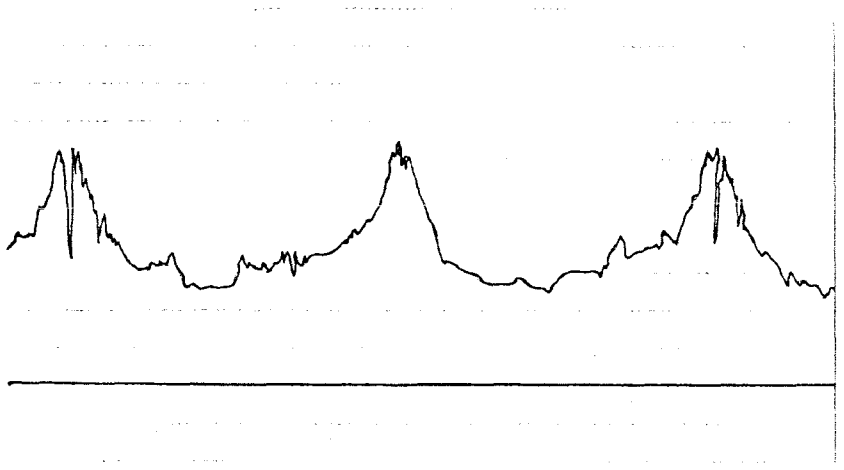

FIG. 5 VORTEX VELOCITY/TIME OUTPUT TRACE.

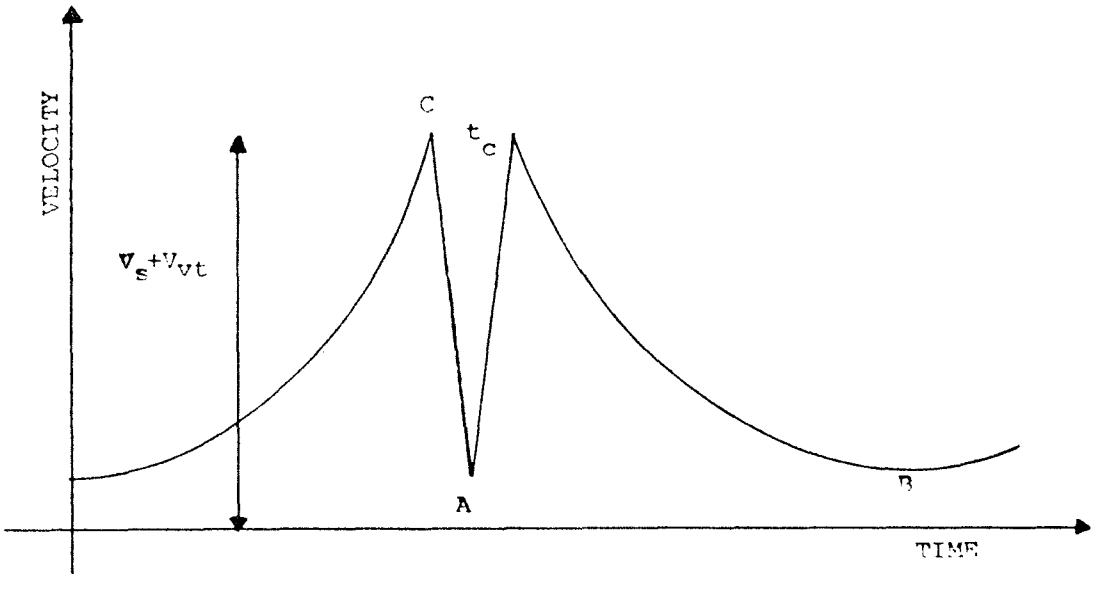

FIG.6 SCHEMATIC DIAGRAM OF A TYPICAL VORTEX VELOCITY/TIME OUTPUT TRACE.

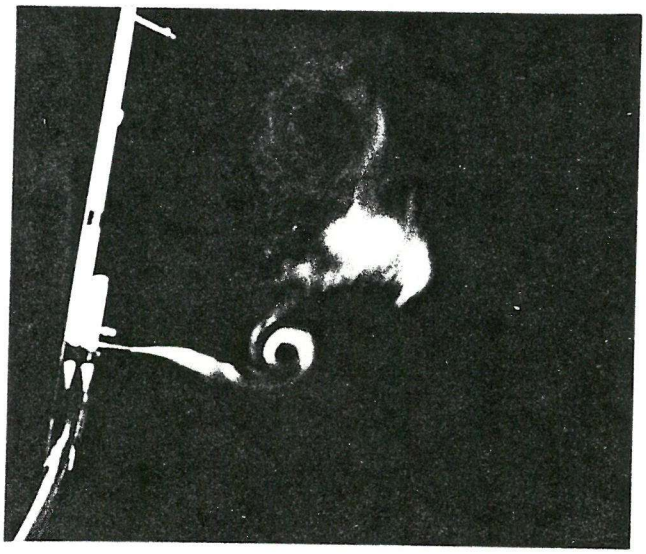

FIG.7 PHOTOGRAPH OF A VORTEX CORE EXPANSION.

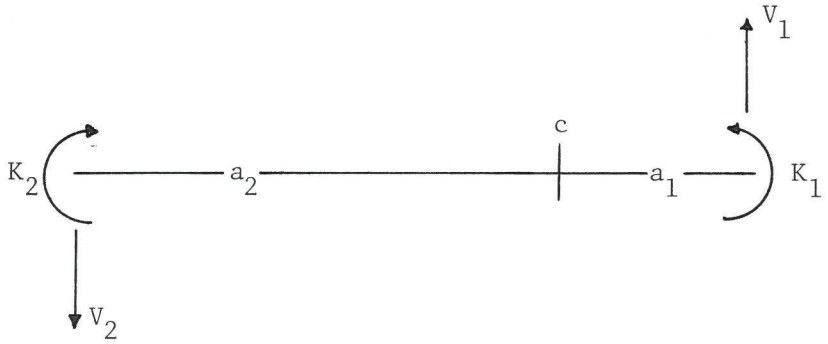

FIG.8 TWO INFINATE RECTILINEAR VORTICES.

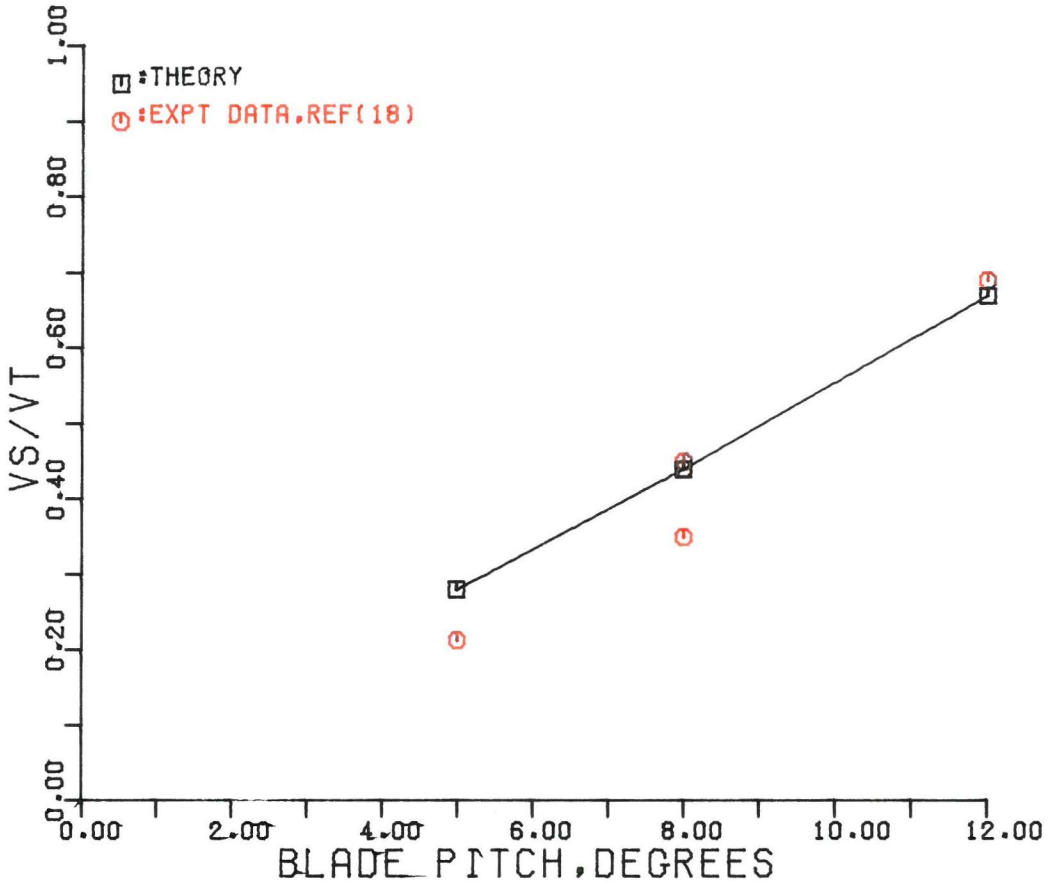

FIG.9 VORTEX CORE EDGE INDUCED VELOCITY.

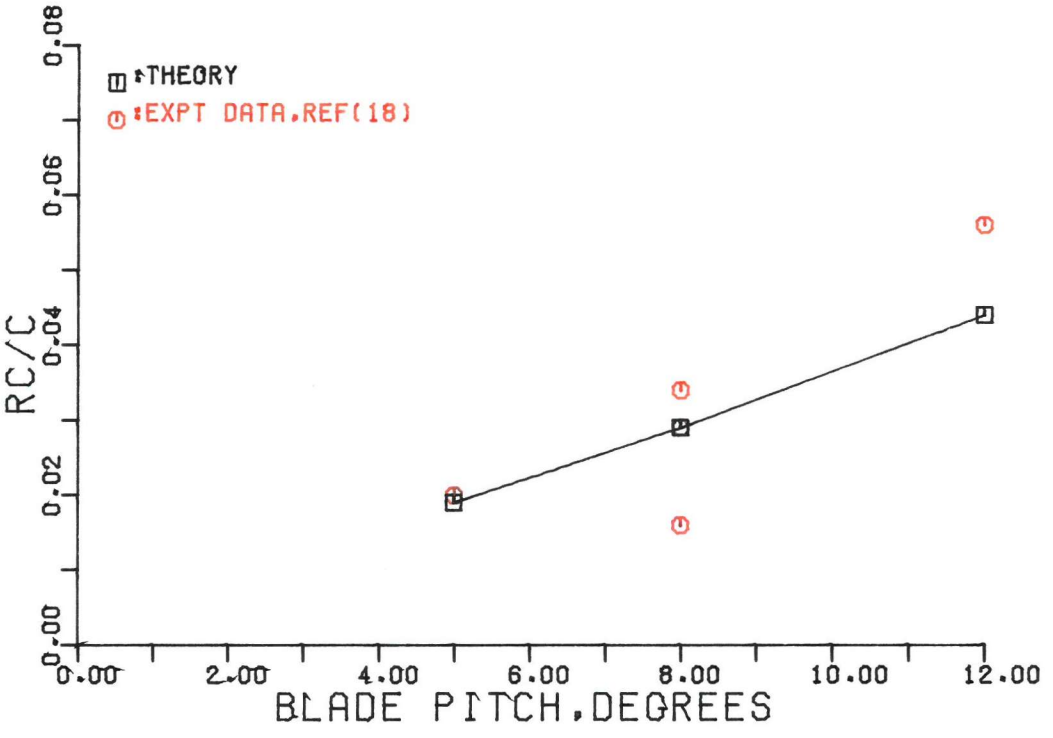

FIG.10 VORTEX CORE RADIUS.

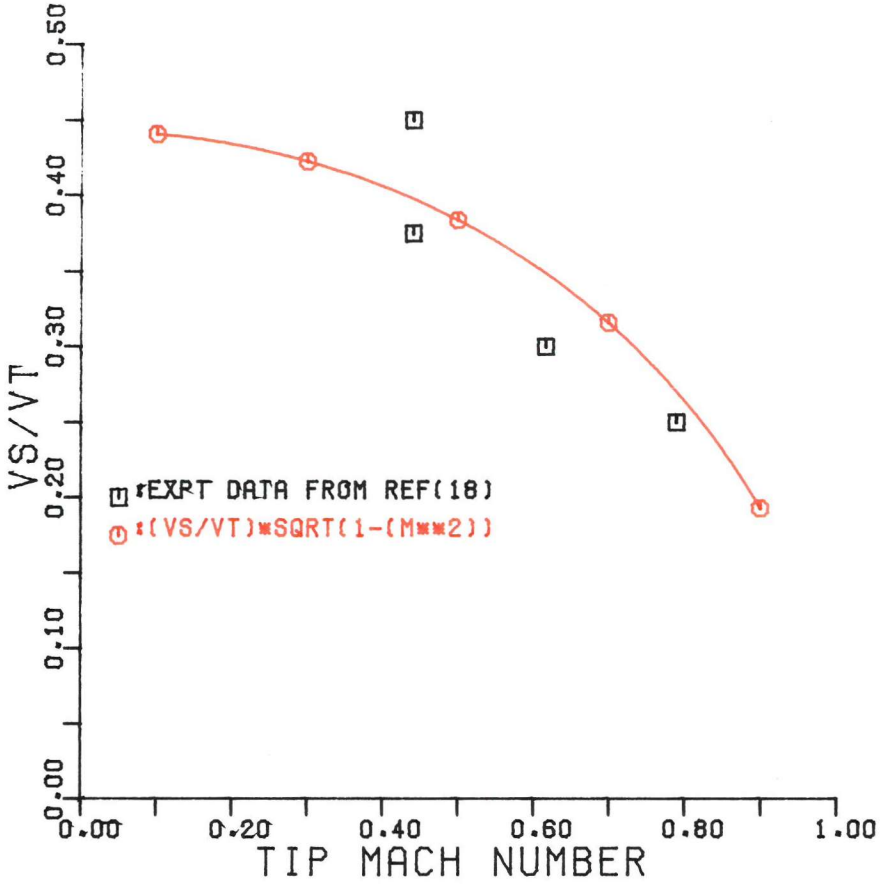

FIG.11 EFFECT OF MACH NO. ON VORTEX INDUCED VEL.

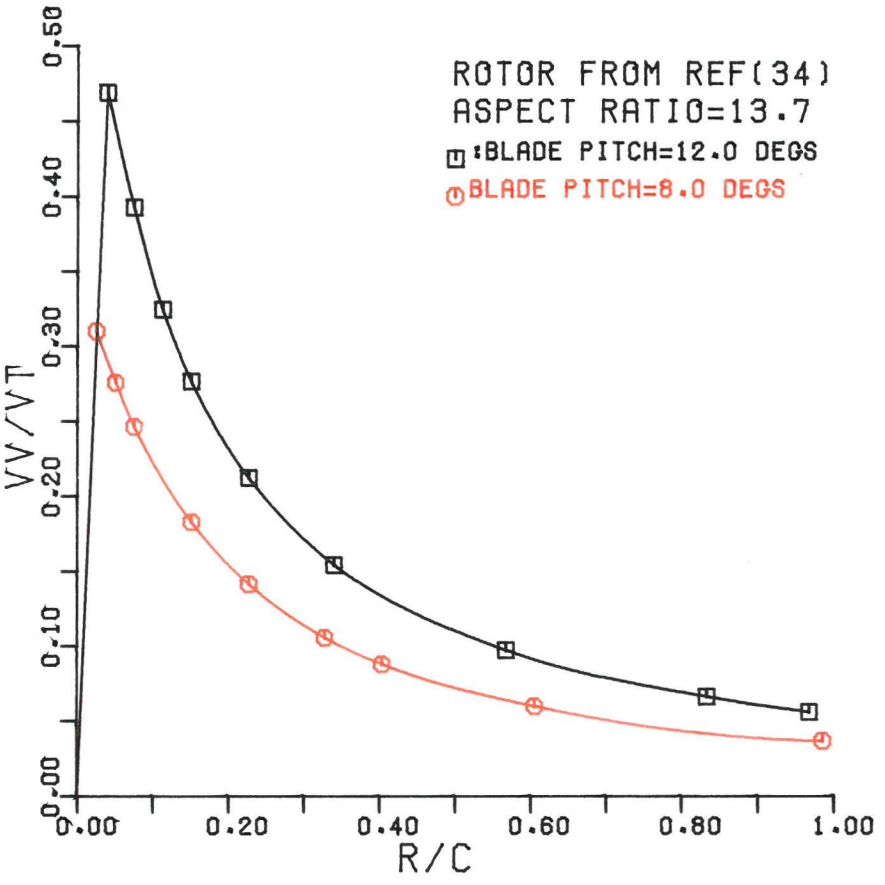

FIG.12 VORTEX VELOCITY (VV) DISTRIBUTION.

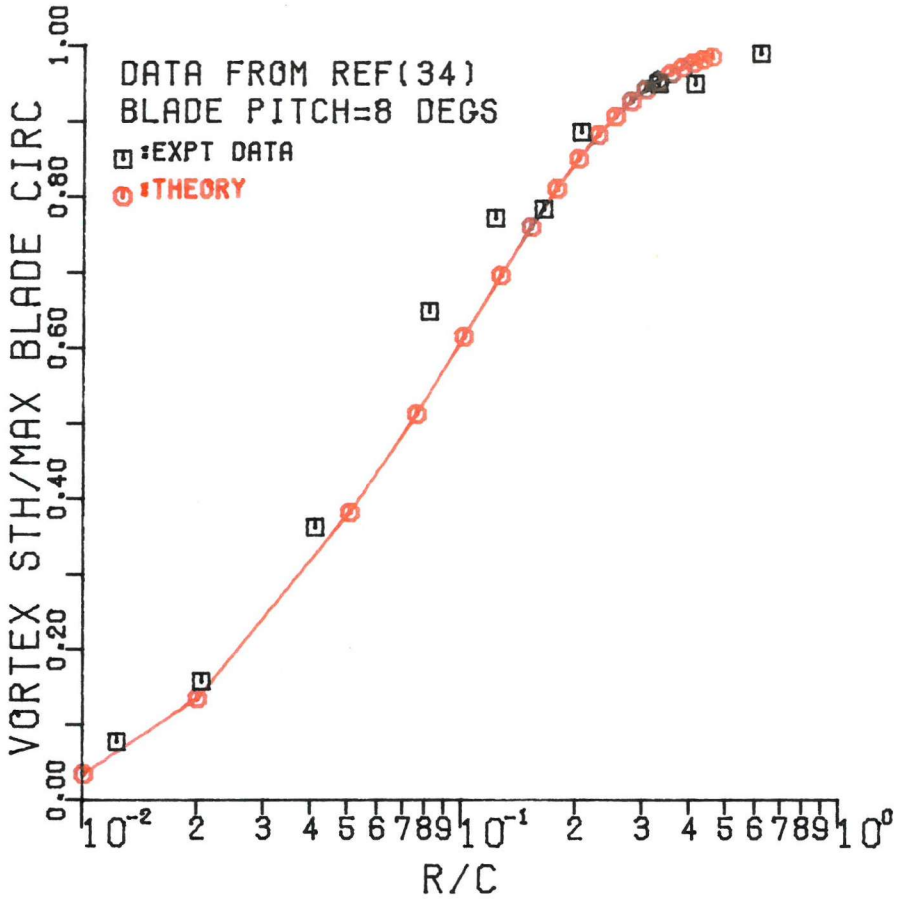

FIG.13 VORTEX CIRCULATION DISTRIBUTION.

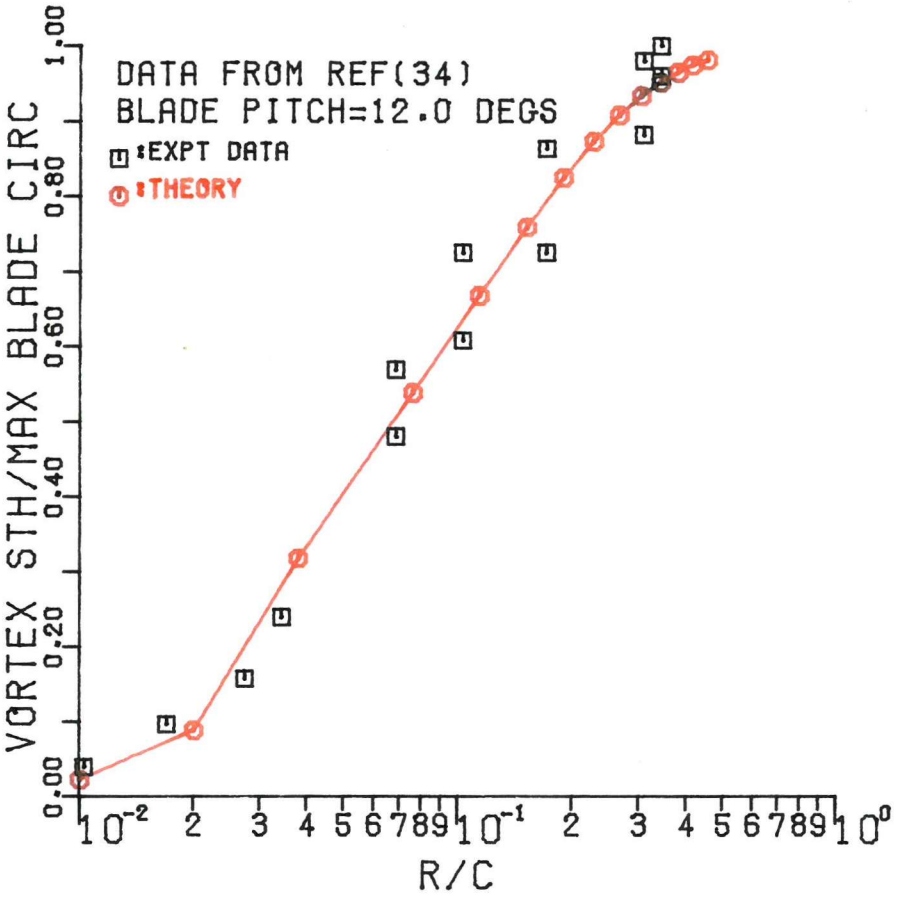

FIG.14 VORTEX CIRCULATION DISTRIBUTION.

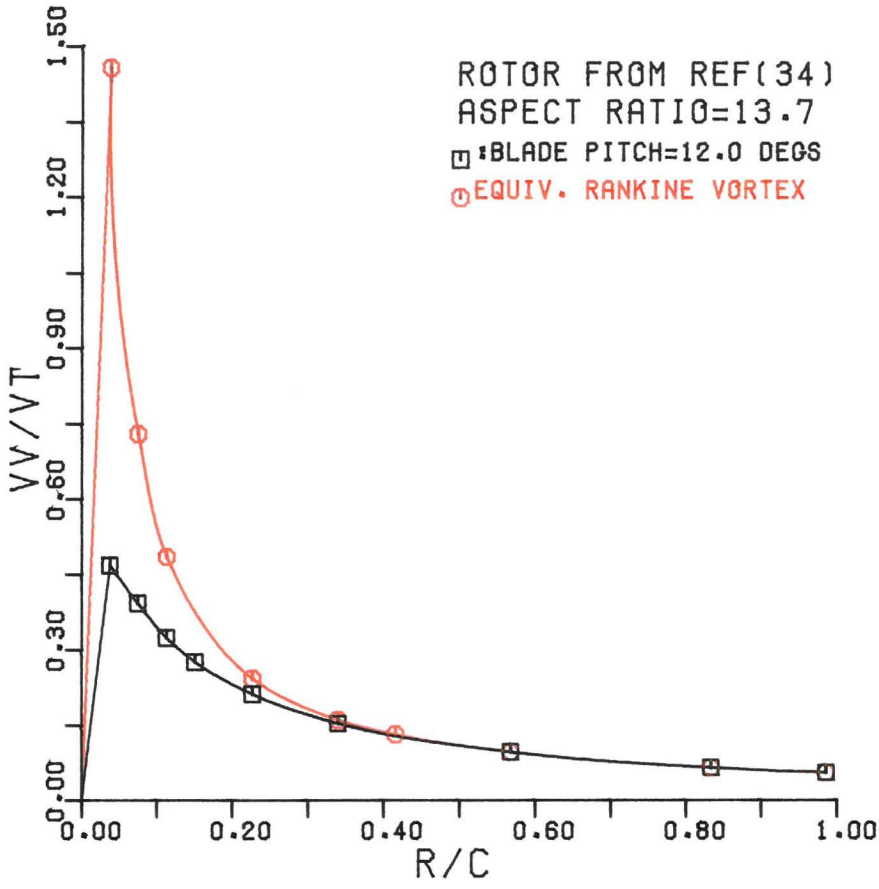

FIG.15 EQUIVALENT RANKINE VORTEX.

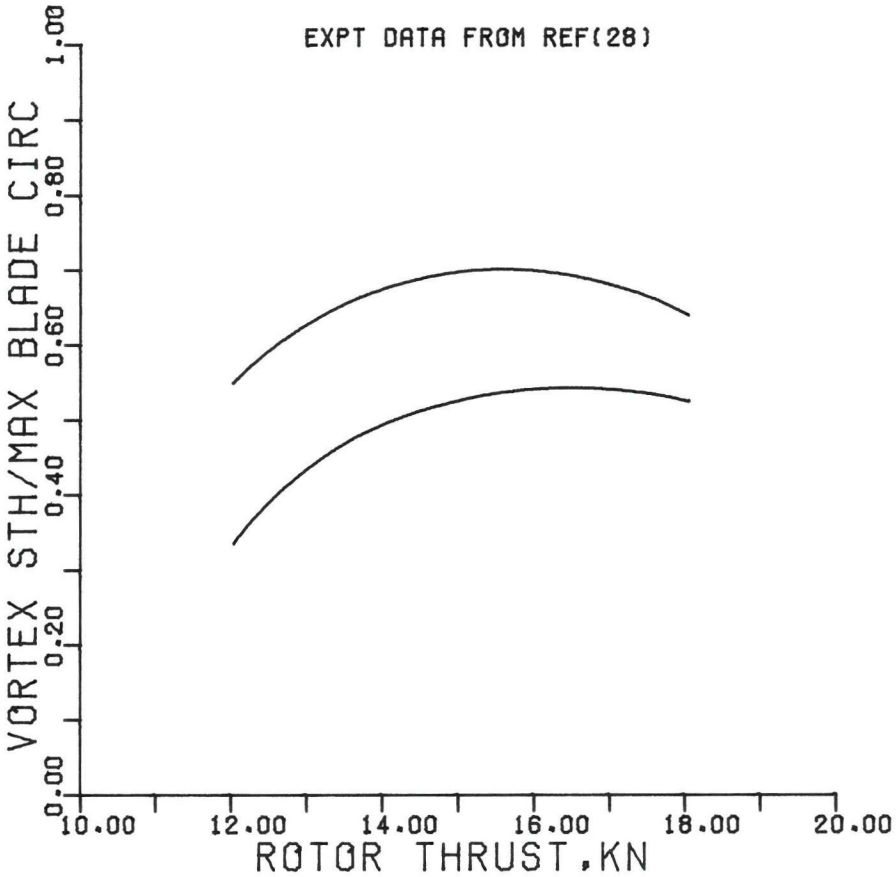

FIG.16 NORMALISED TOTAL VORTEX STRENGTH.

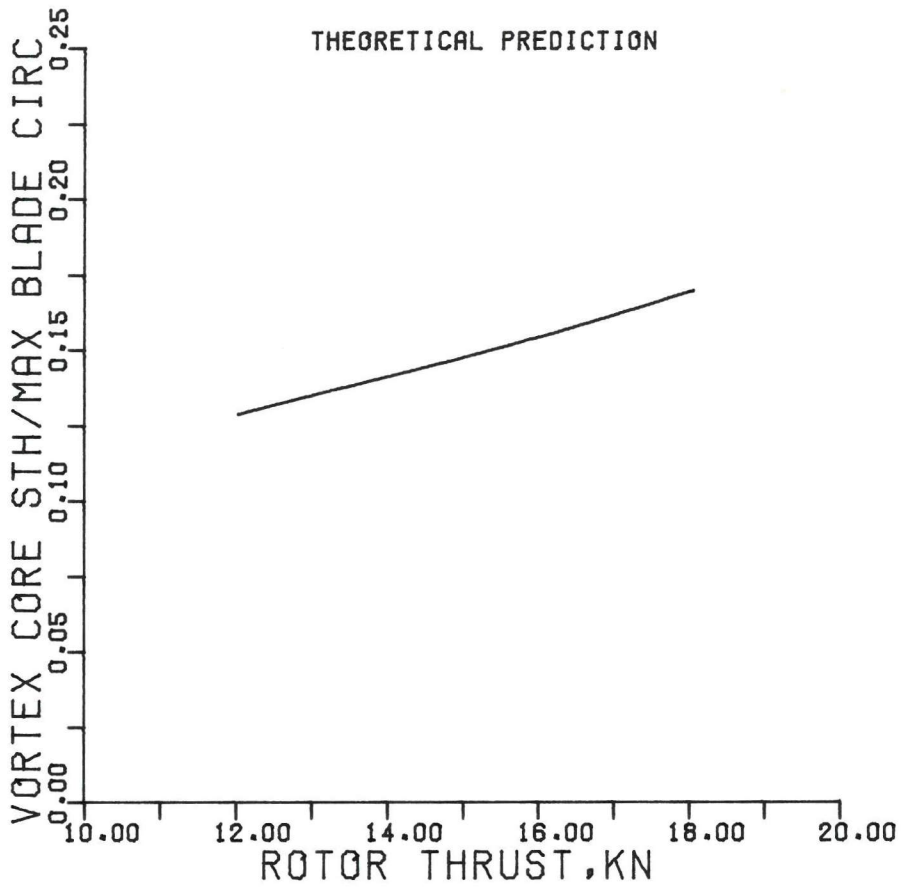

FIG.17 NORMALISED VORTEX CORE STRENGTH.

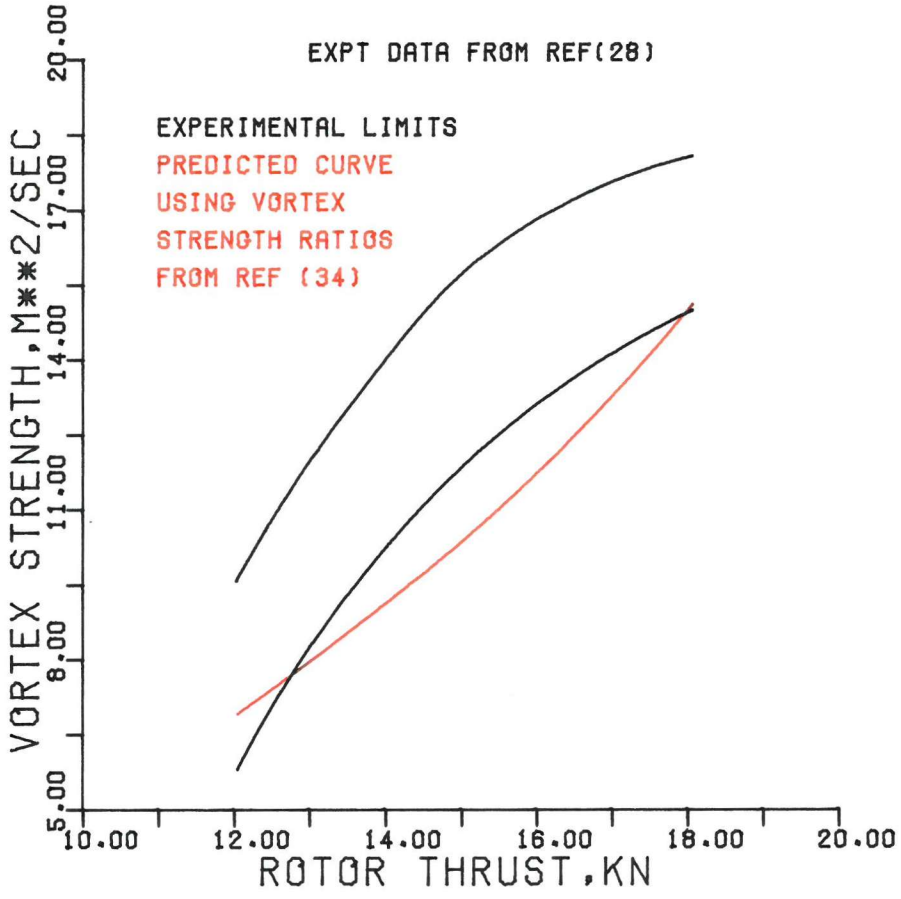

FIG. 18 TOTAL VORTEX STRENGTH.

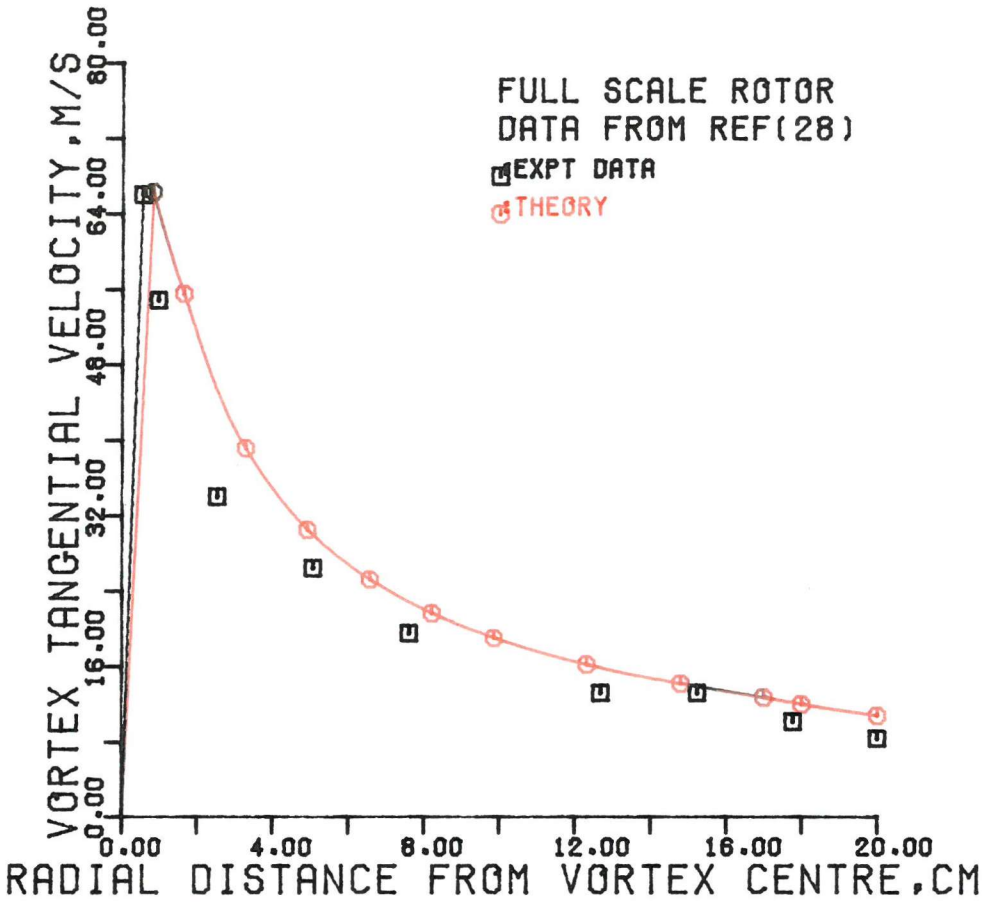

FIG.19 VORTEX VELOCITY DISTRIBUTION.

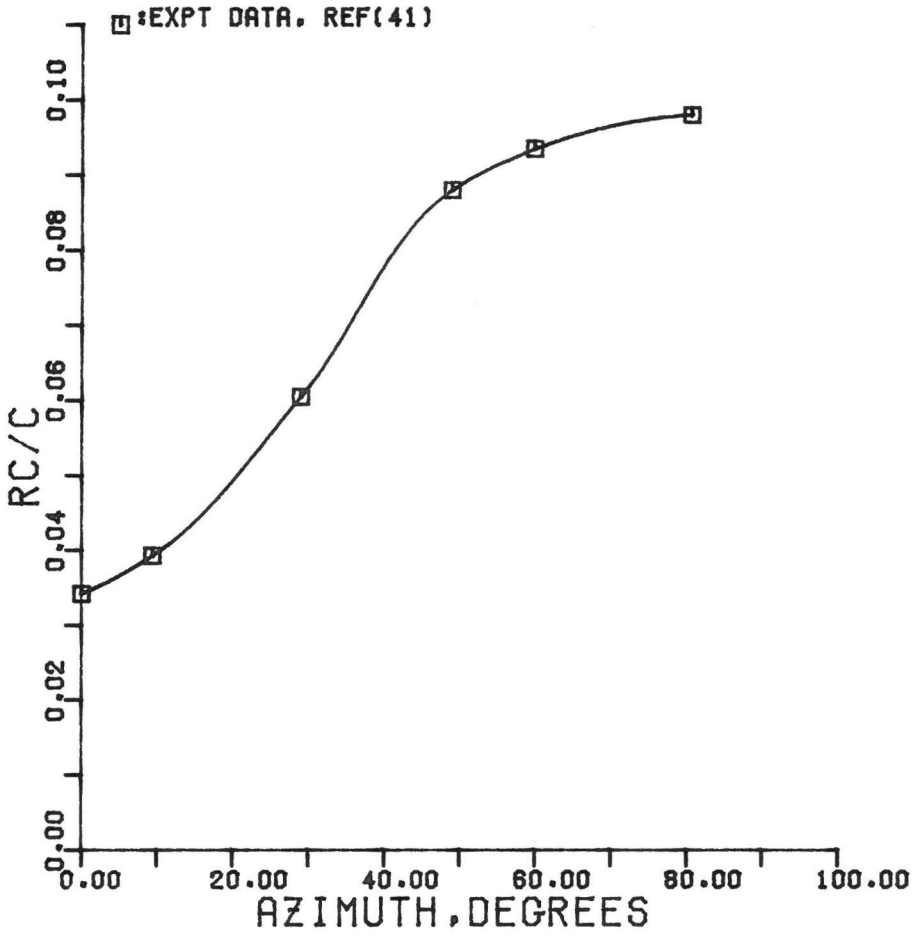

FIG.20 VORTEX CORE VARIATION WITH AZIMUTH.

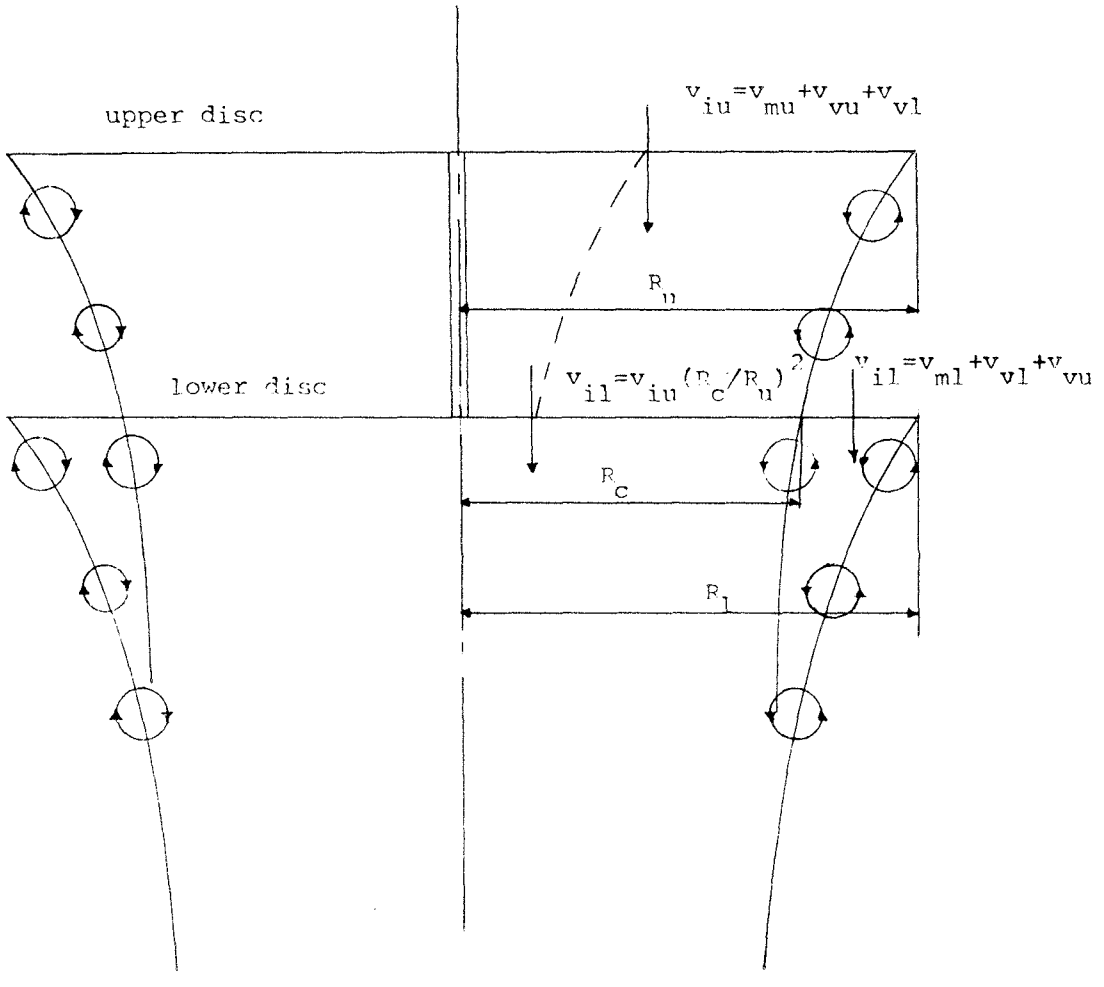

FIG.21 SCHEMATIC REPRESENTATION OF THE CCTR HOVER MODEL.

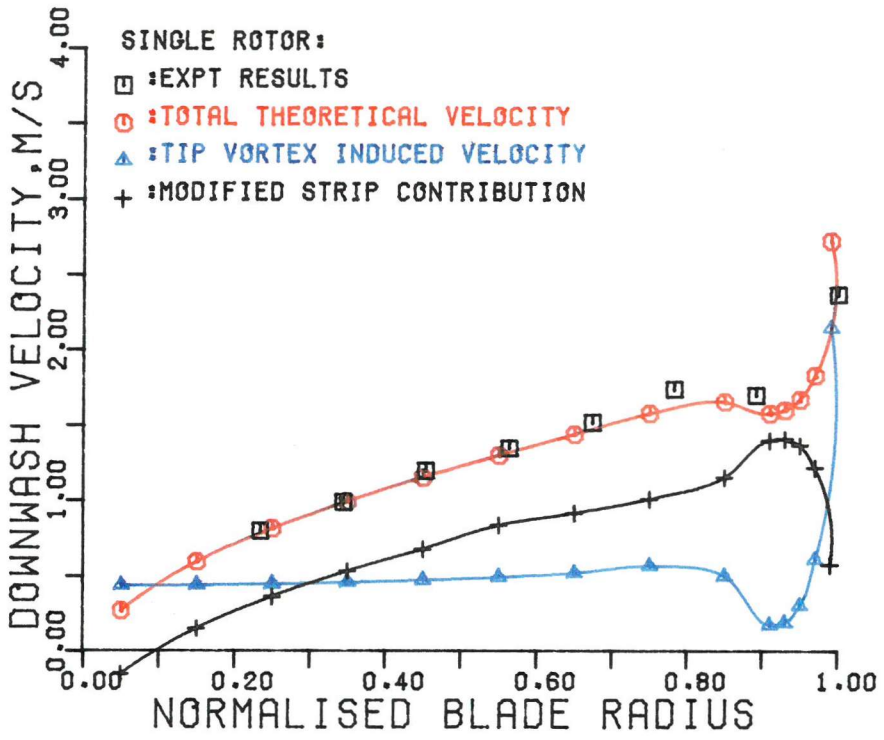

FIG.22 COMPONENT DOWNWASH VELOCITY DISTRIBUTIONS.

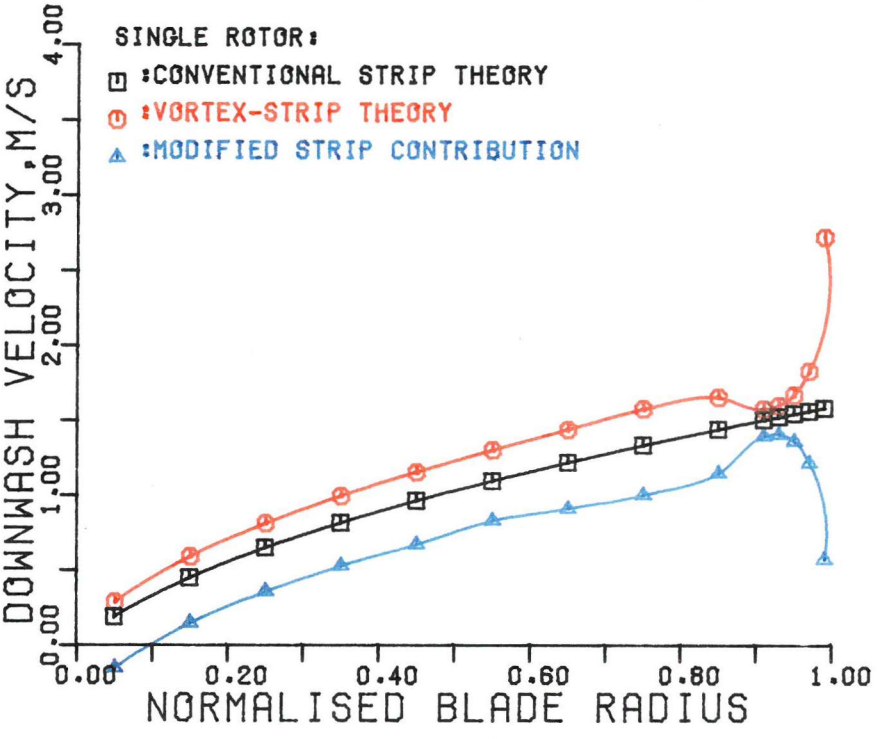

FIG.23 COMPARISON BETWEEN STRIP AND VORTEX-STRIP. THEORIES.

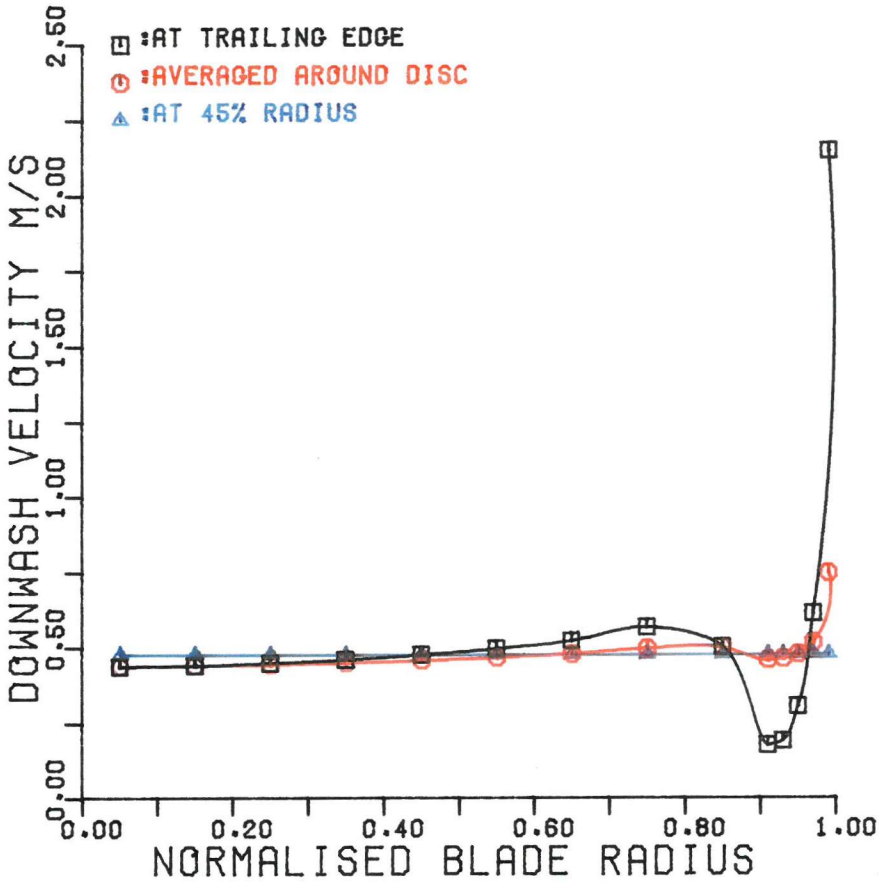

FIG.24 VORTEX VELOCITY COMPONENTS ON UPPER ROTOR.

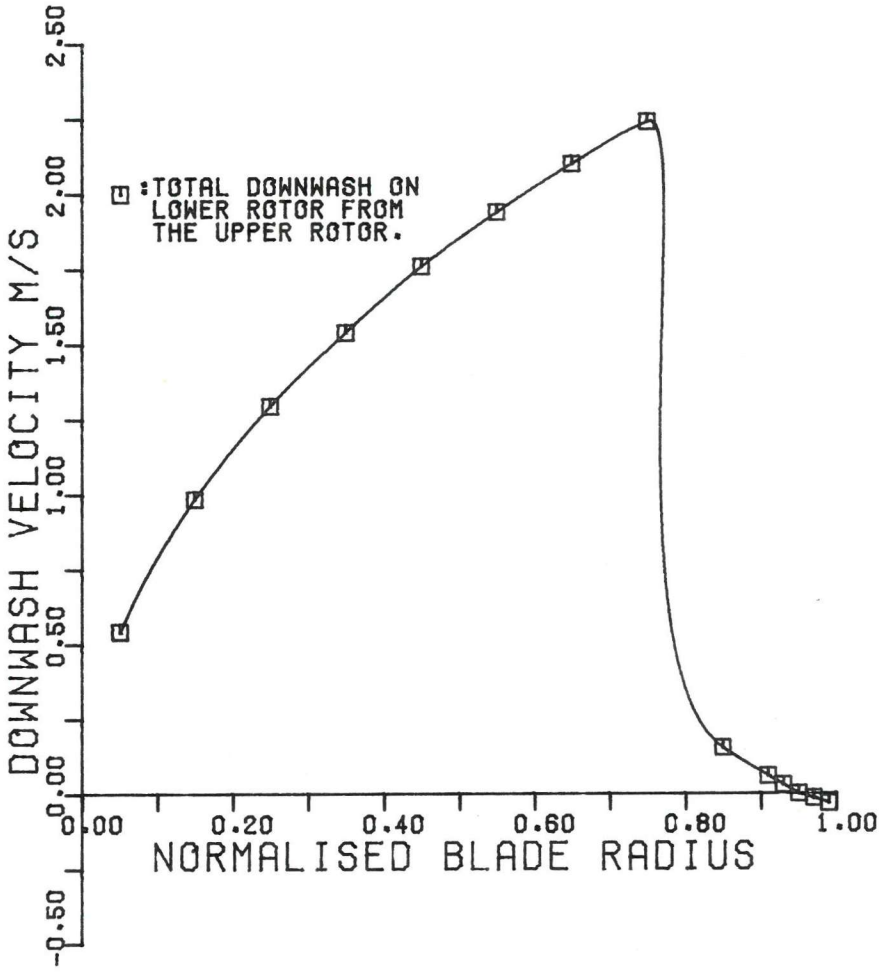

FIG.25 LOWER ROTOR DOWNWASH FROM UPPER ROTOR.

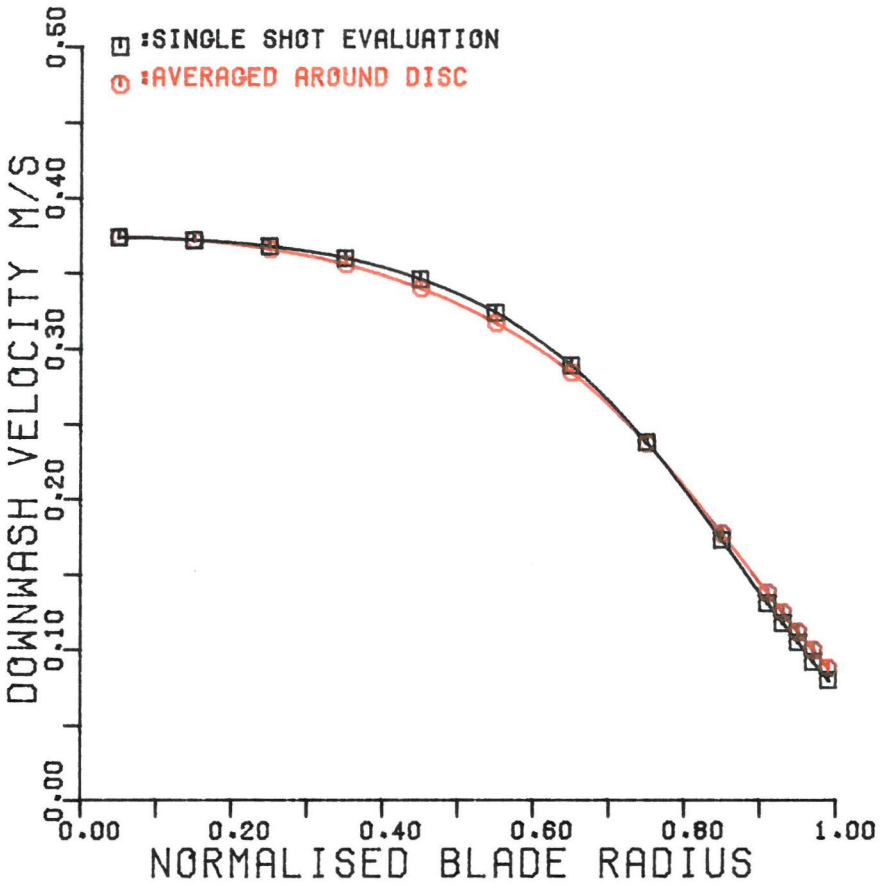

FIG.26 LOWER VORTEX INDUCED VEL ON UPPER ROTOR.

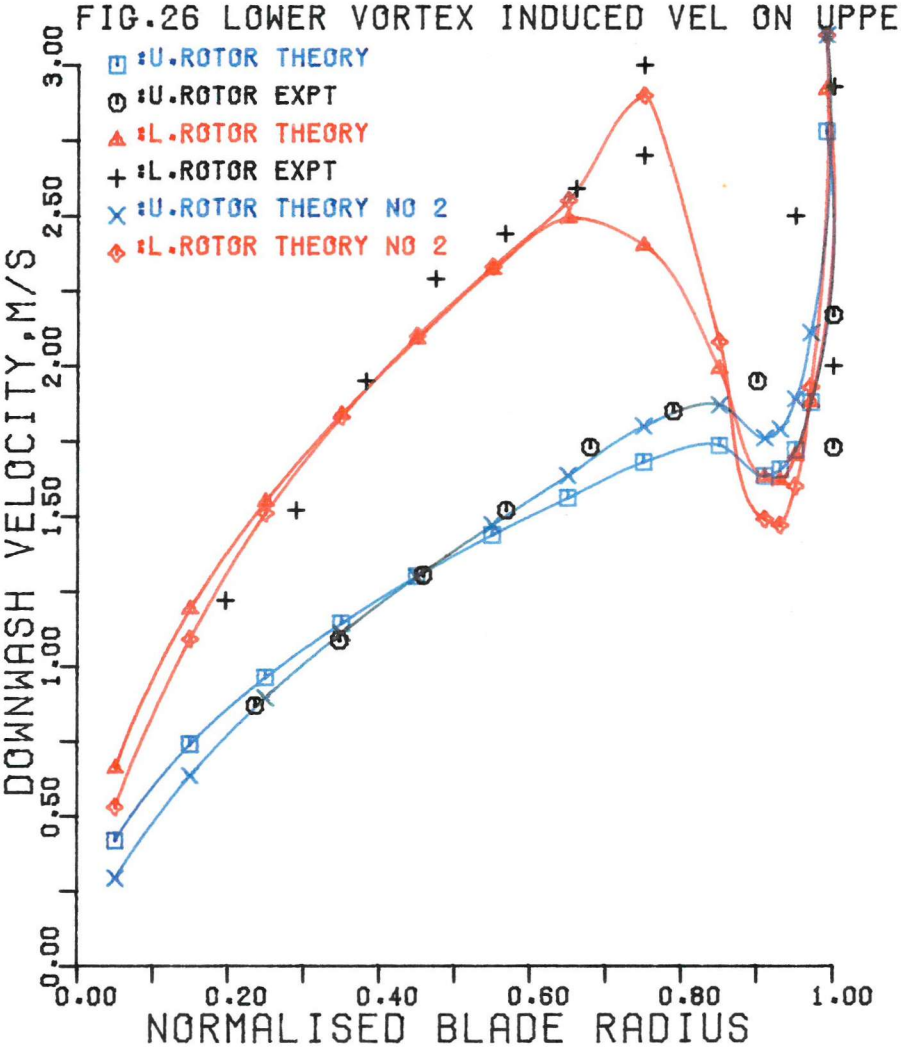

FIG.27 TOTAL DOWNWASH VELOCITY DISTRIBUTIONS.

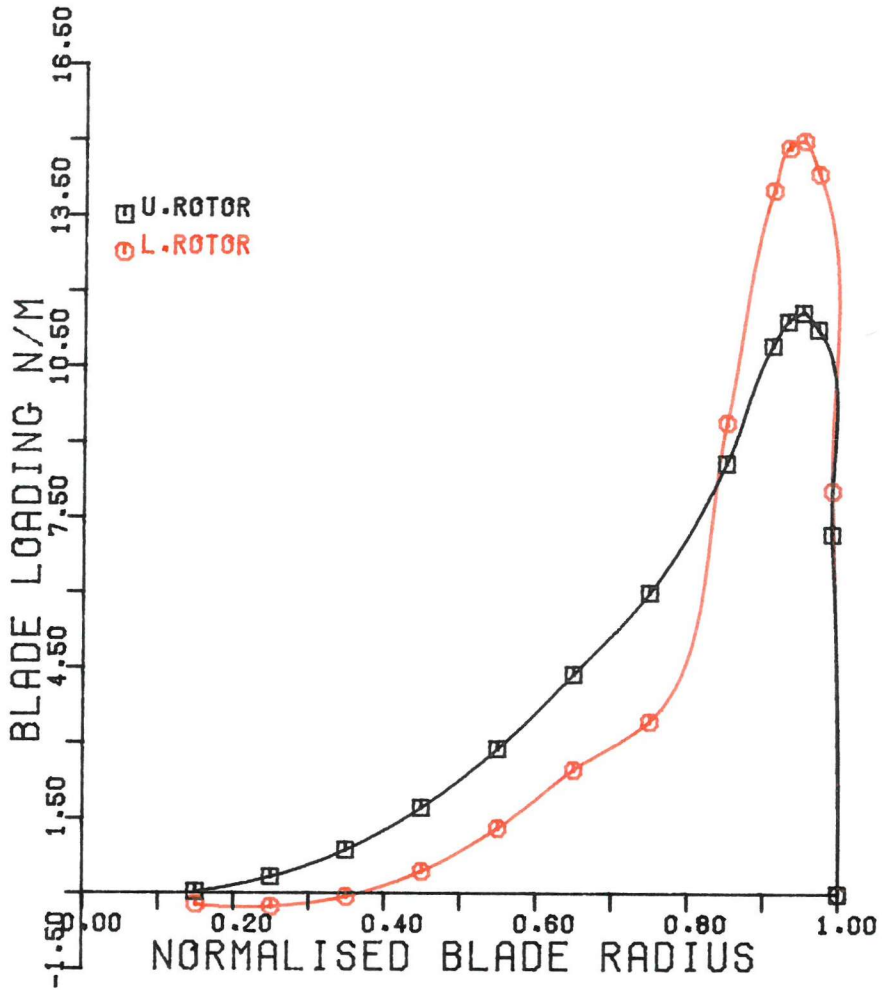

FIG.28 CCTR LIFT DISTRIBUTIONS.

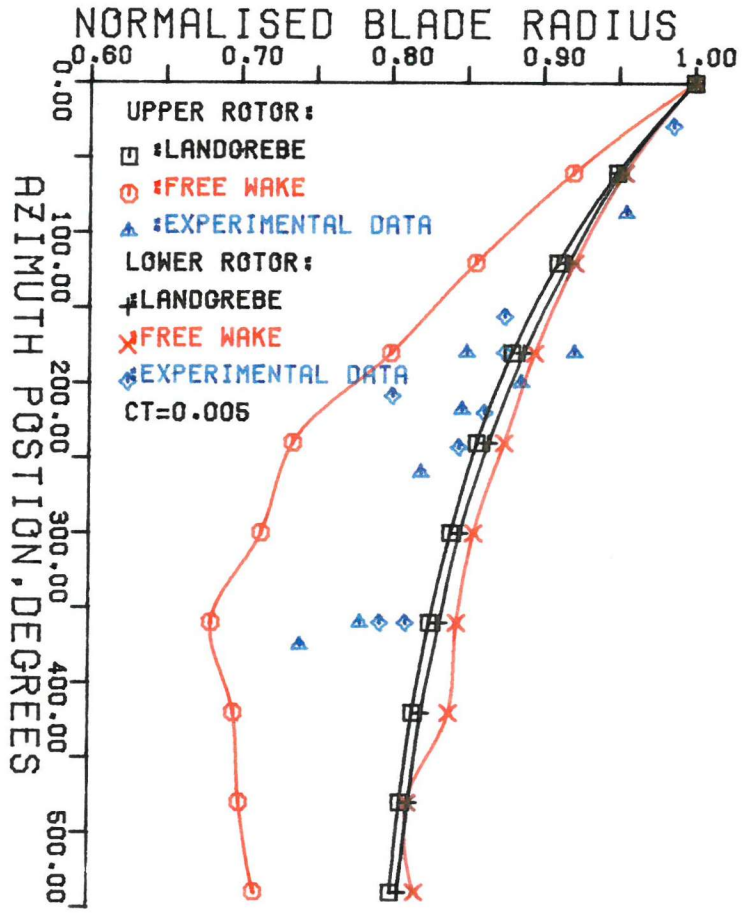

FIG.29 TIP VORTEX WAKE LIMITS.

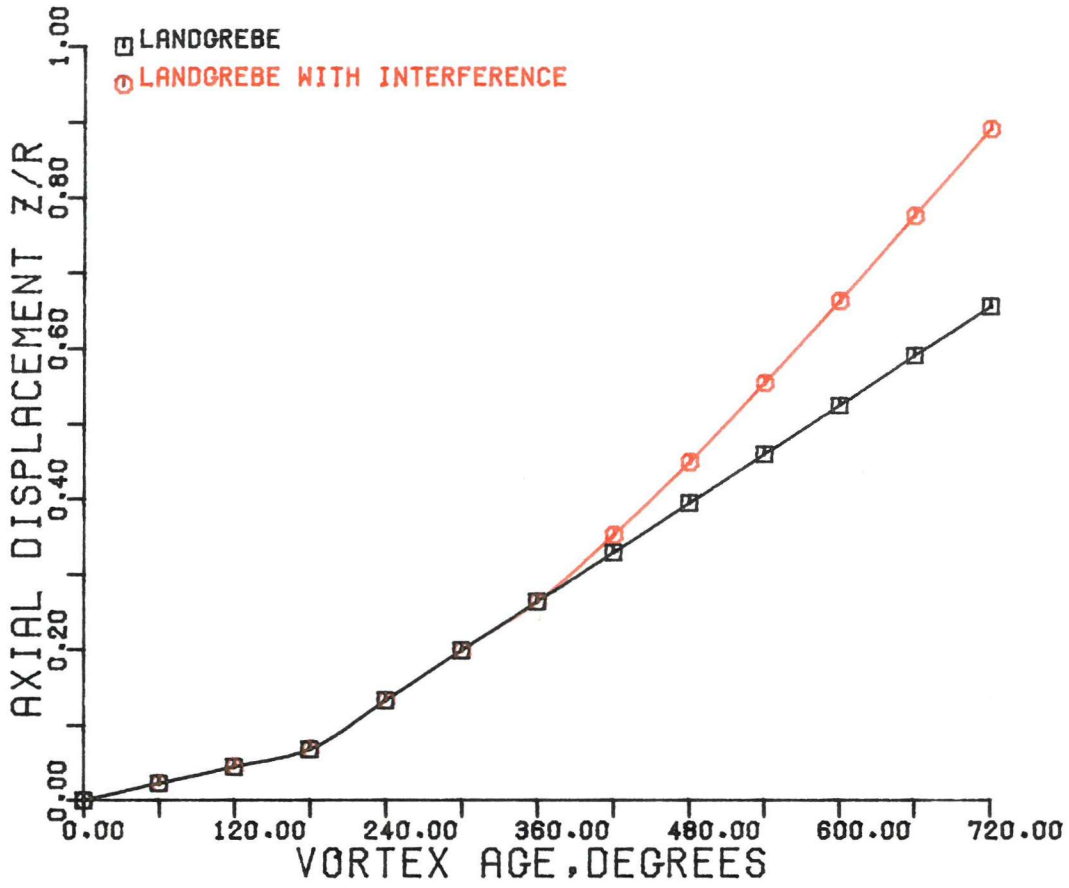

FIG.30 VORTEX AXIAL DISPLACEMENT FROM UPPER ROTOR.

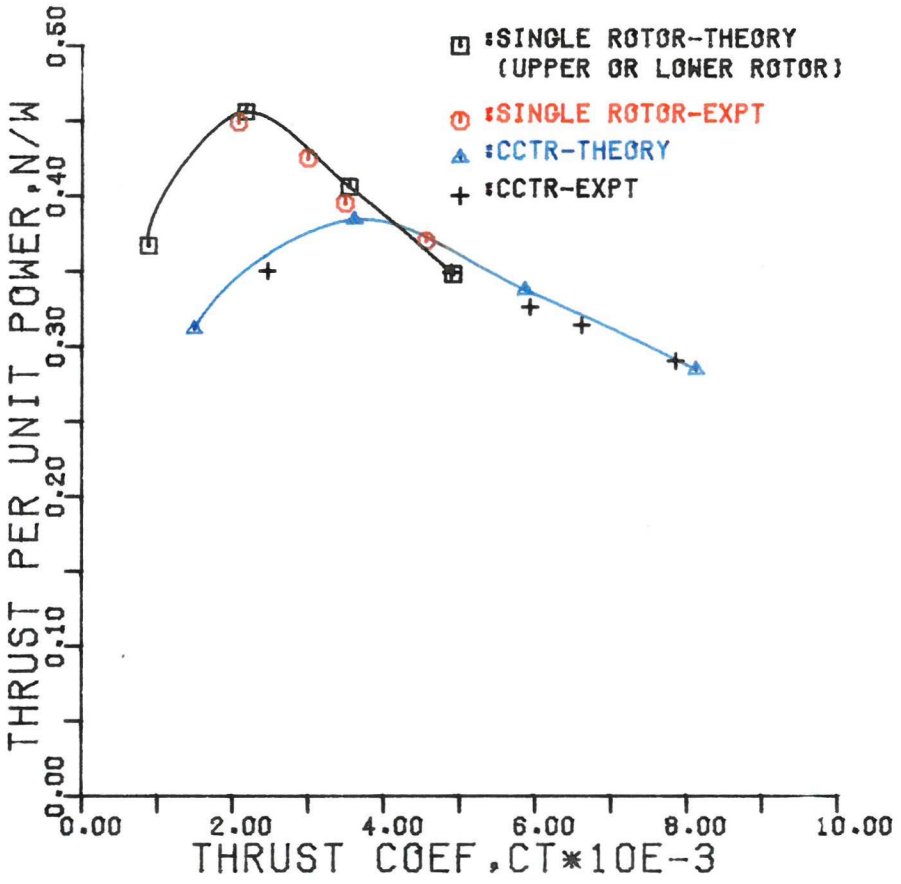

FIG.31 MOTE CCTR PERFORMANCE CHARACTERISTICS.

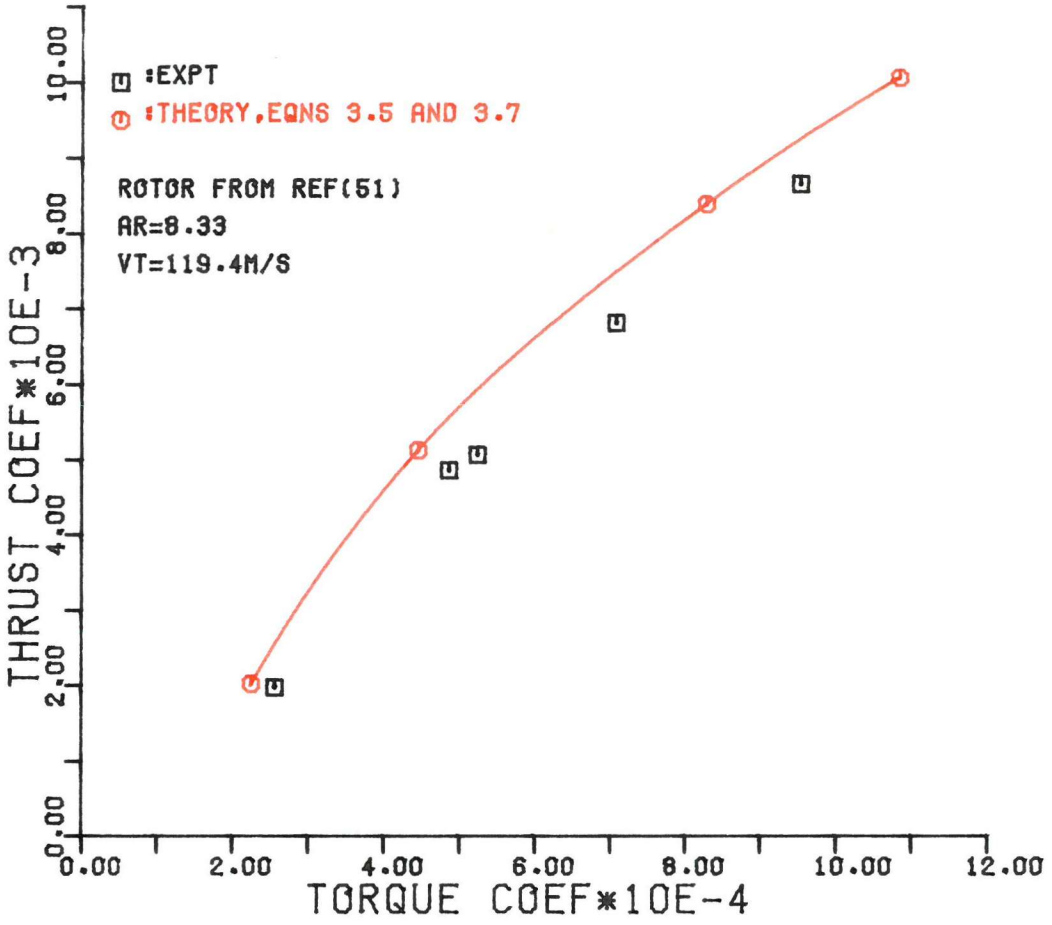

FIG.32 CCTR PERFORMANCE CURVE.

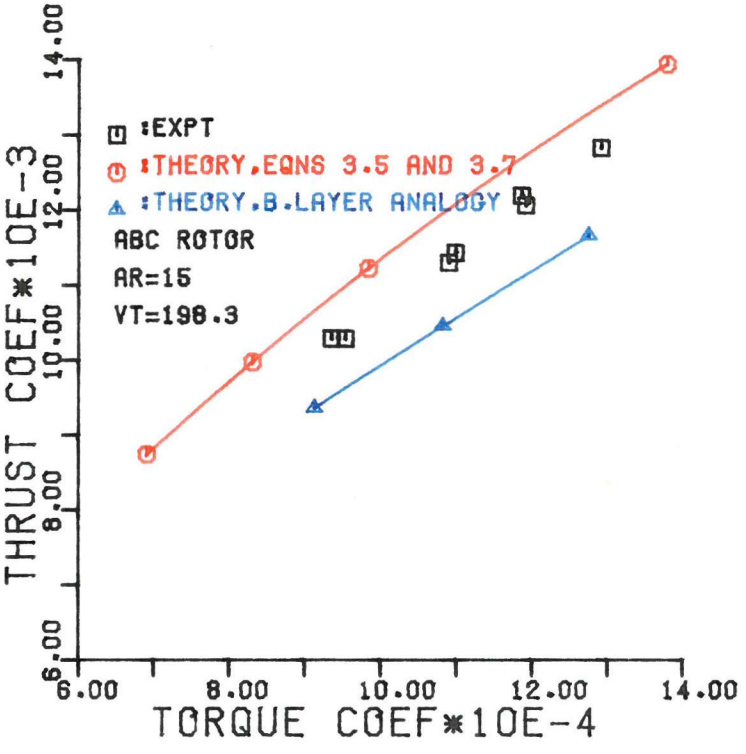

FIG.33 ABC PERFORMANCE CURVE.

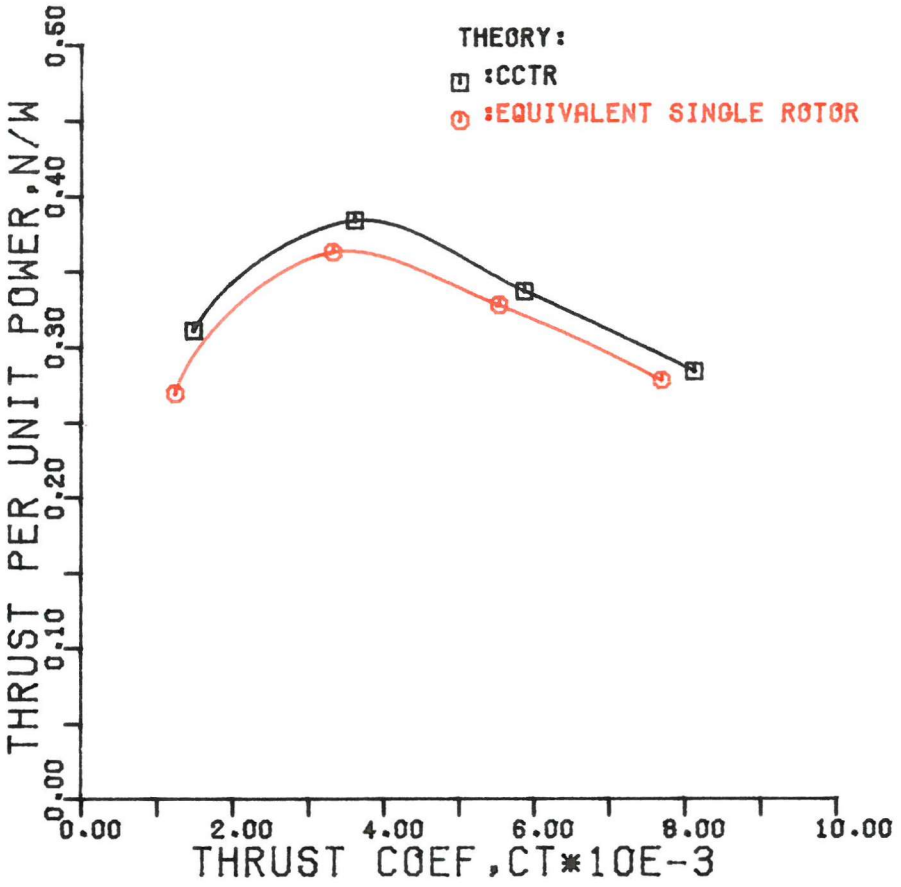

FIG.34 NOTE CCTR COMPARED WITH EQUIVALENT SINGLE. ROTOR.

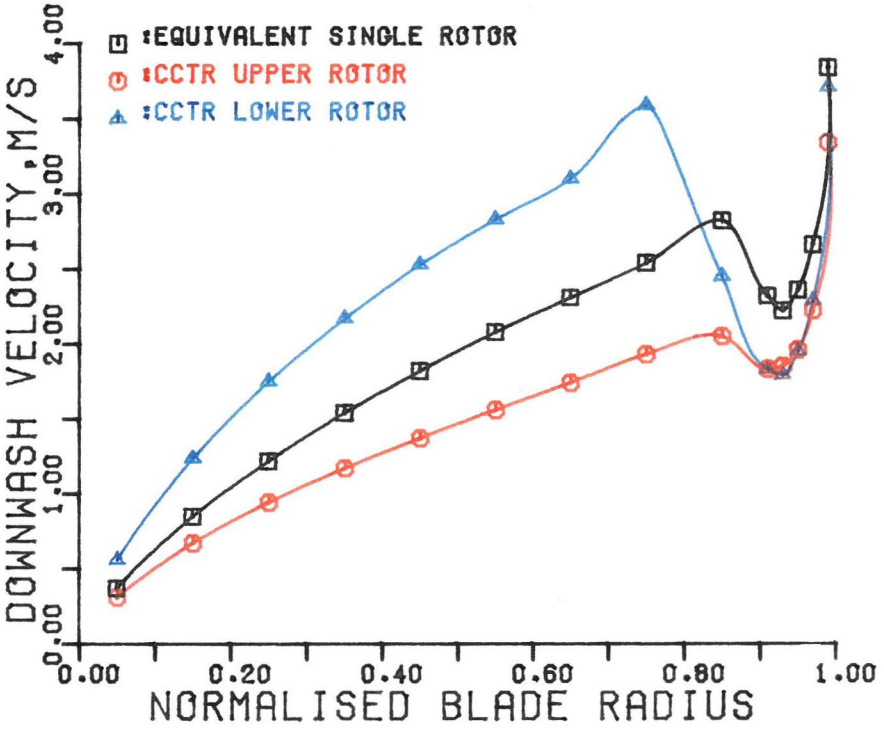

FIG.35 DOWNWASH DISTRIBUTIONS.

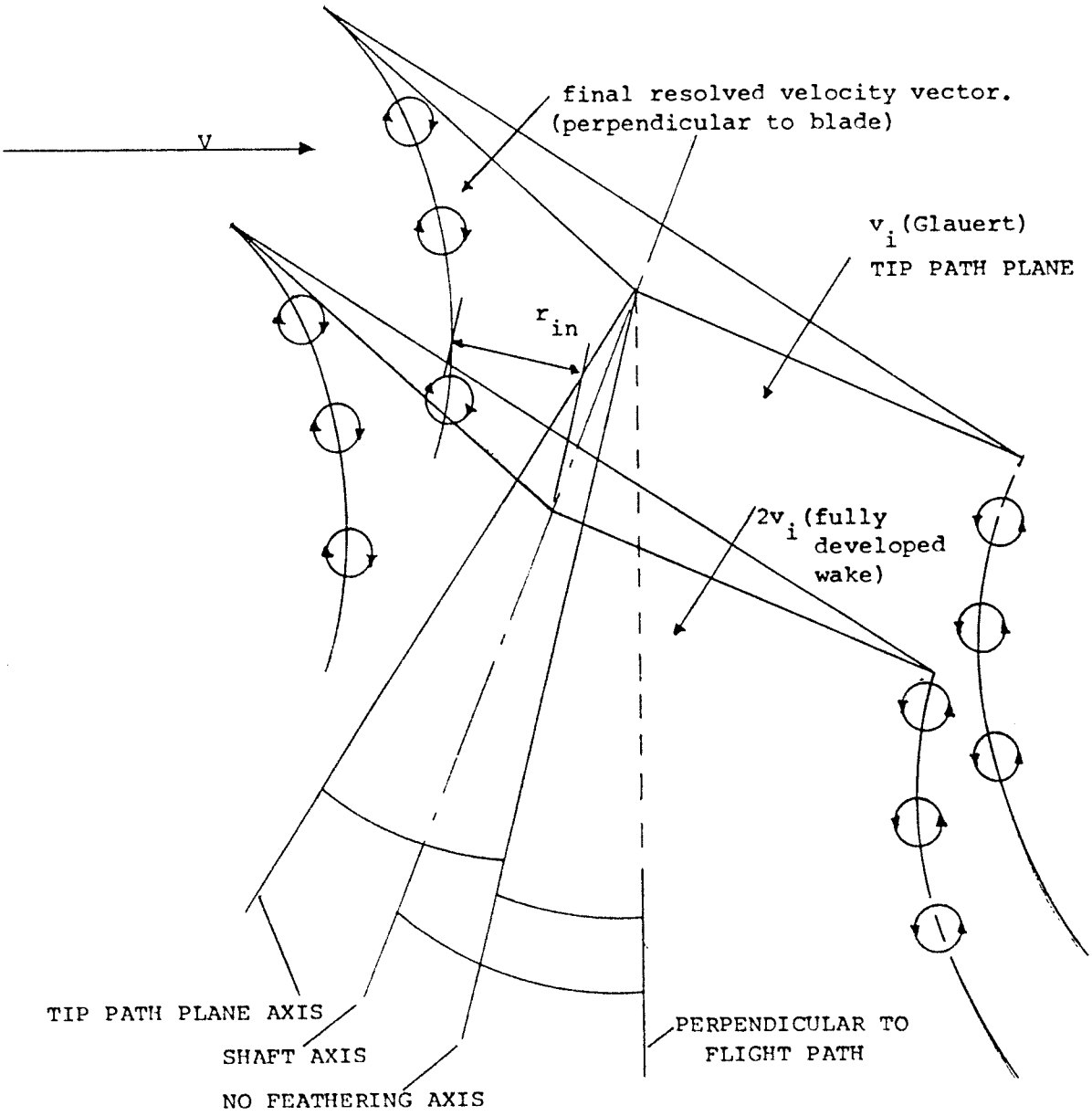

FIG.36 SCHEMATIC REPRESENTATION OF THE FORWARD FLIGHT MODEL.

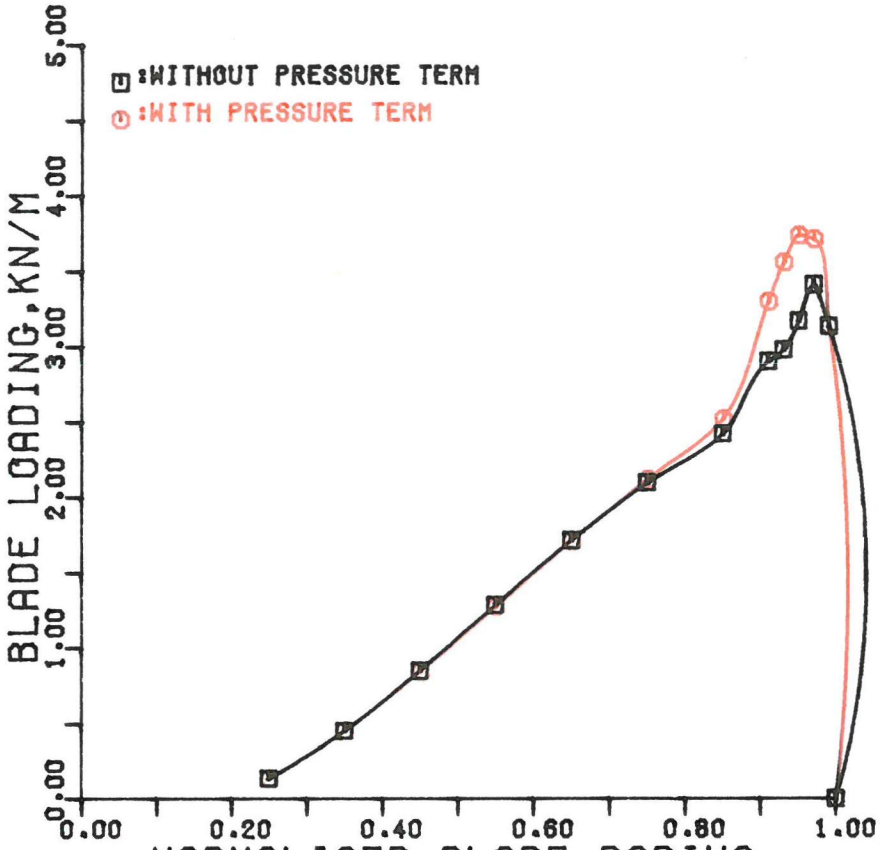

FIG.37 PREDICTED SINGLE ROTOR BLADE LOADING.

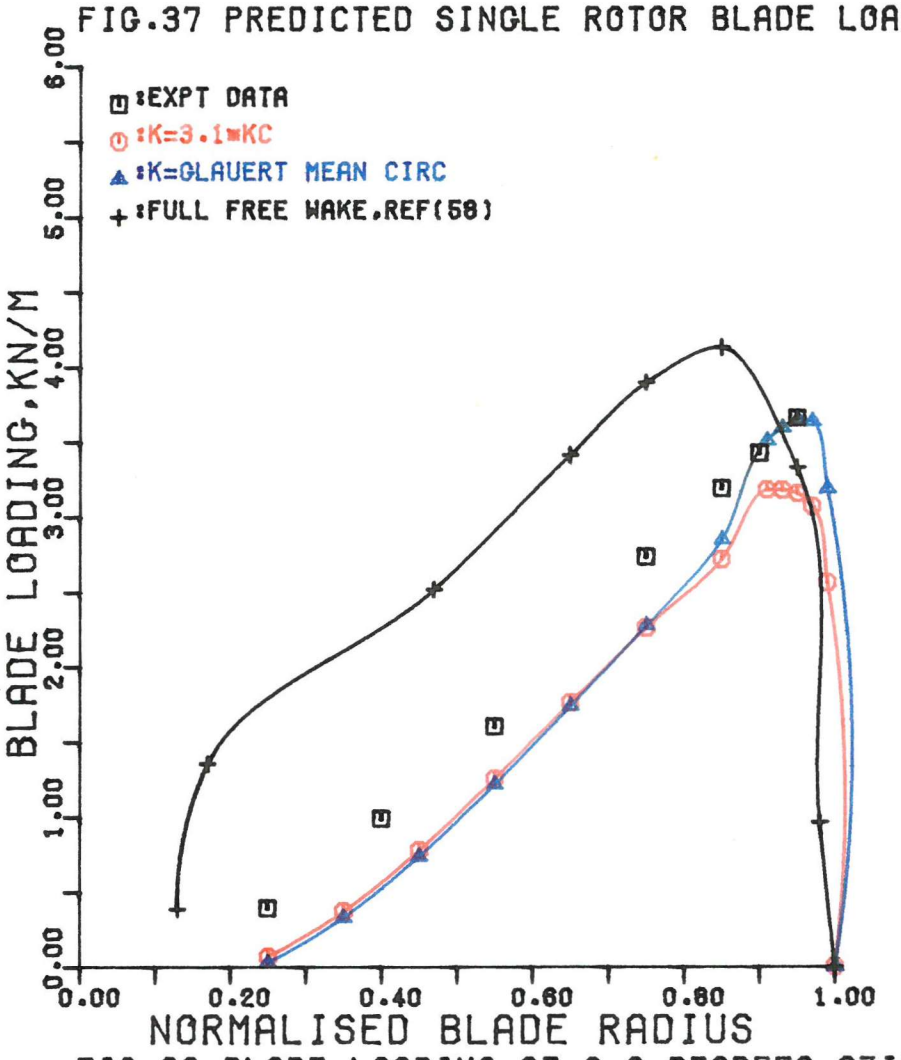

FIG.38 BLADE LOADING AT 0.0 DEGREES AZIMUTH.

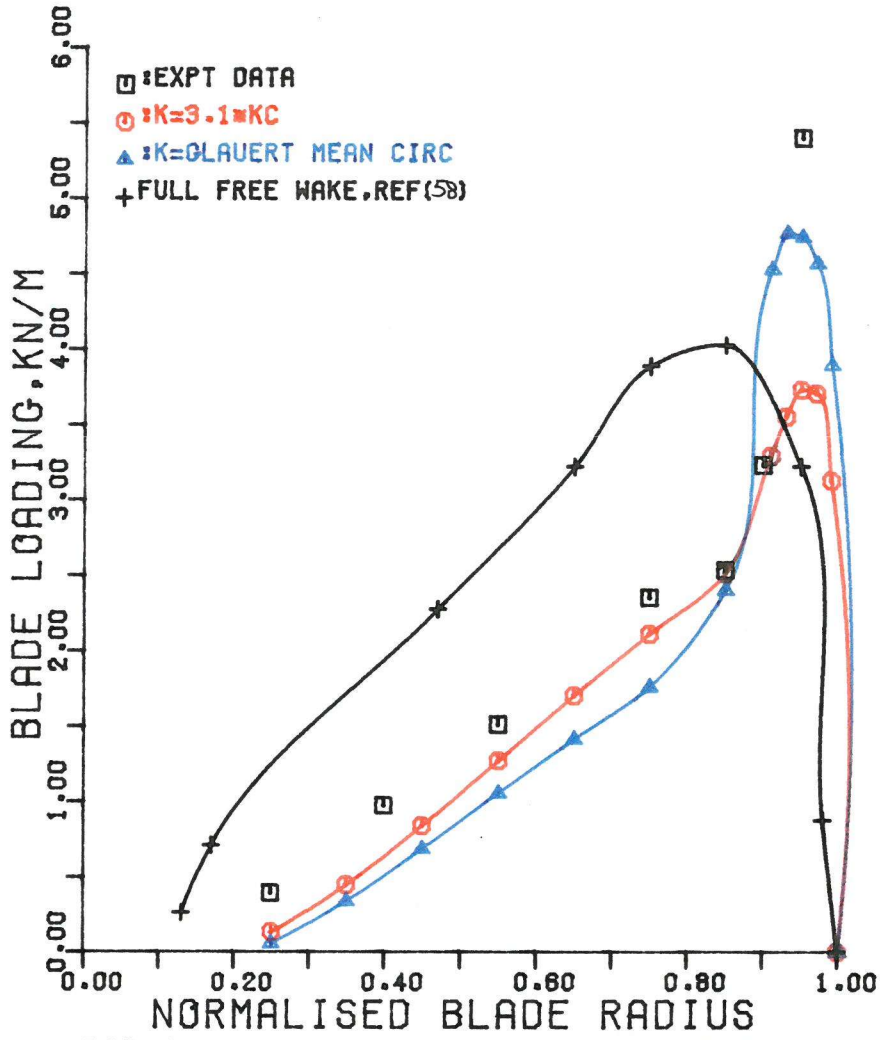

FIG.39 BLADE LOADING AT 90.0 DEGREES AZIMUTH.

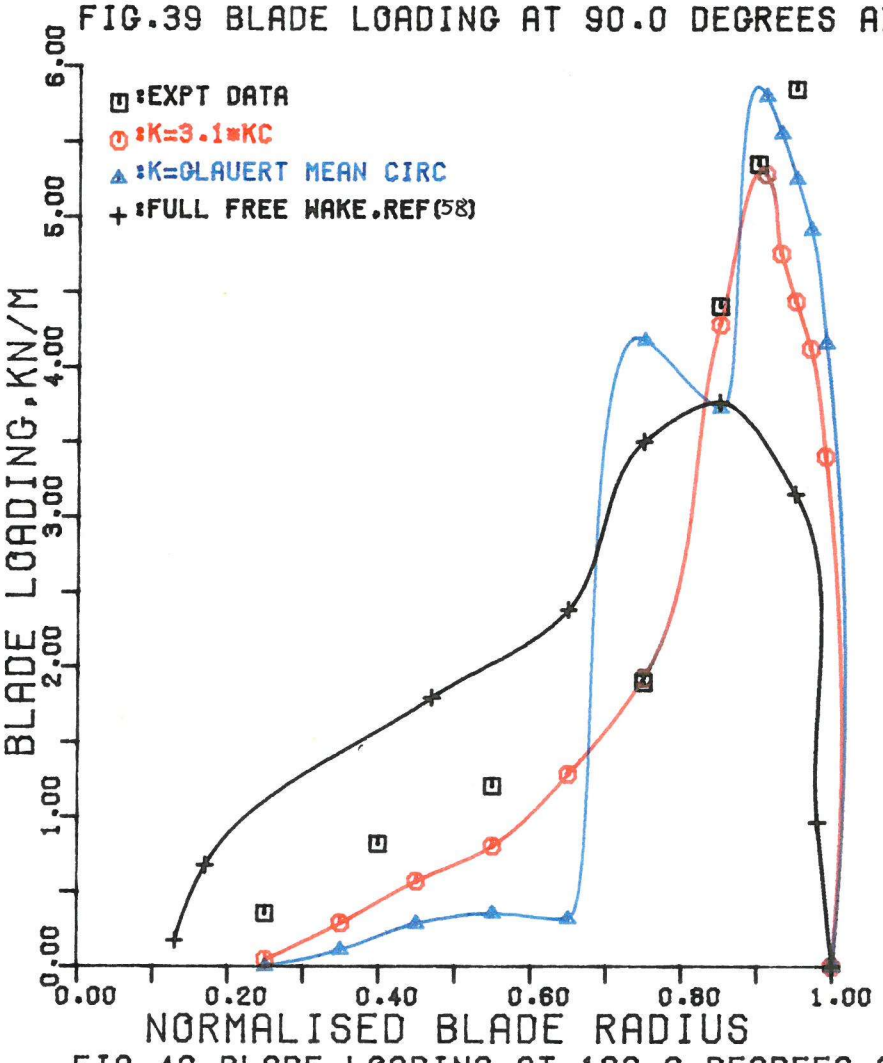

FIG.40 BLADE LOADING AT 180.0 DEGREES AZIMUTH.

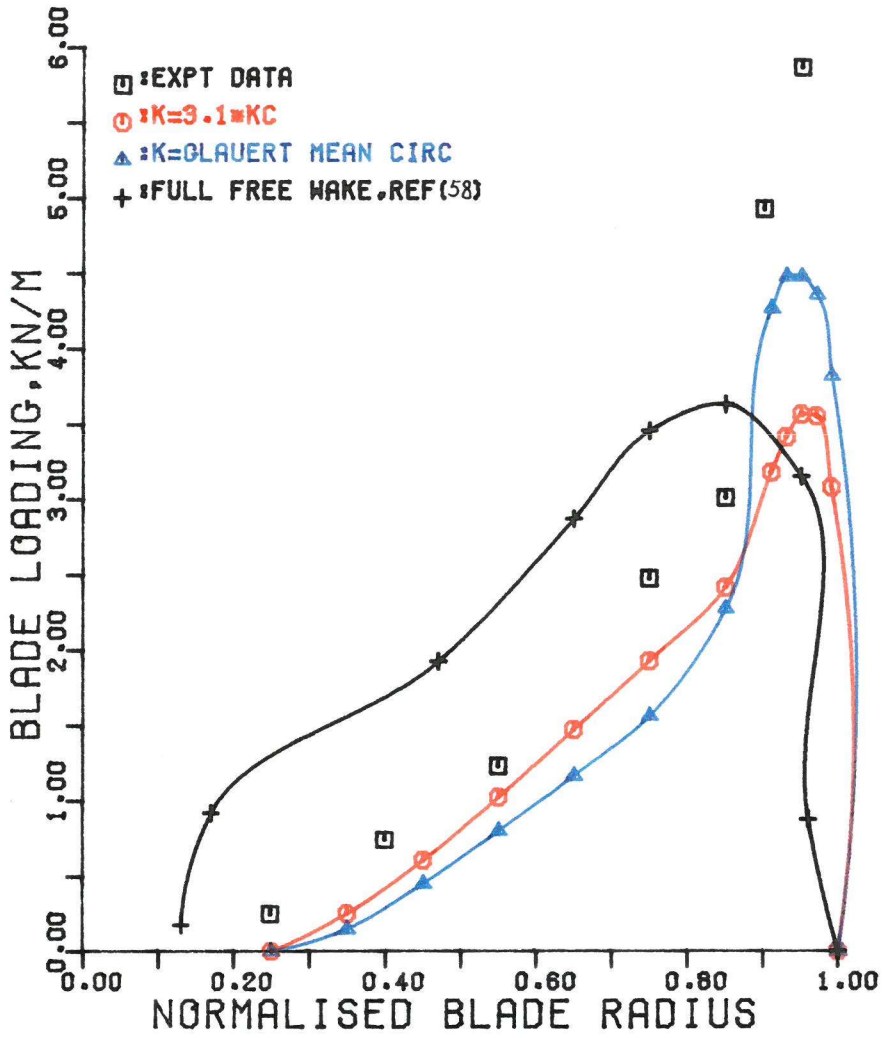

FIG.41 BLADE LOADING AT 270.0 DEGREES AZIMUTH.

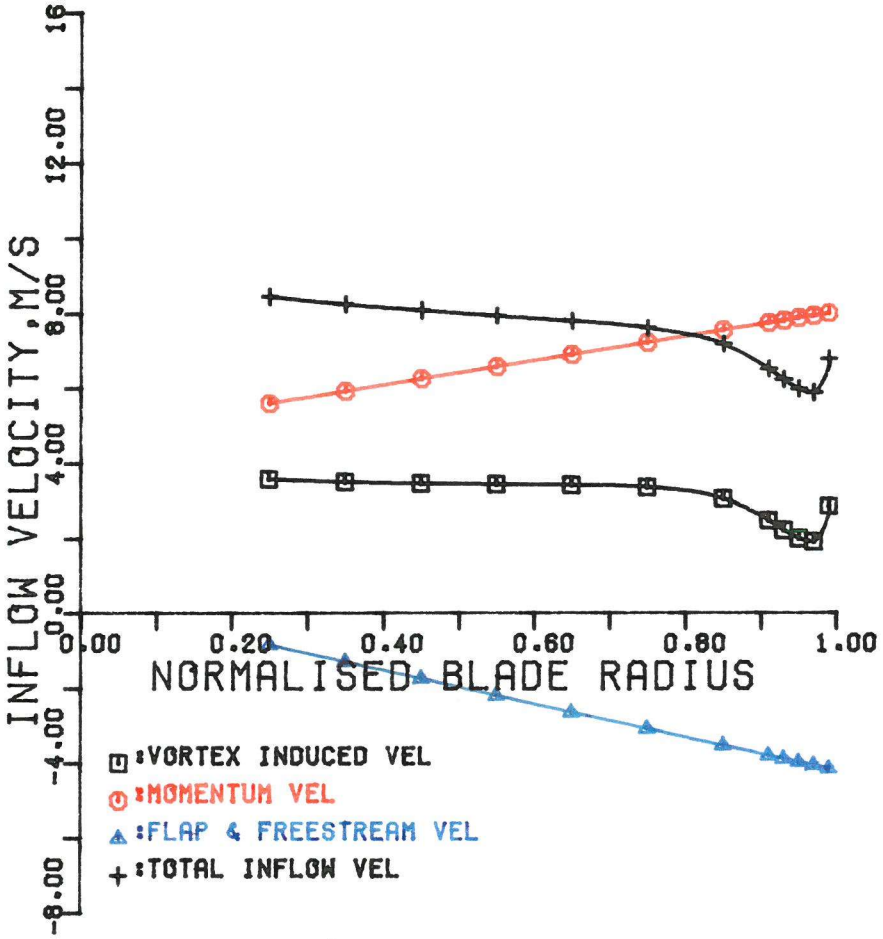

FIG.42 INFLOW DISTRIBUTIONS AT 0.0 DEGREES AZIMUTH.

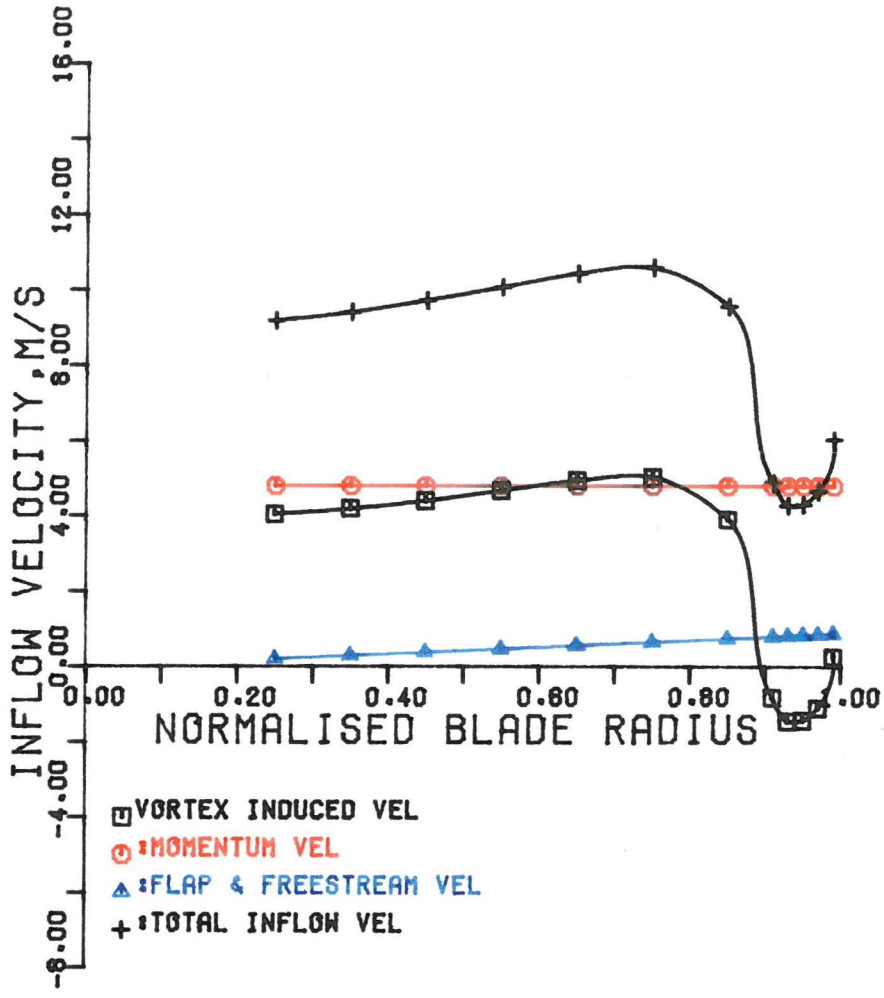

FIG.43 INFLOW DISTRIBUTIONS AT 90.0 DEGREES AZIMUTH.

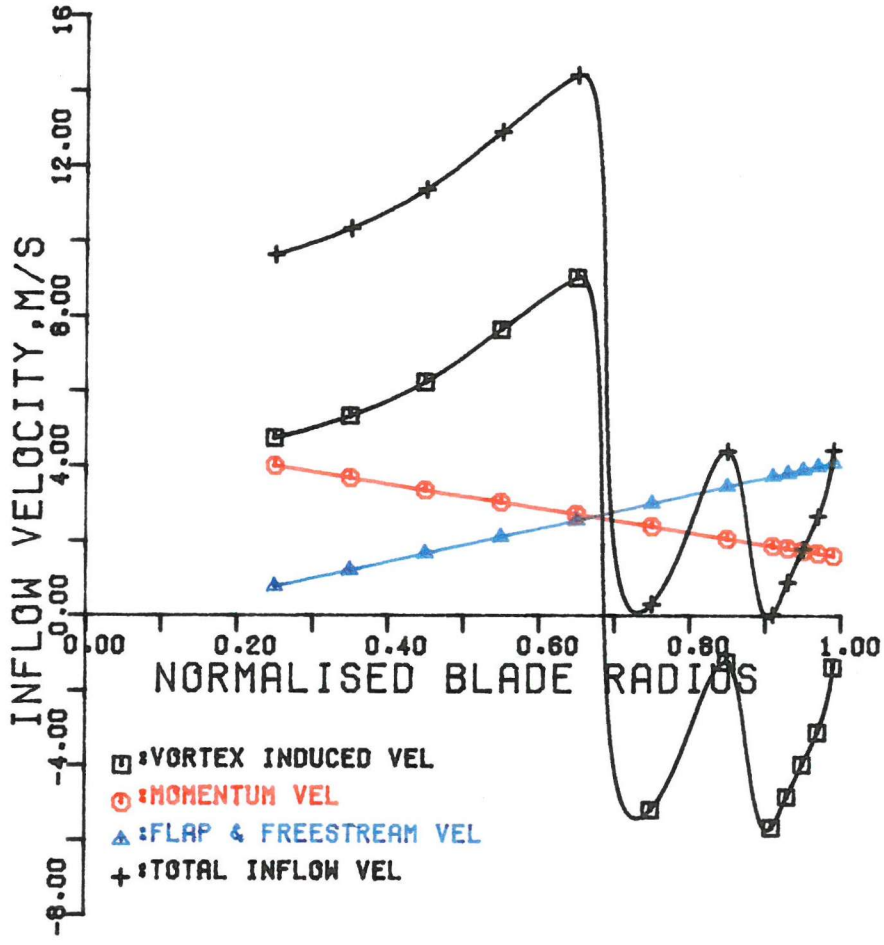

FIG.44 INFLOW DISTRIBUTIONS AT 180.0 DEGREES AZIMUTH

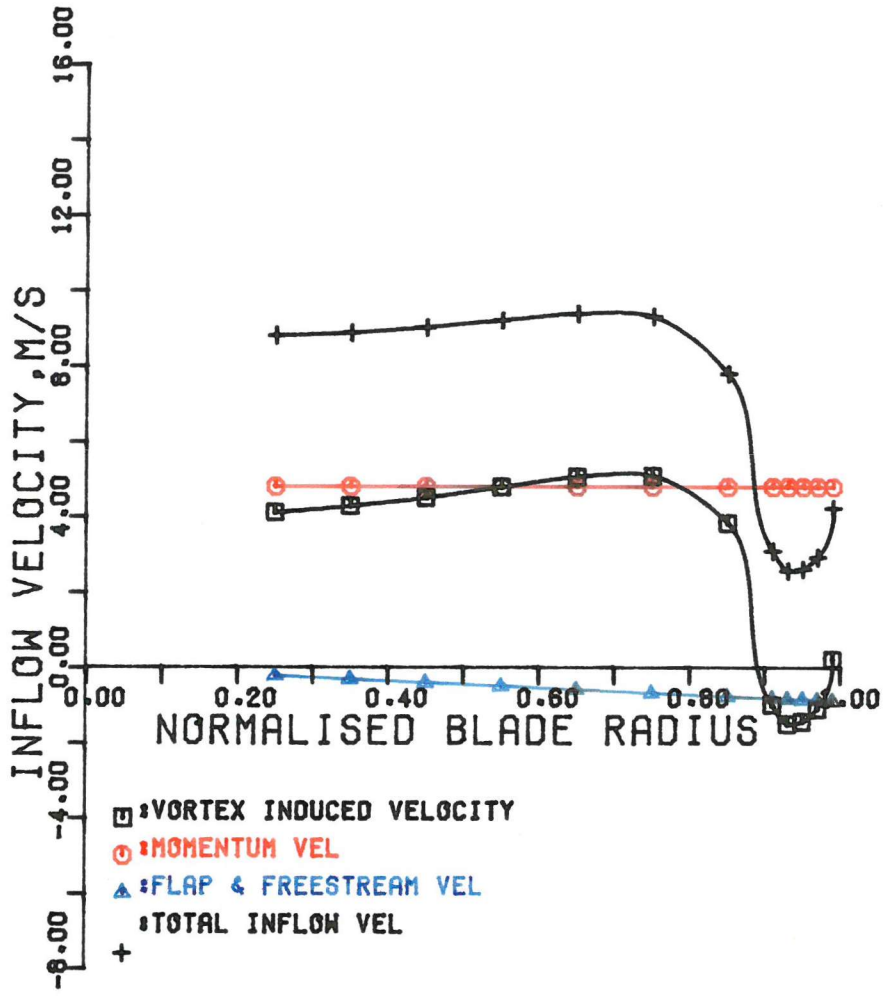

FIG.45 INFLOW DISTRIBUTION AT 270.0 DEGREES AZIMUTH.

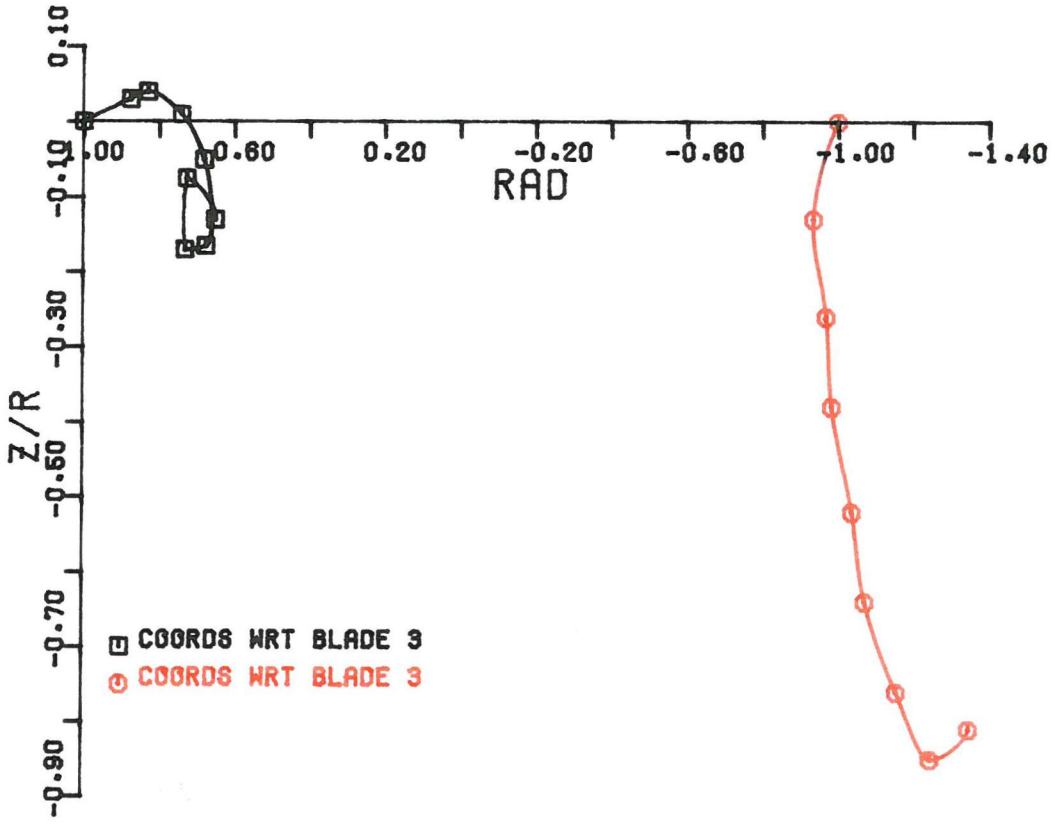

FIG.46 TIP VORTEX PATHS IN LONG.AL PLANE.

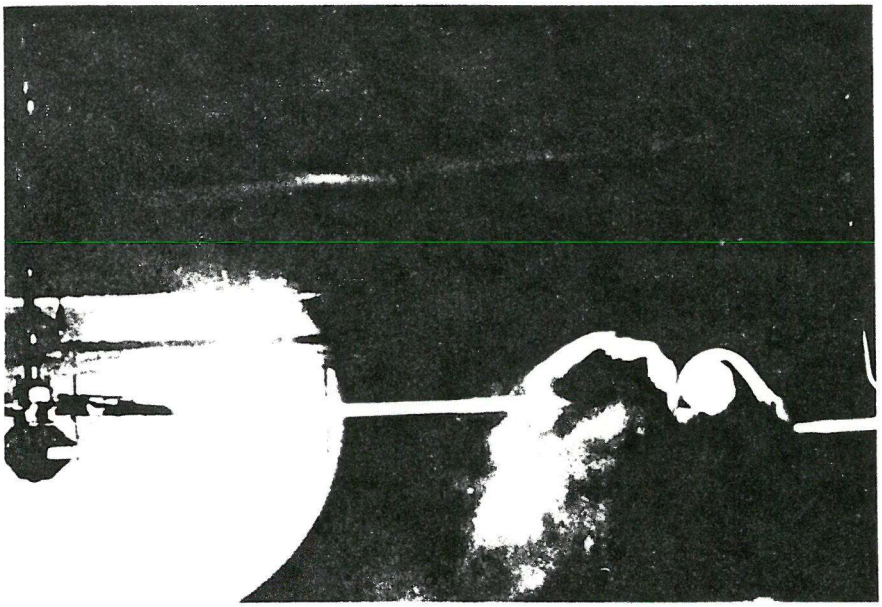

FIG.47 PHOTOGRAPH OF THE TIP VORTEX FORMATION AT THE FRONT OF A CCTR.

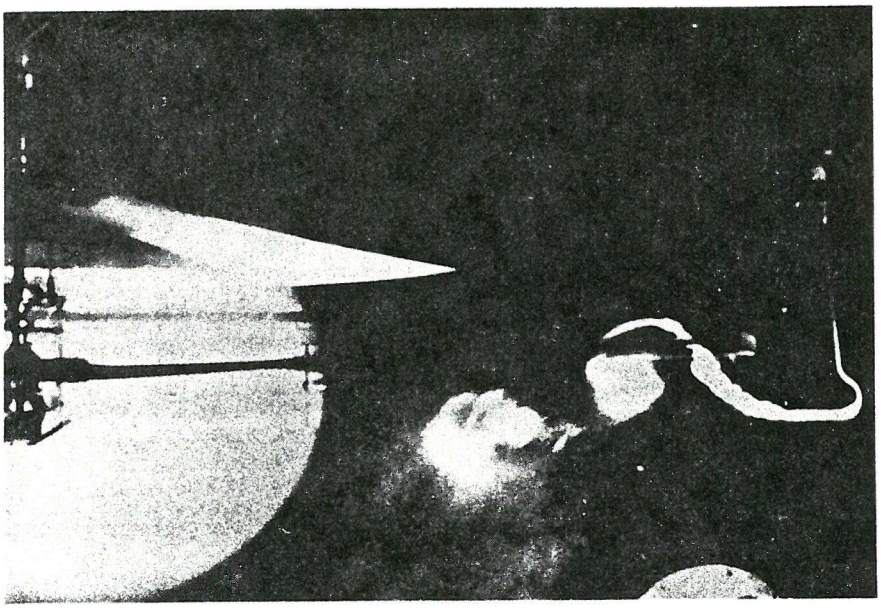

FIG.48 PHOTOGRAPH OF THE UPWASH AT THE FRONT OF A CCTR.

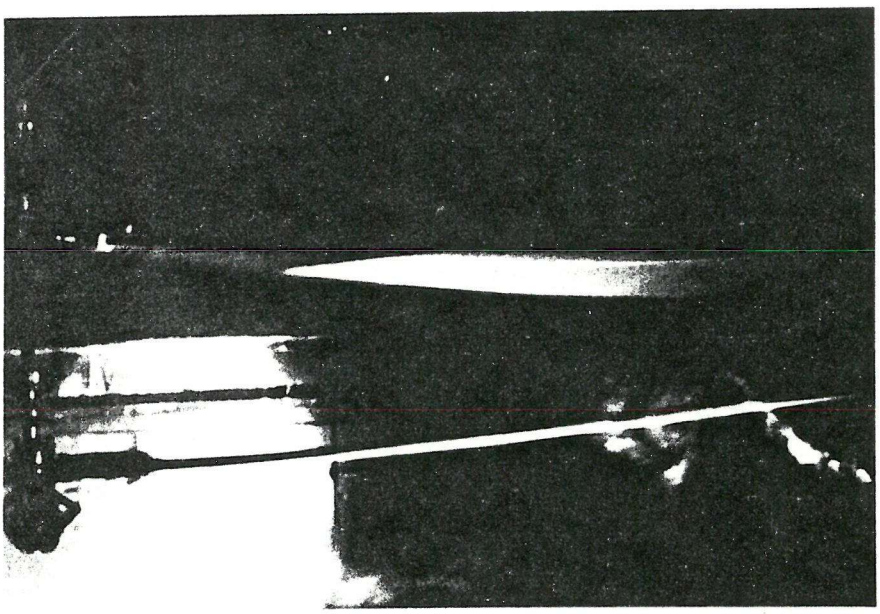

FIG.49 PHOTOGRAPH OF APENDING BLADE VORTEX INTERACTION.

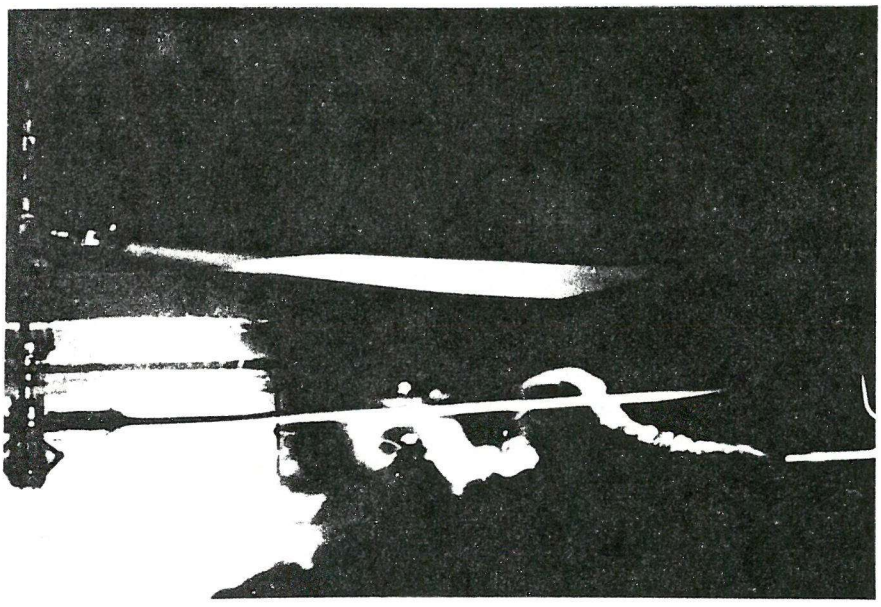

FIG.50 PHOTOGRAPH OF THE FLOW PERIODICITY AT THE FRONT OF A CCTR.

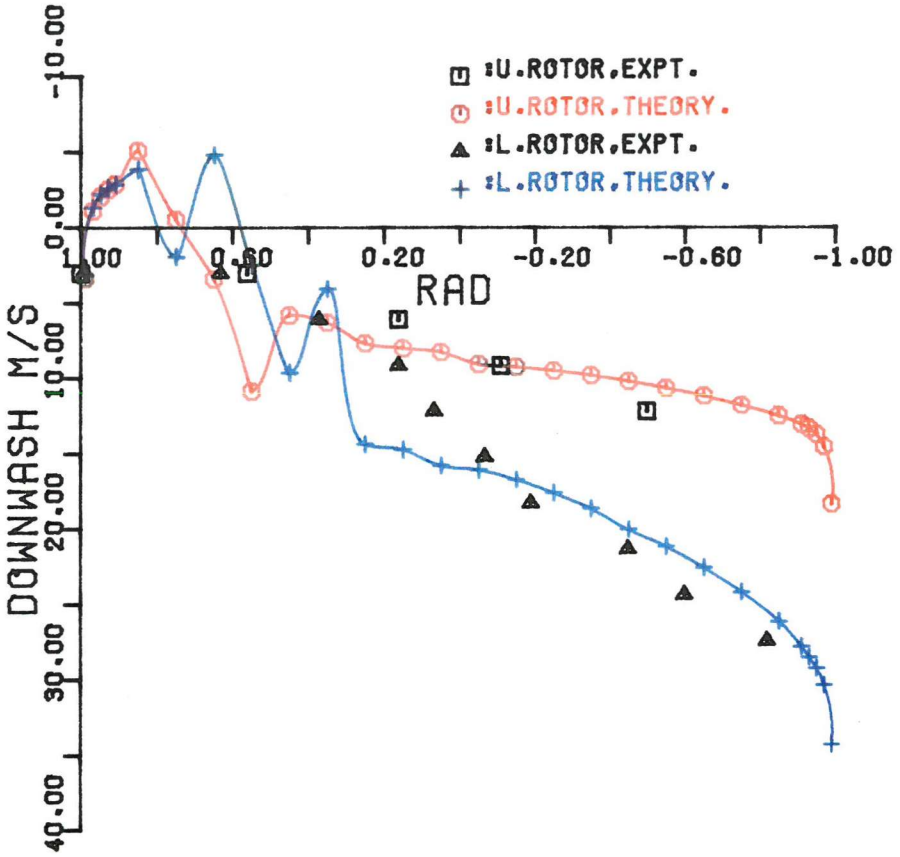

FIG.51 ABC INFLOW DISTRIBUTION,0-180 DEGS PLANE.

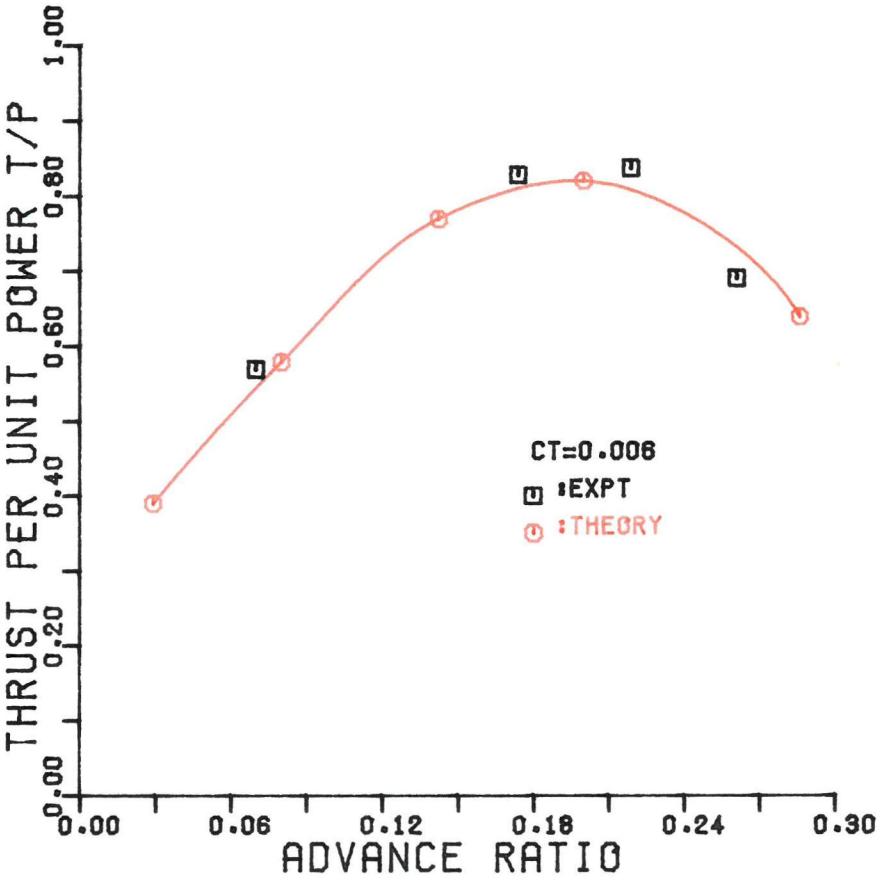

FIG.52 MOTE FORWARD FLIGHT PERFORMANCE.

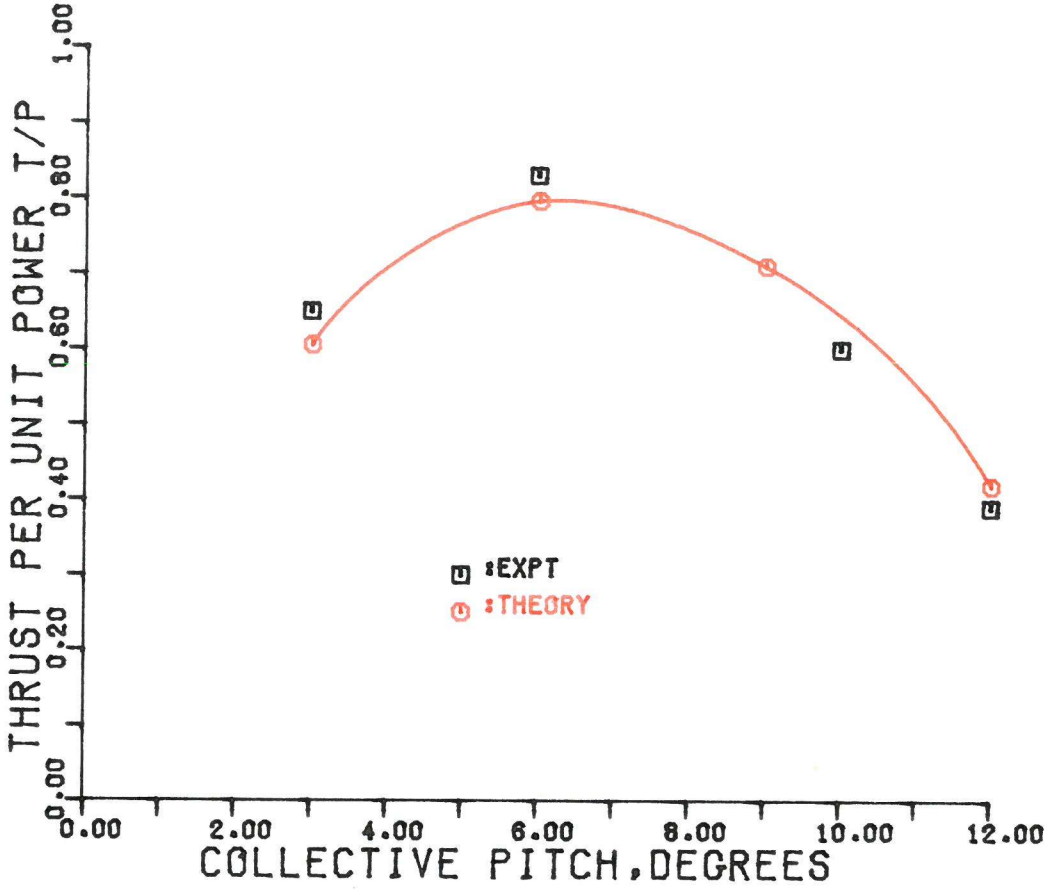

FIG.53 MOTE PERFORMANCE,ADVANCE RATIO=0.174.

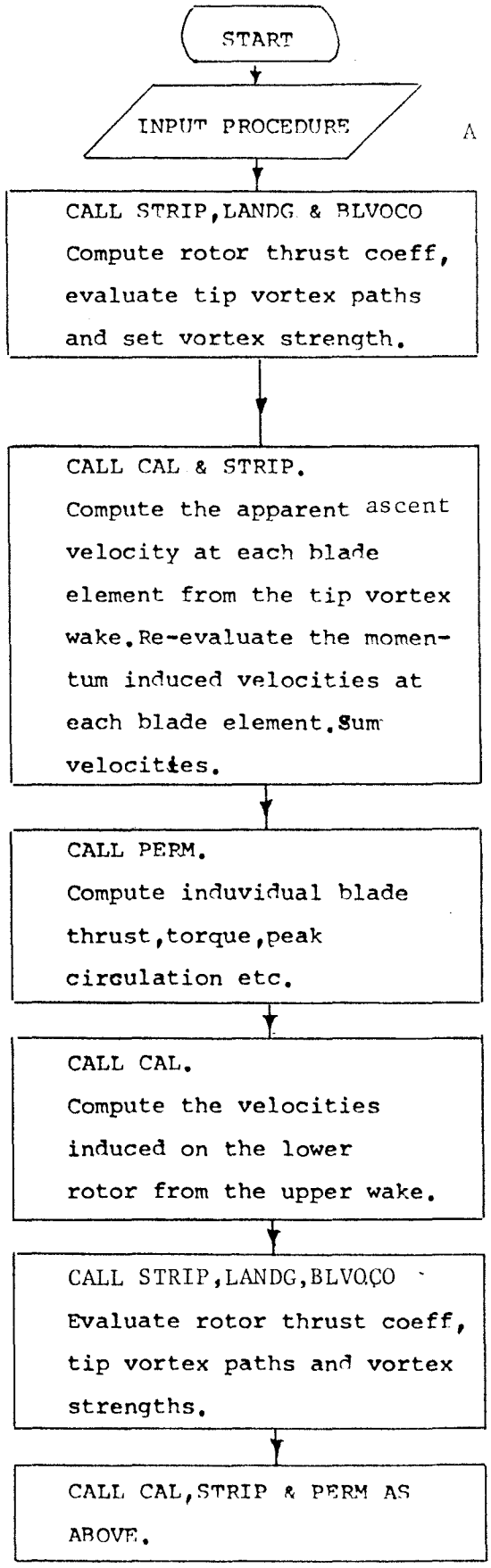

FIG.54 FLOW CHART OF HOVER CODE.

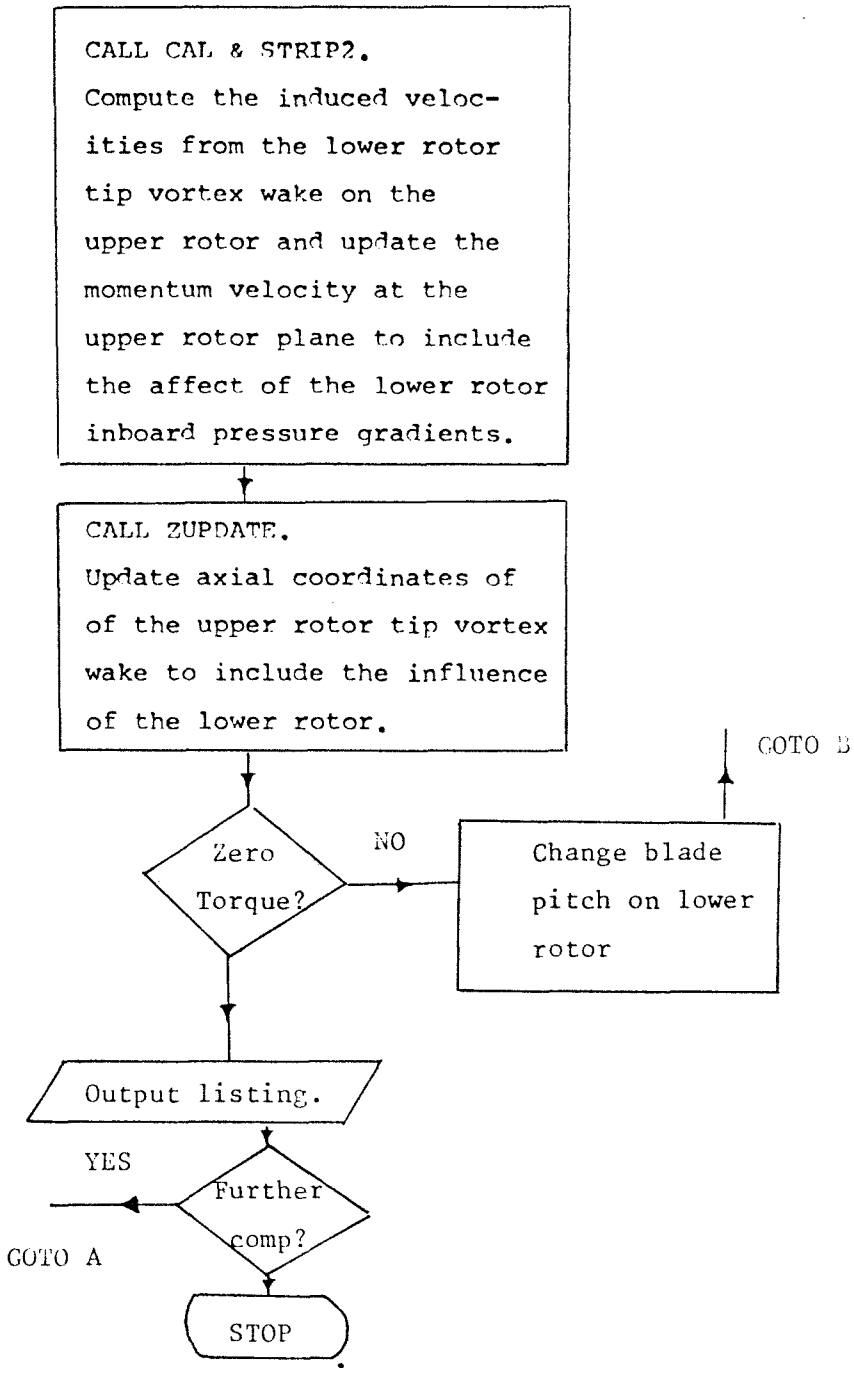

FIG.54 CONTINUED.

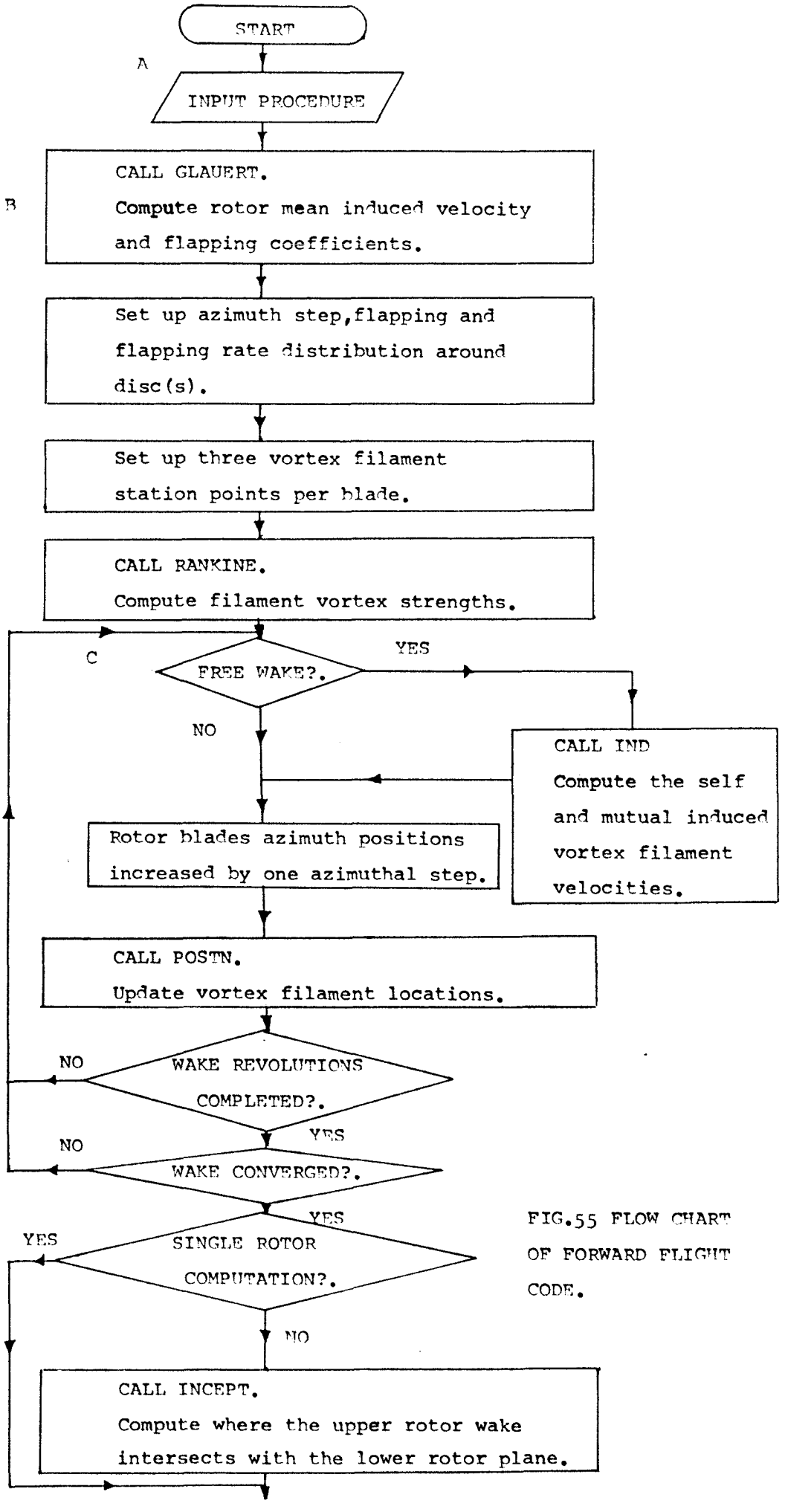

FIG.55 FLOW CHART OF FORWARD FLIGHT CODE.

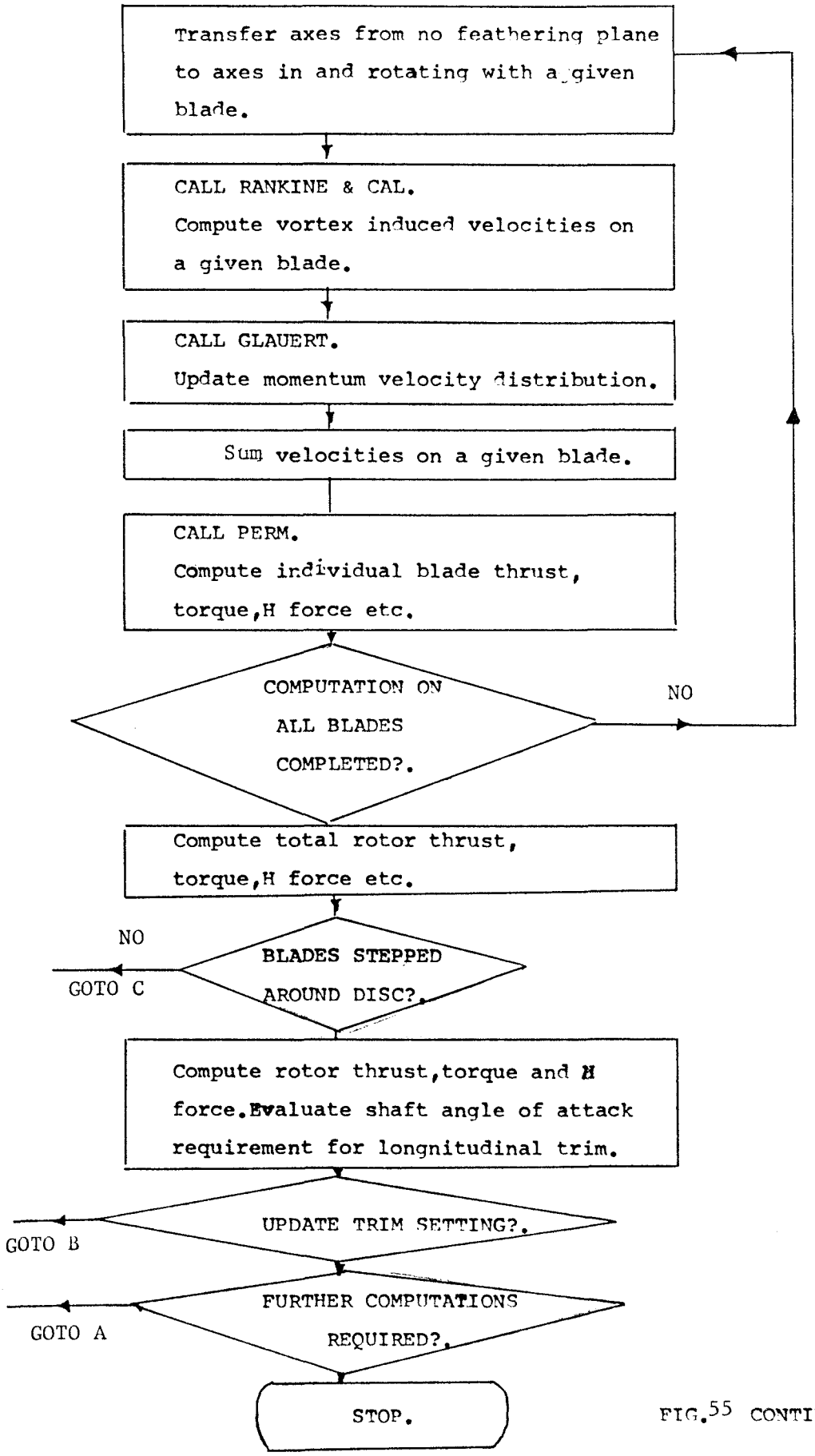

FIG.55 CONTINUED.

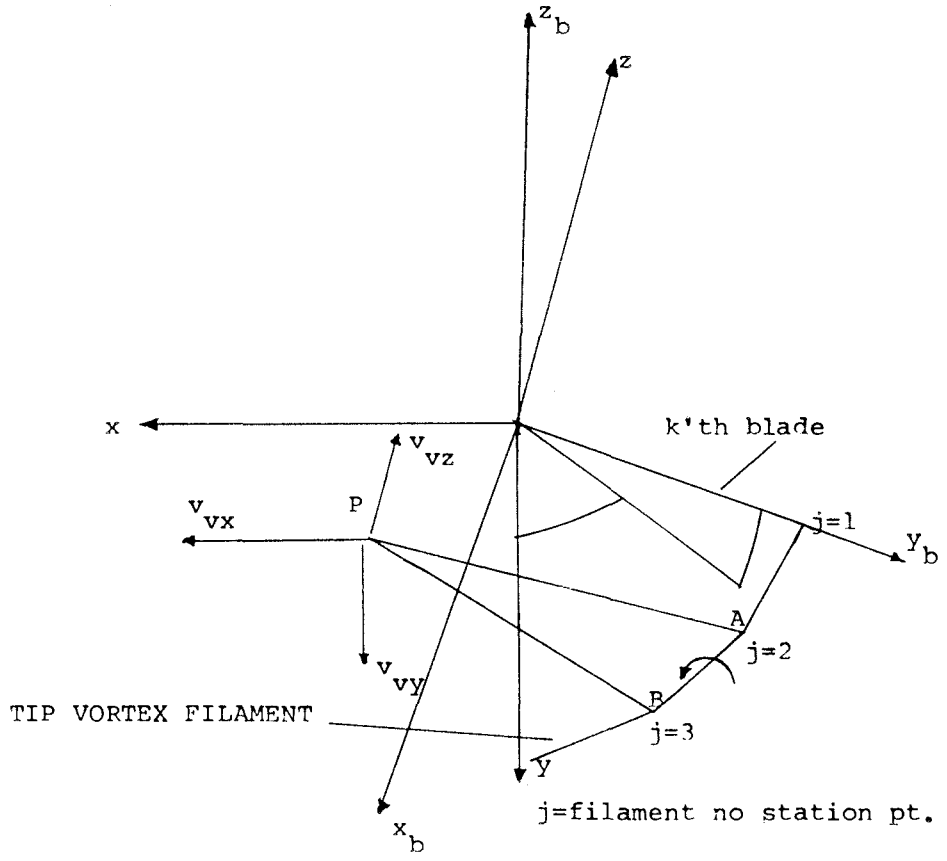

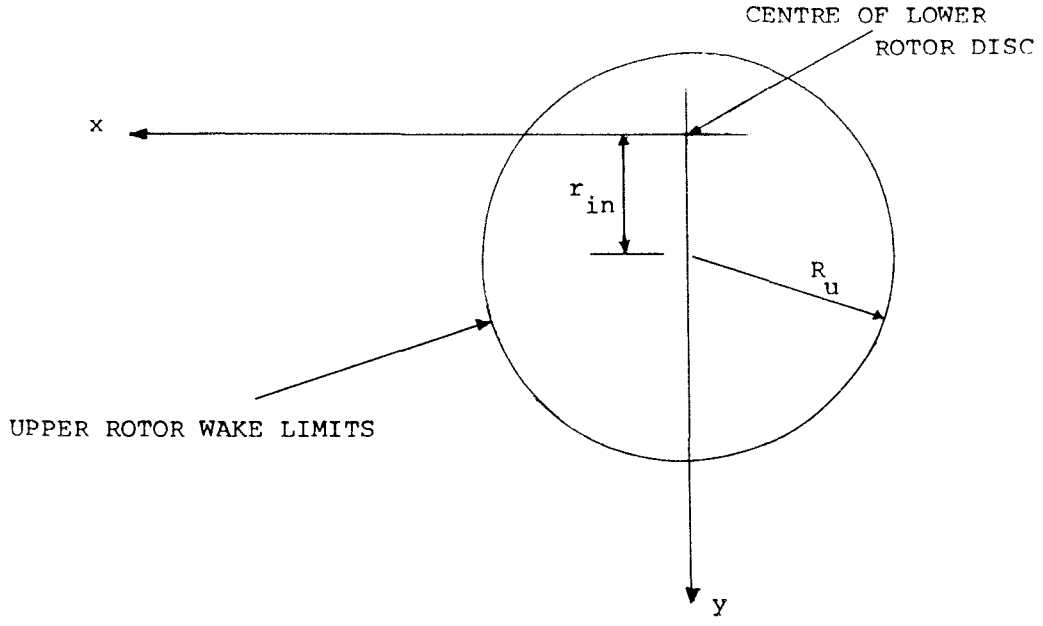

FIG.56 NOTATION OF AXES.

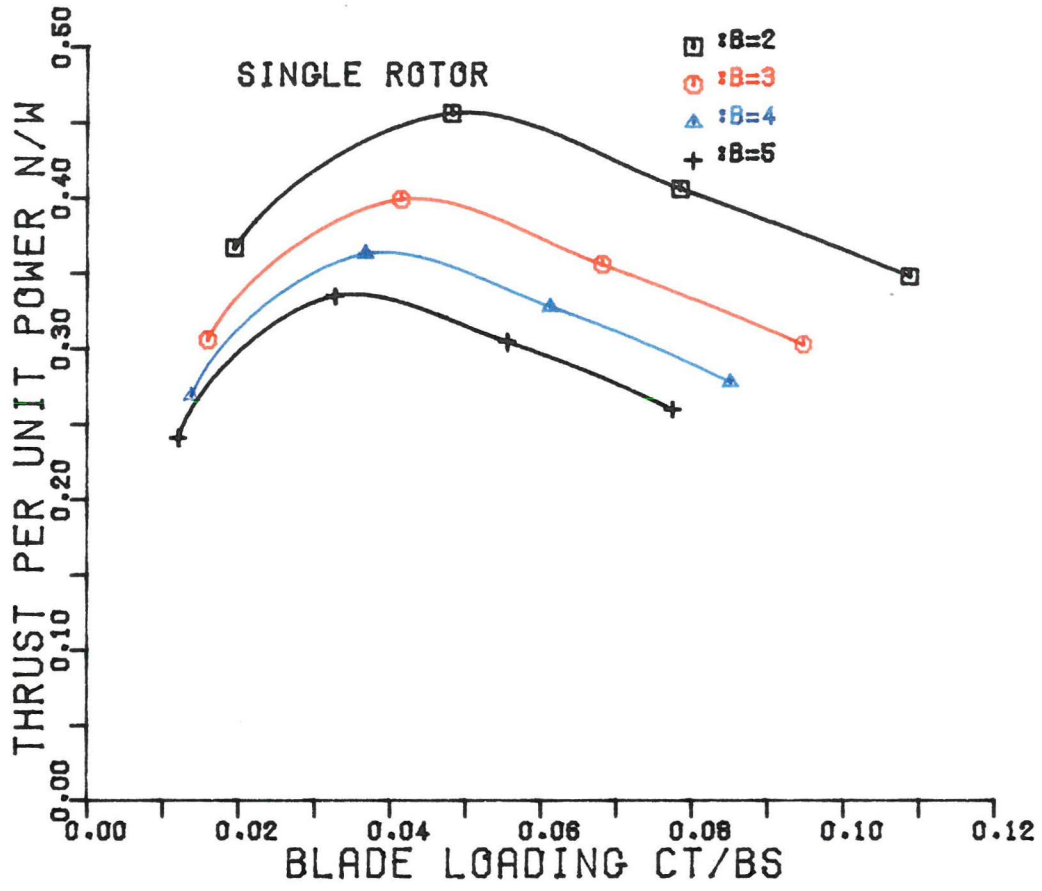

FIG.57 VARIATION IN NUMBER OF BLADES.

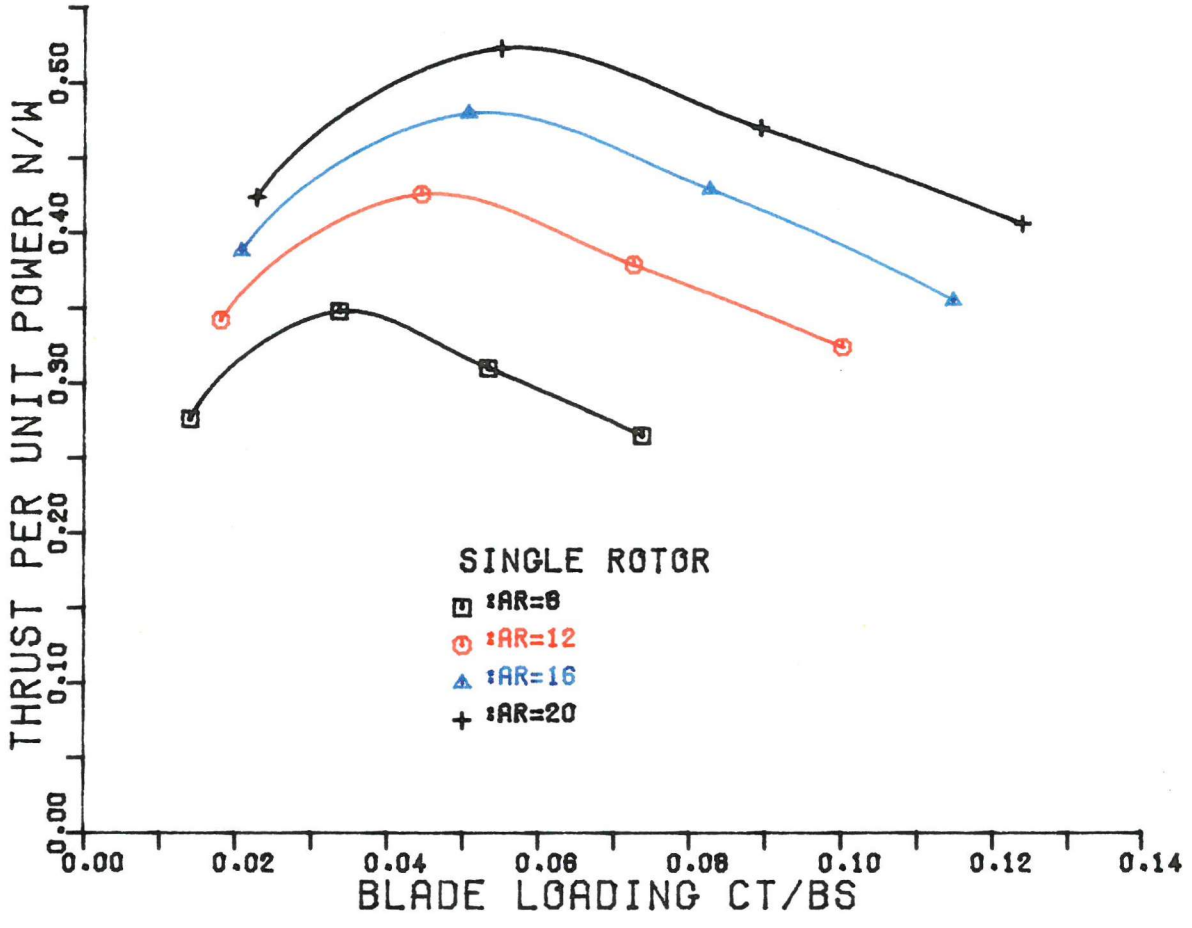

FIG.58 VARIATION IN BLADE ASPECT RATIO.

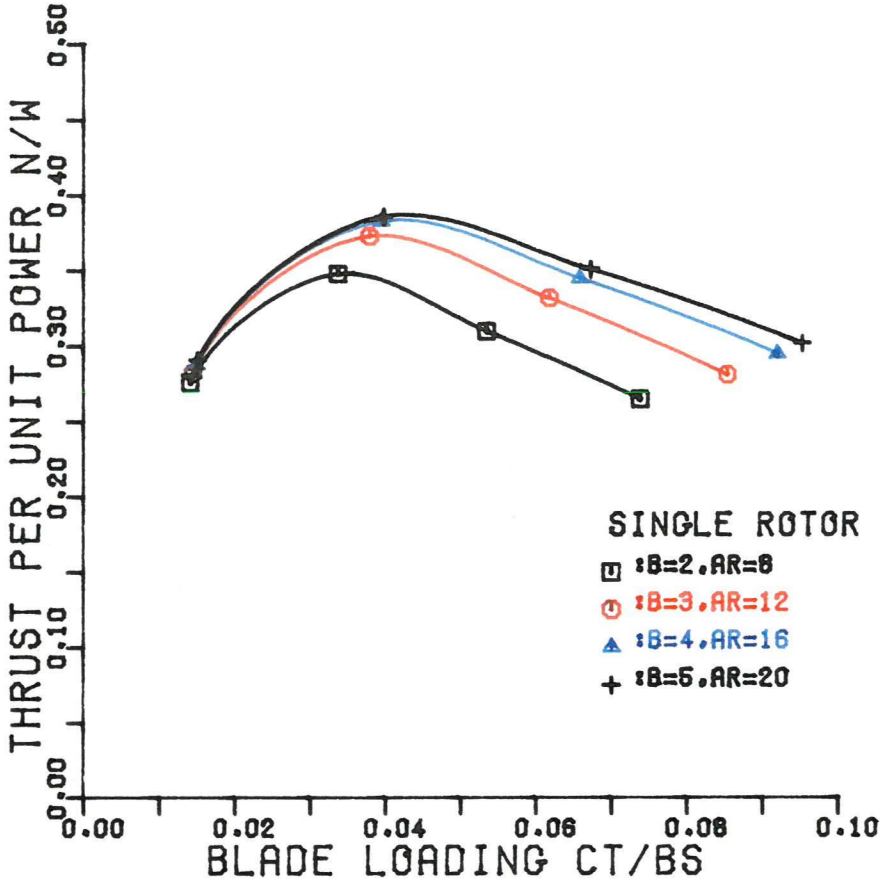

FIG.59 CONSTANT BLADE SOLIDITY.

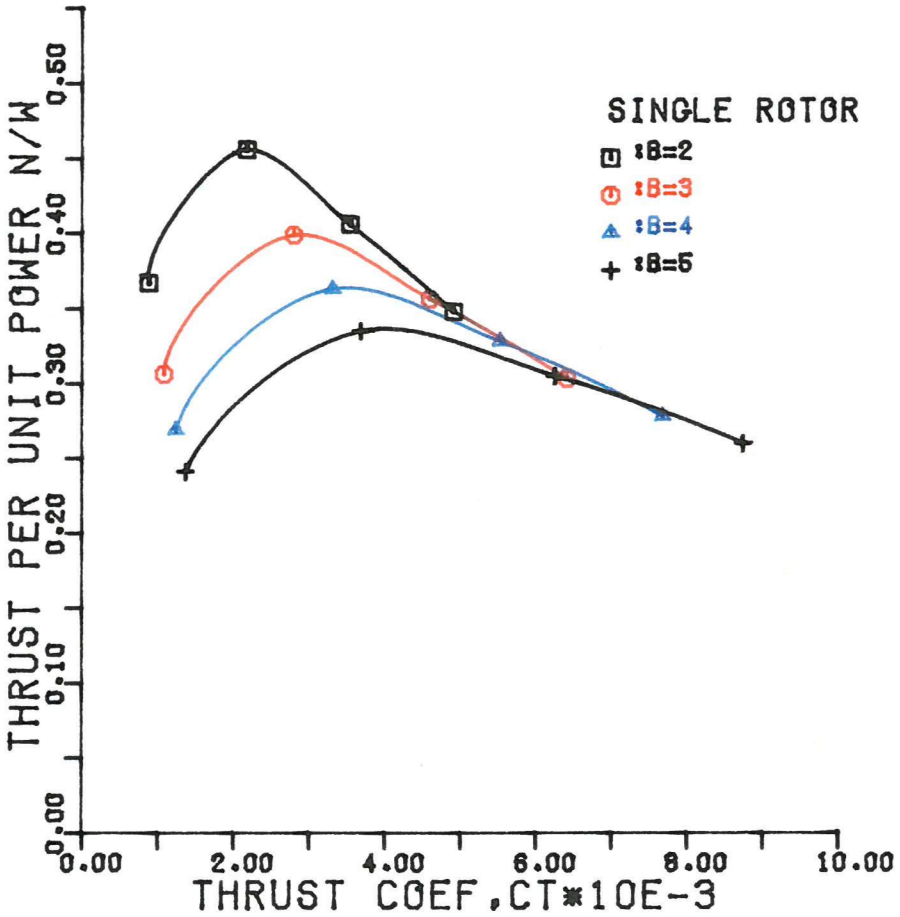

FIG.60 VARIATION IN NUMBER OF BLADES.

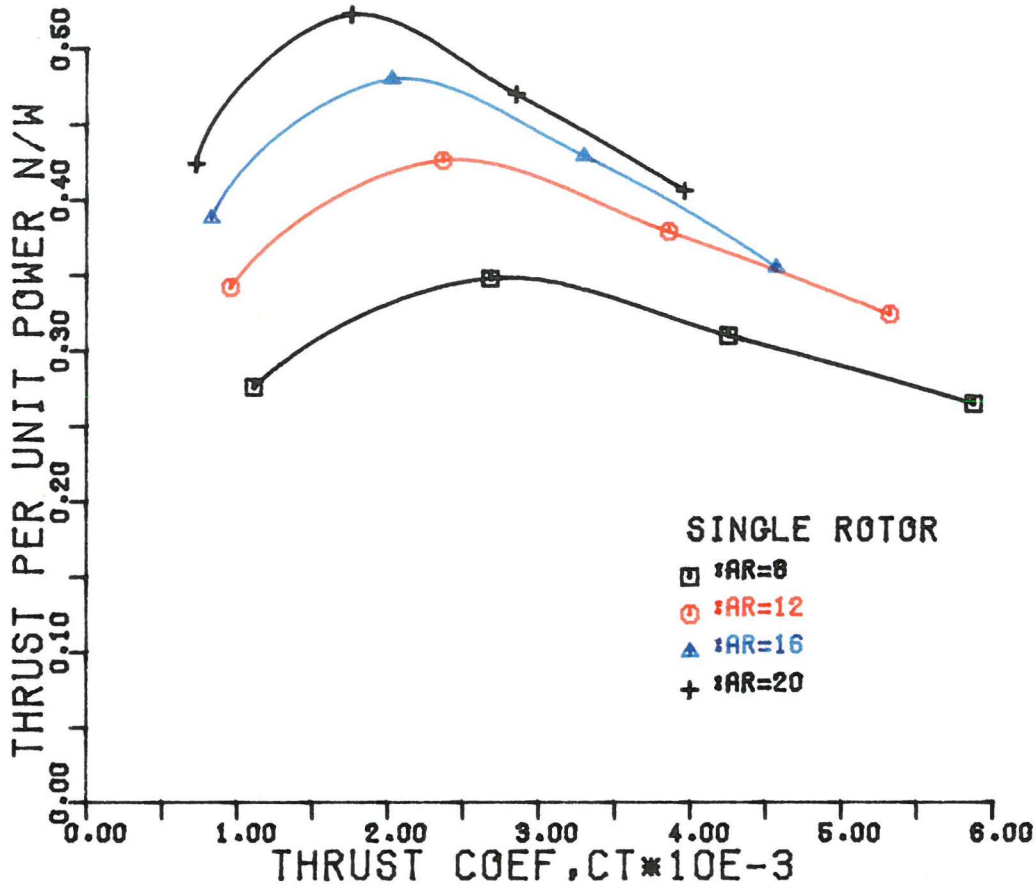

FIG.61 VARIATION IN ASPECT RATIO.

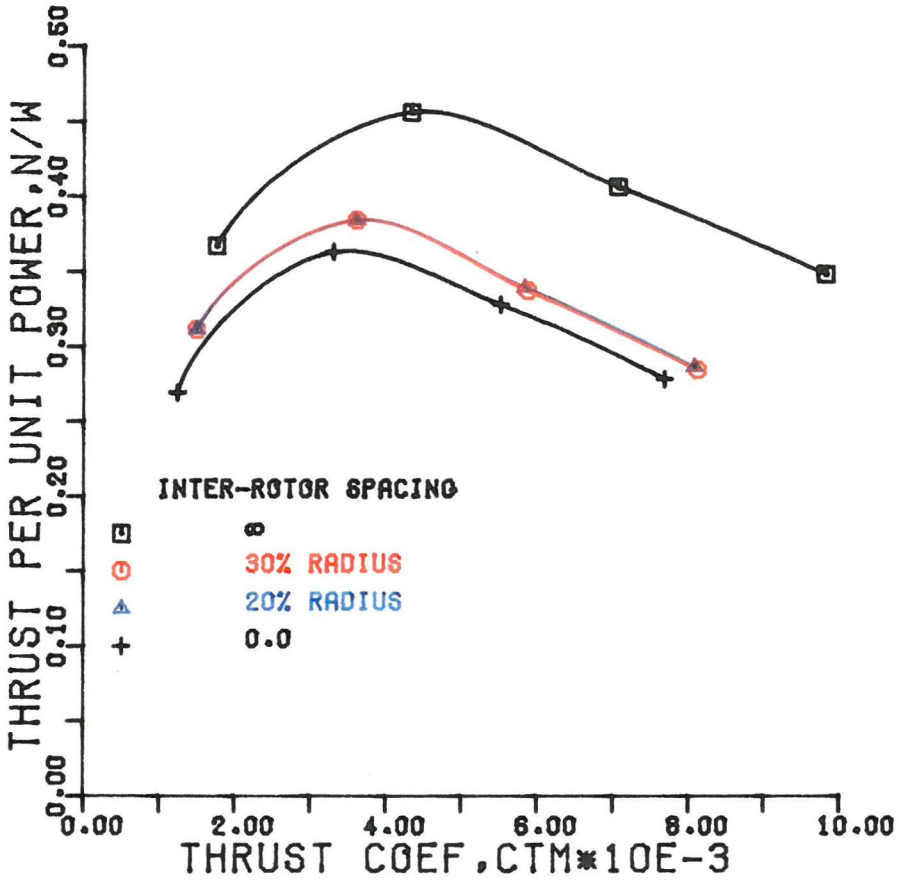

FIG.62 EFFECT OF INTER-ROTOR SPACING.

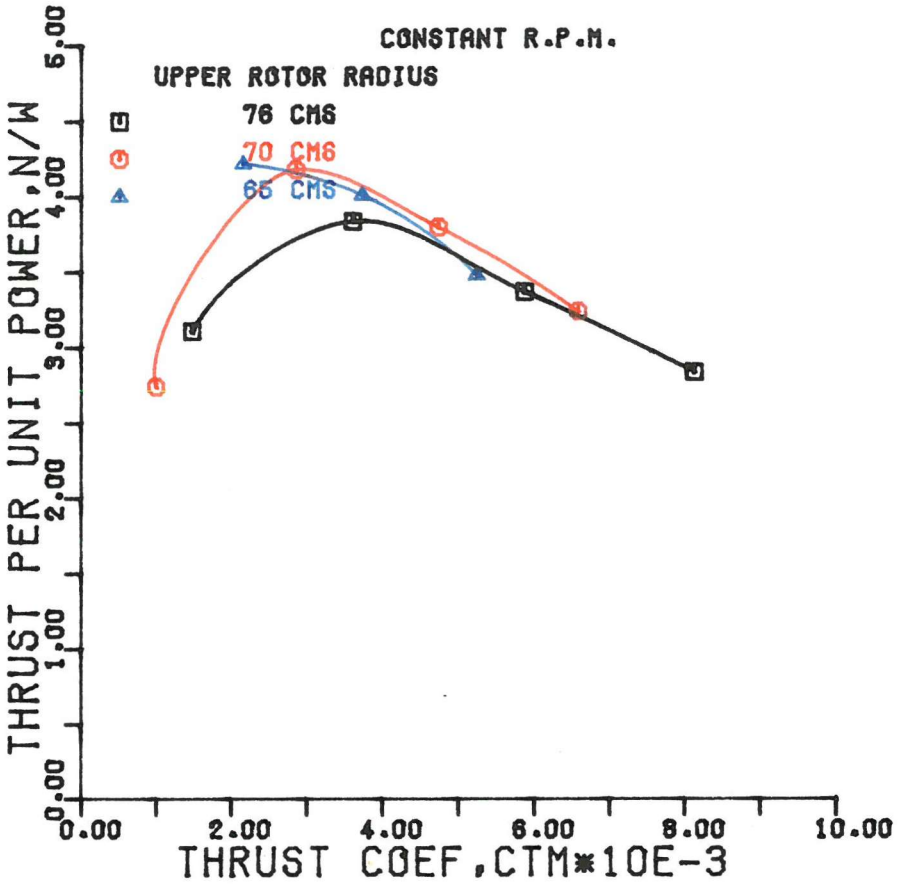

FIG.63 EFFECT OF REDUCING UPPER ROTOR RADIUS.

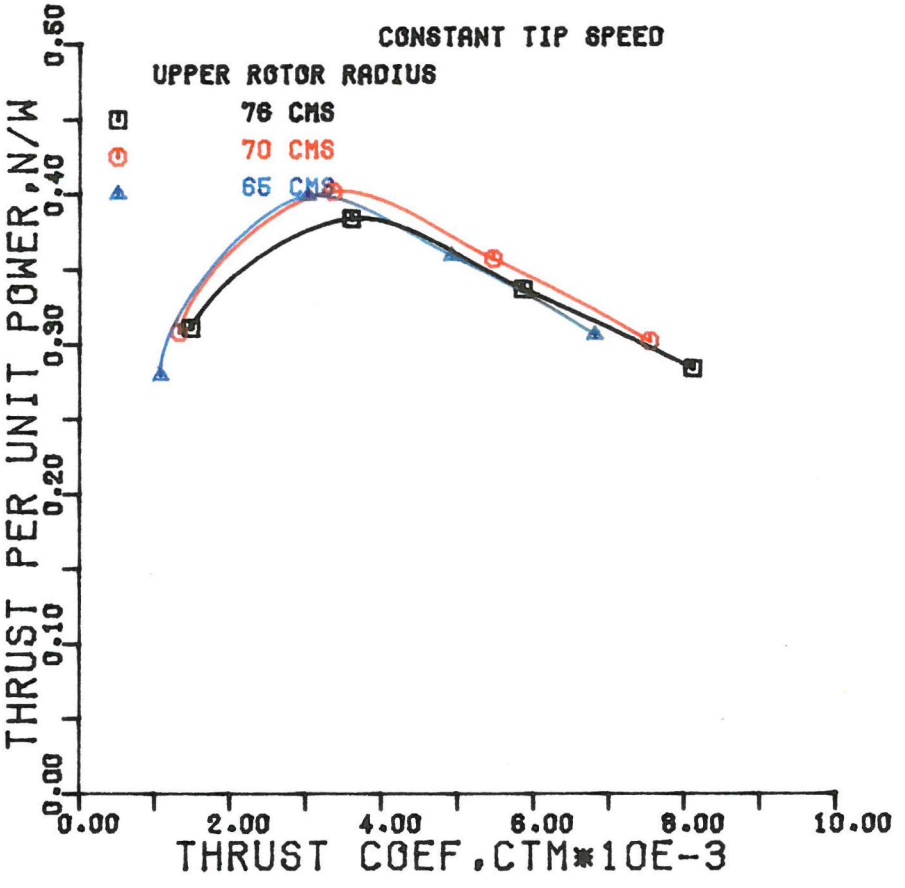

FIG.64 EFFECT OF REDUCING UPPER ROTOR RADIUS.

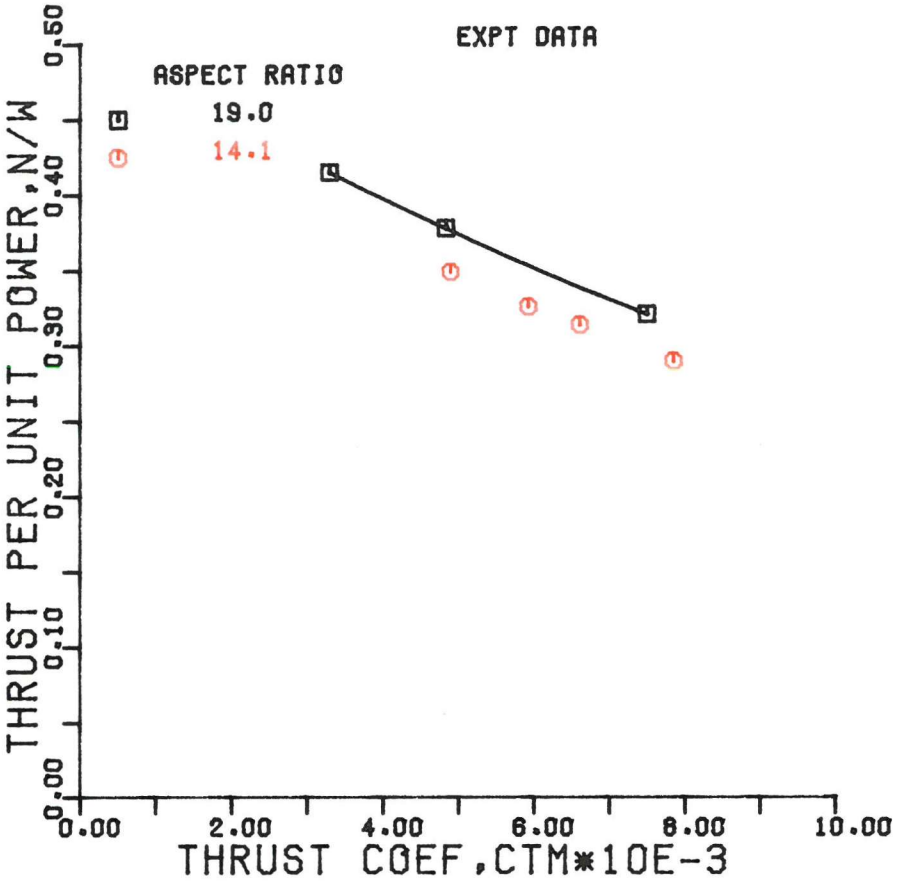

FIG.65 MOTE CCTR COMPARISON-ASPECT RATIO EFFECT.

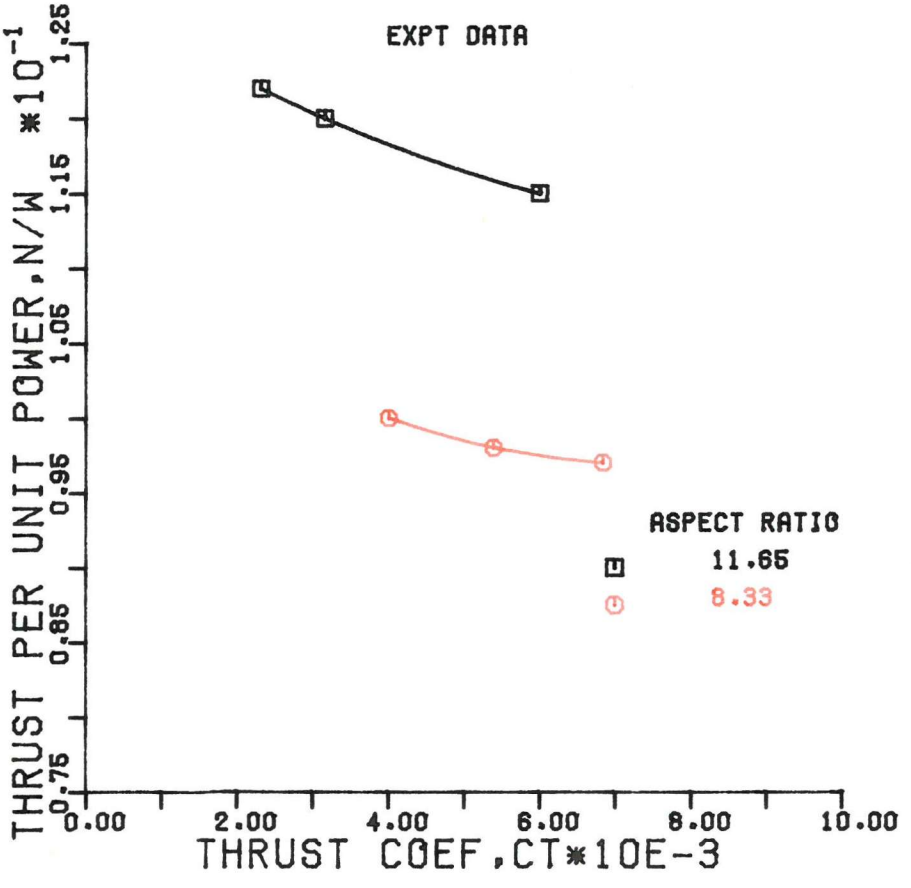

FIG.66 CCTR COMPARISON-ASPECT RATIO EFFECT.